‘FIXED CHARGE’ CHEMICAL DERIVATIZATION AND DATA DEPENDENT MULTISTAGE TANDEM MASS SPECTROMETRY FOR PROTEIN STRUCTURAL ANALYSIS

By

Xiao Zhou

A DISSERTATION

Submitted to
Michigan State University
in partial fulfillment of the requirements
for the degree of

DOCTOR OF PHILOSOPHY

Chemistry

2012

ABSTRACT

'FIXED CHARGE' CHEMICAL DERIVATIZATION AND DATA DEPENDENT MULTISTAGE TANDEM MASS SPECTROMETRY FOR PROTEIN STRUCTURAL ANALYSIS

By

Xiao Zhou

Protein surface accessible residues play an important role in protein folding, protein-protein interactions and protein-ligand binding. With the advantages in sensitivity, speed, and the capability of analyzing complex protein systems, mass spectrometry combined with protein labeling has found increasing utility for the characterization of protein surface. However, a common problem associated with the use of chemical labeling methods for mapping protein solvent accessible residues is that when a complicated peptide mixture resulting from a large protein or protein complex is analyzed, the modified peptides may be difficult to identify and characterize amongst the largely unmodified peptide population (i.e., the 'needle in a haystack' problem). To address this challenge, an experimental strategy was developed involving the synthesis and application of a 'fixed charge' sulfonium ion containing amine-specific protein modification reagent, S,S'-dimethylthiobutanoylhydroxysuccinimide ester (DMBNHS), coupled with capillary HPLC-ESI-MS, automated CID-MS/MS, and data dependent neutral loss mode MS^3 in an ion trap mass spectrometer, to map the surface accessible lysine residues in a model protein, Cellular Retinoic Acid Binding Protein II (CRABP II). After reaction with different reagent : protein ratios and digestion with Glu-C, modified peptides were selectively identified and the number of modifications within each peptide were determined by CID-MS/MS, via the exclusive neutral loss(es) of dimethylsulfide, independently of the amino acid composition and precursor ion charge state (i.e. proton mobility) of the peptide. The observation of these

characteristic neutral losses were then used to automatically 'trigger' the acquisition of an MS^3 spectrum to allow the peptide sequence and the site(s) of modification to be characterized. Using this approach, the experimentally determined relative solvent accessibilities of the lysine residues were found to show good agreement with the known solution structure of CRABP II. With the initial success demonstrated on a model protein, the experimental strategy was extended to reveal the mechanisms corresponding to oxidation induced inactivation of calcineurin (CN), from a structural perspective. CN is a Ca^{2+}/calmodulin (CaM) activated phosphatase that participates in a wide variety of physiological processes. CaN is also reported to be inactivated by H_2O_2- or superoxide-induced oxidation both *in vivo* and *in vitro*. However, the mechanism is still under debate. Here, the relative rates of H_2O_2 induced oxidation of methionine residues within CN were first determined using a multi enzyme digestion strategy coupled with analysis using capillary HPLC-ESI-MS and CID/ETD-MS/MS. Then the developed experimental strategy, i.e., combining protein modification by DMBNHS with data dependent multistage tandem mass spectrometry, was applied to characterize changes in CN conformation before and after oxidation. In addition, targeted ETD-MS/MS was used to characterize and quantify individual unmodified lysine residues from isomers of DMBNHS modified peptides containing multiple modifiable sites. The extent of DMBNHS modification of observed CN lysine residues was found to increase upon oxidation. More importantly, the methionine residues that were highly susceptible towards oxidation and lysine residues exhibited large increase in solvent accessibility upon oxidation all locate in CN functional domains that are involved in Ca^{2+}/CaM binding regulated activation, thus indicating of a role for oxidation induced conformation change in CN as a possible cause of CN inactivation by inhibiting Ca^{2+}/CaM regulated CN activations.

ACKNOWLEGEMENTS

The completion of this dissertation has been one of the most significant challenges I have ever had to conquer and I know I would not have got to this point without the help of many people. It is to them that I owe my sincere gratitude. First and foremost, I would like to thank my advisor, Dr. Gavin E. Reid, for his guidance and support all though my Ph. D studies. His knowledge, experiences, and especially his passion in research have greatly nurtured me. I also must thank my committee members, Dr. Merlin L. Bruening, Dr. A. Daniel Jones, and Dr. Gregory L. Baker, for their valuable suggestion and help on research work. I would also thank Dr. Babak Borhan and his students Mercy Anyika and Wenjing Wang for the supply of CRABP II proteins and especially their knowledge and help on organic synthesis. The synthesis work would not have been accomplished so smoothly without their advices. I would also thank Dr. Paul Stemmer from Wayne State University for his supply of calcineurin protein samples and his suggestions through the extensive discussions of this work. I also give my deepest thanks to the previous and current members from Reid's group, not only for their help on my research work, but also the happiness and encouragement they gave me. I would specially thank Yali Lu for her kindly help at the beginning of my Ph.D research and Jennifer Cox for leading me to the LC-MS world. I would like to thank my parents for their continuously support, not only though graduate school, but for my entire life. My mom, in particular, has always been my source of strength and without her I would not have gone this far. Last, but certainly not least, I truly thank my friends who have accompanied me during the difficult times. Without all the encouragement, caring, and kindness they provided, I would not have had this dissertation accomplished.

TABLE OF CONTENTS

LIST OF TABLES

LIST OF FIGURES

LIST OF SCHEMES

CHAPTER ONE

INTRODUCTION TO MASS SPECTROMETRY-BASED STRATEGIES FOR PROTEIN STRUCTURAL CHARACTERIZATION

1.1 A Brief Introduction to Mass Spectrometry-Based Proteomics

With the evolution and maturation of genomics during the past century, a large number of genes have been sequenced. However, genes only contain the source of information. It is the proteins that carry the information from genes and perform majority of the biological functions. Therefore, proteomics has become a new and important focus of research in the post-genomics era [1]. In general, proteomics studies cellular functions at the protein level and includes identification, characterization, and quantification of proteins in temporal and spatial terms.

The rapid development of proteomics is partially stimulated by the recent development of mass spectrometry (MS) for its advantages in sensitivity, speed, and compatibility with complex samples [1-3]. The introduction of soft ionization techniques, i.e., electrospray ionization (ESI) [4] or matrix-assisted laser desorption ionization (MALDI) [5, 6], allowed analysis of intact peptides or small proteins and revolutionized protein mass spectrometry [7]. Tandem mass spectrometry (MS/MS) is usually used to obtain the amino acid sequence information of the peptide [8]. As the name implies, MS/MS involves two stages of MS. Typically, in the first stage, the m/z of intact analyte ions present in the sample is determined and the ions of defined m/z (precursor ions) are isolated. In the second stage, the isolated precursor ions are dissociated and the m/z of the resulting fragment ions (product ions) is determined. Collision-induced

dissociation (CID) is the classical and still the most widely used fragmentation method. During CID, isolated precursor ions are accelerated in/into a gas-filled collision cell where their translational energy is converted into internal energy through multiple collisions with the inert collision gas. The internal energy gained by collisions is accumulated at a relatively slow time scale (picoseconds to microseconds) and is distributed through the peptide to induce cleavage at the weakest bond. CID dominantly cleaves the C-N amide bonds and generates b type sequence ions with the charge retained on N-terminal or y type sequence ions with the charge retained on C-terminal as Scheme 1.1 shows, where the subscript number indicates the number of amino acid contained within the corresponding sequence ions. Scheme 1.2 illustrates a general mechanism for the formation of b and y type ions [9]. The protonated amide bond, although whether the protonation site is on amide oxygen or amide nitrogen hat not been clearly determined yet [9, 10], is attacked by the preceding carbonyl group and an ion-molecule complex is formed. Dissociation of the complex can happen with or without a proton transfer resulting in a b type or y type ion, respectively. This mechanism indicates that the fragmentation requires the involvement of a proton at the cleavage site. To generate a series of sequence ions, the proton has to migrate along the peptide back bone, i.e., a "mobile proton" has to be present. For many peptides, cleavage occurs almost evenly along the peptide backbone, however, enhanced cleavages at specific peptide amide bonds have also been observed. For example, cleavage at the N-terminal side of Pro residue is usually observed which is assumed to be caused by the higher proton affinity of Pro imide bond [11]. Enhanced cleavage at the C-terminal side of Asp residue is common, especially when the number of protons is less than or equal to the number of Arg residues within the peptide (i.e., "nonmobile") [10, 11]. This is proposed to occur through the formation of a salt bridge by sharing the Asp carboxylic acid hydrogen to the neighboring amide

bond followed by attack of the protonated amide bond by the negatively charged oxygen from Asp carboxyl group. Besides the enhanced cleavage at peptide backbones, facile cleavages at amino acid side chains have also been observed, such as the ready loss of H_3PO_4 from phosphoserine or/and phosphothreonine [12] and facile loss of methane sulfenic acid from oxidized Met residues [13]. The preferential cleavages at certain peptide amid bonds or specific amino acid side chains may dominant the CID-MS/MS spectra and suppress the fragmentation along the peptide backbone, thus resulting in poor sequence information.

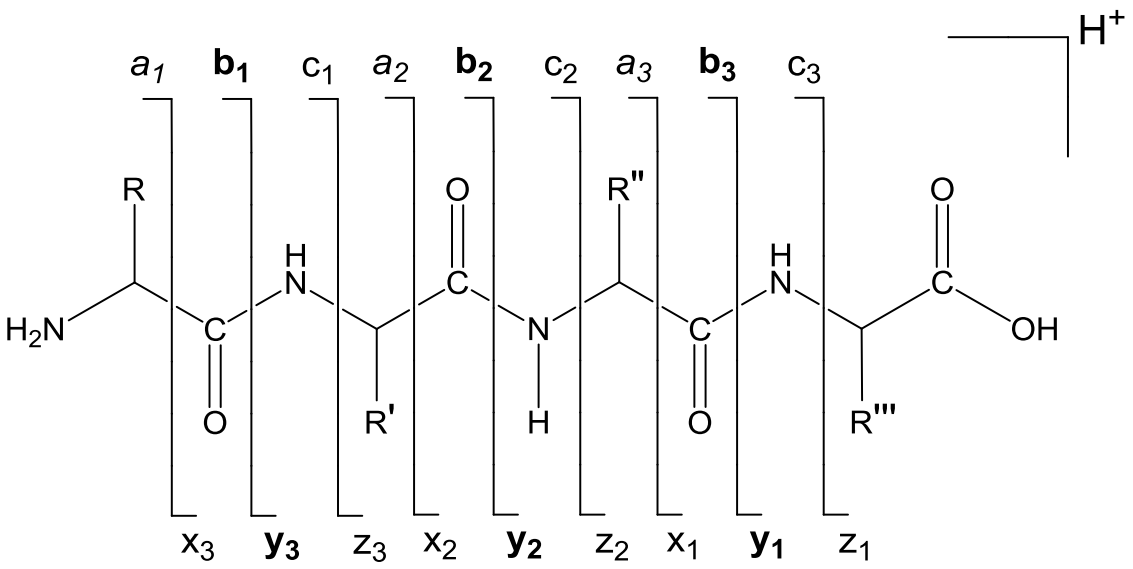

Scheme 1.1 Model peptide showing the cleavage sites for a/x, b/y, and c/z ions. Adapted from Reference [40].

CID-MS/MS can be performed on two main categories of mass spectrometers depending on whether the CID-MS/MS is performed in space or in time. Space-based instruments perform CID in a different region from that used for m/z analysis and precursor ion selection. For example, a triple quadrupole instrument (QqQ), which is frequently used as a space-based tandem mass spectrometer, uses the second quadrupole to perform CID-MS/MS on the precursor ions selected from the first quadrupole and subject the resulting product ions to the third quadrupole for analysis (product ion scan) [14]. A hybrid mass spectrometer with a combination of a quadrupole and a time-of-flight (TOF) analyzer has also been widely used to perform CID-MS/MS in space [15]. Typically, space-based instruments can only perform one stage of MS/MS as Multistage MS/MS (MS^n), i.e., further fragmentation of product ions generated in MS/MS, would require multiple collision cells. This issue is addressed by performing MS/MS and MS^n in time, in which the ions are analyzed, isolated, and fragmented in the same region but at different times. In CID-MS/MS experiments performed on time-based instruments, such as ion trap and Fourier transform-ion cyclotron resonance mass spectrometers (FT-ICR), the isolated ions with a specific m/z are accelerated by applying a radio frequency (RF) characteristic of the specific m/z and then fragmented via the conversion of translational energy to internal energy though multiple collisions with the bath gas. CID-MS^n can be successively performed in the same way without the addition of any physical domain to the instrument.

As mentioned above, the enhanced cleavage at certain peptide amide bonds or amino acid side chains can result in poor peptide sequence coverage. This problem can be overcome by electron-based fragmentation strategies, i.e., electron capture dissociation (ECD) [16] and electron transfer dissociation (ETD) [17-19]. The electron-based dissociation processes precede

by exothermic capture of a low-energy electron by a peptide cation (ECD) or transfer of a low-energy electron from the reagent radical anion to a peptide cation (ETD). The interaction between a peptide cation and an electron produces an odd-electron peptide cation radical which undergoes free-radical-driven cleavage as shown in Scheme 1.3 [20]. Unlike CID, ECD and ETD mainly cleave N-C_α bonds and generate even electron c type sequence ions and odd electron z• type ions (Scheme 1.1). The electron-based fragmentation happens at a relatively short time scale (~ 10^{-15} s) [21] before the redistribution of vibrational energy, thus more comprehensive sequence coverage can be obtained as the cleavage sites are not restricted to the weakest bond. Compared to CID, the electron-based dissociation methods have the advantages of 1) higher sequence coverage of protein or large peptide thereby allowing more specific localization of modification sites and 2) preservation of labile post-translational modifications (PTM) [22, 23]. However, the dissociation efficiency of the electron based fragmentation methods is highly dependent on the charge density of the precursor ions. For example, the electron capture cross section (i.e., the ratio of relative reduction in intensity of the precursor ions divided by electron current passing through the ECD cell) in ECD is proportional to the ionic charge squared [24]. Also, the ETD fragmentation efficiency is improved with decreasing ratio of amino acid residues per precursor charge (residues/charge), which usually appears as decreasing m/z [25]. This is attributed to the higher capability of a lower-charged non-covalent intermediate, which is generated after the capture of an electron, to bind the c/z ion pair together even with the backbone cleaved [25]. A gentle collision activation targeting the charge-reduced precursor ions has been demonstrated to effectively dissociate the c/z ion pair bound though non-covalent interactions and improve the ETD fragmentation efficiency [25, 26]. A similar approach which

applies CID on charge reduced species as it is formed during ECD has also been developed to improve the fragmentation efficiency of ECD [27].

Unlike CID-MS/MS, electron-based fragmentation can only be performed on a limited numbers of instruments. ECD has been mainly performed in FT-ICR for two reasons [20, 28]. First, the electron capture by peptide ions requires at least milliseconds, which can not be realized by beam type instruments, such as quadrupole and TOF. Second, high electron capture efficiency require electron energies < 1 ev [24], which can not be provided by ion trap. However, FT-ICR is the most expensive type of mass instrumentation. Although several methods for modification of the ion trap have been proposed as an alternative instrumentation for ECD experiments [29-31], none have been implemented. ETD has been used more commonly as it can be performed in a radio frequency ion trap in which peptide ions and electron donors can be trapped and reacted [17].

Based on the soft ionization techniques and efficient MS/MS fragmentation methods, a variety of MS-based analytical methods have been established for proteomic analysis. Most of these can be generally divided into two categories depending on whether the protein analyzed is intact or proteolytically digested prior to analysis. The latter is called “bottom-up” proteomics and is currently the dominant proteomic technology, while the former approach is known as “top-down” [32].

In a typical bottom-up proteomic experiment, the proteins are proteolytically digested into peptides that are more amenable to MS analysis. The resultant peptide mixture is separated by chromatography and then analyzed by mass spectrometry equipped with a soft ionization source, i.e., ESI or MALDI. Most bottom-up experiments perform MS for m/z analysis of the intact ions and MS/MS for elucidation of peptide structural information. After data acquisition,

the raw MS and MS/MS data are further analyzed for protein/peptide identification by peptide mass fingerprinting [33] based on MS data only, de novo sequencing [34], or database search algorithms, where the latter two methods are based on both MS and MS/MS data. Database search algorithms [35-39] are the most popular proteomic data processing methods in which experimental MS/MS spectra are compared with predicted patterns of *in silico*-fragmented peptides from available databases of known proteins.

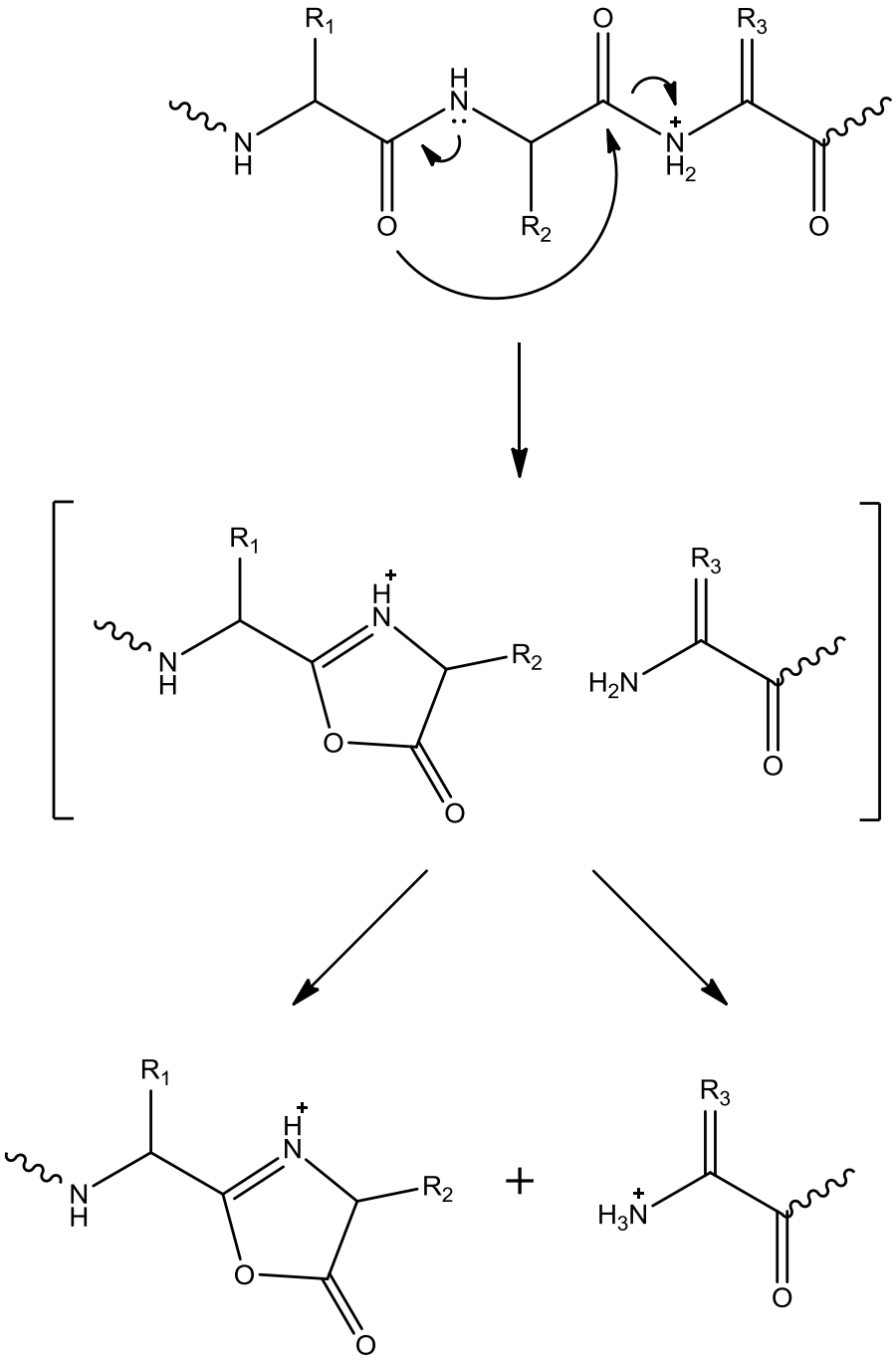

Scheme 1.2 Generally accepted mechanism for formation of b and y ions following CID-MS/MS.

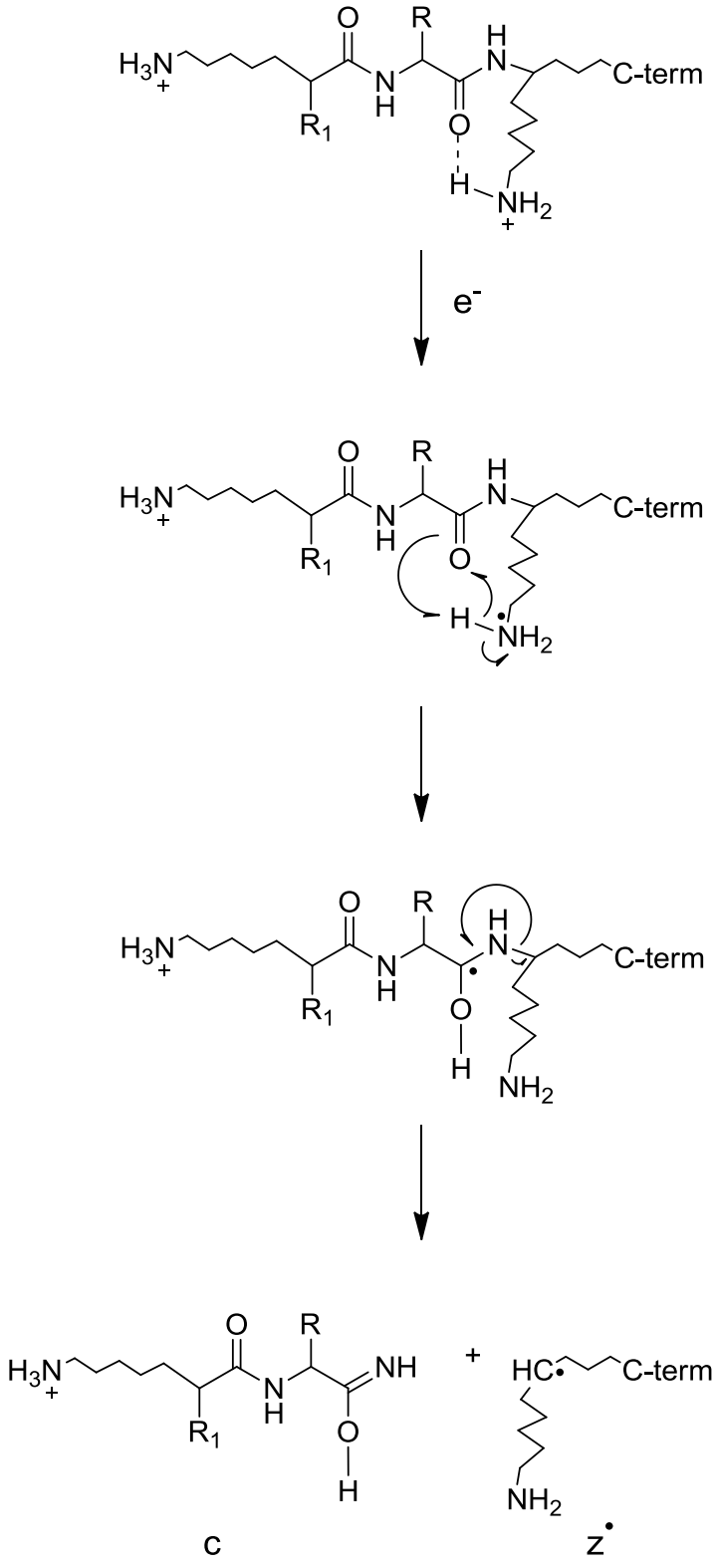

Scheme 1.3 Proposed mechanism for formation of c and z ions following ECD- or ETD-MS/MS.

The bottom-up approach is powerful in analyzing high-complexity samples for its variable front-end separation techniques, especially liquid chromatography (LC). Two major separation methods used in proteomics are Gel-LC-MS/MS [41-43] and multidimensional protein identification technology (MudPIT) [44, 45]. In Gel-LC-MS/MS, intact proteins, usually from a cell lysate, are separated by SDS-PAGE in one dimension according to their molecular weight or, in two dimensions, based on molecular weight and isoelectric point. The separated proteins are in-gel digested and the resultant peptides from each protein digestion are on-line separated by LC, usually using reversed phase (RP) columns, followed by MS and MS/MS analysis. MudPIT is a two-dimensional separation approach developed in John Yates's group in 1999 [44]. In MudPIT, the proteins are proteolytically digested in solution without prior separation. The complex peptide mixtures are then separated by a biphasic microcapillary chromatography column, in which strong cation exchange (SCX) material and RP material are packed in serial. The peptides are separated by SCX according to acidity to different fractions in the first dimension. Each fraction is then further separated by RP based on hydrophobicity in the second dimension. The separated peptides are on-line analyzed by a mass spectrometer. Gel-LC-MS/MS requires much more protein material than MudPIT; however, it separates peptides for each protein individually thereby reducing the ambiguities of peptide-to-protein mapping.

In contrast to bottom-up proteomic strategies, top-down is an emerging technique analyzing the intact proteins without the need for proteolytic digestion [22, 32, 46-49]. Similarly to bottom-up approaches, top-down proteomic analysis often involves 1) front-end separation of protein mixtures, 2) protein analysis by MS and MS/MS, and 3) protein identification and characterization by database search algorithms. MS/MS analysis in top-down strategies often

prefers electron-based fragmentation strategies, i.e., ECD and ETD, for their relative independence of fragmentation efficiencies on peptide length or compositions [22, 23]. However, top-down proteomics still suffers from several technological limitations. For example, the front-end separation techniques for proteins are not as developed as peptide fractionation methods. This requires the use of high resolution and high mass accuracy instruments such as FT-ICR [50] and Orbitrap [51] for analyzing co-eluting proteins. Also, due to the size and complex tertiary structure of large proteins [52], no generic methods are available to efficiently fragment proteins larger than 50 kDa [22, 23, 53].

Bottom-up and top-down approaches, with their complementarities, are and will be the main strategies upon which the MS-based proteomic are built and developed.

1.2 Mass-Spectrometry Based Methods for the Study of Protein Structure, Folding, Dynamics, and Interactions

1.2.1 Introduction

Proteins perform a variety of biological functions within every living organism, such as enzyme catalysis, communication, energy conversion, cell growth and apoptosis. Most proteins are only functional when they adopt a compact three dimensional structure. This close relationship between structure and functions has attracted scientists to study protein structure. How proteins adapt themselves into highly specific and biologically active three dimensional structures from disordered polypeptides is still under study [54]. It is generally accepted that all the information needed for the specific protein folding pathway is contained within the amino

acid sequence and most native conformations correspond to the lowest free energy. Many diseases are reported to be related to protein unfolding [55]. Protein dynamics also play an essential role in protein function. In an organism, which involves a solution environment, proteins are continuously experiencing internal motions, either locally or globally, and thus usually exist in more than one conformation [56, 57]. In the native state, most proteins exist in one or more dominant forms which are usually the most compact conformations and represent the lowest energy state, with the presence of a small population of less folded conformations at relatively higher energy states [58-60]. Also, some proteins tend to exist in disordered states and only fold into a more structured conformation upon binding to another molecule [61, 62]. Nonetheless, every protein molecule alternates between different conformations which is considered to be essential in biological functions [63]. In most cases, the biological activities are not realized by a single protein but by a complex network between proteins and other proteins or ligands. Therefore, the study of protein-protein interaction and protein-ligand binding is also very important in order to understand cell functions.

It is clear that protein structure, folding, dynamics, and interactions are closely related to protein function in cells. Understanding of this relationship will benefit the understanding of disease development and drug action mechanisms. X-ray crystallography and nuclear magnetic resonance (NMR) remain the gold standard for high-resolution protein structural analysis. X-ray crystallography requires protein crystals, which limits its usage to highly pure proteins at well structured conformation. Moreover, whether the protein structure within the crystal is the same as in the solution phase is still not clear. The structure obtained from X-ray crystallography usually represents a snapshot of the static structure and cannot provide information on protein dynamics or folding. NMR spectroscopy provides structural information of proteins in solution.

However, this technique is generally limited to proteins smaller than 50 kDa and requires relatively high protein concentrations. Computational modeling can predict protein structure with high-throughput based on the protein's primary amino acid sequence, but it requires experimental data to validate the predicted models [64]. As an alternative to current high-resolution techniques, MS has become a powerful tool for protein higher order structural analysis, especially with the introduction of ESI [4] and MALDI [5, 6] as soft ionization techniques. The current MS-based approaches for the study of protein structure, folding, dynamics, and interactions mainly involve two categories, i) a non-labeling method which is represented by protein charge-state distributions and ii) labeling methods which include hydrogen-deuterium exchange (HDX), hydroxyl radical probes, and selective chemical modification.

1.2.2 ESI Charge State Distributions for Protein Structure Analysis

1.2.2.1 Relationship between Protein Conformation and Charge State Distribution

In the electrospray (ESI) process, analyte solution is sprayed through a metal or silica capillary where a high voltage is applied. Driven by the high voltage, charges are accumulated at the surface of the solution at the end of the capillary tip and a Taylor cone is formed. The Taylor cone elongates due to Columbic repulsion and finally breaks into a fine mist of charged droplets. Solvent evaporation shrinks the charged droplets and increases their charge density until the Rayleigh limit is met (i.e. the Columbic repulsion is equal to the liquid surface tension). The droplets become unstable at or close to the Rayleigh limit and a series of smaller offspring

droplets are formed. Two mechanisms have been proposed to describe the process after the droplets reach the Rayleigh limit, the ion evaporation model (IEM) [65] and the charge residue model (CRM) [66]. The IEM proposes that ions are directly ejected from the intact droplet surface to the gas phase. In contrast, the CRM predicts that successive solvent evaporation and droplet breakage happens until a single analyte molecule is isolated. Further drying of this single-molecule containing droplet will produce a molecule with retaining charges. Most experimental observations suggest that gas-phase ions of macromolecules such as proteins are produced by CRM, while small molecules are ionized through the IEM pathway [67].

It is assumed that the charge retained on protein molecules is dependent on the three-dimensional structure of the polypeptide chain in solution [68], although whether proteins can preserve their native solution structures during ESI process is still under debate [69]. Nonetheless, proteins that are in tightly folded states generally result in lower charge states than those with disordered conformations [68]. However, the physical reasons responsible for this correlation are still not clear. The mechanism that came along with the first observation of conformational effects on ESI charge state distributions suggested that the higher charge states observed for unfolded proteins were caused by the higher solvent accessibility of basic amino acid residues, which were the protonation sites during the ESI process [70]. However, this mechanism overlooked the fact that most Arg and Lys residues were already protonated in bulk solutions. Therefore, it has been proposed that the charge state is determined by the neutralization of acid residues [71-73]. The relatively higher charge state of unfolded proteins is not considered to result from more solvent-exposed basic residues. Instead, the lower charges state of proteins at compact conformations is caused by the lack of neutralization of acid residues exposed on the protein surface. Another hypothesis argued that the unfolded conformations

could accommodate more charges because the protonation sites were further apart and the Coulombic repulsion was reduced [74]. Similarly, the exposed residues experience less steric effects and electrostatic shielding and thus are more likely to capture protons from solvent in the extended conformations [75].

1.2.2.2 Analysis of Protein Dynamics, Conformational Change, and Interactions

Due to the close correlation between protein conformations and ESI charge state distributions, ESI-MS has served as a straightforward tool for the study of protein dynamics, structural changes, and interactions [68, 76, 77].

The vital biological functions realized by intrinsically disordered protein has gained particular attentions recently [61, 62]. Due to the highly dynamic structure of intrinsically disordered proteins, several conformations may co-exist in solution. ESI-MS has showed great promise for the characterization of the compactness of different protein conformations in solution. Kaltashov *et. al.* probed the higher order structure of α-synuclein, which is a neuronal protein and is believed to be involved in the development of Parkinson's disease [78]. Four co-existing conformations were observed with charge states centered ranging from +8 to +19. By plotting ratios of average charges accommodated by random coil over natively folded proteins as a function of protein mass, the lowest charge state was determined to be a highly structured conformation, and the highest charge state was assigned as a random coil. By correlating with available circular dichroism (CD) and Raman spectroscopic measurements, one less-folded semi-compact intermediate with relatively high charge states was found to contain significant helical content while the other relatively ordered semi-compact intermediates was determined to be a β-

sheet-rich conformation. A recent study by Grandori's group [79] analyzed conformations of the N-terminal and C-terminal fragments of an intrinsically disordered protein, Sic1. The two regions of Sic1 are reported to perform different biological functions and proposed to have different structural flexibility. This hypothesis was confirmed by the difference in relative abundances of compact, semi-compact, and unfolded forms from the two regions. In addition to dynamic characterization of intrinsically disordered proteins, charge state distributions was also used to distinguish the conformational difference of IgG1 with varied post-translational modifications isolated from different cell lines [80].

In 1990, ESI-MS was used successfully for the first time to study the acid induced unfolding of bovine cytochrome c [70]. More recently, Douglas's lab developed a method which coupled a continuous flow mixing device with ESI-MS for time-resolved conformational study of horse heart cytochrome c [81]. Cytochrome c has 5 pH-dependent conformations labeled as I-V [82] and was reported to transition from a largely unfolded state (II) to a native form (III) under apparent pH at roughly 2.5. In this time-resolved conformational study [81], the acid-denatured cytochrome c at pH=2.4 was refolded by mixing with a higher pH buffer to reach a final pH of 3.0. After being mixed over a range of reaction times from 0.1 to 15.5 s, the protein solutions were analyzed by ESI-MS and the obtained charge state distribution was used to study the refolding process. By analyzing the relative intensity of two different conformations (unfolded state, II, and folded state, III) using "global analysis" [83], the refolding process was found to include two pathways with different lifetimes of roughly 0.17 and 8.1 s. This indicated two refolding subpopulations of cytochrome c in solution and was consistent with previous studies. A similar method was used to study the Ca^{2+} induced interaction between calmodulin and melittin and the corresponding structural change of calmodulin-melittin complex [84]. By

monitoring the charge state distribution, another study revealed the folding and assembly mechanisms of hemoglobin from unfolded apo-α- and β-globin state in denatured condition to native state with the presence of heterotetrameric structures in equilibrium with αβ dimers and α- and β- monomers [85]. Charge state distribution studies by ESI-MS can also be coupled with ion-mobility MS for protein structure analysis. A recent study of 2,2,2-trifluoroethanol (TFE) induced fibrillation of β2-microglobulin showed the presence of a less compact structure with the introduction of TFE by charge state distribution analysis and this result was confirmed by ion-mobility MS with the appearances of a new series of signal with higher drift times under TFE conditions [86].

1.2.3 Hydrogen Deuterium Exchange Mass Spectrometry for Protein Structure Analysis

1.2.3.1 Hydrogen Deuterium Exchange Fundamentals

Hydrogen atoms on protein backbone amide bonds are most easily studied by hydrogen deuterium exchange (HDX) mass spectrometry. Hydrogens covalently bonded to carbons almost never exchange while those that are located on side chains, such as S-H and O-H, and N- or C-termini exchange too fast and can hardly be detected due to rapid back exchange. Note that every amino acid residue (except proline and the N-terminal residue) possesses an amide hydrogen, therefore, HDX has the advantage to potentially probe the entire protein backbone.

Amide hydrogens that are completely exposed to solvents exchange very rapidly with rates of 10-1,000 s^{-1} at pH 7 [87]. The exchange rates of the exposed amide hydrogens are affected by solvent pD, temperature, and the adjacent amino acid side chains [88]. HDX

reactions can be either acid-catalyzed by D_3O^+ or base-catalyzed by OD^- [89]. The exchange rate reaches its minimum at around pD 2.5 and increase by an order of magnitude with each pD unit at higher or lower pD. Also, the exchange rate would be slowed by a factor of 10 with roughly every 22^oC decrease in temperature [87]. HDX rates are also sensitive to neighboring amino acid side chains due to both inductive and steric effects. The adjacent side chains can affect the HDX rates as much as tenfold, while the protein structural effect (as described below) can decrease the exchange rates as much as 10^8.

Besides pD, temperature, and side-chain effects, HDX rates are largely affected by the solvent accessibility and hydrogen bonding of the corresponding amide hydrogens. These two factors are key to the application of HDX for protein tertiary structure analysis [90]. Fast HDX is indicative of solvent exposure and weak hydrogen bonding, while slow exchange corresponds to solvent protection and strong hydrogen bonding. Slow HDX rates are usually interpreted as low solvent accessibility; however, one must pay attention that this may be caused by high hydrogen bonding even when the amide hydrogens are solvent exposed. Another disadvantage is that when only the side chains are experiencing fluctuations or interactions, the solvent accessibility of backbone hydrogens may remain the same and can not be detected. In these cases, covalent labeling approaches (described later) may be more appropriate and can at least serve as good complementary methods.

1.2.3.2 General Procedure of Hydrogen Deuterium Exchange Mass Spectrometry for Protein Structure Mapping

One of the most commonly used HDX MS methods for protein structure analysis is continuous HDX labeling, which monitors the deuteration level of proteins as a function of D_2O incubation time [91], as illustrated in Scheme 1.4. The deuterium labeling reaction is initiated by dilution of the protein equilibrated in a physiologically conditioned H_2O into a fully deuterated solvent with the same pH and temperature. After incubation in D_2O for various times, usually ranging from several seconds to many hours, the HDX is quenched by decreasing the pH to 2.5 and the temperature to 0^oC. At this condition, the HDX rate decreases by approximately five orders of magnitude [89] with an average half life of 30-60 min [92] to allow enough time for downstream sample analysis. After quenching, the protein sample can be directly sprayed into a mass spectrometer, with or without HPLC separation at the front end, to monitor the overall mass change of the intact protein. The quenched protein sample can also be proteolytically digested into peptides followed by HPLC-MS analysis to obtain better spatial resolution and identify where the deuterium labels are located on particular parts of the protein. Note that the digestion must be conducted under quenched conditions and thus require the use of acidic proteases, such as pepsin. During analysis by mass spectrometry, MS is used to obtain the number of deuterium exchanged in for a whole protein or peptide. To acquire protein/peptide sequence information and to determine the HDX sites at a higher resolution, tandem mass spectrometry (MS/MS) must be performed. Finally, the relative deuteration level of each protein/peptide or protein/peptide fragment is plotted against the HDX time and the global or local HDX rate is determined.

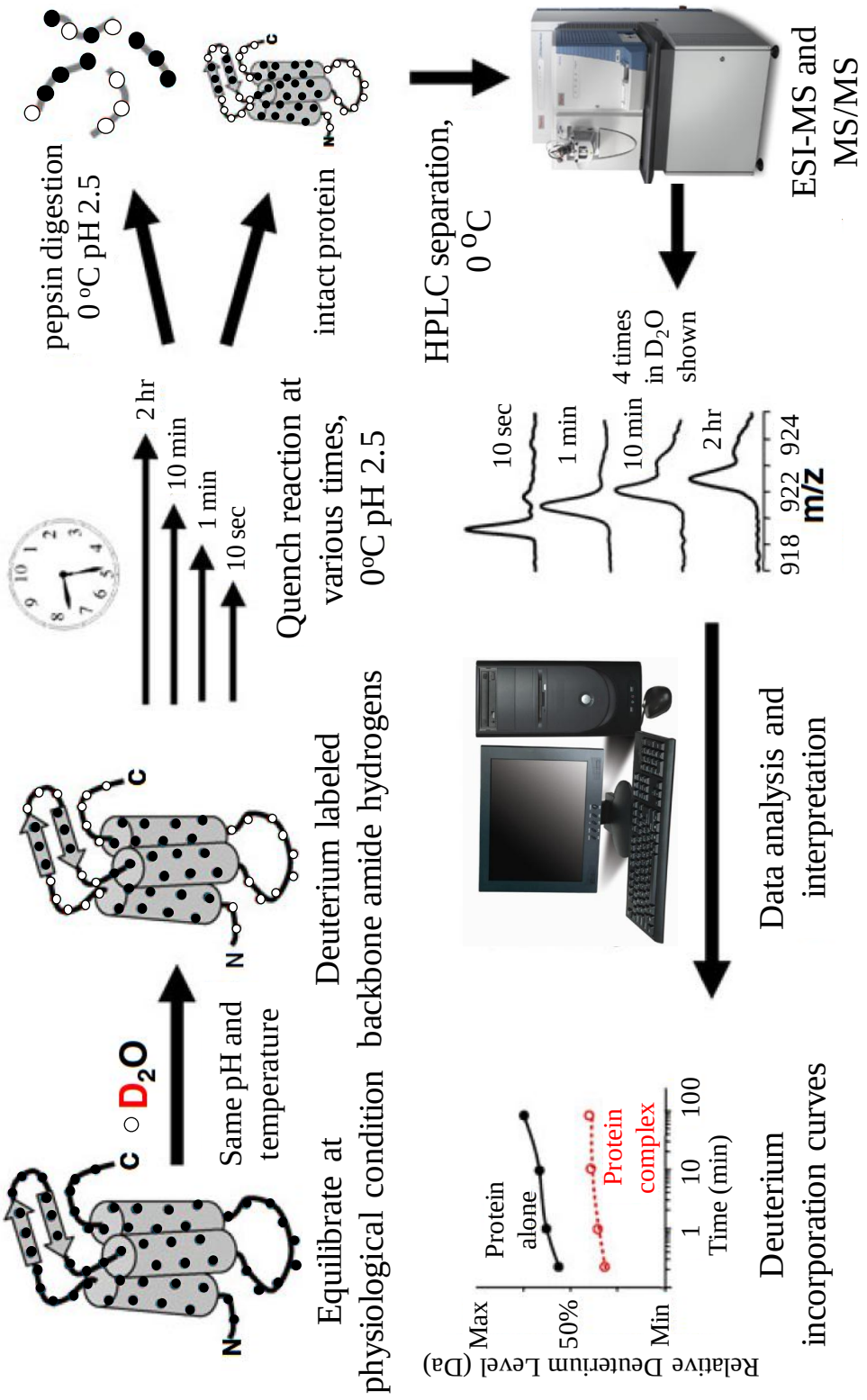

Scheme 1.4 Workflow of a typical continuous protein HDX labeling experiment monitored by mass spectrometry. Adapted from Reference [93]. For interpretation of the references to color in this and all other figures, the reader is referred to the electronic version of this dissertation.

Another commonly used HDX labeling method is pulsed HDX [91, 94]. In contrast to continuous HDX labeling in which the protein is exposed to D_2O continuously for various time, during a pulsed HDX labeling experiment, a perturbation reagent is added to induce a conformational change to the protein and, after a well defined fixed time, the perturbed protein sample is exposed to deuterium for a very brief time (pulsed). Usually pulsed HDX experiments are conducted under basic conditions (pH 8-10) to ensure sufficient HDX during the short labeling time. Pulsed HDX labeling is generally applied to characterize short-lived protein unfolding/refolding intermediates and protein complexes to study the corresponding unfolding/folding and interaction mechanisms and kinetics.

1.2.3.3 Ongoing Improvement of Hydrogen Deuterium Exchange Mass Spectrometry

1.2.3.3.1 Elimination of Deuterium Back Exchange

One major challenge for HDX MS is the back exchange of deuterium to hydrogen after the deuterium labeling process. Following HDX labeling, all the sample preparation processes, including protein digestion and HPLC separation, are performed in undeuterated aqueous solutions to avoid artificial exchange-in of deuterium, thus the Ds can be back exchanged to Hs and the labeling information may be lost. Although all these processes are done under quenched conditions in which the HDX reaction is slowed by roughly five orders of magnitude [89], the HDX can still occur with a half life of 30-60 min [92]. Therefore, shortening the time for post-HDX processes is very important and has been realized mainly by two strategies, i.e. increasing the digestion rate and shortening the peptide separation time, as described in detail below.

To efficiently digest proteins under quenched conditions within a short time (usually ~ 5 min), a relatively large pepsin:substrate ratio is required to achieve sufficient digestion efficiency [95, 96]. The use of a large amount of pepsin might be problematic to the analysis. First of all, the presence of pepsin may interfere with the proteins and complicate the MS spectra. Second, the pepsin retained on the HPLC column may remain active and digest proteins injected onto the column later. Finally, plugging of the HPLC column with pepsin and large undigested substrate has also been observed especially when the HPLC column is packed with small particles. To circumvent these problems, digestion methods using immoblized pepsin columns have been developed [96, 97]. In 2002, Smith's group chemically immoblized pepsin onto POROS-20AL support (PerSeptive Biosystems) and packed them into a stainless steel column, with 2-mm inner diameter × 50-mm length [96]. The column packed with immoblized pepsin was then incorporated on-line into a HPLC system. The protein samples were injected into the sample loop and then driven through the pepsin column during which the proteins were digested. The resultant peptic peptides were concentrated and desalted on the peptide trap and finally separated by a C18 column. The high local pepsin concentration of the immobilized pepsin can greatly improve the digestion efficienty without the potential of contaminating or plugging the LC analytical column. Using triosephosphate isomerase as a model protein, a higher digestion efficiency was obtained using the on-line immobilized pepsin digestion system with 20 s digestion time compared to a 5 min in-solution digestion. Busby *et. al.* reported that the pepsin activity can be improved by immobilizing pepsinogen, which is the inactive precursor of pepsin, to POROS AL-20 support [98]. It has also been demonstrated that digestion conducted at high pressure can effectively increase the enzymatic activity of pepsin [99, 100]. Nowadays, most HDX MS experiments are performed with an online column packed with immoblized pepsin and

commercial products are also available [101]. The recent rapid development of microfluidic devices can also be used for HDX MS by incorporating protein digestion and ESI into a single chip [102, 103]. “Top-down” approaches can avoid the digestion step and thus significantly reduce the deuterium back exchange, however, with the cost of losing spatial resolution. This problem can be partially resolved by using tandem mass spectrometry and will be discussed later.

It has been reported that even under quenched conditions, 30% of deuterium labels could be lost during HPLC separation [104]. Therefore, much effort has been invested to reduce back exchange during the separation process. Replacement of HPLC with supercritical fluid chromatography which uses CO_2 as the mobile phase has been used to reduce the back exchange [105]. However, the separation efficiency is not competitive with reversed-phase HPLC. Deuterium back exchange can also be effectively reduced by decreasing the separation time, but with the cost of compromised separation efficiency especially at 0 ^{o}C [106]. The use of ultra performance liquid chromatography (UPLC) which employs particle smaller than 2 μm in diameter can significantly improve the separation resolution, speed, and sensitivity [107-110] compared with conventionally HPLC whose particle sizes are usually 3-5 μm in diameter.

1.2.3.3.2 Elimination of Deuterium Scrambling

Proteolytic digestion can generally provide peptide fragments with 5-10 residues and allow the exchange site to be located within 5-10 residues. To obtain better or even single residue resolution, tandem mass spectrometry (MS/MS) can be performed. Conventional CID involves slow collisional activation of the precursor ions and causes intramolecular hydrogen and

deuterium migration (deuterium scrambling) [111, 112]. This observation is consistent with the well accepted "mobile proton" peptide fragmentation model [10]. Deuterium scrambling can obscure the original deuterium localization in solution which carries protein conformational information. Fortunately, this scrambling effect can be largely reduced to a negligible extent by using ECD and ETD fragmentation techniques [113-115]. ECD and ETD are both very rapid fragmentation techniques and the precursor ions can be dissociated before the deuterium has a chance to migrate along the peptide backbones. Coupled with the "bottom-up" approach, Jorgensen's group was able to achieve single-residue resolution for 65% of the backbone amides of a 99-residue protein [116]. With the "top-down" method and ECD-MS/MS, Konermann's group reported the observation of 83 fragments from a 153-residue protein, indicative of an average spatial resolution of less than 2 residues [117]. This strategy involving "top-down" and ECD fragmentation was further extended to study the short-lived folding-intermediates of apo-myoglobin (153 residues) using the pulsed HDX labeling method [118]. In this study, the earliest studied folding point was 10 milliseconds. With a continuous-flow mixing device, a quench step was shortened to 1 second prior to the immediate analysis by ESI. Therefore, the back exchange was virtually eliminated. The disadvantage of this strategy was the low signal/noise ratio which required an average of 60 min for each ECD spectrum. "Top-down" combined with ECD-MS/MS has also been applied to study the protein dynamics by characterizing each of the coexisting conformers of a protein in solution [119].

1.2.3.4 Development of Hydrogen Deuterium Exchange Mass Spectrometry

1.2.3.4.1 Measurement of Stability of Proteins from Rates of Hydrogen Deuterium Exchange

Stability of unpurified proteins from rates of HDX (SUPREX) is a technique first developed by Ghaemmaghami *et.al.* to quantify protein stabilities in a high-throughput fashion [120]. In a typical SUPREX experiment, proteins are diluted into a series of HDX buffers containing a chemical denaturant (such as guanidine hydrochloride or urea) at different concentrations, usually ranging from 0 to 8 M. After the exchange occurs for a specified amount of time, the mass of each deuterated protein is determined by MALDI MS. MALDI is chosen here mainly because of its tolerance to moderate amounts of guanidine hydrochloride or urea. A SUPREX curve is generated by plotting the amount of deuterium incorporation (ΔM) of each protein against the denaturant concentration at a specific time. Using a nonlinear regression routine in SigmaPlot (SYSTAT Software, Inc., San Jose, CA), $\mathbf{C_{SUPREX}^{1/2}}$ (the [denaturant] at the transition midpoint of the curve), can be calculated form equation:

$$\mathbf{\Delta M = \Delta M_0 + \frac{a}{1+e^{-\left(\frac{[denaturant]-C_{SUPREX}^{\frac{1}{2}}}{b}\right)}}}$$, where ΔM and [denaturant] are determined experimentally, $\mathbf{\Delta M_0}$ is ΔM before global HDX, a is the amplitude of the curve in Da, and b is a parameter that describes the steepness of the transition [121]. If a protein unfolds in a cooperative two-state process (no stable intermediates are present), ΔG_f (i.e. the free energy of folding in the absence of denaturant) and m ($\mathbf{m = \frac{\delta \Delta G_f}{\delta [denaturant]}}$; m is indicative of the sharpness of the transition of ΔM vs. [denaturant]) can be determined using $\mathbf{-RTln\left(\left(k_{int} \times\right.\right.}$

$\frac{\mathbf{t}}{\mathbf{0.693}}\right) - \mathbf{1}\right) = \mathbf{mC}_{\mathbf{SUPREX}}^{\mathbf{1/2}} + \mathbf{\Delta G_f}$, where R is the gas constant, T is the temperature in Kelvin, and k_{int} is the HDX rate of unprotected hydrogen which can be estimated based on experiment temperature and pH [87]. ΔG_f can be used to quantify protein-ligand binding affinities by calculating $\Delta\Delta G_f$ (the change of ΔG_f upon ligand binding). Furthermore, the $\Delta\Delta G_f$ values can be used to determine the dissociation constant of protein-ligand complexes [121, 122]. In the case of proteins unfolding through multiple stable intermediates, the transition in the SUPREX curve is broadened and ΔG_f and m values are not meaningful by themselves. However, many proteins have multiple domains and their unfolding processes often involve the population of several transition states. In order to extend the application of SUPREX to study the stability of individual domains in multi-domain proteins, a rapid protease digestion step is incorporated into the basic SUPREX protocol after the HDX step [123]. Rapid partial digestion of proteins generates relatively large peptide fragments (2-10 kDa) from which the thermodynamic stabilities of each individual domain can be derived.

The main advantage of SUPREX is its capability of high-throughput analysis for its ability to analyze unpure proteins. A recent SUPREX study reported the screening of two chemical libraries, with a total of 10,880 compounds, for cyclophilin A binding ligands at a rate of 6 s/ligand [124]. Despite these benefits brought by MALDI MS analysis, SUPREX is not amenable to analyze relatively large proteins or proteins in complex mixtures. Also, as SUPREX is designed to provide thermodynamic stability information of proteins at the domain level. The obtained structural resolution is not comparable with continuous HDX labeling method.

1.2.3.4.2 Quantification of Protein-Ligand Interactions by Mass Spectrometry, Titration, and Hydrogen Deuterium Exchange

Quantification of protein-ligand interactions by mass spectrometry, titration, and H/D exchange (PLIMSTEX) is a novel technique developed in Gross's lab to determine the association constants for protein-ligand interactions, as well as to quantify the conformational changes associated with ligand binding to proteins [125]. In PLIMSTEX, the protein is first equilibrated with different concentrations of ligand in aqueous buffer to create different [ligand]/[protein] ratios. Then, HDX is initiated by diluting the sample in to D_2O with the same salt concentration and pH as the starting solution. When HDX reaches a near steady state (1-3 hr, optimized from a previous kinetic study using continuous HDX method), where the fast exchangeable Hs have reached equilibrium while the slow exchangeable ones have not, the exchange is quenched by lowering the pH to 2.5 and temperature to 0 ^{o}C The sample is on-line desalted and analyzed by MS. Ligands are dissociated from the protein during the quenching and desalting process, thus allowing the mass measurement of the free protein. A PLIMSTEX curve is generated by plotting the D uptake versus the various [ligand]/[protein] ratios, and the D uptake of the apo-protein and the difference in D uptake associated with ligand binding can be obtained. By fitting the resultant data to appropriated equations [126], the binding constant of the ligand can be determined. Also, a digestion step can be incorporated after the quenching of HDX to improve the spatial resolution of the D uptake [127]. PLIMSTEX has been demonstrated to effectively and accurately determine the binding affinity of Ca^{2+} to calmodulin (CaM) in the

presence or absence of three different CaM-binding peptides [128] and the affinity and the order of Ca^{2+} binding to the four EF hands of troponin C [129].

Compared to SUPREX, the biggest advantage of PLIMSTEX is that it can quantify the association constant of a protein-ligand complex involving multiple interaction sites and even multiple binding ligands while SUPREX can only accurately determine the dissociation constant when the binding stoichiometry is 1:1. Another advantage of PLIMSTEX over SUPREX is that PLIMSTEX avoids the use of a chemical denaturant which may alter the protein-ligand binding [130]. However, the ability of PLIMSTEX to determine the association constant of more complicated systems comes at the expense of taking more time and material.

1.2.4 Hydroxyl Radical Modification Combined with Mass Spectrometry for Protein Structure Analysis

1.2.4.1 Introduction

Hydroxyl radicals covalently modify protein side chains based on the intrinsic chemical reactivity and solvent accessibility of the specific amino acid residue. Similarly to HDX, the resulting mass shift marks the modification site and can be used to characterize the accessibility of that site.

1.2.4.1.1 Generation of Hydroxyl Radicals

Many methods have been developed for the generation of hydroxyl radicals [131], and each of them has its advantages and disadvantages. Fenton chemistry has been used to chemically produce hydroxyl radicals from hydrogen peroxide, where a chelated metal (such as EDTA-Fe(II)) is used as the catalyst [132]. Fenton chemistry is a low-cost and simple way to generate hydroxyl radicals. However, the presence of a high concentration (~mM) of metal, chelator, and ascorbate may perturb the protein native structure, especially for metal containing proteins. Radiolysis of water by electron pulse [133], X-rays [134-136], and γ-rays [134, 137-140] have also been used together with mass spectrometry to study protein structures and protein interactions. These methods generate hydroxyl radicals from water and avoid the requirement of chemical reagents, although the solution needs to be buffered to resist pH changes caused by water decomposition. Synchrotron radiolysis can generate high flux hydroxyl radicals and modify proteins on millisecond time scales [135, 141], thus allowing time-resolved studies of protein dynamics. However, synchrotron radiation sources are out of reach to most researchers. In 2004, UV photolysis of H_2O_2 was combined with mass spectrometry for the first time to map protein solvent accessibilities [142]. To reduce the concentration of H_2O_2 and exposure time, a technique utilizing a pulsed laser to photodissociate H_2O_2 on the nanosecond scale was developed [143]. Also, the H_2O_2 concentration was lowered from 30% [142] to 0.3-1%. At the same time, Gross's lab utilized laser flash to photolysis H_2O_2 at 0.04% concentration and controlled the exposure time of the protein to hydroxyl radicals on a microsecond time scale using catalase and glutamine as the scavengers for H_2O_2 and •OH, respectively [144]. These fast photochemical oxidation methods are reported to modify proteins before they undergo super-

secondary unfolding events and can map their native structure [145]. Alternatively, sulfate radical anion ($SO_4^{-\bullet}$) generated by laser photolysis of $Na_2S_2O_8$ can also oxidatively label proteins as rapidly as •OH [146]. However, these techniques require the mix of oxidizing reagent (H_2O_2 or $S_2O_8^{2-}$) at millimolar concentration with protein sample prior to analysis. This may introduce oxidation induced protein unfolding before hydroxyl labeling [147] and secondary oxidation of amino acid side chains after hydroxyl exposure [148]. Nonetheless, laser photolysis of H_2O_2 has been become more and more prevalent over the past decade.

1.2.4.1.2 Hydroxyl Radical Mediated Oxidation of Amino Acid Residue Side Chains

Hydroxyl radical attack of proteins can lead to both protein backbone cleavages and oxidation of amino acid side chains [149]. Because hydrogen abstraction from the Cα carbon, which is the initial step of protein backbone cleavage, occurs (at a rate of ~10^7 $M^{-1}s^{-1}$) much slower than reaction with most side chains (at a rate of 10^8-10^9 $M^{-1}s^{-1}$) [150, 151], protein backbone cleavage can be avoided by carefully controlling the concentration and presence time of hydroxyl radicals. The reactivity order of the side chains of 20 amino acids and cystine towards hydroxyl radical are: Cys > Met > Trp > Tyr > Phe > cystine > His > Leu, Ile > Arg, Lys, Val > Ser, Thr, Pro > Gln, Glu > Asp, Asn > Ala > Gly [149]. The first 14 residues (i.e. Cys, Met, Trp, Tyr, Phe, cystine, His, Leu, Ile, Arg, Lys, and Val) provide both sufficient reactivity and mass shift for the confident qualitative and quantitative analysis by MS and are typically used for protein footprinting. Hydroxyl radical mediated oxidation occurs through

different mechanisms depending on the chemistry of specific amino acid side chains and causes a variety of mass shifts as illustrated in Table 1.1 [149].

Table 1.1 Primary products and corresponding mass changes for amino acid side chains subjected to hydroxyl radical mediated modification. Adapted from Reference [149].

Residue	Modification and Mass Changes
Cys	sulfonic acid (+48 Da), sulfinic acid (+32 Da), hydroxyl (-16 Da)
cystine	sulfonic acid (+48 Da), sulfinic acid (+32 Da)
Met	sulfoxide (+16 Da), aldehydes (-32 Da), sulfone (+32 Da)
Trp	hydroxy (+16, +32, +48 Da, etc.), imidazole-ring opening (+32 Da)
Tyr	hydroxy (+16, +32 etc.)
Phe	hydroxy (+16, +32 etc.)
His	Oxo (+16 Da), pyrrole-ring opening (-22, -23, -10 Da, +5 Da)
Leu	hydroxy (+16 Da), carbonyl (+ 14 Da)
Ile	hydroxy (+16 Da), carbonyl (+ 14 Da)
Arg	deguanidination (-43 Da), hydroxy (+16 Da), carbonyl (+14 Da)
Lys	hydroxy (+16 Da), carbonyl (+ 14 Da)
Val	hydroxy (+16 Da), carbonyl (+ 14 Da)
Ser	hydroxy (+16 Da), concomitant oxidation and loss of water (-2 Da)
Thr	hydroxy (+16 Da), concomitant oxidation and loss of water (-2 Da)
Pro	hydroxy (+16 Da), carbonyl (+ 14 Da)
Gln	hydroxy (+16 Da), carbonyl (+ 14 Da)
Glu	decarboxylation (-30 Da), hydroxy (+16 Da), carbonyl (+14 Da)
Asp	decarboxylation (-30 Da), hydroxy (+16 Da)
Asn	hydroxy (+16 Da)
Ala	hydroxy (+16 Da)

1.2.4.1.3 General Approaches for Hydroxyl Radical and Mass Spectrometry Based Protein Structure Mapping

The protein footprinting experiment by hydroxyl radical labeling and mass spectrometry is very similar to HDX MS methods. Proteins are exposed to hydroxyl radicals generated by any of the methods describe above. Specially, in a microsecond-timescale laser photolysis of H_2O_2 experiment [144], protein samples containing ~15 mM H_2O_2 are activated by a pulse laser shot while they flow though silica tubing. The flow rate and laser pulse frequency are adjusted so that the proteins only experience one irradiation. This assures that proteins are only labeled as they are in the native conformation, as oxidation events may induce protein unfolding [152]. The samples are collected at the end of the tubing and the residual H_2O_2 and hydroxyl radicals are immediately removed by catalase and •OH scavengers (such as glutamine or methionine). The lifetime of hydroxyl radicals is estimated to be less than 1 microsecond with the presence of an appropriate scavenger [145]. Subsequent to hydroxyl modification, proteins are generally digested with site-specific enzymes. The resultant samples are analyzed by mass spectrometry usually coupled with HPLC. The proportion of modified forms of each peptide are obtained and correlated with the solvent accessibility. MS/MS of the modified peptides identifies the specific modification site(s) and improves the structural resolution.

1.2.4.2 Recent Development and Applications of Hydroxyl Labeling and Mass Spectrometry for Protein Structure Mapping

Computational modeling has been used to construct high-resolution protein three-dimensional structures from known sequences and simulate protein dynamics in solution in a high-throughput fashion [153]. These models need to be optimized and validated by experimental data. Hydroxyl radical labeling combined with mass spectrometry serves as a low-resolution protein surface mapping method and provides constraints and experimental support for structural modeling. For instance, proinsulin (the biosynthetic precursor of insulin) misfolding can lead to diabetes mellitus. However, proinsulin is refractory to crystallization and the high-resolution structure is hard to obtain. With computational modeling, a monomeric human proinsulin model was generated [154] using a template of engineered DKP-proinsulin [155] with known NMR structure. The experimentally determined oxidation rates showed good agreement with the solvent accessibilities predicted from the constructed model. A zinc-stabilized human proinsulin hexamer model was also constructed [154] based on the known insulin hexameric crystal structure. The regions predicted to be buried in the hexamer interfaces showed more protection from hydroxyl labeling in the hexamer assembly than in the monomeric form.

Hydroxyl radical labeling combined with mass spectrometry has also been widely used to probe protein kinetic folding/unfolding processes and detect interfaces and conformational changes due to protein interactions. A lot of studies have been done to probe protein structure and protein-protein interaction interfaces under equilibrium conditions [156-161]. Stocks and Konermann developed a pulsed oxidative labeling method to explore the mechanism of protein unfolding [162]/folding [163] at the millisecond time scale. The pulsed oxidative labeling technique uses a continuous-flow mixing device which allows the rapid mixing and incubation of

proteins with unfolding/folding initiators for milliseconds (the shortest reported time is 10 ms) followed immediately by pulsed hydroxyl labeling at the microsecond scale. Using this approach, the kinetic mechanism for the folding and assembly of a protein complex, S100A11 homodimer, was tracked at the millisecond time scale [164]. Using a 1900 nm laser to cause a nanosecond temperature jump for protein refolding and a 248 nm laser to quickly photochemically oxidize the protein refolding intermediates, Chen *et. al.* was able to explore the protein folding mechanism at the sub-millisecond time scale [165].

Hydroxyl radical labeling in conjunction with mass spectrometry has also emerged as a method for structural characterization of membrane proteins [166, 167]. Although membrane proteins play a key role in numerous biological processes, their studies are falling far behind soluble proteins mainly due to their extreme hydrophobicity and tendency to aggregate. Oxidative labeling has been used to probe water-soluble protein structures since the late 1990s [168], but only recently has this approach been used to study membrane proteins. The native structure of a membrane protein, bacteriorhodopsin, has been examined in its natural lipid bilayer [169]. Hydroxyl radicals generated by nanosecond photolysis of H_2O_2 were used to label bacteriorhodopsin containing membrane suspensions for about 1 μs. The oxidatively labeled protein sample was digested by trypsin and then analyzed by LC-MS. Of the nine methionine residues, 4 were highly oxidized suggestive of their location in the solvent-exposed loop region, while the other 6 showed severalfold less oxidation indicating they are buried in the membrane. These results are consistent with the known crystal structure of bacteriorhodopsin. Using the same approach, bacteriorhodopsin structure in a non-native state has also been characterized [170]. More sequence coverage of bacteriorhodopsin was obtained by individually mutating two residues to methionine residues, thus allowing all of the 7 helices in bacteriorhodopsin to be

characterized [171]. With pulsed oxidation labeling, the kinetic folding mechanism of bacteriorhodopsin has been studied by characterizing the transient folding intermediates [172]. Another study used synchrotron X-ray radiolysis of water to generate hydroxyl radicals at millisecond time scales and characterized the potassium channels, i.e. membrane proteins that undergo conformational changes to regulate the flow of K^+ across the membrane, at open and closed states provided an insight on the gating mechanism of KirBac3.1 [173].

1.2.4.3 Summary

In contrast to deuterium labeling, hydroxyl radical modification generates stable modification products that are amenable to a variety of analysis methods, including proteolysis by different kinds of proteases, extensive HPLC separation, and various fragmentation techniques in MS/MS, because back exchange and deuterium scrambling are eliminated. However, there is a concern that the oxidation may alter protein conformation [143, 152, 174-176]. Also, due to the variety of modifiable amino acid side chains and the resultant different mass changes, the MS spectrum may be complicated and hard to interpret. Moreover, when the oxidation sites are distributed among several modifiable amino acid residues, the relative intensities of some modified peptides may be too low to be detected. These problems can be overcome by residue-specific labeling methods as described below.

1.2.5 Other Protein Labeling Methods Combined with Mass Spectrometry for Protein Structure Analysis

In spite of the rapid development and demonstrated application of HDX and hydroxyl labeling methods for protein structure mapping, they are not universally suited for all kinds of protein samples. As mentioned above, HDX suffers from back exchange and D scrambling, and analysis of large proteins or protein complexes remains challenging. Hydroxyl radical oxidation introduces stable labels and alleviates these problems, however, there is a concern that the oxidation may alter protein conformation [143, 152, 174-176]. Also, due to the variety of modifiable amino acid side chains and the resultant different mass changes, the MS spectrum may be complicated and hard to interpret. Moreover, when the oxidation sites are distributed among several modifiable amino acid residues, the relative intensities of some modified peptides may be too low to be detected. Residue specific labeling can overcome these problems as described below. Table 1.2 summarizes of these reagents and their reactions with corresponding targeted residues.

1.2.5.1 Lysine-Specific Reagents

Lysine is one of the most popular candidates for studying protein surfaces because it is usually located at protein surfaces due to its polar side chain which is usually positively charged under physiological pH conditions. It is also often involved in protein-protein/protein-ligand interactions [177, 178]. Many reagents have emerged for targeting the primary amine on the side chain of lysine residues or protein N-termini.

The earliest used reagents for lysine modification are a series of organic acid anhydrides, such as acetic anhydride [179, 180], maleic anhydride [181], and succinic anhydride [180, 182],

for the acylation of amino groups, as shown in Table 1.2. Due to its high tendency towards hydrolysis, acetic anhydride is often added in at least 1,000 molar excess over protein and the addition of base during the modification process may be needed to maintain the proper pH [183, 184]. Since the early proof-of-principle studies, in which the surface topology of several model proteins probed by amino-acetylation and mass spectrometry were demonstrated to correlate well with the corresponding crystal structures [179, 180], more and more literature has appeared this method to probe protein structures [185-187], protein interactions and the associated structural changes [181, 184, 188, 189]. Lysine acetylation was also used together with PLIMSTEX to study the interaction of human telomeric repeat binding factor 2 (TRF2) with the telomeric DNA. With the backbone solvent accessibility mapped by HDX and lysine side chains probed by selective acetylation, complementary information was obtained for the binding region of TRF2:DNA [127].

Over the past years, N-hydroxysuccinimide (NHS) esters have been increasingly used for selective lysine side chain modification due to their higher selectivity and lower reagent excess compared to acetic anhydride [187, 190, 191]. One of the most commonly used NHS esters is NHS-biotin from Pierce (Rockford, IL), but the biotin moiety in these studies is commonly not used for isolation or purification purposes. An early study in 1991 mapped the structure of Aplysia egg-laying hormone and provided some information on the regions that are critical for function [192]. Since 2000, many studies have emerged using NHS-biotin to indentify the interface involved in protein-protein interactions [191], protein-DNA/RNA interactions [193, 194], and binding induced protein conformational changes [195, 196]. Sulfo-NHS-biotin, with increased aqueous solubility, has also been widely used to probe protein surface topology [197, 198] and ligand-binding induced conformational change [199]. A study used three reagents,

sulfo-NHS-biotin, sulfo-NHS-6-(biotin-amido)-hexanoate (sulfo-NHS-LC-biotin), and sulfo-NHS-6-(biotin-amido)-6-hexanamido (sulfo-NHS-LC-LC-biotin), in parallel to footprint changes of a methyltransferase upon binding its tRNA substrate [200]. In this approach, labeled peptides gave rise to 3 characteristic MS pattern with a mass difference of 113 Da between the adjacent peaks, thus allowing the easy identification of modified peptides. Another group of widely used NHS ester reagents are NHS acetate and its derivative, sulfo-NHS acetate, which has better water solubility [190, 201-205]. Compared to NHS biotin, NHS acetate has a smaller molecular size and better solubility in aqueous solution.

S-methylthioacetimidate is another amine-specific reagent for protein tertiary structure mapping. The biggest advantage of S-methylthioacetimidate is that it reacts with lysine amino-groups without altering their positive charge which may reduce the possibility of perturbing protein native conformation. S-methylthioacetimidate was first developed by Thumm and co-workers for protein surface labeling [206]. Differential amidination by S-methylthioacetimidate and S-methylthiopropionimidate enabled easier identification and relative quantitation of peptides based on the sizable mass differential of 14 Da per added label [207]. Selective amine amidination by S-methylthioacetimidate has also been used to probe protein surface topology [208], study the structure and activity of trypsin [209], and map the structure of a large protein complex, *Caulobacter crescentus* ribosome, which consists of more than 50 proteins [210]. Similarly to SUPREX as described previously, S-methylthioacetimidate can also be used for the thermodynamic analysis of protein folding and protein-ligand interactions by substituting the HDX labeling with selective lysine amidination [211].

Table 1.2 Chemical reagents and the corresponding reactions used for specific and nonspecific protein labeling

Residue	Modification Reagent	Reaction
lysine	acetic anhydride: 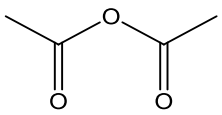	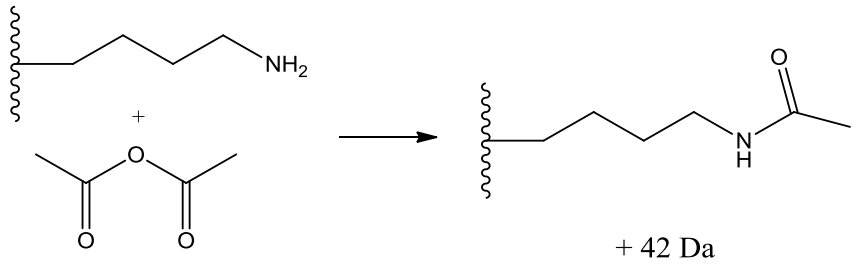 + 42 Da
	succinic anhydride: 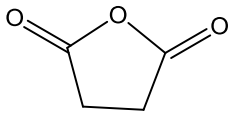	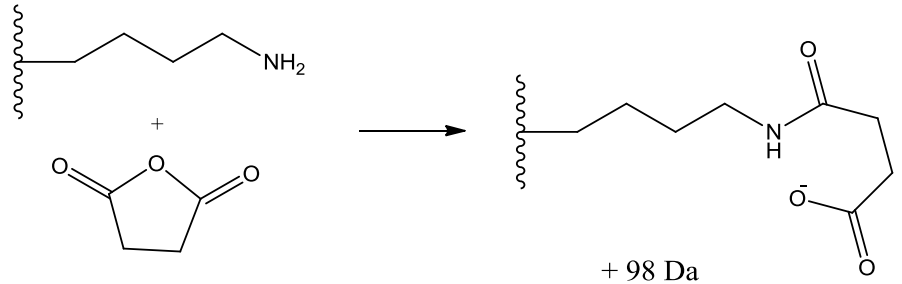 + 98 Da

Table 1.2 (cont'd)

lysine (cont'd)	(sulfo)-NHS-biotin: 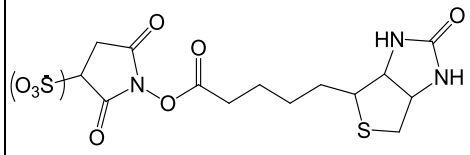	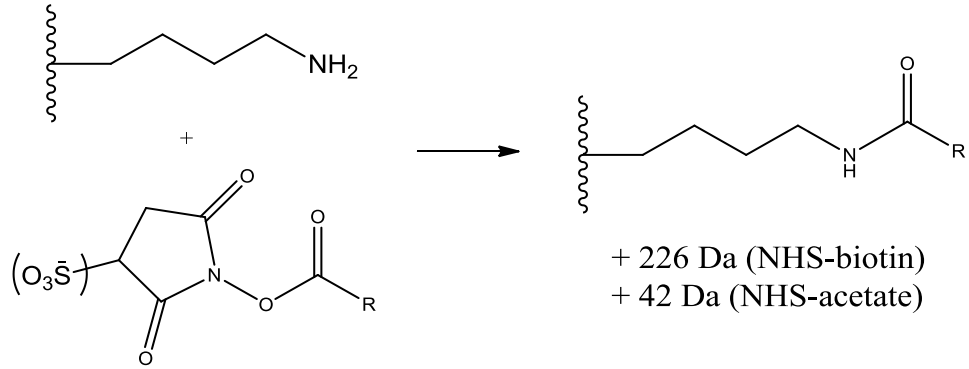
	(sulfo)-NHS-acetate: 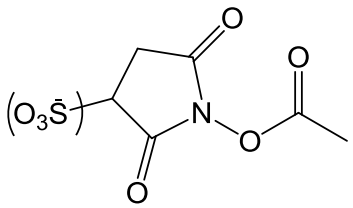	

Table 1.2 (cont'd)

lysine (cont'd)	S-methylthioacetimidate: 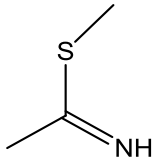	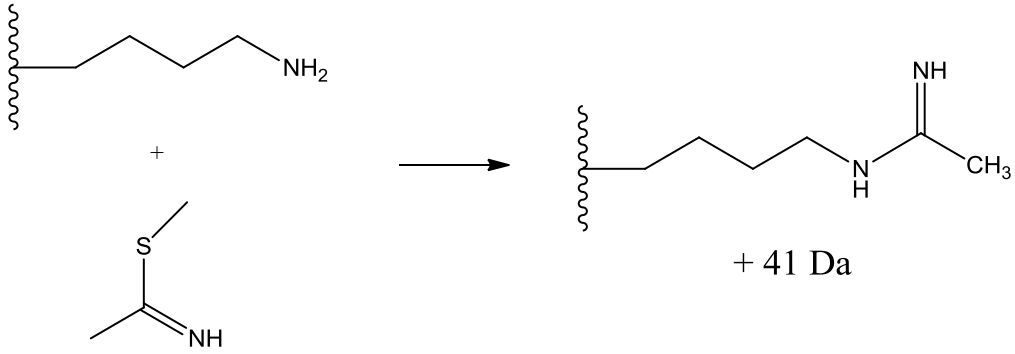
arginine	1,2-cyclohexanedione: 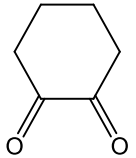	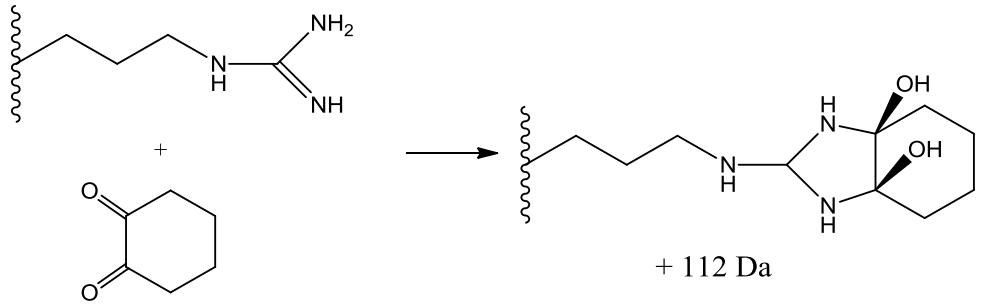

Table 1.2 (cont'd)

arginine (cont'd)	phenylglyoxal: 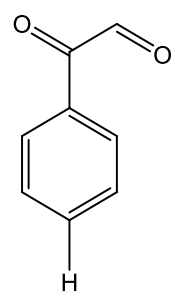	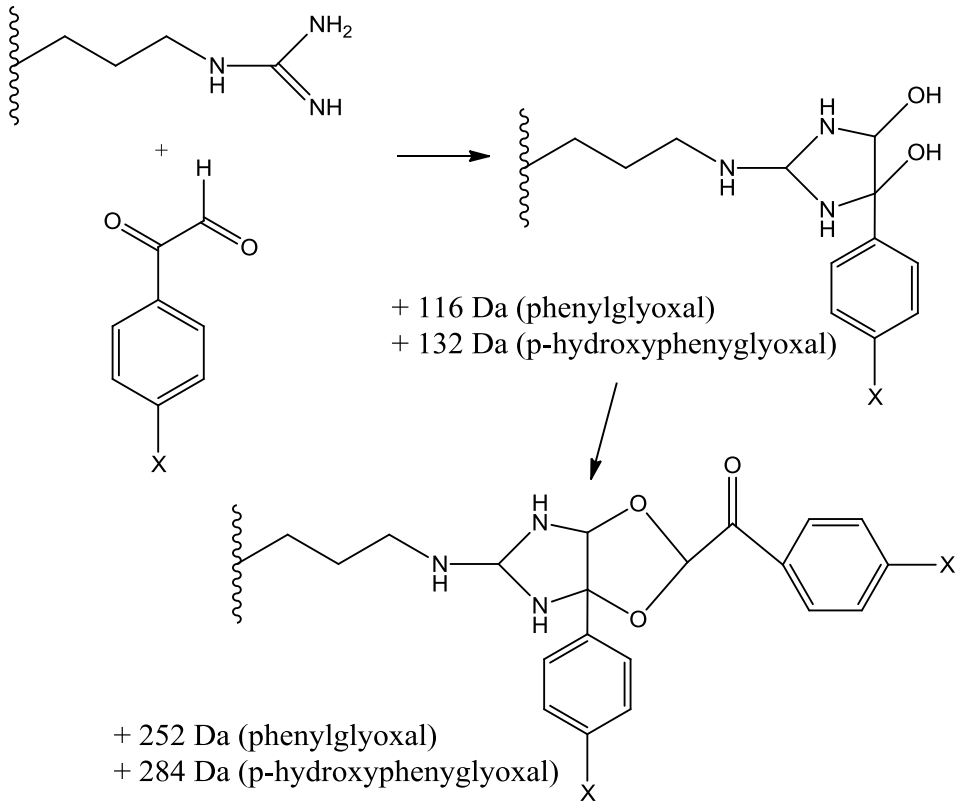
	p-hydroxyphenylglyoxal: 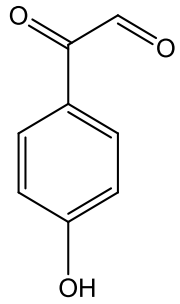	

Table 1.2 (cont'd)

arginine (cont'd)	2,3-butanedione: 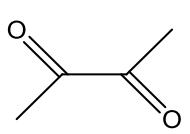	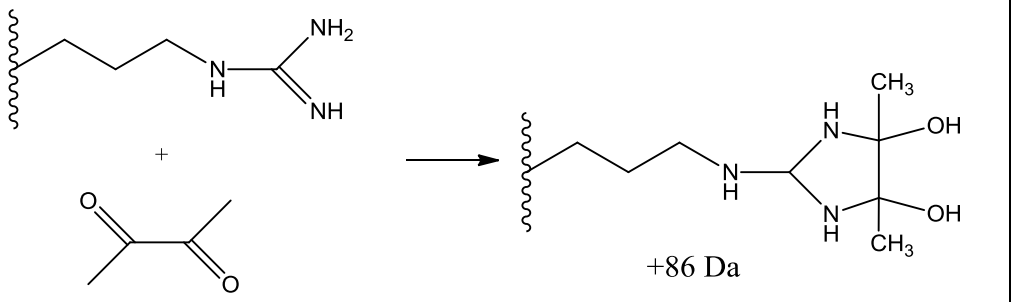
	kethoxal (3-ethoxy-2-ketobutanal): 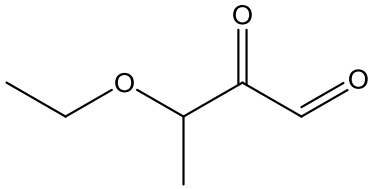	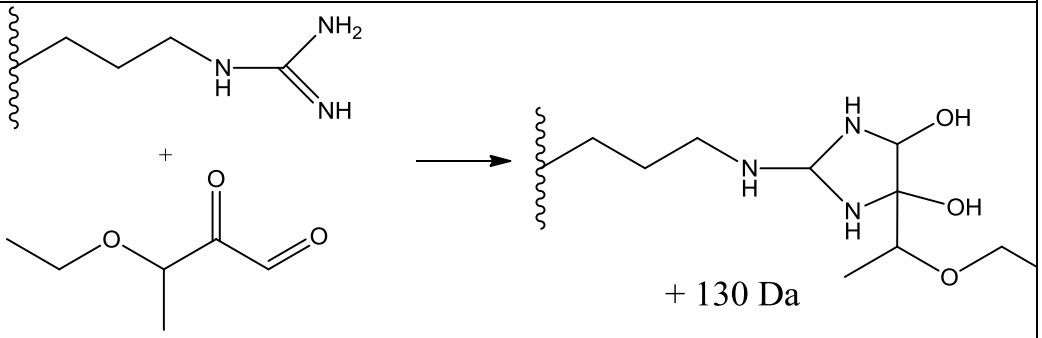

Table 1.2 (cont'd)

histidine	diethylpyrocarbonate (DEPC) 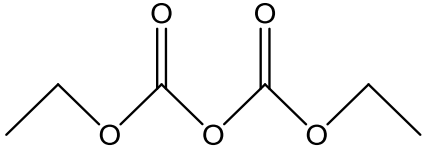	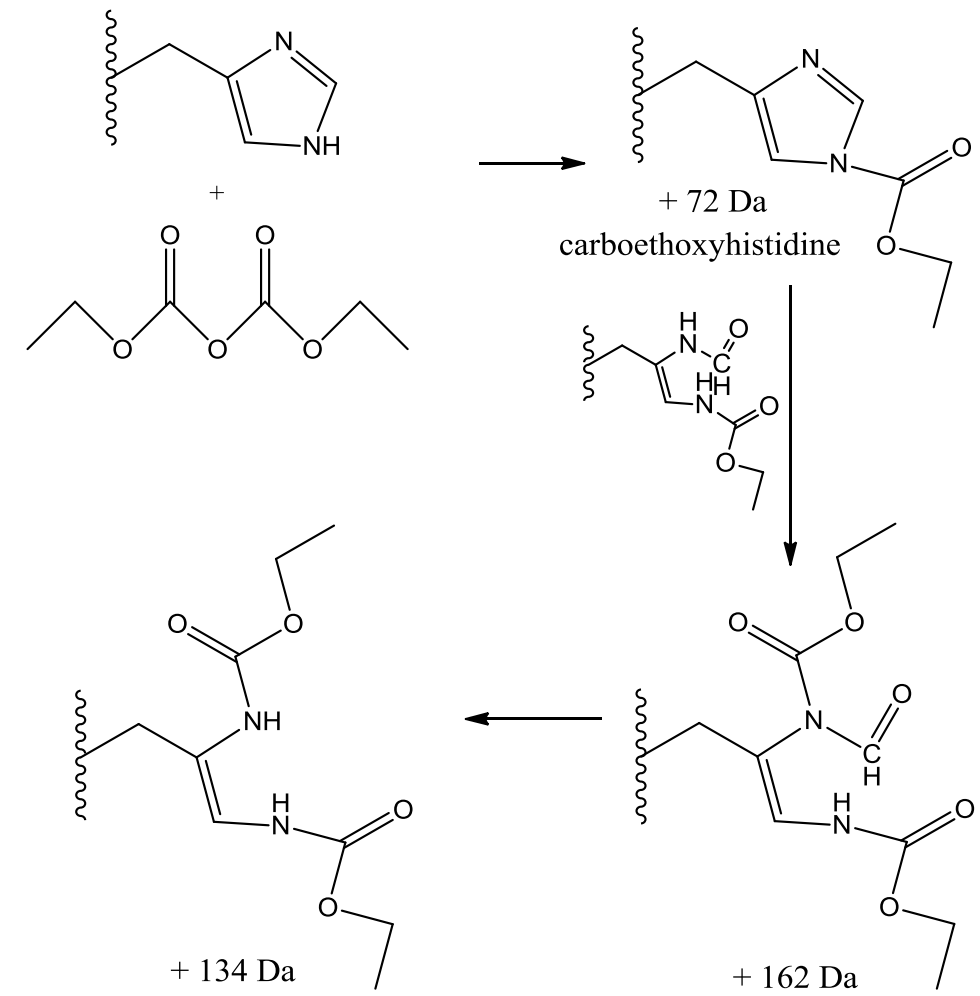

Table 1.2 (cont'd)

glutamic acid & aspartic acid	5-ethyl-3-(3-dimethylaminopropyl) carbodiimides (EDC): 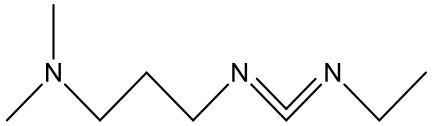	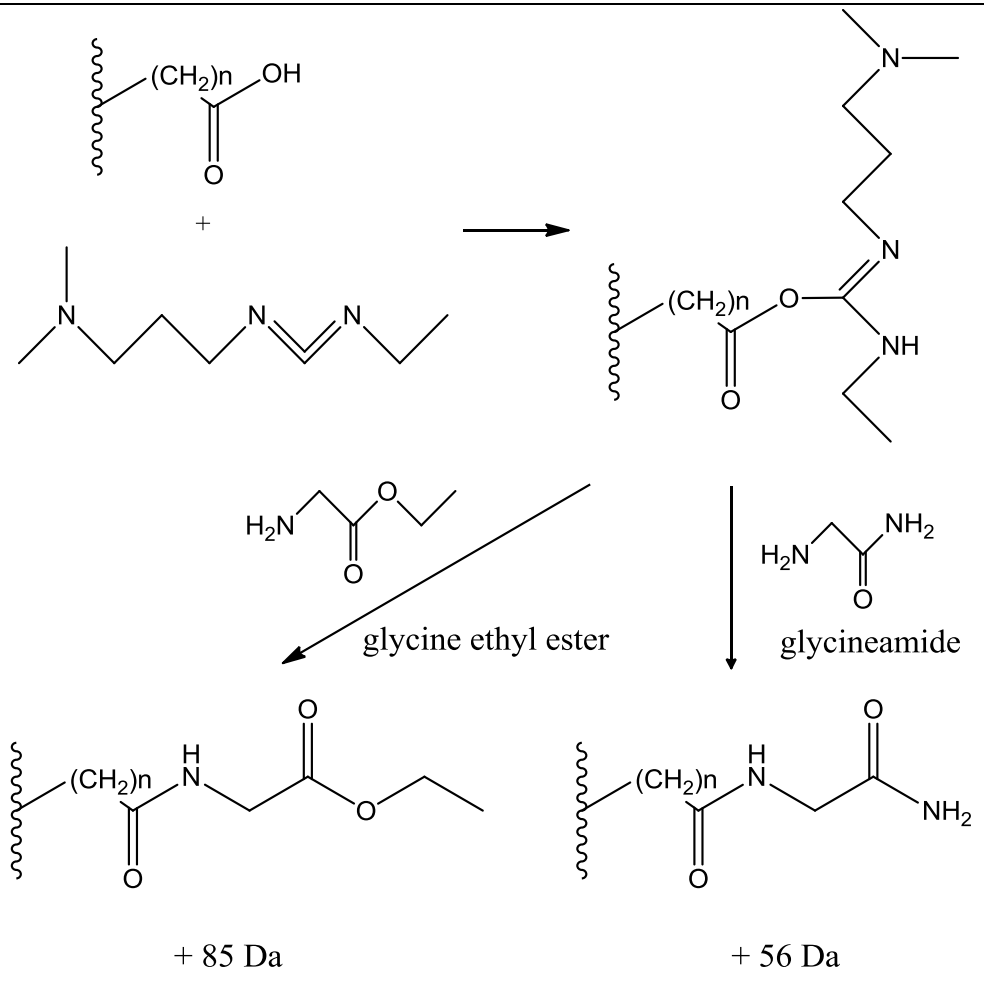

Table 1.2 (cont'd)

cysteine	iodoacetamide: 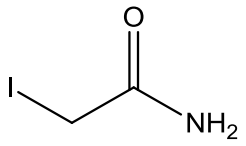	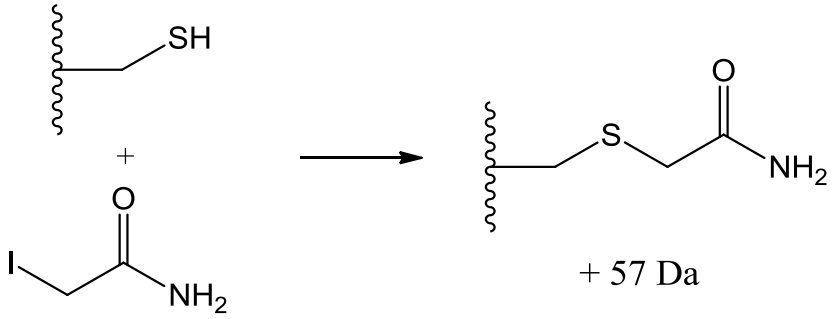 + 57 Da
	N-alkylmaleimide: 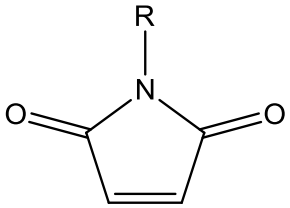	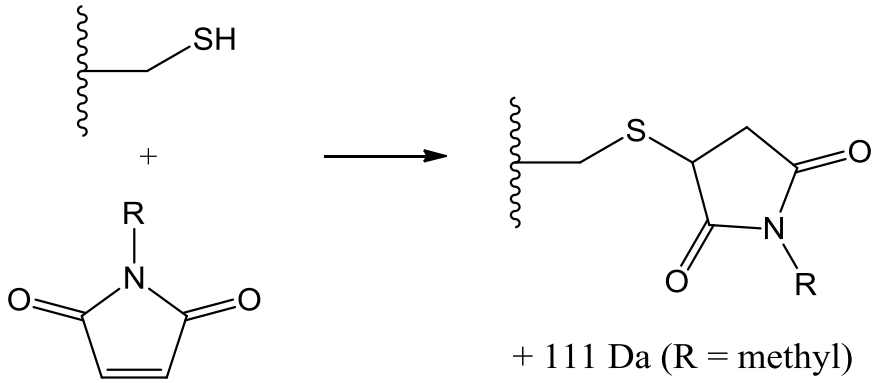 + 111 Da (R = methyl)
	4-vinylpyridine: 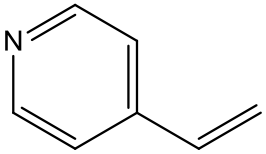	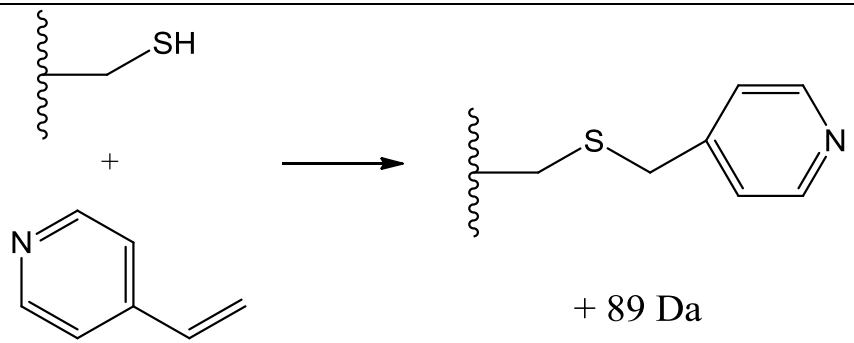 + 89 Da

Table 1.2 (cont'd)

cysteine (cont'd)	5-((((2-iodoacetyl)amino)ethyl)amino)naphthalene-1-sulfonic acid (IAEDANS): 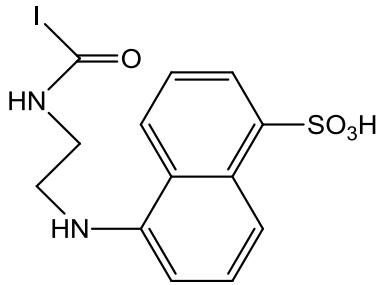	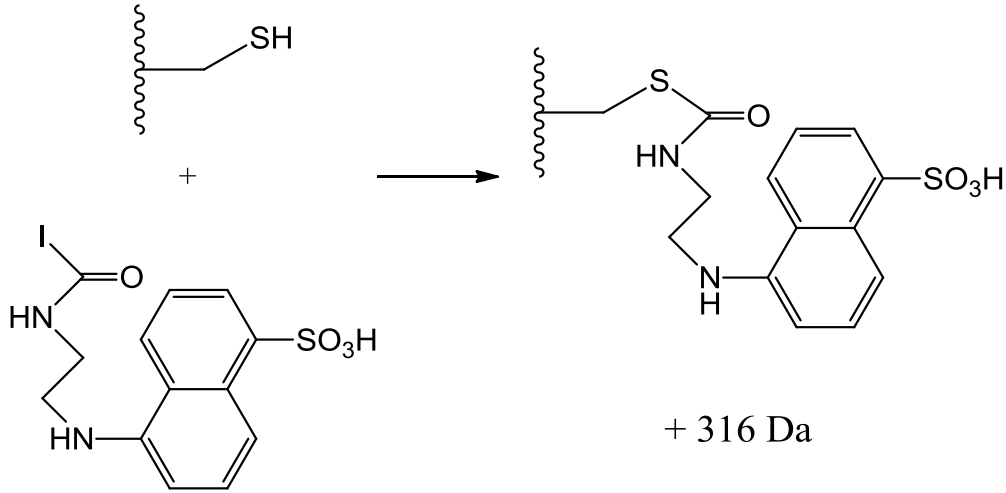
	melarsen acid: 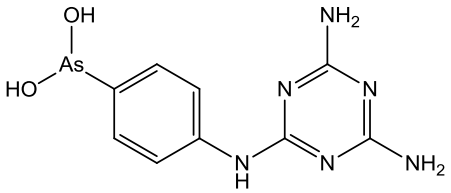	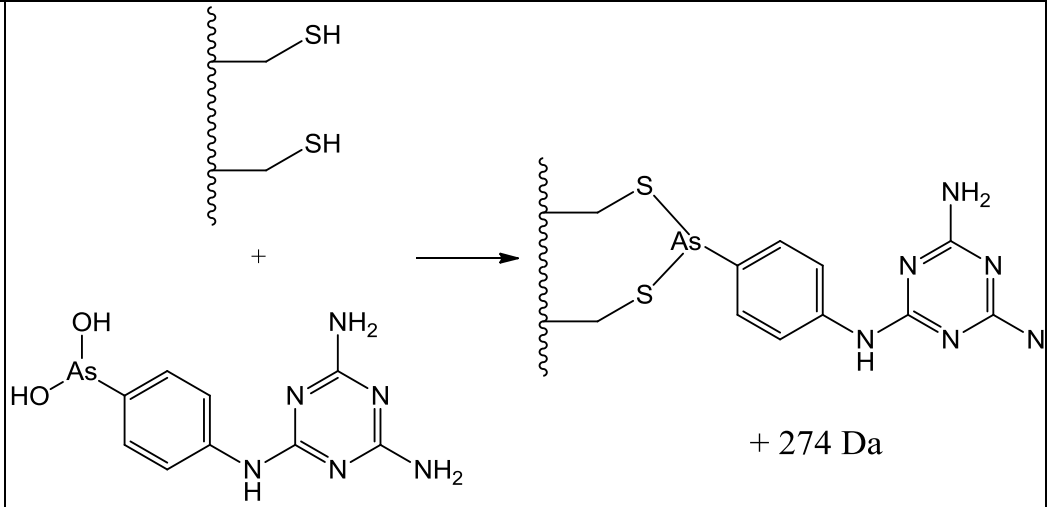

Table 1.2 (cont'd)

tyrosine	N-acetylimidazole: 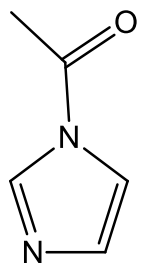	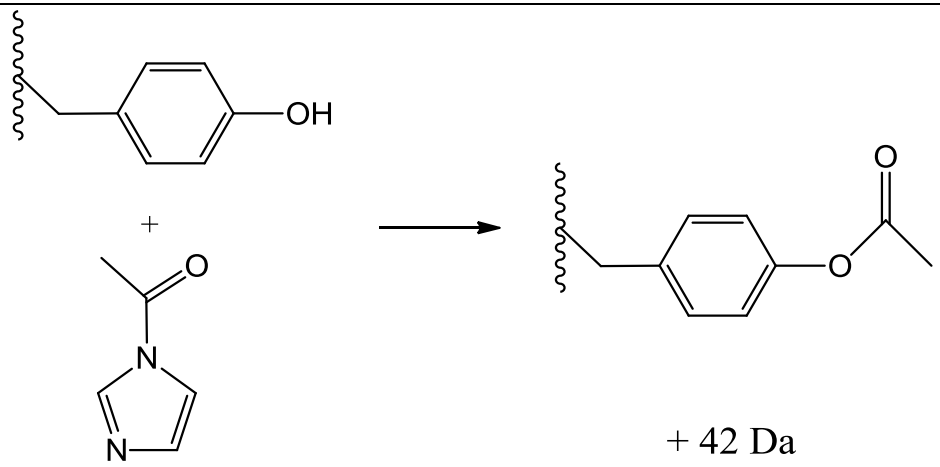 + 42 Da
	tetranitromethane: 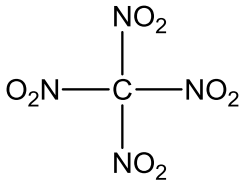	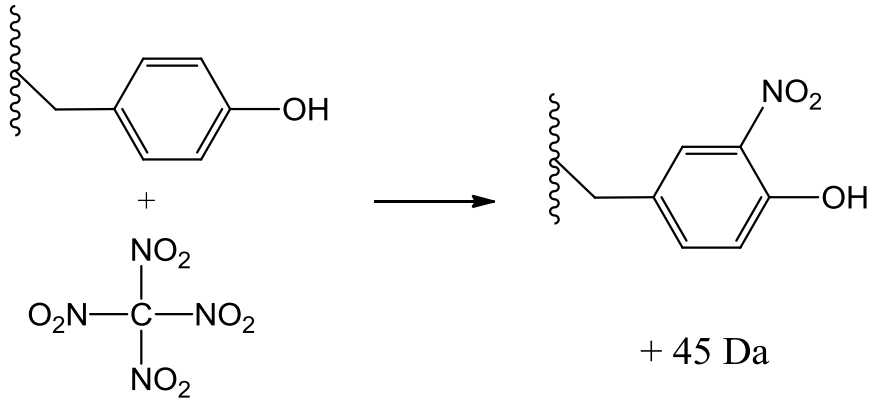 + 45 Da

Table 1.2 (cont'd)

tyrosine (cont'd)	I_2 + KI	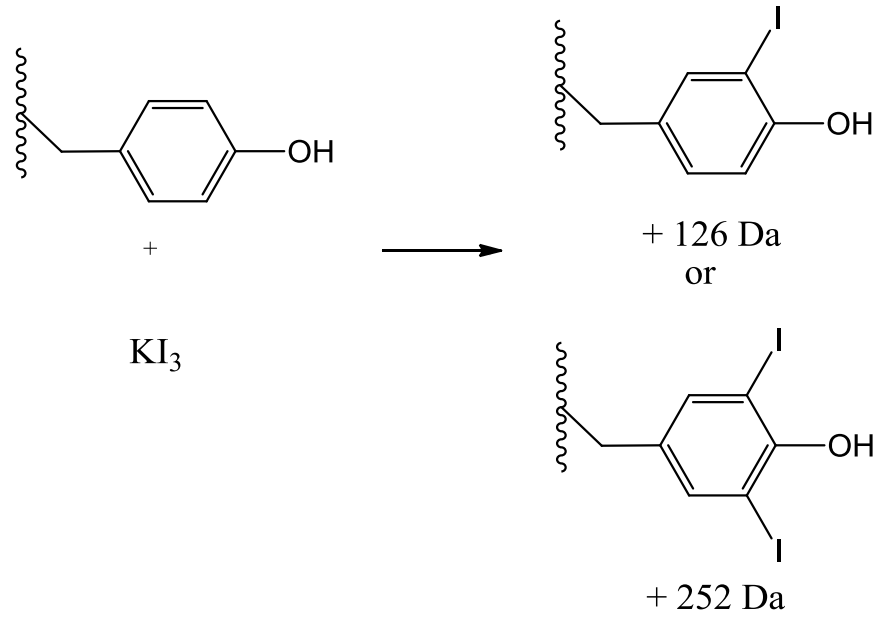

Table 1.2 (cont'd)

tryptophan	2-hydroxy-5-nitrobenzyl bromide (Koshland's reagent): 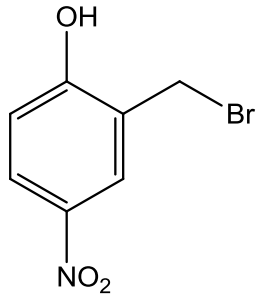	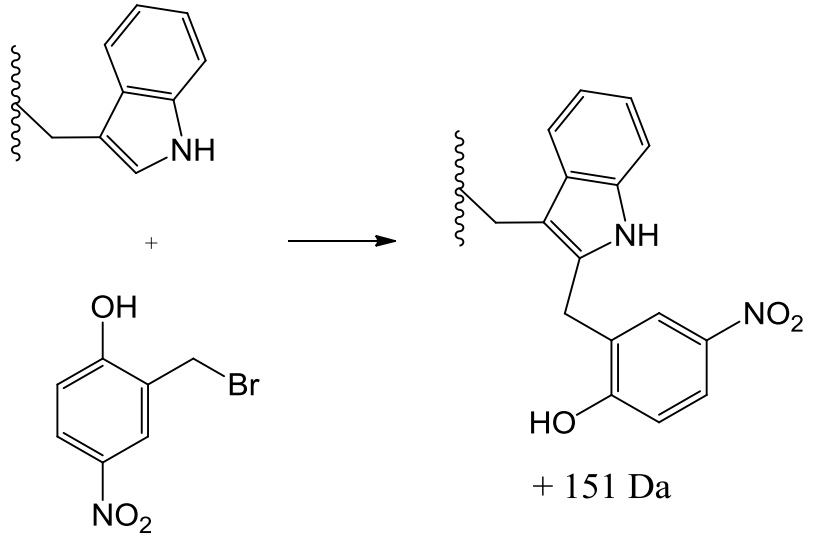 + 151 Da

Table 1.2 (cont'd)

tryptophan (cont'd)	N-bromosuccinimide: 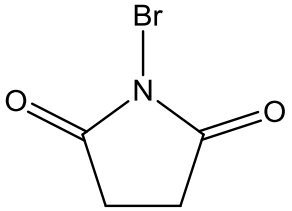	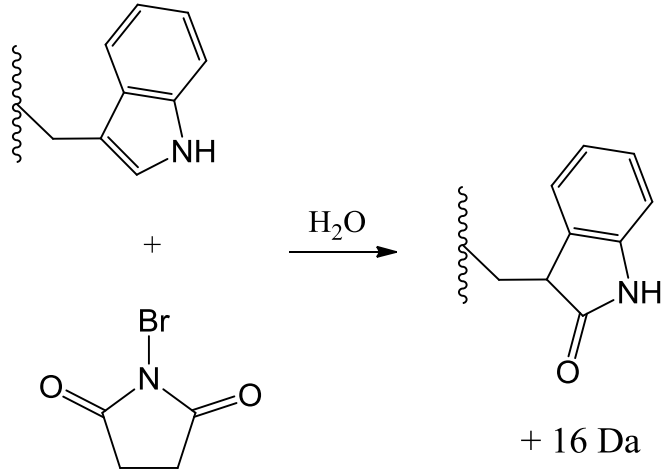
	2-nitrophenylsulfenyl chloride: 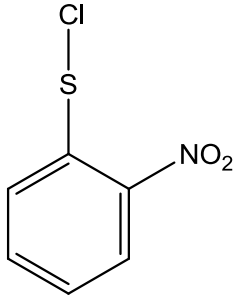	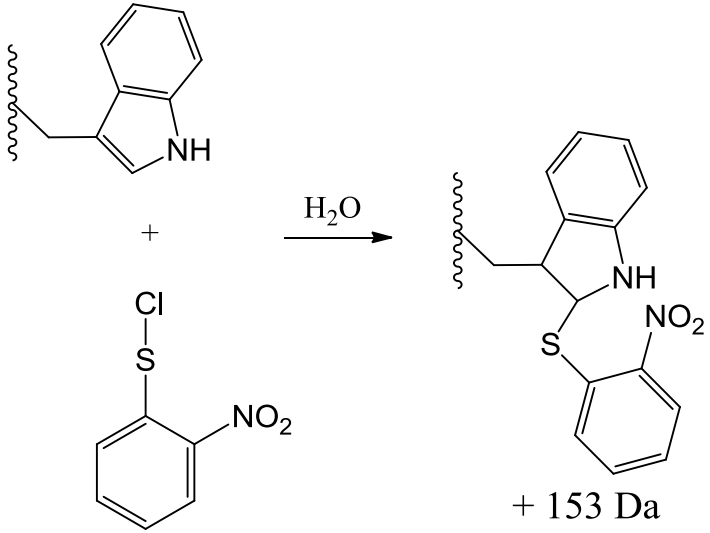

Table 1.2 (cont'd)

non-selective	diazirine: 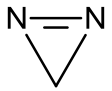	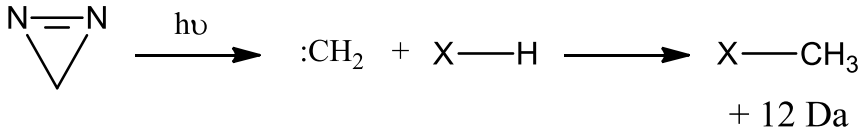

1.2.5.2 Arginine-Specific Reagents

Arginine is the most basic amino acid with pKa at 12.48 and is almost always protonated under physiological pH. Due to partial double bond character of each of the C-N bonds, the arginine guanidium side chain can form multiple salt bridges with carboxylates which reduces its reactivity with labeling reagents. This feature makes arginine a valuable probe for the study of protein-ligand and protein-protein interactions [212]. Arginine-specific protein labeling reagents are usually vicinal dicarbonyl compounds, such as 1,2-cyclohexanedione, phenylglyoxal, p-hydroxyphenyglyoxal, and 2,3-butanedione, which form a cyclic product with the arginine guanidinium cation [213] as shown in Table 1.2. Kethoxal, an RNA footprinting reagent, has also been demonstrated to react specifically with the arginine guanidium group under mild conditions [214]. The addition of borate can stabilize the cyclic product as shown in Scheme 1.5 [215-217]. Some early studies found that the presence of proton acceptors, such as carboxylate groups, in proximity to the arginine guanidium groups can catalyze the cyclization reaction because the guanidium groups become more nucleophilic after being deprotonated by carboxylate groups [179, 186]. Since the early 1990s, many studies have used arginine-specific protein labeling methods coupled with mass spectrometry to map protein surface topology [218, 219] and charge distribution [220], to probe the active sites of enzymes [221-224], and to characterize the interface and associated conformational changes involved in protein-ligand binding [214, 225, 226] and protein-protein interactions [227-229].

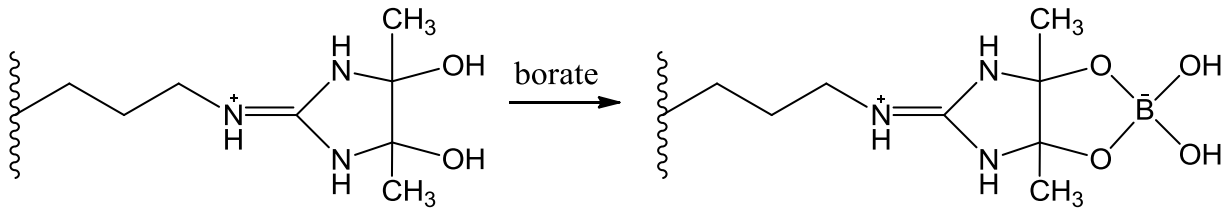

Scheme 1.5 Reaction showing how borate stabilizes the cyclic products formed by reaction of arginine with 2,3-butanedione.

1.2.5.3 Histidine-Specific Reagents

Histidine has an imidazole side chain with pKa ~6.0. It is usually involved in protein biochemistry due to its moderate basicity, aromaticity, H-bonding capacity, and divalent metals binding capability. Diethylpyrocarbonate (DEPC) has been used almost exclusively for specific histidine modification [230]. As shown in Table 1.2, at low DEPC concentrations, mono-modification of histidine gives carboethoxyhistidine as the predominant product. In the presence of excess DEPC, formyl-dicarboethoxyhistidine can be formed. Further reaction may lead to ring opening to form urethane-dicarboethoxyhistidine. The mono-modification reaction of histidine, i.e. generation of carboethoxyhistidine, is reversible under acidic or basic conditions, or in the presence of nucleophiles such as tris(hydroxymethyl)aminomethane (Tris) and hydroxylamine [230]. Under 25 ℃, the half-life of carboethoxyhistidine is 55 hr at pH 7, 2 hr at pH 2, and 18 min at pH 10 [231]. The formation of dicarboethoxyhistidine, however, is irreversible. Because of the various products that may be generated from DEPC modification of histidine, care must be taken when performing the modification experiments and interpreting the mass spectra. However, the ability of DEPC to modify both the δ-nitrogen and ε-nitrogen of histidine to form dicarboethoxyhistidine can improve the spatial resolution of this probe. In a study to characterize the DEPC reaction with insulin, both histidine residues, His5 and His10, were modified. Biscarbethoxylation was only observed on His10, whereas only one nitrogen on the imidazole ring of His5 was modified [232]. This is consistent with the crystal structure where both imidazolyl nitrogen atoms on His10 have high solvent accessibility while His5 only has one side of the imidazole ring exposed on the surface. Besides histidine, DEPC modification of lysine, tyrosine, cysteine, serine, threonine, and occasionally arginine has also been reported [230, 233-

235]. In a study conducted by Dage and coworkers, DEPC modification of histidine was almost exclusive at pH 6, however, an increase in lysine modification was observed as the pH increased from 6 to 8 [236]. Due to the complexity of DEPC modification products, peptide mass mapping is not sufficient to identify the modified residue and MS/MS is required. The poor selectivity of DEPC modification may also be beneficial since multiple residues can be monitored at a time and higher protein sequence coverage can be obtained. DEPC has been used in many studies to characterize protein structures [232, 234-236], investigate the interface involved in formation of protein complexes [204, 205], map conformational changes induced by Ca(II) [237] or Cu(II) [238] binding, and probe the metal binding sites [233, 239].

1.2.5.4 Carboxylic Acid-Specific Reagents

Protein carboxyl groups are typically modified by glycine ethyl ester and glycineamide via the activation using carbodiimides, such as 1-ethyl-3-(3-dimethylaminopropyl)carbodiimide as shown in Table 1.2. Carbodiimides can also react with cysteines and tyrosines [240]. Similarly to other selective protein modification reagents, numerous studies have used glycine ethyl ester / glycineamide in the presence of carbodiimides to probe protein structures [241, 242] and analyze protein-protein complex [241, 243, 244]. A recent study by Gau *et. al.* [160] characterized the conformation difference of apolipoprotein E3 (ApoE3) between its native state (WT-ApoE3) and monomeric mutant (ApoE3MM) to probe the regions that are involved in self-association. They compared the footprinting results obtained from fast photochemical •OH labeling and selective carboxylic acid modification and found a good consistency except for the region 183-205. They proposed three reasons responsible for this discrepancy. First, fast •OH labeling mapped the

protein structure at a microsecond time scale whereas carboxylic acid modification presented the protein conformation averaged over several minutes. Second, compared with EDC and GEE, interaction of •OH with protein amino acid residues are much easier since the size of •OH is much smaller and comparable to water molecules. Finally, the reaction sites in the two modification methods are different. Attack of EDC by the carboxylic group is the first step in carboxyl-specific labeling while •OH abstracts hydrogen from the β/γ carbon from aspartic/glutamic acid [131].

1.2.5.5 Cysteine-Specific Reagents

Due to the relatively high activity and biological importance of cysteine residues, a large number of reagents have been used to modify cysteine residues. Iodoacetamide, iodoacetic acid, and N-alkylmaleimides are the most common probes whereas other reagents, such as chloroacetamide, acrylamide, arsonous acids, 4-vinylpyridine, and fluorescent reagents including crylodan and 5-((((2-iodoacetyl)amino)ethyl)amino)naphthalene-1-sulfonic acid (IAEDANS) have also been used. Some commonly used reagents for cysteine modifications are shown in Table 1.2. Besides solvent accessibility, local electrostatic environment is also a determinant of cysteine reactivity. In a study using tubulin as the model protein, reactive cysteine residues were found to be located within 6.5 Å of positively charged groups (i.e. arginine and lysine side chains and positive edges of aromatic ring) presumably due to the stabilization of the negative thiolate by the neighboring positive charges. Some less reactive cysteine residues, even if they were exposed on the surface, were found in the vicinity of carboxyl groups and their inactivity were ascribed to the suppression of thiol dissociation caused by surrounding negative charges [245].

As with other amino acid residues, cysteine residues have been targeted by numerous studies for protein structural characterization [246-253]. More interestingly, a recent study used cysteine shotgun-mass spectrometry to probe the protein structural changes in stressed cells. In comparison to cells in the native states, enhanced cysteine labeling of whole blood ghosts was observed under shear stress at 1.5 Pa for 30 and 60 min [254]. Moreover, as disulfide bonds play a vital role in protein folding, cysteine-specific labels have been used to map the bridging of vicinal cysteine residues. It is generally considered that cysteine residues in a disulfide form are less active. However, control experiments are necessary to distinguish whether this low activity is caused by disulfide bond formation or simply burial in the protein interior. While mapping of disulfide bonds are generally achieved indirectly based on the identification of free thiols [250, 255, 256], Glocker's group directly probed protein disulfide bonds by reducing the protein prior to selective bridging of bis-cysteinyl groups by arsonous acid [257]. In this study, 4 arsonous acid derivatives, phenylarsonous acid, 4-aminophenylarsonous acid, pyridinyl-3-arsonous acid, and melarsen oxide, were examined in terms of their reactivity and specificity in the bridging reaction of bis-cysteinyl residues. Melarsen oxide was found to be most suitable (as shown in Table 1.2) and was used to characterize the structure of partially reduced bovine pancreatic trypsin inhibitor.

1.2.5.6 Methionine-Specific Reagents

Methionine is one of the main residues targeted by hydroxyl radicals and not many reagents have been developed for specific methionine modification. Inspired by SUPREX, Fitzgerald's lab developed a technique, termed SPROX (stability of proteins from rates of

oxidation), that utilizes hydrogen peroxide as a protein methionine oxidation reagent to measure the extent of oxidation as a function of denaturant concentration [258]. Similarly to SUPREX (see Section 1.2.3.4.1), with the denaturant concentration dependence of the oxidation rate being determined, the protein folding free energy and protein-ligand affinities can be obtained. SPROX differs from SUPREX in terms of protein labeling method where SPROX uses irreversible oxidative labeling and SUPREX uses HDX. The utilization of stable labeling allows more complicated manipulation of proteins, such as protein fractionation and enrichment after labeling. The validity of this method has been proved on several model proteins and protein-ligand complexes using either chemical denaturant [258] or heat to cause protein unfolding [259]. A recent report demonstrated the ability of the SPROX method to identify protein targets for drug molecules [260]. However, the potential protein conformational change induced by oxidation [143, 152, 174-176] casts doubt on the future application of SPROX. Alternatively, methionine residues can be modified by phenacylbromide [261-263]. Although this approach has not been used to map protein surface, the initial application of phenacylbromide in peptide quantification (see Section 1.3) showed this reagent is a promising method for methionine labeling eliminating the concerns of any protein conformational changes induced by oxidation.

1.2.5.7 Tyrosine-Specific Reagents

The generally used reagents for tyrosine-specific protein labeling are N-acetylimidazole targeting tyrosine phenolic groups, and tetranitromethane and I_2/KI or NaI/chloramines T mixtures targeting the tyrosine aromatic ring as illustrated in Table 1.2. At pH $\geq$ 8, side reactions

of tetranitromethane with histidine, methionine, and tryptophan can occur [264]. Modification of lysine and serine by N-acetylimidazole was also observed [265]. Iodine modification is less specific and reactions with histidine, tryptophan, methionine, and cysteine have been reported [266]. Mild acidic conditions (pH ~6) were usually used to avoid undesired side reactions. Digestion pH was generally kept low for reduced hydrolysis of O-acetyl-tyrosine [186] and kept relatively high (pH ~9) for the stabilization of nitrotyrosine [267]. Due to the two different labeling sites on tyrosine residues, more detailed insights can be obtained about the microenvironment at different sites. An early study used N-acetylimidazole and tetranitromethane to probe the structure of a minibody, a *de novo*-designed 61-residue protein, and found three tyrosine residues were labeled by both reagents whereas Tyr24 and Tyr47 were only modified by tetranitromethane. The reactivities of the five modified tyrosine residues are consistent with the previous limited proteolysis results while the absence of N-acetylimidazole modified Tyr24 and Tyr47 was attributed to possible hydrogen bonding of the phenolic group with other amino acid residues [186]. Tyrosine-specific modification coupled with mass spectrometry has been widely used to map protein structures [267-269] and characterize protein-ligand binding [226, 270] and protein-protein interactions [227].

1.2.5.8 Tryptophan-Specific Reagents

Commonly used reagents for specific tryptophan modification are 2-hydroxy-5-nitrobenzyl bromide (also known as Koshland's reagent), N-bromosuccinimide, and O-nitrophenylsulfenyl chloride as shown in Table 1.2. Side reactions of Koshland's reagent with cysteine and tyrosine residues was observed at acidic and basic pH, respectively [271]. N-

bromosuccinimide modification of arginine, tyrosine, histidine, lysine, and cysteine side chains has also been reported [272]. Modification of tryptophan by the above reagents is more specific at lower pH. Mapping of tryptophan solvent accessibility has been utilized to map protein conformation [273, 274] and protein interactions with other molecules [275]. Recently, Ladner and coworkers investigated the light-driven reactivity of a series of halocompounds towards tryptophan. UV irradiation of chloroform, 2,2,2-trichloroethanol, 2,2,2-trichloroacetate, and 3-bromo-1-propanol attaches a formyl, hydroxyethanone, carboxylic acid, and propanol group, respectively, onto the tryptophan indole ring. These reagents were used to determine the solvent accessibility of carbonic anhydrase [276].

1.2.5.9 Nonspecific Chemical Reagents

Carbene ($:CH_2$) is one of the most reactive organic chemicals with low specificity and thus essentially useless for synthesis. However, its indiscriminate reactivity with proteins makes it promising in protein structural characterization [277]. Carbene is an electron deficient species and is generally generated by UV irradiation of diazirine at > 300 nm (usually at 320 nm) to avoid damage to protein chromophores. Diazirine is a chemically inert gas unless being irradiated or heated and does not introduce any undesired reactions with protein. Photolysis of diazirine usually extends for ~ 45 min (the half life is 10.3 min [278]) and the reaction cuvette is immersed in 20 ℃ water bath to avoid heating. Carbene can modify both protein backbones and amino acid side chains by insertion of a methylene group into double bonds or any X-H bond where X = C, O, N, or S. The modification is a random and non-specific process which has been

proved by observation of uniform modification of unfolded bovine α-lactalbumin [278, 279] and *Bacillus licheniformis* β-lactamase [280]. The extreme reactivity of carbene (with a life-time < 50 ps in solution [281]) makes it only capable of reacting with targeting groups within its immediate molecular cage. As a result, methanol, which is formed by reaction of carbene with high concentration of H_2O in modification solution, builds up quickly and may pose a disturbance to protein conformation. Due to the poor solubility of diazirine in aqueous solution (~ mM), it has been shown that the generated methanol does not cause any putative change to protein structure [278]. This feature, however, also poses a limitation, i.e. the level of protein labeling is also very low (4×10^{-3} labels per molecule of α-lactalbumin [280]) and may fall below detection limit. A recent study from Delfino's group developed a photolysis device for continuous generation and photolysis of diazirine to enhance the modification extent and assessed different protein conformations in their native and non-native states [282]. Jumper and Schriemer explored a new carbene precursor, diazirine-modified leucine, which was soluble in water, and achieved greater extent of protein modification which was sufficient for detection by mass spectrometry [283].

1.2.6 Chemical Cross-Linking Combined with Mass Spectrometry for Protein Structure Analysis

1.2.6.1 Introduction

In contrast to protein surface labeling reagents described above, which have only one functional group, a protein cross-linking reagent has two or more functional groups connected by a spacer or linker and can react with multiple amino acid residues located in proximity within the same protein or between the individual components of a multi-protein complex. Furthermore, the functional groups are usually connected by a linker or spacer whose length serves as a ruler to estimate the distance between the two linked residues. As a result, non-covalently interacting protein regions can be captured into a stable covalent complex and analyzed either by "bottom-up" or "top-down" approach from which the cross-linked peptides can be identified. Accordingly, the low-resolution protein structure or protein interactions can be characterized [284].

The main challenges in protein cross-linking combined with mass spectrometry for the identification of protein interactions sites arise from the high complexity of the reaction mixtures. First of all, cross-linking reaction can result in a variety of products which can be basically characterized into three types: dead-end modified peptides, intra-cross-linked peptides, and inter-cross-linked peptides [285]. In dead-end modified peptides, one of the functional groups from the cross-linker is incorporated into the protein while the other functional group is deactivated, for example, hydrolyzed. Intra-cross-linked peptides have the amino acid residues cross-linked within the same peptide. Inter-cross-linked peptides are generated by connecting

two amino acid residues from different peptides that are spatially close. Combination of these three cross-linking types can generate an even larger number of products and hamper the identification of cross-links. This problem would become even more severe as the size of the protein or the number of subunits in protein complexes increases.

To overcome the challenges motioned above, a number of strategies have been developed to facilitate the identification of cross-linked peptides from complex mixtures by introducing a variety of functionalities to the cross-linker as well as software development for improved automated data analysis [286]. The recent developments in cross-linkers will be discussed in details below.

1.2.6.2 Recent Development of Cross-Linking Reagents Coupled with Mass Spectrometry for Protein Structure and Protein Interaction Analysis

A straightforward way to simplify the reaction products to be analyzed by mass spectrometry is to enrich the cross-linked peptides prior to mass analysis. A typical method involves the incorporation of a biotin group into the cross-linker so the cross-linked peptides can be enriched by affinity purification on avidin beads [287, 288]. However, the "enrichable" cross-linkers are always bulky and may affect the reaction efficiency with interacting proteins. Chowdhury and coworkers developed a compact cross-linker with an alkyne tag. After the protein cross-linking reaction, the alkyne can react with an affinity agent containing an azide moiety and biotin via "click chemistry" [289].

Incorporation of differential isotopes enables the easy identification of cross-linked peptides from a complex mixture via the presence of distinct isotope patterns in the MS spectra.

Isotopes can be incorporated into the cross-linker region by reacting proteins with 1:1 mixtures of isotope-labeled and non-labeled cross-linking reagents, from which the cross-linked peptides can be distinguished as doublet peaks with 1:1 ion signal ratio in MS spectra [290]. The isotopes can also be introduced to the peptide chain. For example, inter-cross-linked peptides can be differentiated from other peptides (including intra-cross-linked, dead-end modification, and free peptides) by reaction with equal amount of isotope-labeled and non-labeled N-terminal modification reagent as they have two N-termini showing a characteristic 1:2:1 isotope pattern while the others only contain one N-terminus [291]. Combination of isotope-encoded N-terminal modification reagents and isotope-encoded cross-linking reagents has been developed to discriminate free peptides containing lysine residues, whose ε-amino groups can also be modified by an N-terminal modification reagent, from inter-cross-linked peptides [292]. Proteolytic digestion of proteins in ^{18}O-labeled water incorporates two ^{18}O atoms into each digested peptide. In this scenario, inter-cross-linked peptides can be easily identified based on the observation of an 8-Da mass shift while the other peptides all exhibit a common 4-Da mass increment [293, 294].

Another solution for the facilitated identification of cross-linked peptides is the utilization of cleavable cross-linkers. A traditional chemical-cleavable cross-linker is 3,3’-dithio-bis(succinimidylpropionate) (DTSSP) which contains a disulfide bond [295]. After reduction of the disulfide bond, inter-cross-linked and dead-end modification peptides give rise to linear peptides with half of the cross-linker while intra-cross-linked peptides contain two halves of the cross-linker. Reduction in the complexity and size of reaction products allows more confident peptides identification by MS and MS/MS. DTSSP has been combined with isotope-labeling for unambiguous identification of the cross-linked products via the characteristic isotope patterns

[296]. A photo-cleavable cross-linker, bimane bisthiopropionic acid N-succinimidyl ester, (BiPS), whose partial cleavage can be induced by MALDI was also developed [297]. In contrast to the cleavage prior to MS analysis, CID induced cross-linker cleavage during MS/MS has been rapidly developed. Back and coworkers developed a bifunctional cross-linker, N-benzyliminodiacetoyloxysuccinimide (BID), which yields stable benzyl cation marker ions under low-energy CID-MS/MS. Observation of these marker ions was used for straightforward identification of cross-linked peptides from the complex mixture, although products ions from cleavage of other sites were also present [298]. Bruce's lab developed a novel type of cross-linker called protein interaction reporter (PIR) [299]. PIRs contain two low-energy CID-MS/MS cleavable bonds in the spacer chain. Cleavage of inter-cross-linked peptides produces two separate linear peptides, thus giving rise to simplified fragmentation spectra. Also, a reporter ion can be released based on the cleavage of the two labile bonds, allowing the cross-linked peptides to be tracked. However, this reagent is too bulky with a length of 43 Å and precludes informative protein-protein interactions. Afterwards, Soderblom employed a set of labile Asp-Pro bond containing cross-linkers with linker length of 11.2 and 15.1 Å. The preferred cleavage of Asp-Pro bond releases two separate peptides with unique mass modification. Further fragmentation of the individual peptides produces sequence ions allowing the peptide sequence and cross-linking residue to be identified [300]. Similar approaches employing a cross-linker featuring a preferred cleavage of Gly-Pro bond by an intramolecular attack of the sulfur from a thiourea moiety [301], incorporating simply a thiourea [302] or urea [303] moiety with enhanced cleavage at N-C bond, and utilizing a facile cleavage of C-N bonds adjacent to a quaternary diamine moiety [304] have also been developed. However, the enhanced CID cleavage of the "labile" bonds for either the generation of report ions or separation of the cross-linked peptides are highly dependent on the

peptide composition and precursor ions charge state, i.e. proton mobility [11, 305], and thus limiting the sensitivity and extensive applicability of these approaches. Recently, Lu *et. al.* developed a sulfonium ion containing, amine reactive cross-linking reagent, S-methyl 5,5'-thiodipentanoylhydroxysuccinimide, as shown in Scheme 1.6 A. Exclusive cleavage of the C-S bond adjacent to the sulfonium ion under CID occurs via the fragmentation pathway illustrated in Scheme 1.6 B, independently of the proton mobility. With this approach, different types (i.e., dead-end, intra, and inter) of cross-linking products can be distinguished and further fragmentation of the exclusive products by CID-MS^3 enables the determination of peptide identify and specific cross-linking sites [306].

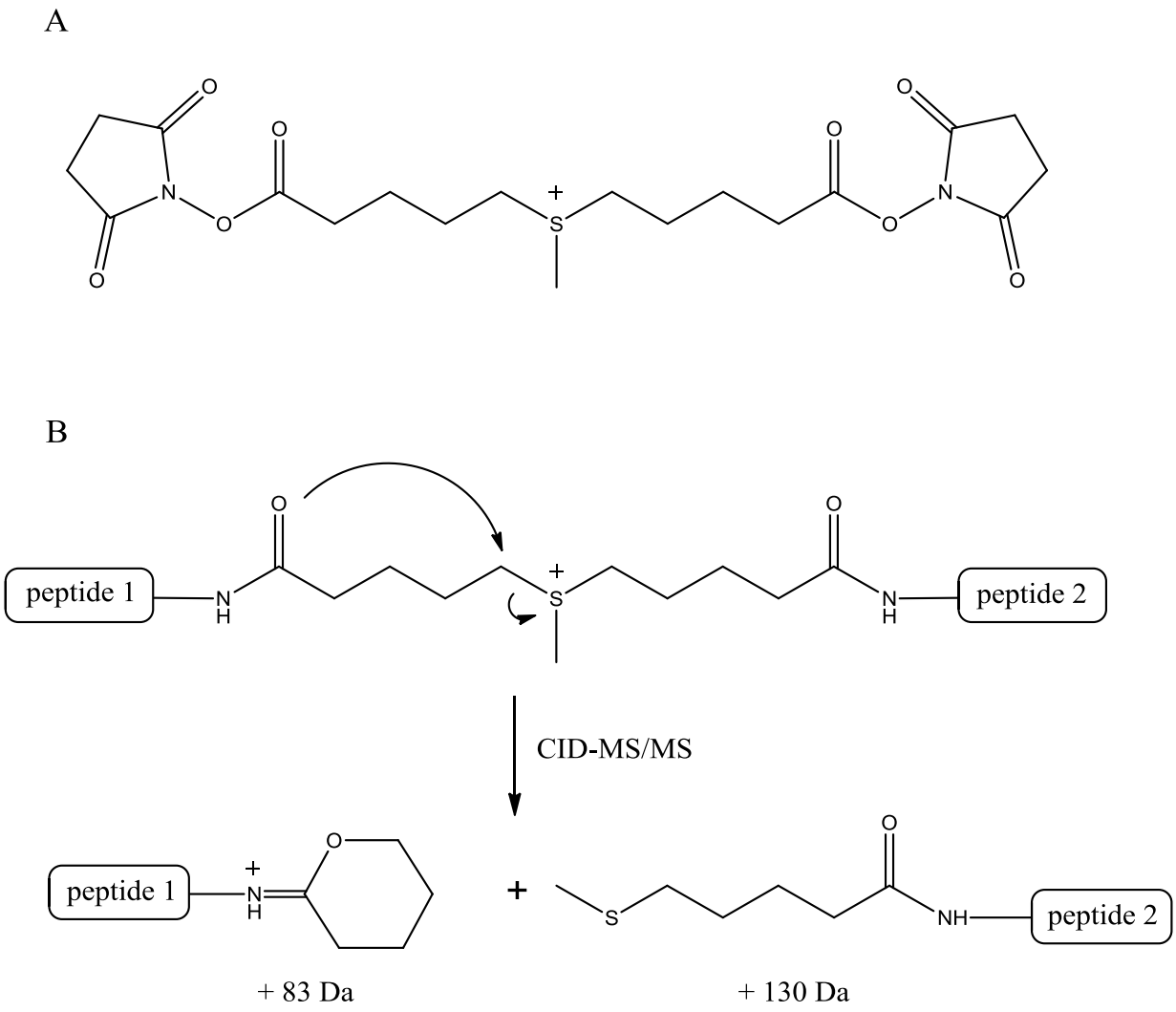

Scheme 1.6 Sulfonium ion containing (A) cross-linker structure and (B) proposed fragmentation mechanism of the cross-linked peptides under CID-MS/MS.

1.3 Chemical Labeling Strategies for Quantitative Proteomics

In addition to protein identification and characterization studies, quantification of protein expression levels at different cell states is another major goal of proteomics. Generally, protein quantification strategies can be classified into two categories: label-free methods and labeling methods [307]. Label-free quantification strategies are mainly based on measurement of the mass spectral peak intensities determined at the peptide level [308, 309] or spectral counting at the protein level [310, 311]. In a typical isotope-labeling based protein quantification experiment, protein under different conditions (usually normal versus stressed) are differentially labeled by "light" and "heavy" reagents, after which the samples are pooled together, fractionated by chromatography, and finally analyzed by mass spectrometry. Relative quantitation is achieved by comparing the abundance of "light" and "heavy" labeled peptide pairs, assuming the differentially labeled peptides exhibit the same chemical properties during chromatography and only differ in mass. Isotope incorporation is generally realized by i) the metabolic method in which stable-isotope labeled amino acids are used in cell growth medium; ii) enzymatic method in which ^{18}O is incorporated onto terminal carboxylic groups during digestion; and iii) chemical derivatization of amino acid residues at the protein or peptide level [307]. Chemical derivatization based quantification strategies have become one of the most prevalent approaches and will be described below.

Similarly to specific-labeling methods for protein structure analysis described in Section 1.2.5, isotope-labeling strategies target a variety of protein/peptide functional groups, such as primary amines (including N-termini and lysine residues), sulfhydryl groups, and carboxylic acids (including C-termini and aspartic/glutamic acid residues) [312]. The isotope-coded affinity

tag (ICAT) developed by Gygi et. al. in 1999 [313] represents a breakthrough in this field. The ICAT reagents have three functional moieties: i) an iodoacetamide group that reacts with free thiol groups from cysteine residues, ii) a biotin moiety that enables subsequent enrichment by avidin affinity chromatography, and iii) a linker region that is differentially labeled, i.e., containing either eight hydrogens ("light" label) or eight deuteriums ("heavy" label). The first generation ICAT reagents suffered from some limitations. First, incorporation of deuterium labels can preclude the co-elution of "light"-labeled and "heavy"-labeled peptides, making quantitation less accurate. Second, fragmentation of the bulky biotin group can complicate the CID-MS/MS spectrum of the peptides thereby hampering peptide identification. Hence, a newer version of ICAT reagents were generated, which have a photo- or acid- cleavable linker to aid the removal of biotin after enrichment and replace ^{2}H with ^{13}C as the isotope labels [314].

ICAT reagents are now widely used and commercially available, however, they are limited to cysteine containing peptides and thus have poor coverage over the whole proteome. A global labeling technique, isotope dimethyl labeling, has been rapidly developed for quantitative proteomics since 2003 [315-317]. In this method, all primary amines (the N-terminus and lysine side chains) in a peptide mixture are converted to dimethylamines by several combinations of isotopomers of formaldehyde and cyanoborohydride, providing a minimum of 4 Da mass shift between peaks in the resultant isotope-labeled peptide triplet (as shown in Scheme 1.5). Besides its global quantitation capability, isotope dimethyl labeling also has advantages of high reaction efficiency and, especially, low cost.

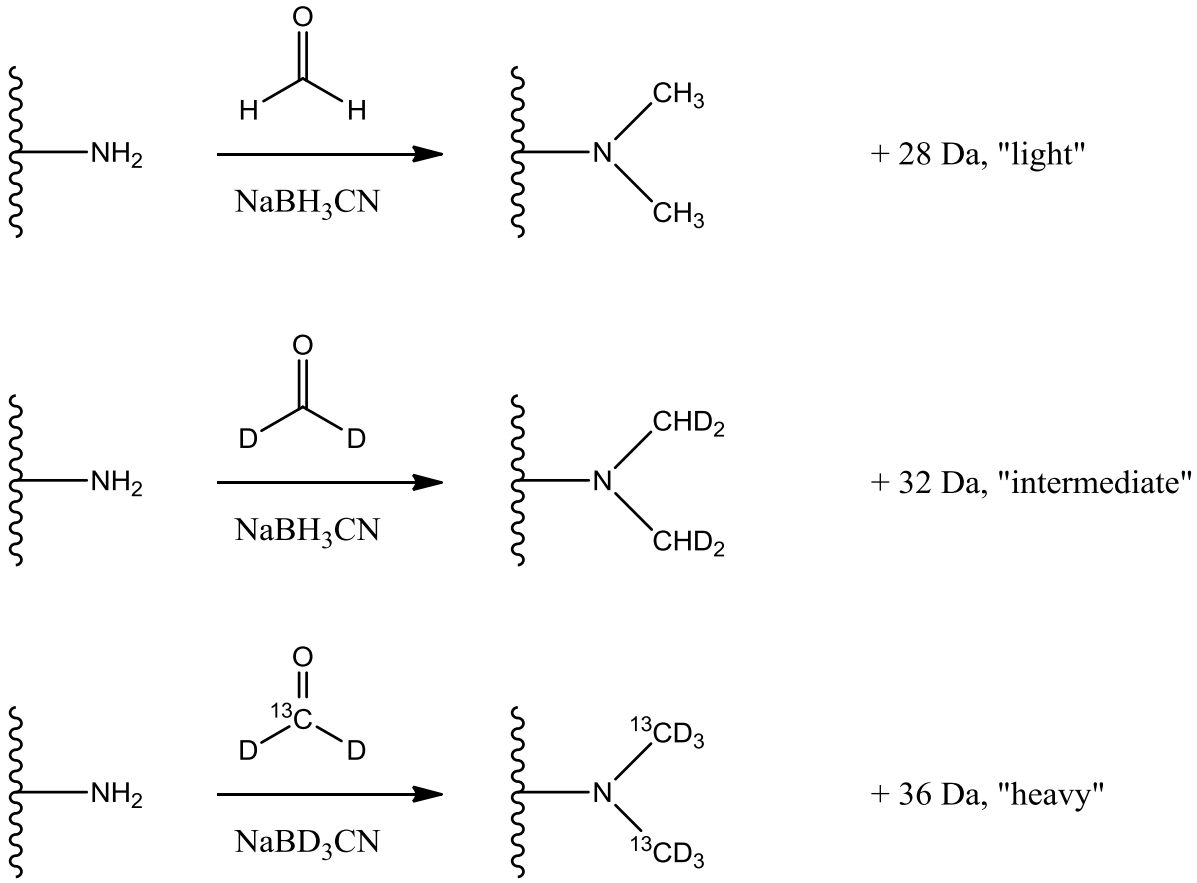

Scheme 1.5 Schemes of triplex isotope dimethyl labeling of primary amines. Adapted from Reference [317].

In contrast to performing quantitation based on ion intensities at MS stage, differential labeling by isobaric mass tagging reagents results in identical mass and allows the quantitation to be realized at MS/MS stage based on the intensities of reporter ions from peptide fragments. Isobaric tags for relative and absolute quantitation (iTRAQ) is a commonly used isobaric tagging reagent [318, 319]. The iTRAQ reagents consist of three groups: i) an NHS-ester moiety that reacts specifically with peptides N-terminus and lysine residue side chains, ii) a reporter group that can contain up to 8 isotope labels with mass ranging from 113 to 121 (skip 120) Da, and iii) a balance group with mass ranging from 184 to 192 (skip 185) Da to offset the mass difference from the reporter group. During CID-MS/MS, the differentially labeled reporter groups are released with retained charge and their intensities are indicative of the abundance of the corresponding peptide.

Another widely used isobaric chemical tagging reagent is tandem mass tags (TMT), which employs the same quantitation principle as iTRAQ and developed about the same time [320]. The latest version of TMT allows up to 6 samples to be analyzed simultaneously [321]. Cleavable isobaric labeled affinity tag (CILAT) is another isobaric tagging reagent which allows the quantitation to be performed at MS/MS stage, however, it also incorporates an affinity group for the enrichment of tagged peptides and a cleavable linker for the release of differently labeled isobaric peptides [322].

Isobaric mass tagging is superior to mass difference tagging in several aspects. First, incorporation of the same numbers of isotope labels minimizes the chromatographic separation of differentially labeled peptides and improves the quantitation accuracy. Second, isobaric tagging of a peptide from multiple samples results in a single peak in MS, which does not increase the complexity of MS spectra and also increases sensitivity and throughput.

Additionally, in the mass difference tagging approach, a variety of m/z differences arises from the variation of charge states and number of modifications, while the m/z of reporter ions liberated from isobaric mass tagging reagents are constant. A potential problem of mass difference tagging is the possible interference caused by the overlapping of differentially labeled peptides with other non-labeled peptides, while this shortcoming is avoided in isobaric mass tagging methods.

Recently, Reid's group developed a MS/MS based quantitation strategy utilizing differential isotope-encoded sulfonium ion derivatization of methionine containing peptides [261, 262]. CID-MS/MS of the isotope-coded sulfonium ion derivatized peptides gives rise to characteristic product ions resulting from the exclusive neutral loss of "light" or "heavy" phenacyl methyl sulfide, independently of the proton mobility of the precursor ion. Quantitation of protein expression can be achieved via measurement of the abundance of "light" and "heavy" neutral loss product ions. This exclusive neutral loss product ion enables the targeted identification of labeled peptides from the complex mixture without the requirement of extensive fractionation or enrichment prior to mass analysis. Later, a pair of isotope-encoded sulfonium ion containing isobaric mass tagging reagents was also developed targeting the lysine residue [323]. Similarly to iTRAQ, the derivatized peptides are not distinguishable during MS analysis, but exhibit differentiable product ions resulting from the exclusive "light" or "heavy" neutral loss(es) allowing quantitation be to realized. Unlike other isobaric tagging reagents (such as iTRAQ and TMT), which have dissociation pathway for release of reporter ion as one of the many competing fragmentation channels thereby "diluting" the signature ion intensity, the isobaric sulfonium ion labeling technique only has one dissociation pathway thus increasing the sensitivity and accuracy. Moreover, the incorporation of fixed charge within peptides can enhance peptide

ionization efficiencies and increase the presence or abundance of high charge state precursor ions for improved ETD analysis.

1.4 Aims of This Dissertation

The aims of this dissertation include:

1. Design and synthesis of a series of isotope-coded sulfonium ion containing protein modification reagents targeting primary amines including the N-terminus and lysine residue side chains.
2. Evaluation of the gas-phase fragmentation behavior of the developed reagents on a model peptide.
3. Proof-of-principle demonstration of an analytical strategy involving the sulfonium ion derivatization of amines coupled with capillary HPLC-ESI-MS, automated CID-MS/MS, and data-dependent neutral loss mode MS^3 for surface mapping of a model protein.
4. Application of the developed analytical strategy to the study of oxidation induced conformational changes in calcineurin.

CHAPTER TWO

DEVELOPMENT OF A FIXED-CHARGE SULFONIUM ION CONTAINING PROTEIN MODIFICATION REAGENT AND ITS INITIAL APPLICATION ON A MODEL PROTEIN

2.1 Introduction

Despite the demonstrated benefits of the current protein labeling methods for mapping protein structures and protein-protein interactions (as described in Chapter One), a common problem is that when a complicated peptide mixture resulting from a large protein or protein complex is analyzed, the modified peptides may be difficult to identify amongst the largely unmodified peptide population.

To overcome this problem, the Reid group has developed a chemical derivatization and multistage MS/MS (MS^n) based analysis strategy, involving the introduction of a 'fixed-charge' sulfonium ion to peptides or proteins containing certain structural features (e.g., the side chains of selected amino acids such as methionine [261-263, 324] or cysteine [325], or within a cross-linking reagent targeting lysine residues [306]), for selective gas-phase identification and quantitative analysis. The sulfonium ion derivatization strategy was first developed on the

---

Part of the results described in Chapter Two were published in: Zhou, X., Lu, Y., Wang, W., Borhan, B. and Reid, G.E., 'Fixed Charge' Chemical Derivatization and Data Dependant Multistage Tandem Mass Spectrometry for Mapping Protein Surface Residue Accessibility. *J. Am. Soc. Mass Spectrom.* **2010**, *21*, 1339-1351.

methionine side chain by alkylating the thioether sulfur atom with readily available alkylation reagents (as shown in Scheme 2.1) [262, 263, 324]. Under low-energy CID-MS/MS conditions, these sulfonium ion-containing peptides give rise to a single characteristic product ion resulting from the exclusive neutral loss of dialkylsulfide (as shown in Scheme 2.1), independent of the amino acid composition or precursor ion charge state (i.e. proton mobility). Therefore, the fixed-charge containing peptides can be readily identified from the complex mixtures by CID-MS/MS. This method may, therefore, be considered a gas phase enrichment strategy. Moreover, the modification site and sequence information can be obtained by subjecting the identified peptides to further dissociation by multistage MS/MS (MS^3) in a quadrupole ion trap, or by energy resolved "pseudo MS^3," at higher CID energy in a triple quadrupole. The differential quantitative analysis of the fixed-charge sulfonium ion-containing peptides has also been achieved by measuring the abundances of the neutral loss product ions resulting from the "light" and "heavy" labeled peptide ions [261, 262]. The mechanism responsible for the exclusive neutral loss of dialkylsulfide in gas phase has been proposed to occur via the charge-directed nucleophilic attack of the carbon atom connected to sulfur by adjacent N- or C-terminal amide bonds, resulting in stable cyclic five- or six-membered cyclic product ions, respectively [263], as illustrated in Scheme 2.1. Based on the derivatization strategy developed on methionine residues, sulfonium ion-containing cysteine-specific peptide modification reagents [325] and an amine-specific cross-linking reagent [306] have also been developed. CID-MS/MS of the peptides with sulfonium ion derivatized cysteine residue [325] or with sulfonium ion containing cross linker [306] both showed exclusive loss of a dialkylsulfide moiety, independent of the proton mobility.

Here, as an initial step toward extending this strategy toward the improved analysis of higher order protein structures, this chapter describes the synthesis, characterization and initial

application of an amine-specific sulfonium ion containing protein modification reagent using a model protein, human cellular retinoic acid binding protein II (CRABP II).

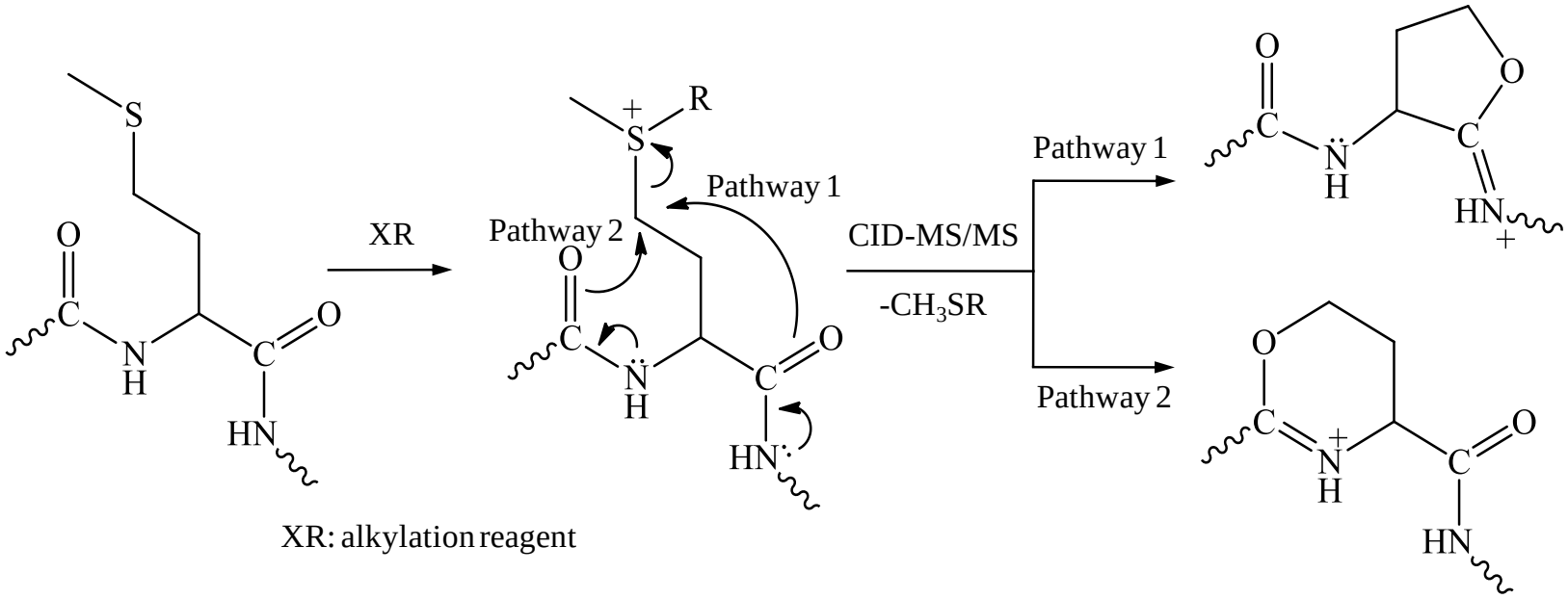

Scheme 2.1 Fixed charge sulfonium ion derivatization of methionine residues and the gas-phase fragmentation of the derivatized peptides. Adapted from Reference [263].

2.2 Design of the Sulfonium Ion Containing Amine-Specific Protein Modification Reagent

The protein modification reagent developed here was designed to have favorable solution phase reactivity towards amines and exclusive fragmentation pathways in CID-MS/MS for the 'targeted' identification and characterization of modified peptides. First, it has an NHS-ester moiety which enables the reagent to react specifically in solution at physiological pH towards the ε-amino groups on lysine residue side chains and/or free N-termini within the protein/peptide of interest. It also contains a sulfonium ion moiety, whose permanent charge can enhance the ionization efficiency [323], and which serves as an efficient leaving group to facilitate the thermodynamically favored exclusive neutral loss(es) of dimethylsulfide upon CID-MS/MS, independent of proton mobility, thereby allowing modified peptides to be readily identified from within a mixture of unmodified peptides. Finally, the NHS-ester moiety and sulfonium ion moiety are connected by an alkyl chain, which includes 3 methylene groups, to facilitate the formation of a stable five-membered cyclic product ion allowing for the exclusive neutral loss of $S(CH_3)_2$ to be thermodynamically favored, as well as the product ion to be stable through dissociation during subsequent CID-MS^3.

Based on the criteria described above, an amine-specific sulfonium ion containing protein modification reagent, S,S'-dimethylthiobutanoylhydroxysuccinimide ester (DMBNHS) (**(3)** in Scheme 2.2), was developed and synthesized as described in Chapter Three. An isotopic version, d_3-DMBNHS, was also synthesized for differential quantitative analysis and its initial evaluation was performed on a model peptide.

2.3 Initial Evaluation of the Reactivity of DMBNHS towards Lysine on a Model Peptide and the Gas-phase Fragmentation Behavior of the Modified Peptide

The reactivity and selectivity of the synthesized reagent, DMBNHS, towards the amino group was first evaluated on a model peptide to validate its further application on proteins.

As shown in Scheme 2.2, after reacting with DMBNHS, the peptide carries a 'fixed charge' sulfonium ion. CID-MS/MS of the derivatized peptide ions is expected to give rise to an exclusive product ions corresponding to the neutral loss of $S(CH_3)_2$. The product ion is proposed to contain a five-membered cyclic iminohydrofuran. Further fragmentation of the neutral loss product ions by CID-MS^3 is expected to give rise to peptide sequence ions, thus allowing the peptide sequence and the site of modification to be characterized.

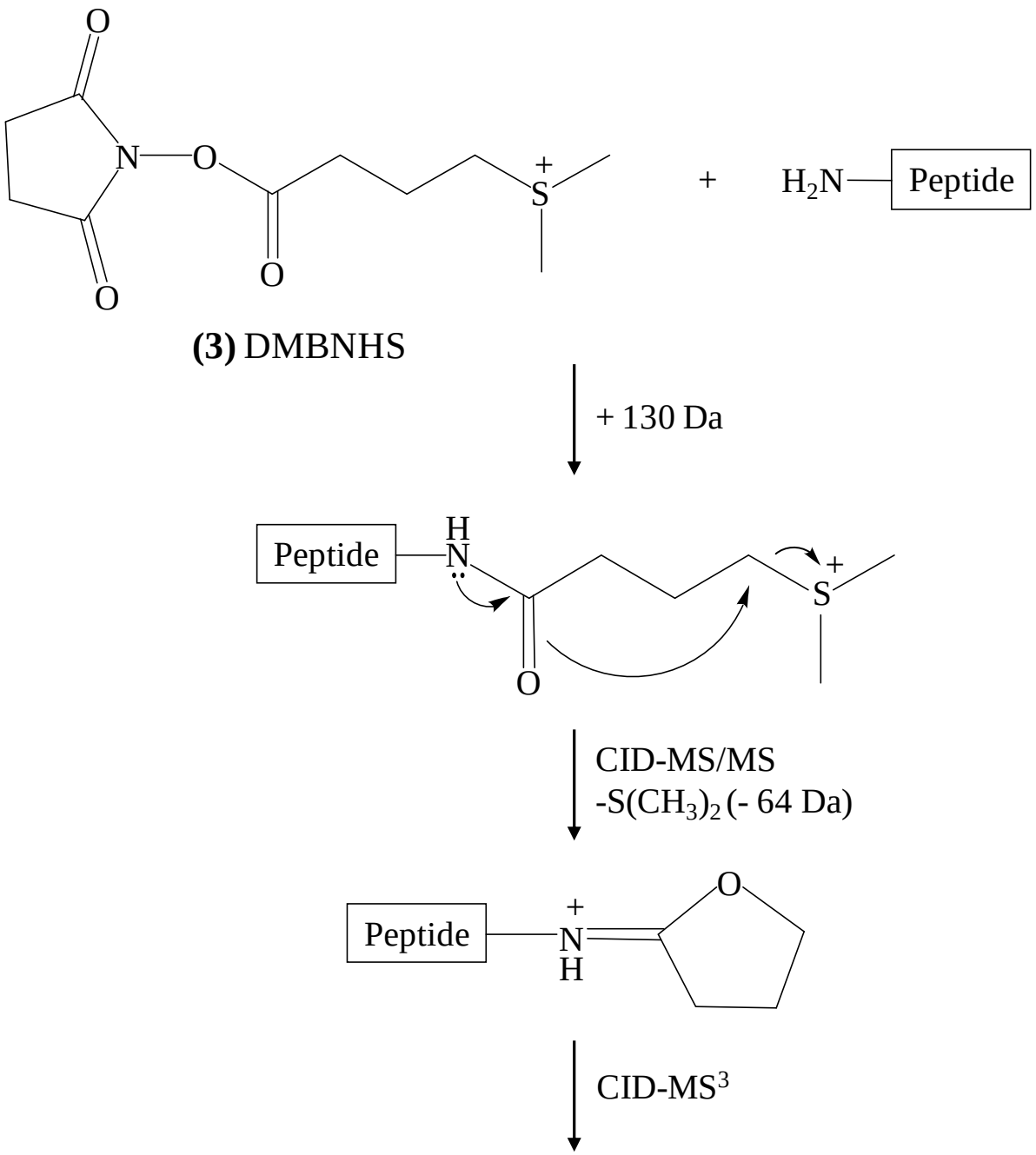

Scheme 2.2 Schematic of the solution phase DMBNHS **(3)** peptide modification and gas-phase CID-MS/MS and -MS^3 fragmentation reactions of DMBNHS modified peptide ions.

Here, neurotensin (*p*ELYENKPRRPYIL) was chosen as the model peptide. The glutamic acid on the N-terminus is cyclized, thus only a ε-amino group on the lysine residue is available to be modified. The peptide modification reaction was performed as described in Chapter Three. Briefly, neurotensin was incubated with DMBNHS or d_3-DMBNHS at a 1:1 molar ratio in PBS buffer with 1% DMF. The percentage of DMF was kept low to mimic the physiological conditions. After 1 hr reaction at room temperature, the reaction solution was desalted and subjected to ESI-MS, CID-MS/MS, and -MS^3 analysis without further purification.

The ESI-MS of the modified neurotensin peptides are shown in Figure 2.1. Figure 2.1 A shows the MS spectrum of the DMBNHS modified neurotensin (neurotensin+DMB) at +2 and +3 charge states. Some unmodified neurotensin was also observed, however, the reaction could potentially be driven to completion by increasing the amount of DMBNHS or reaction time. Since this was a proof of principle experiment, the reaction towards neurotensin was not optimized further. Figure 2.1 B shows the MS spectrum of the d_3-DMBNHS modified neurotensin (neurotensin+DMB(d_3)) at +2 and +3 charge states. It can be seen from the comparison between Figure 2.1 A and 2.1 B that the protonated unmodified neurotensin ions are present at the same m/z, while charged modified neurotensin ions are present at different m/z corresponding to a difference of 3 Da from the incorporation of 3 deuterium of d_3-DMBNHS. It can also be seen from both Figure 2.1 A and 2.1 B that the abundance of modified peptide is lower than the unmodified from at +2 charge state but higher at the +3 charge state. This indicates the sulfonium ion can increase the abundance of higher charge state ions, which is consistent with previously published results [323].

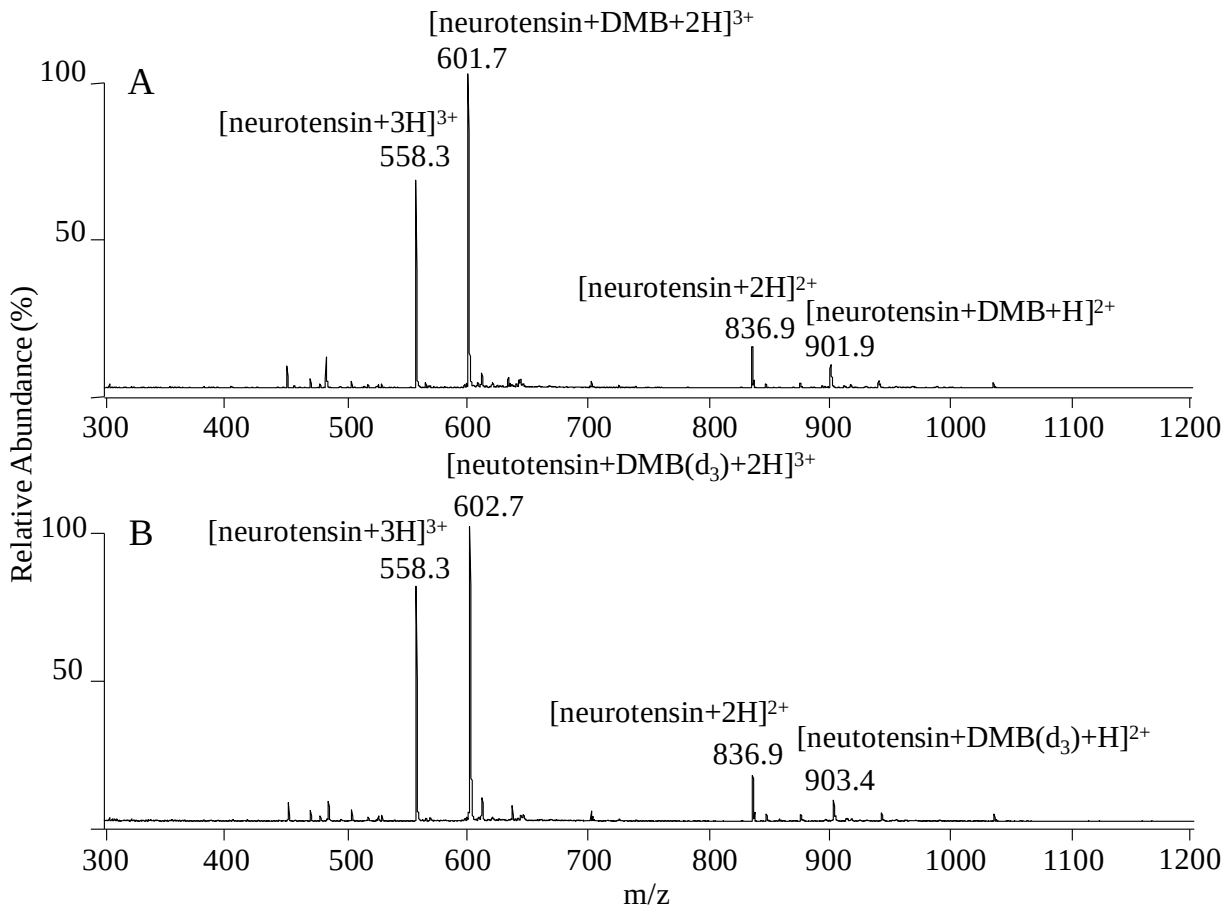

Figure 2.1 Ion trap mass spectrometry characterization of DMBNHS and d_3-DMBNHS modified neurotensin. ESI-MS of (A) DMBNHS modified and (B) d_3-DMBNHS modified neurotensin (labeled as [neurotensin+DMB] and [neurotensin+DMB(d_3)], respectively).

CID-MS/MS of both the doubly (Figure 2.2 A) and triply (Figure 2.2 B) charged DMBNHS modified neurotensin ions gave rise to exclusive product ions corresponding to the neutral loss of 62 Da. This is consistent with the neutral loss of $S(CH_3)_2$ as proposed in Scheme 2.2. CID-MS/MS of both the doubly (Figure 2.2 C) and triply (Figure 2.2 D) charged d_3-DMBNHS modified neurotensin ions generated exclusive product ions corresponding to the neutral loss of 65 Da. Again, this indicates the facile loss of SCH_3CD_3 as illustrated in Scheme 2.2. The observation of exclusive product ions from CID-MS/MS of both the doubly and triply charged DMBNHS/d_3-DMBNHS modified neurotensin ions resulting from the neutral loss of $S(CH_3)_2$/SCH_3CD_3 indicates that the characteristic fragmentation pathways is not dependent on the proton mobility. These results were consistent with previous publications showing the dominant loss of dialkylsulfide from the sulfonium ion derivatized peptides in CID-MS/MS as the favored fragmentation pathway, independent of the proton mobility [261-263, 306, 324, 325].

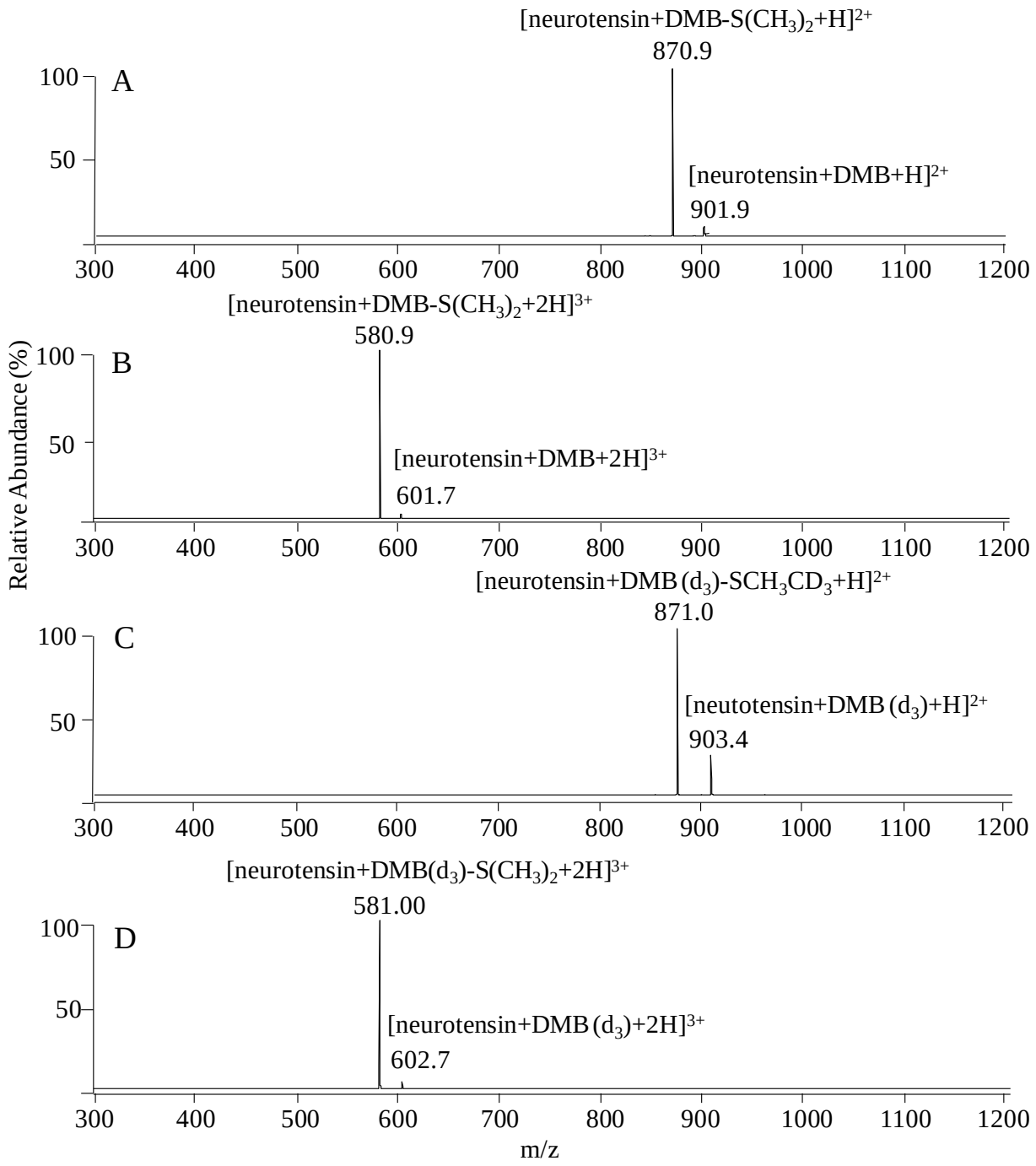

Figure 2.2 Ion trap mass spectrometry characterization of DMBNHS and d_3-DMBNHS modified neurotensin. CID-MS/MS of (A) $[neurotensin+DMB+H]^{2+}$, (B) $[neurotensin+DMB+2H]^{3+}$, (C) $[neurotensin+DMB(d_3)+H]^{2+}$, and (D) $[neurotensin+DMB(d_3)+2H]^{3+}$.

Due to the loss of isotope labeling information during the neutral loss of $S(CH_3)_2/SCH_3CD_3$ upon CID-MS/MS, further fragmentation of the neutral loss product ions from DMBNHS modified neurotensin and d_3-DMBNHS modified neurotensin would give the same sequence ions. This is confirmed by the experimental data as CID-MS^3 of $[neurotensin+DMB\text{-}S(CH_3)_2+2H]^{3+}$ (as shown in Figure 2.3. A) and $[neurotensin+DMB(d_3)\text{-}SCH_3CD_3+2H]^{3+}$ (as shown in Figure 2.3. B) gave rise to identical sequence ions. Based on the observation of the unmodified sequence ion, y_7^{2+}, and modified ions, $y_8^{\dagger 2+}$, $y_9^{\dagger 2+}$, $y_{10}^{\dagger 2+}$, $y_{11}^{\dagger 2+}$, and $y_{12}^{\dagger 2+}$, the modification was easily located on the lysine residue. For comparison, the CID-MS/MS of triply charged unmodified neurotensin is shown in Figure 2.3 C. The y_7^{2+} ions from unmodified and modified neurotensin have the same m/z, while the y_8, y_9, y_{10}, y_{11}, and y_{12} ions from modified neurotensin ($y_8^{\dagger 2+}$, $y_9^{\dagger 2+}$, $y_{10}^{\dagger 2+}$, $y_{11}^{\dagger 2+}$, and $y_{12}^{\dagger 2+}$ in Figure 2.3 A and 2.3 B, where a dagger (†) indicates sequence ions with one modified residue) shift to higher m/z compared to those from unmodified form (y_8^{2+}, y_9^{2+}, y_{10}^{2+}, y_{11}^{2+}, and y_{12}^{2+} in Figure 2.3 C). This further confirms the modification site at the lysine residue.

Unexpected reactions of NHS esters with cysteines, tyrosines, serines, and threonines were reported [326-328]. Neurotensin (*p*ELYENKPRRPYIL) contains two tyrosine residues as the potential targets of DMBNHS; however, no sequence ions were observed indicating the modification site at either of the two tyrosine residues. This is probably due to the low DMBNHS:neurotensin reaction molar ratio (1:1) and the physiological pH utilized here, as tyrosine modification by NHS esters was found to be favored under acidic conditions [328].

The initial study on neurotensin demonstrated the selective reactivity of DMBNHS towards lysine residues and the exclusive gas-phase fragmentation behavior of the derivatized peptides.

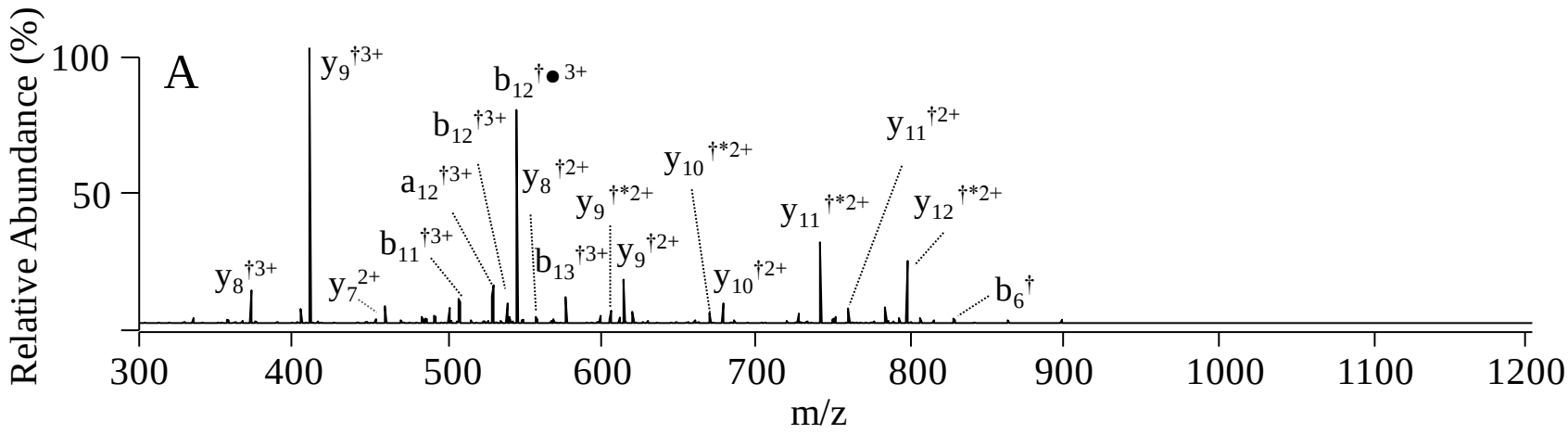

Figure 2.3 Ion trap mass spectrometry characterization of DMBNHS and d_3-DMBNHS modified neurotensin. CID-MS^3 of (A) [neurotensin+DMB-$S(CH_3)_2$+2H]$^{3+}$ from Figure 2.2 B and (B) [neurotensin+ DMB(d_3)-SCH_3CD_3+2H]$^{3+}$ from Figure 2.2 D. CID-MS/MS (C) of triply unmodified neurotensin, [neurotensin+3H]$^{3+}$, from Figure 2.1 A. †: sequence ions containing the modified residue. A superscript * indicates the loss of NH_3. A superscript ○ indicates the loss of H_2O. A superscript ● indicates the addition of H_2O.

Figure 2.3 (cont'd)

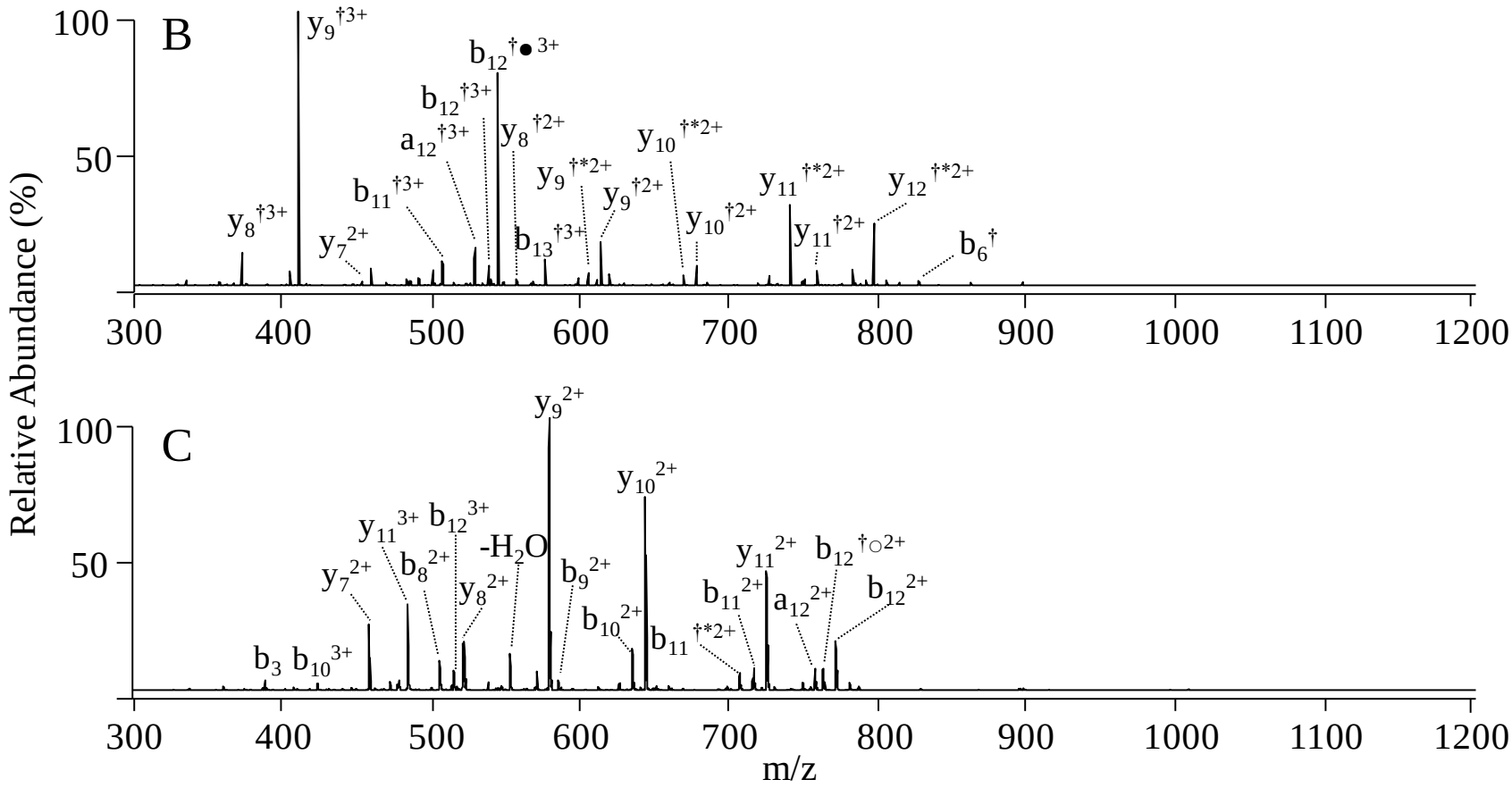

2.4 Application of DMBNHS on a Model Protein for Quantitative Characterization of Protein Surface Residue Accessibility

The utility of the DMBNHS based protein modification and 'targeted' multistage tandem mass spectrometry strategy for the identification and characterization of modified peptides for mapping protein surface residue accessibilities was demonstrated here using a model protein, human cellular retinoic acid binding protein II (CRABP II). The complete sequence of CRABP II is shown in Scheme 2.3, with the 13 lysine residues distributed throughout the protein sequence and the N-terminal residue labeled in bold text. The solvent-accessibilities (SA) of these lysine amino acid side chains and the N-terminal amino group are predicted by the GetArea program [329] which performs the calculation based on the Cartesian coordinates of each atom obtained from the determined NMR solution structure of CRABP II [330]. The solvent-accessibilities are predicted to range from 26.0% to 93.1% (Table 2.1).

^{1}**P**NFSGNW^{8}**K**IIRS*E*NF*EE*LL^{20}**K**VLGVNVM

LR^{30}**K**IAVAAAS^{38}**K**PAV*E*I^{44}**K**Q*E*GDTFYI^{53}**K**

TSTTVRTT*E*INF^{66}**K**VG*EE*F*EE*QTVDGRPC^{82}

KSLV^{86}**K**W*E*S*E*N^{92}**K**MVC*E*Q^{98}**K**LL^{101}**K**G*E*G

P^{106}**K**TSWTR*E*LTNDG*E*LILTMTADDVVCTR

VYVR*E*

Scheme 2.3 Amino acid sequence of cellular retinoic acid binding protein II (CRABP II). The DMBNHS modification sites are indicated in bold text, while the Glu-C digestion sites are indicated in italic text.

Table 2.1 Summary of observed CRABP II Glu-C digestion peptide sequences, retention time ranges, modifiable residues, and predicted amino acid solvent accessibilities.

Peptide residues	Sequence	Retention time range (min)	Modifiable residues present	Predicted solvent accessibilities (%)[a]
97-112	QKLLKGEGPKTSWTRE	11.51 - 13.93	Lys_{98}	49.6
			Lys_{101}	72.7
			Lys_{106}	42.6
63-70	INFKVGEE	14.49 - 15.46	Lys_{66}	60.5
47-62	GDTFYIKTSTTVRTTE	15.54 - 16.71	Lys_{53}	38.3
1-13	PNFSGNWKIIRSE	18.99 - 19.85	Pro_{1}	57.8
			Lys_{8}	45.7
63-72	INFKVGEEFE	20.06 - 21.10	Lys_{66}	60.5
1-17	PNFSGNWKIIRSENFEE	22.04 - 23.61	Pro_{1}	57.8
			Lys_{8}	45.7
63-96	INFKVGEEFEEQTVDGRPCK SLVKWESENKMVCE	23.94 - 25.20	Lys_{66}	60.5
			Lys_{82}	28.1
			Lys_{86}	56.2
			Lys_{92}	26.0
18-42	LLKVLGVNVMLRKIAVAAA SKPAVE	29.25 - 31.94	Lys_{20}	49.3
			Lys_{30}	58.1
			Lys_{38}	93.1

[a] Solvent accessibilities were predicted based on the known solution phase structure of CRABP II [330], by using the GetArea program [329].

2.4.1. Protein Modification by DMBNHS and HPLC-ESI-MS Analysis of the Resultant Glu-C Digested Peptides

CRABP II was subjected to reaction with varying amounts of DMBNHS, with reagent/protein excesses ranging from 5 to 100. After 30 min, the modification was quenched and the modified protein was digested overnight with Glu-C prior to being subjected to HPLC-MS, -MS/MS and -MS^3 analysis. No reduction or subsequent alkylation was performed prior to protein digestion in the current study, as there are no disulfide bonds in the CRABP II protein sequence.

The base peak chromatograms obtained following LC-MS of each of the labeled CRABP II Glu-C digests are shown in Figure 2.4. The identities of the peaks in each chromatogram (determined following interpretation of the MS/MS and MS^3 spectra obtained from each peak as discussed in detail below) are labeled in Figure 2.4, and summarized in Table 2.1. The observed peptides represented 79% of the protein sequence and contained all 13 lysine residues and the N-terminus. For each of the peptides, it can be seen that the extent of modification increases with increasing reagent to protein ratio, albeit to different extents depending on the identity of the peptide, indicating that each of the lysine residues are exposed on the surface of the protein, which is consistent with the known solution structure [329].

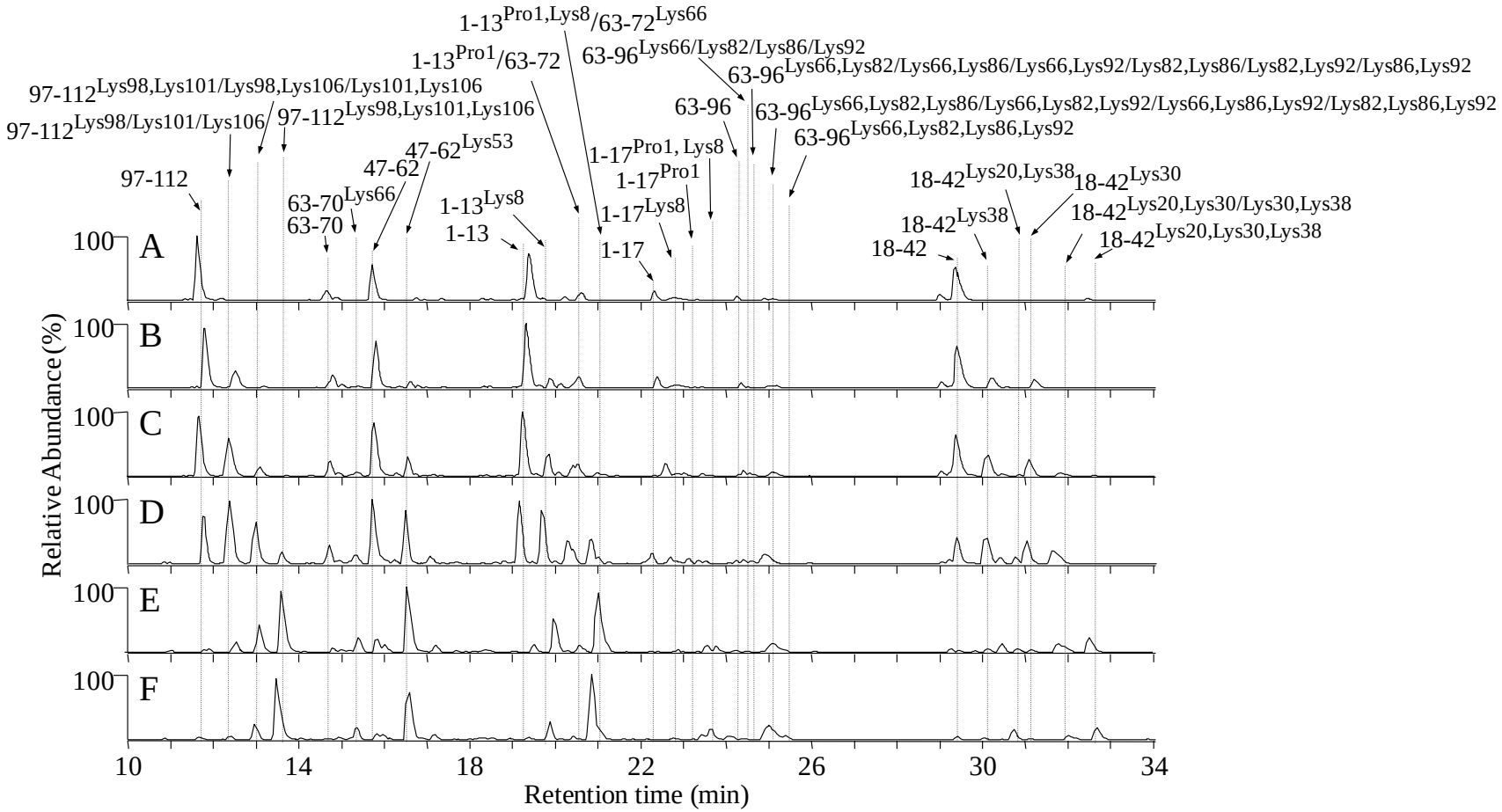

Figure 2.4 Base peak chromatograms of the Glu-C digests from (A) unmodified CRABP II and CRABP II modified with DMBNHS using (B) 5-fold, (C) 10-fold, (D) 20-fold, (E) 50-fold, and (F) 100-fold molar excess. Peaks are annotated as: $\#_x$-$\#_y^n$, where the $\#_x$ and $\#_y$ indicate the residue numbers within the protein and the superscript n indicates the residue(s) that is modified. A superscript / indicates that isomeric forms of a modified peptide were observed within a single co-eluting peak.

2.4.2. CID-MS/MS and -MS^3 Analysis of Peptides Formed by Glu-C Digestion of the DMBNHS Modified CRABP II Protein

Following the acquisition of each MS scan, the three most abundant precursor ions were automatically subjected to CID-MS/MS. Following each MS/MS event, if product ions were observed at m/z values corresponding to the neutral loss of one or more dimethylsulfide groups from a singly, doubly or triply modified precursor ion with a charge state ranging from +1 to +5 (see Table 1), the most abundant of these product ions was automatically isolated and subjected to further dissociation by CID-MS^3.

Figure 2.5 shows the CID-MS/MS spectra acquired from peptide 1-13 (PNFSGNWKIIRSE), which contains two modifiable residues, i.e., the secondary amino group of the N-terminal proline residue and the ε-amino of the lysine residue Lys_8. Thus, it is expected that two singly modified peptides (i.e., $1\text{-}13^{Pro1}$ (where the superscript letter and number indicate the modified residue) and $1\text{-}13^{Lys8}$, with the same mass but different modification sites), and one doubly modified peptide ($1\text{-}13^{Pro1,Lys8}$) should be observed. Figures 2.5 A and 2.5 B show the product ion spectra obtained by CID-MS/MS of the triply charged $[1\text{-}13^{Lys8}+2H]^{3+}$ and $[1\text{-}13^{Pro1}+2H]^{3+}$ precursor ions from the peaks at approx. 19.8 min and 20.6 min in Figure 2.4. Both of these MS/MS spectra are identical, each giving rise to a single product ion via the exclusive loss of dimethylsulfide ($S(CH_3)_2$). Similar results were obtained by dissociation of the doubly charged ($[1\text{-}13^{Lys8}+H]^{2+}$ and $[1\text{-}13^{Pro1}+H]^{2+}$) precursor ions (shown in the Figures 2.5

C and 2.5 D). Notably, the presence of a ‘mobile’ proton in the triply charged precursor ions (the doubly charged precursor ions are in a ‘non-mobile’ charge state) did not affect the MS/MS fragmentation reaction involving the exclusive loss of $S(CH_3)_2$, consistent with previous studies demonstrating that the selective dissociation of sulfonium ion derivatized peptides occurs independently of the proton mobility of the precursor ion, i.e., that ionizing protons simply act as ‘spectators’ rather than participating in competing fragmentation reactions [261-263, 306, 324, 325].

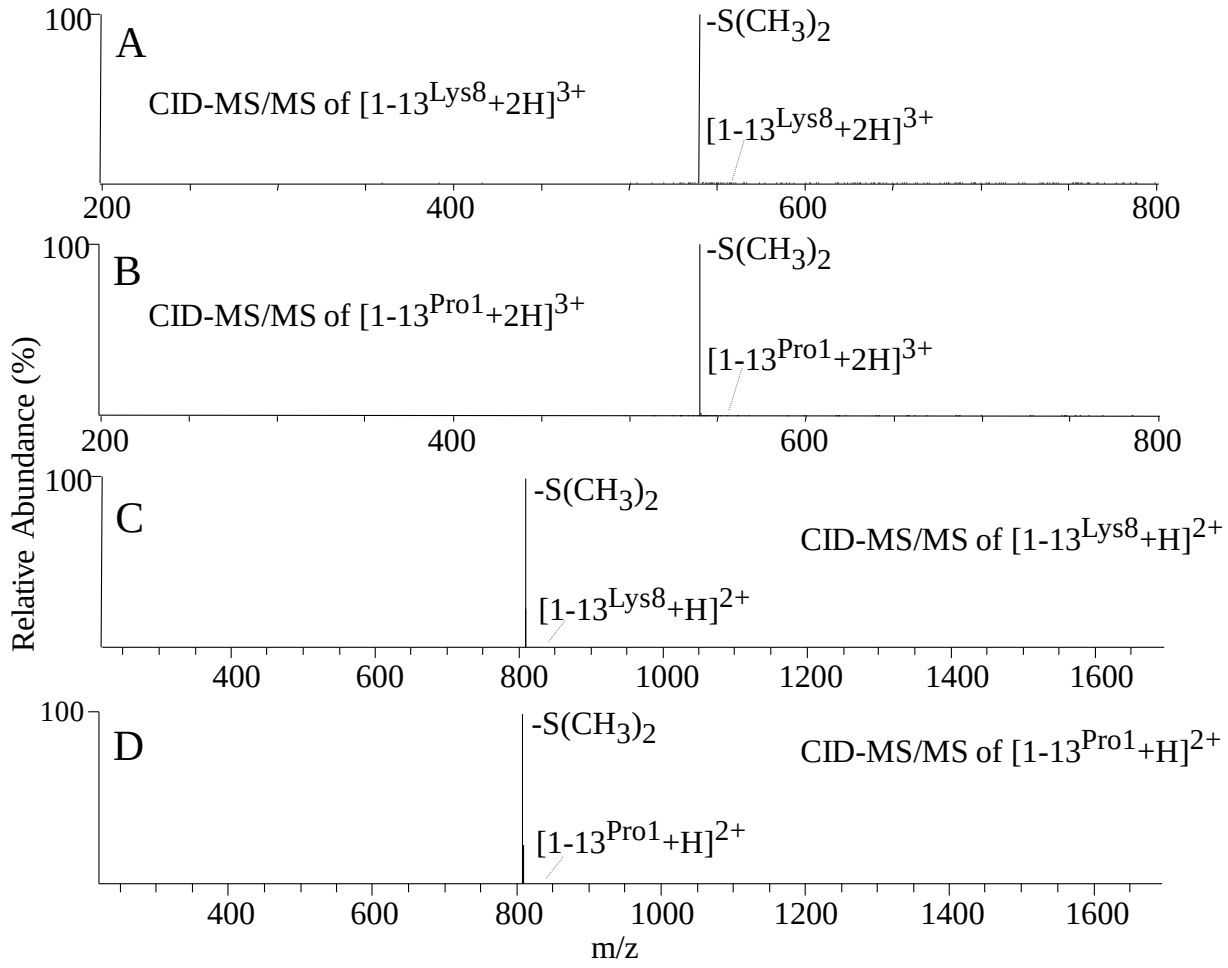

Figure 2.5 Ion trap mass spectrometry characterization of the isomeric DMBNHS singly modified CRABP II peptides, i.e., 1-13^{Lys8} and 1-13^{Pro1}. CID-MS/MS of the triply charged (A) [1-13^{Lys8}+2H]$^{3+}$ and (B) [1-13^{Pro1}+2H]$^{3+}$ precursor ions. CID-MS/MS of the doubly charged (C) [1-13^{Lys8}+H]$^{2+}$ and (D) [1-13^{Pro1}+H]$^{2+}$ precursor ions.

CID-MS^3 of the $[1\text{-}13^{Lys8}+2H\text{-}S(CH_3)_2]^{3+}$ and $[1\text{-}13^{Pro1}+2H\text{-}S(CH_3)_2]^{3+}$ product ions from Figures 2.5 A and 2.5 B gave rise to the spectra shown in Figures 2.6 A and 2.6 B, respectively. Interpretation of the spectra in Figure 2.6 A resulted in the assignment of a series of modified $y_6^{\dagger 2+}$, $y_7^{\dagger 2+}$, $y_8^{\dagger 2+}$, $y_9^{\dagger 2+}$, $y_{10}^{\dagger 2+}$, $y_{11}^{\dagger 2+}$ and $y_{12}^{\dagger 2+}$ and unmodified y_4, b_2 and b_3 product ions, where † indicates sequence ions containing one modified residue. These ions allowed the modification site to be located at the Lys_8 residue. In contrast, Figure 2.6 B contained a series of modified b-type product ions ($b_3^{\dagger}$, $b_5^{\dagger}$, $b_6^{\dagger}$, $b_7^{\dagger}$, $b_8^{\dagger}$, $b_8^{\dagger 2+}$, $b_{11}^{\dagger 3+}$ and $b_{12}^{\dagger 3+}$) and a series of unmodified y-type ions, indicating the site of the modification is localized to the Pro_1 residue.

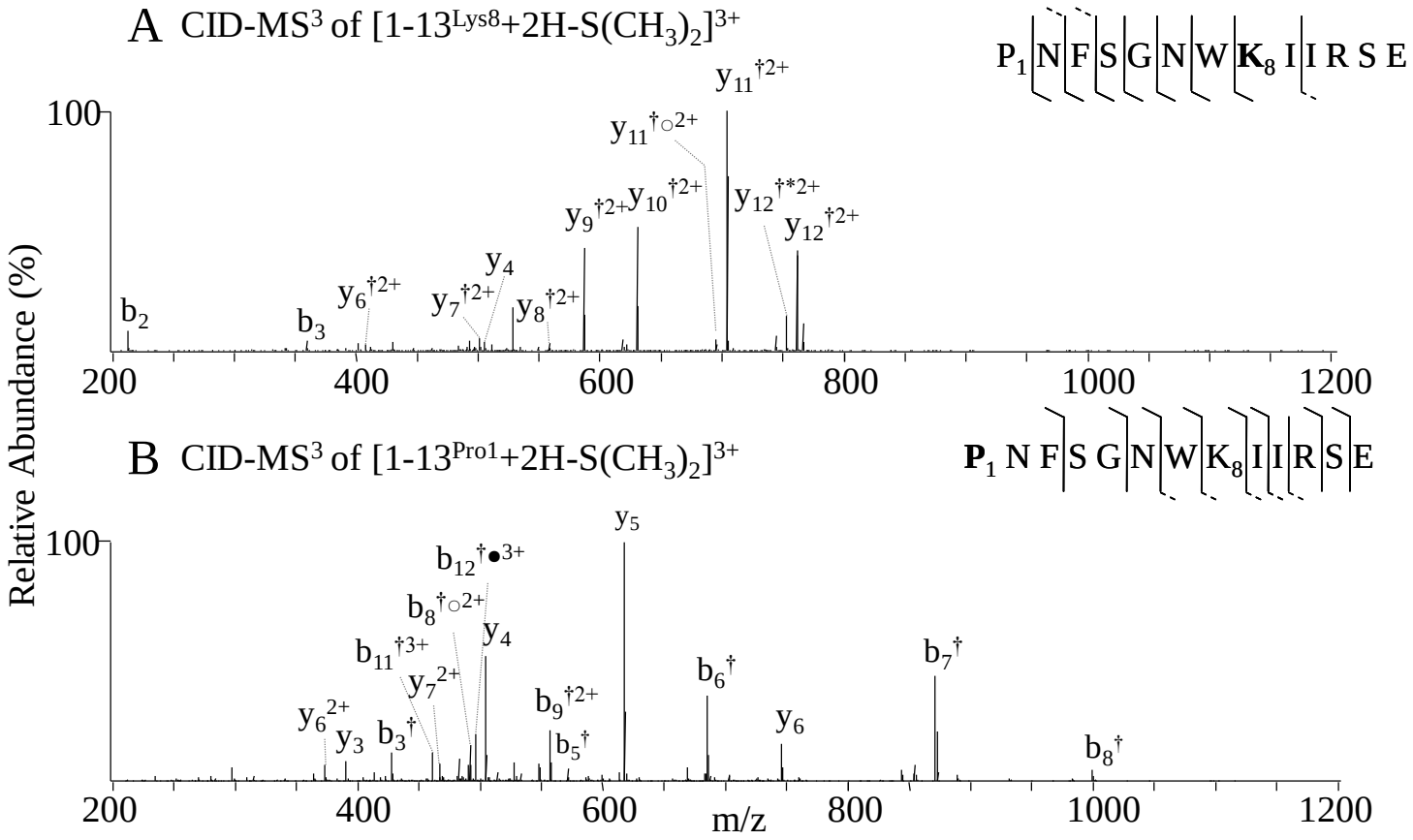

Figure 2.6 Ion trap mass spectrometry characterization of the isomeric DMBNHS singly modified CRABP II peptides, i.e., 1-13^{Lys8} and 1-13^{Pro1}. CID-MS^3 of (A) the [1-13^{Lys8}+2H-S(CH$_3$)$_2$]$^{3+}$ product ion from Figure 2.5 A, and (B) the [1-13^{Pro1}+2H-S(CH$_3$)$_2$]$^{3+}$ product ion from Figure 2.5 B. A superscript † indicates sequence ions containing one modified amino acid residue. A superscript * indicates the loss of NH_3. A superscript ○ indicates the loss of H_2O. A superscript ● indicates the addition of H_2O. A dashed line indicates an unmodified sequence ion was observed. A solid line indicates a sequence ion was observed with one modified amino acid.

Figure 2.7 A and 2.7 B show the CID-MS/MS product ion spectra obtained from the doubly modified ($1\text{-}13^{Pro1,\ Lys8}$) peptide, in its doubly (i.e., $[1\text{-}13^{Pro1,\ Lys8}]^{2+}$) and triply (i.e., $[1\text{-}13^{Pro1,Lys8}+H]^{3+}$) charged precursor ion charge states, respectively. In each case, two characteristic neutral loss product ions were observed, corresponding to the neutral losses of one and two $S(CH_3)_2$ groups, indicative of the presence of two modifications within the peptide. Notably, for both spectra, product ions corresponding to the neutral loss of two $S(CH_3)_2$ groups were significantly more abundant than those corresponding to the neutral loss of only one $S(CH_3)_2$ group. Thus, it was these product ions that were automatically selected for further dissociation by MS^3. As shown in Figure 2.7 C, MS^3 dissociation of the $[1\text{-}13^{Pro1,Lys8}\text{-}2S(CH_3)_2+H]^{3+}$ product ion from Figure 2.7 B allowed the expected modification sites at the Pro_1 and Lys_8 residues to be readily assigned.

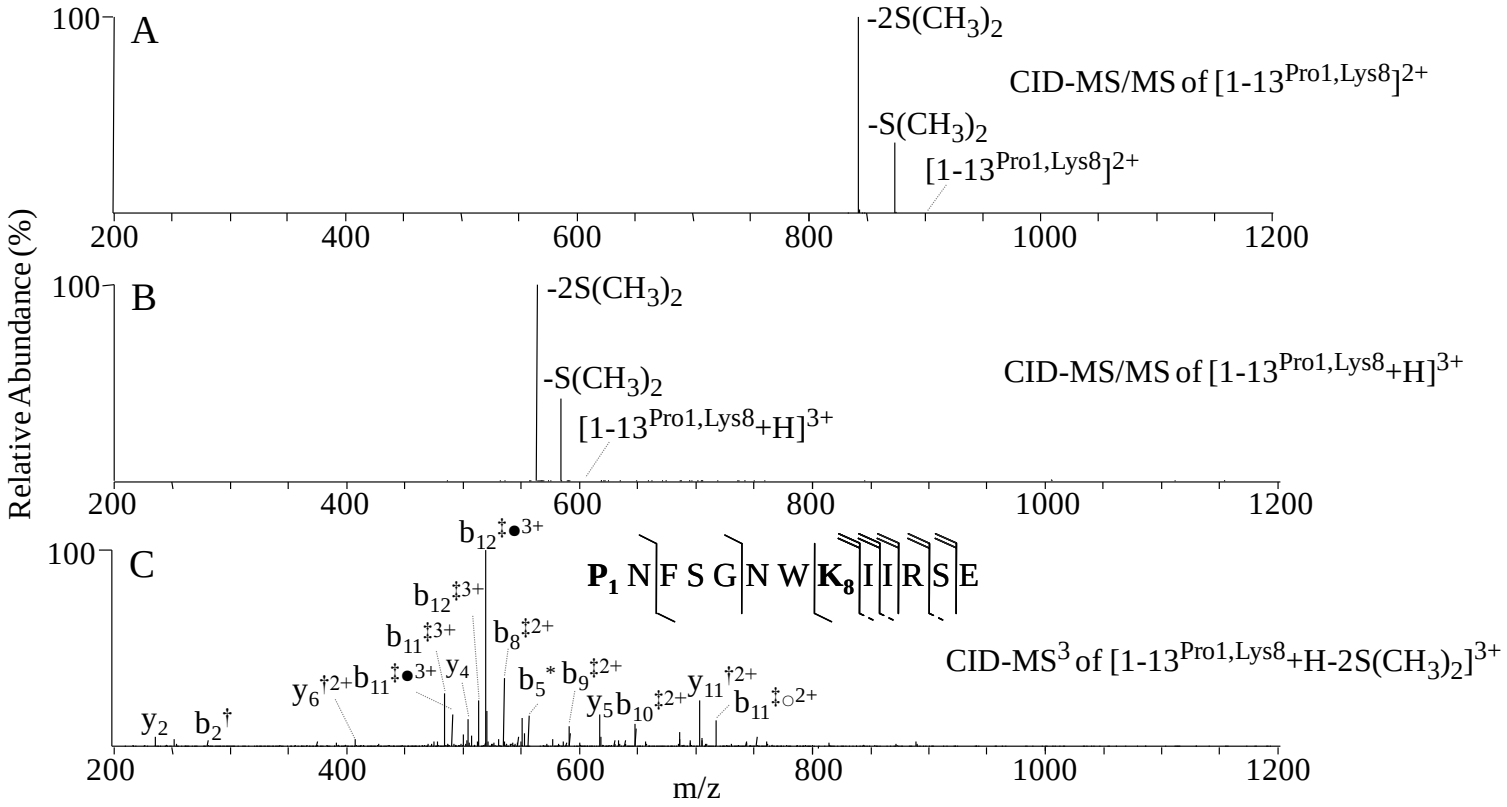

Figure 2.7 Ion trap mass spectrometry characterization of the DMBNHS doubly modified CRABP II peptide, 1-13^{Pro1,Lys8}. CID-MS/MS of (A) the doubly charged ([1-13^{Pro1,Lys8}]$^{2+}$) and (B) triply charged ([1-13^{Pro1,Lys8}+H]$^{3+}$) precursor ions. CID-MS^3 of (C) the [1-13^{Pro1,Lys8}+H-2S(CH$_3$)$_2$]$^{3+}$ product ion from panel B. A superscript † indicates sequence ions containing one modified amino acid residue. A superscript ‡ indicates sequence ions containing two modified amino acid residues. A superscript ○ indicates the loss of H_2O. A superscript ● indicates the addition of H_2O. A dashed line indicates an unmodified sequence ion was observed. A single solid line indicates a sequence ion was observed with one modified amino acid. A double solid line indicates a sequence ion was observed with two modified amino acids.

It is expected that the proton affinity of the iminohydrofuran containing functional group that is formed following the loss of $S(CH_3)_2$ from a DMBNHS sulfonium ion modified peptide would be higher than that of an unmodified amino group. If so, this could potentially result in a decreased 'proton mobility' within the MS/MS product ion, and could thereby limit the extent of sequence information that is obtained following MS^3 for determination of the identity of the peptide and localization of the site of the modification, compared to that obtained from an unmodified peptide. Calculation of the proton affinity of the simplest model for the iminohydrofuran containing functional group (i.e., N-methyl iminohydrofuran), at the MP2/6-311+G(2d,p)//B3LYP/6-311+G(d,p) level of theory, resulted in a proton affinity of 228.2 kcal mol^{-1} (see Table 2.2). This value is 17.2 kcal mol^{-1} higher than that calculated for the simplest model for lysine (methylamine, 211.0 kcal mol^{-1}), and is intermediate between the calculated values for the simplest models for histidine (4-methyl imizadole, 223.5 kcal mol^{-1}) and arginine (N-methyl guanidine, 234.2 kcal mol^{-1}), at the same level of theory. Despite this result, a comparison of the MS^3 product ion spectra obtained from the modified 1-13 peptide ions (e.g., the $[1\text{-}13^{Lys8}\text{-}S(CH_3)_2+2H]^{3+}$ and $[1\text{-}13^{Pro1}\text{-}S(CH_3)_2+2H]^{3+}$ ions in Figure 2.6 A and 2.6 B, and the $[1\text{-}13^{Pro1,\ Lys8}\text{-}2S(CH_3)_2+H]^{3+}$ ion in Figure 2.7 C, with the MS/MS spectra of the unmodified 1-13 peptide in the same charge state (i.e., the $[1\text{-}13+3H]^{3+}$ ion) (see Figure 2.8), revealed that the sequence coverage obtained following MS^3 of the modified peptide ions was equivalent to, or greater than, that of the unmodified MS/MS spectrum. Interestingly, the MS^3

spectrum obtained from the modified $[1\text{-}13^{Lys8}\text{-}S(CH_3)_2+2H]^{3+}$ product ion (Lys_8 modified) was very similar to that obtained by MS/MS of the unmodified $[1\text{-}13+3H]^{3+}$ ion. This is consistent with the expected sites of proton localization in both peptides being at the arginine, lysine (or iminohydrofuran) and N-terminal residues (considered to be 'non-mobile', 'partially mobile' and 'mobile', respectively). In contrast, the MS^3 spectra from the modified $[1\text{-}13^{Pro1}\text{-}S(CH_3)_2+2H]^{3+}$ product ion (Pro_1 modified) and the $[1\text{-}13^{Pro1,Lys8}\text{-}2S(CH_3)_2+H]^{3+}$ product ion (Pro_1 and Lys_8 modified) were substantially different from the MS/MS spectrum from the unmodified peptide, presumably due to differences in the site(s) of protonation or the decreased proton mobility of the N-terminal within these peptides (a protonated iminohydrofuran moiety located at the N-terminal residue of the modified peptide would be expected to result in a 'partially mobile' rather than 'mobile' proton).

Table 2.2 Calculated proton affinities (MP2/6-311+G(2d,p)//B3LYP/6-311+G(d,p) level of theory) for the model side chain functional groups of lysine, histidine and arginine, and the methyl iminohydrofuran side chain moiety formed via the loss of dimethylsulfide from DMBNHS sulfonium ion derivatized peptides.

	E_{total} (Hartree)	ZPVE (kcal mol^{-1})	ZPVE (Hartree)	E_{total}+ZPVE (Hartree)	E_{vib} (kcal mol^{-1})	E_{vib} (Hartree)	Calculated Proton Affinity (kcal mol^{-1})	NIST Proton affinity (kcal mol^{-1}) [a]
Methylamine (Lys)								
Protonated	-95.9661019	49.66893	0.079152538	-95.88694936	50.062	0.000626397	211.0	214.9
Neutral	-95.6121272	40.02914	0.063790543	-95.54833666	40.411	0.000608533		
4-methyl imizadole (His)								
Protonated	-265.264969	70.55813	0.112441622	-265.1525274	72.201	0.002618082	223.5	227.7
Neutral	-264.8923635	61.70744	0.098337139	-264.7940264	63.331	0.00258731		
N-methyl guanidine (Arg)								
Protonated	-244.4941467	72.88049	0.116142541	-244.3780042	75.466	0.004120276	234.2	
Neutral	-244.1063413	65.19224	0.103890526	-244.0024508	67.156	0.003129453		
N-methyl iminohydrofuran								
Protonated	-325.5052987	95.34483	0.151941773	-325.3533569	98.159	0.004484669	228.2	
Neutral	-325.1247869	86.22782	0.137412882	-324.987374	88.988	0.00439863		

[a] Cited from: Hunter, E.P.; Lias, S.G. Evaluated Gas Phase Basicities and Proton Affinities of Molecules: An Update. *J. Phys. Chem. Ref. Data*, 1998, *27*, 413-656.

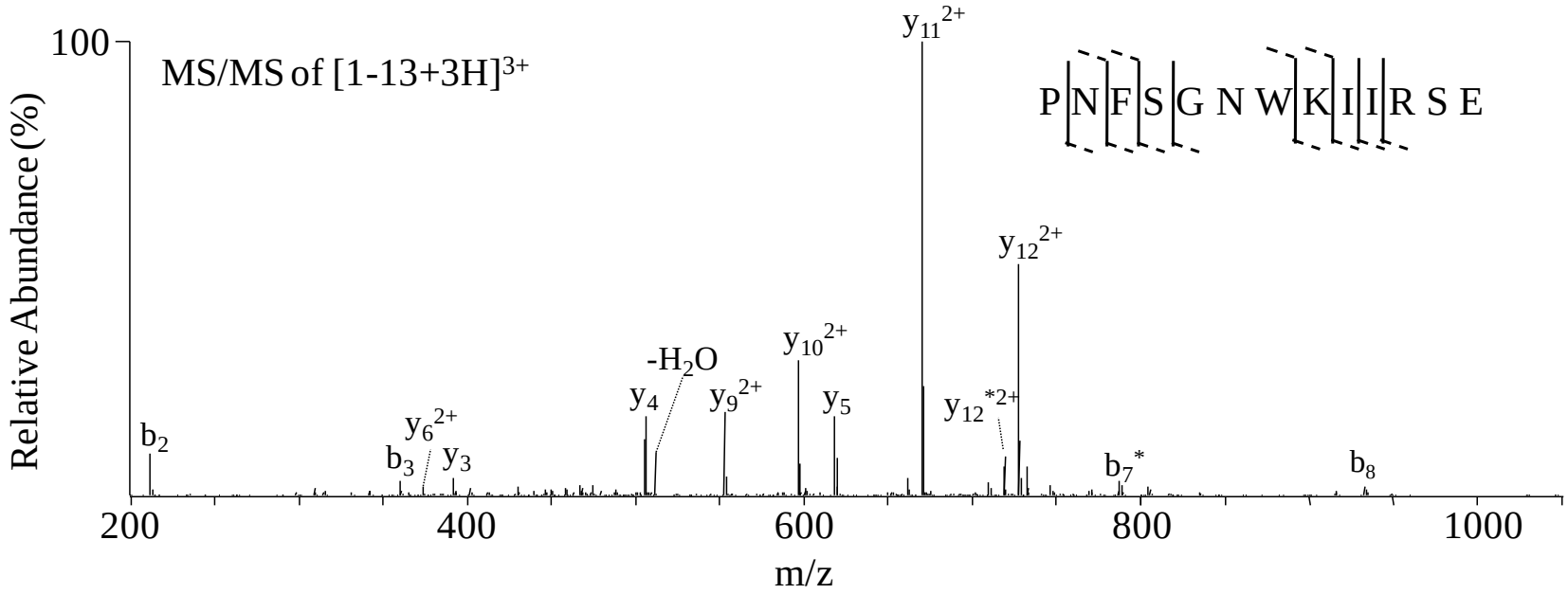

Figure 2.8 CID-MS/MS of the triply protonated unmodified CRABP II peptide 1-13, $[1\text{-}13+3H]^{3+}$. A dashed line indicates an unmodified sequence ion was observed.

Peptide 1-17 (PNFSGNWKIIRSENFEE) shares a similar sequence to peptide 1-13 and contains the same two modifiable residues, i.e., the secondary amino group of the N-terminal proline residue Pro_1 and the ε-amino of the lysine residue Lys_8. Thus, it is expected that peptide 1-17 would give similar chromatographic pattern and DMBNHS modification products. Figure 2.4 shows two peaks corresponding to isomeric singly modified peptide 1-17, with the one eluted earlier at approx. 21.7 min identified as $1\text{-}17^{Lys8}$ and the one eluted later at approx. 23.2 min identified to be $1\text{-}17^{Pro1}$, which is consistent with elution order of $1\text{-}13^{Lys8}$ and $1\text{-}13^{Pro1}$. CID-MS/MS spectra of $[1\text{-}17^{Lys8}+2H]^{3+}$ (Figure 2.9 A) and $[1\text{-}17^{Pro1}+2H]^{3+}$ (Figure 2.9 B) both show a single product ion corresponding to the exclusive neutral loss of $S(CH_3)_2$. Further fragmentation of the neutral loss product ions, i.e., $[1\text{-}17^{Lys8}+2H\text{-}S(CH_3)_2]^{3+}$ and $[1\text{-}17^{Pro1}+2H\text{-}S(CH_3)_2]^{3+}$, in CID-$MS^3$ gave a series of sequence ions as shown in Figure 2.9 C and 2.9 D, respectively. Interpretation of these two spectra allowed the assignment of the modification site to be Lys_8 for the earlier eluted peptide and Pro_1 for the later one. Interestingly, comparison of the MS^3 spectra of $[1\text{-}17^{Lys8}+2H\text{-}S(CH_3)_2]^{3+}$ with $[1\text{-}13^{Lys8}+2H\text{-}S(CH_3)_2]^{3+}$ revealed that the observed sequence ions were very similar, and the MS^3 spectrum of $[1\text{-}17^{Pro1}+2H\text{-}S(CH_3)_2]^{3+}$ was comparable to $[1\text{-}13^{Pro1}+2H\text{-}S(CH_3)_2]^{3+}$. This similarity again confirmed that $1\text{-}17^{Lys8}$ and $1\text{-}13^{Lys8}$ have the same modification site at Lys_8, while $1\text{-}17^{Pro1}$ and $1\text{-}13^{Pro1}$ have the same modification site at Pro_1.

Figure 2.10 A shows a CID-MS/MS product ions spectrum of the doubly modified 1-17, i.e., $1\text{-}17^{Pro1,Lys8}$. Again, the characteristic neural loss of one and two $S(CH_3)_2$ was observed. CID-MS^3 of the neutral loss product ion $[1\text{-}17^{Pro1,Lys8}+H\text{-}2S(CH_3)_2]^{3+}$ (Figure 2.9 B) allowed the modification sites and peptide sequence to be characterized, and showed similar sequence coverage as MS^3 of $[1\text{-}13^{Pro1,\ Lys8}+H\text{-}2S(CH_3)_2]^{3+}$.

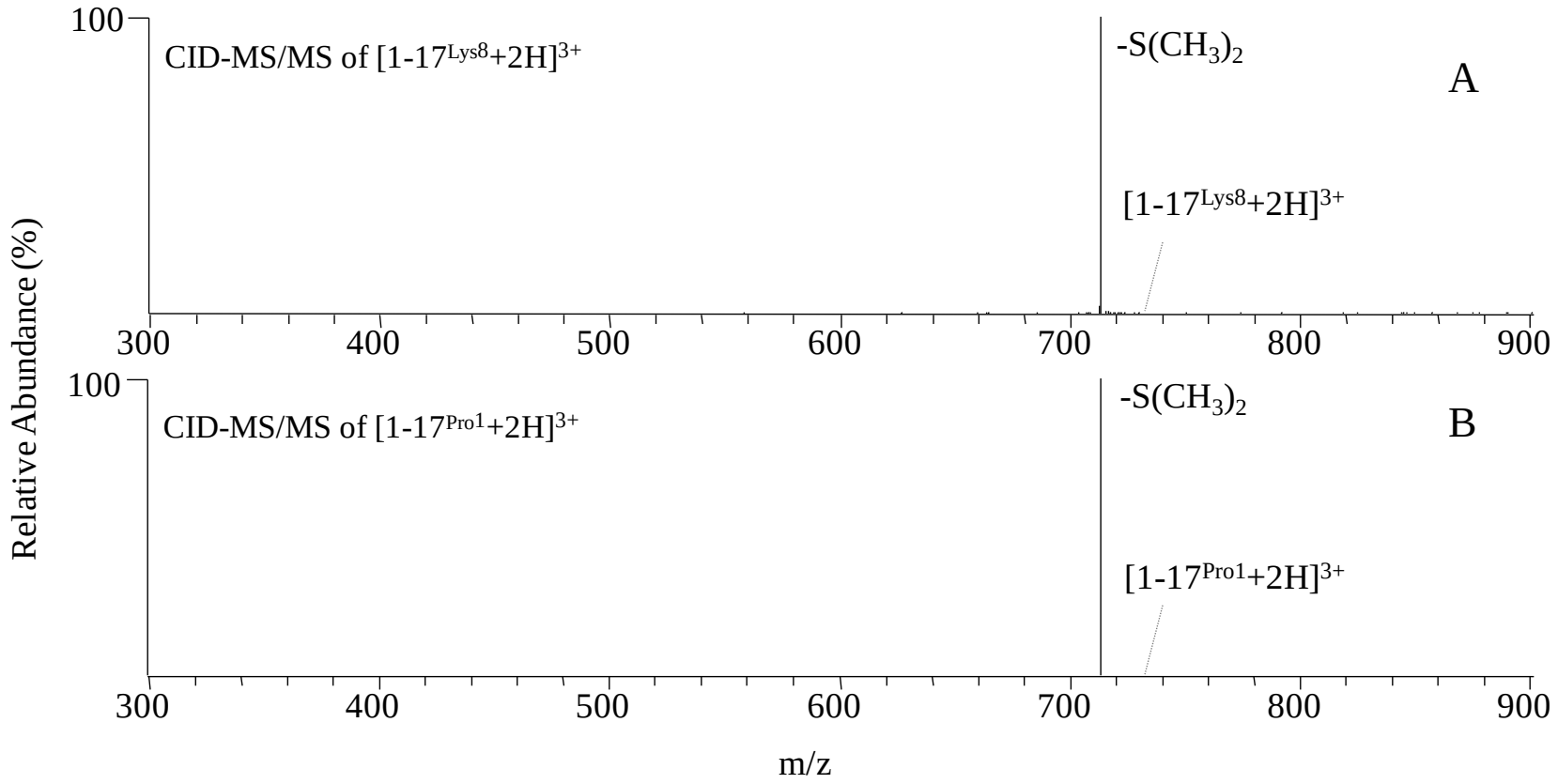

Figure 2.9 Ion trap mass spectrometry characterization of the isomeric DMBNHS singly modified CRABP II peptides, 1-17^{Lys8} and 1-17^{Pro1}. CID-MS/MS of the triply charged (A) [1-17^{Lys8}+2H]$^{3+}$ and (B) [1-17^{Pro_1}+2H]$^{3+}$ precursor ions. CID-MS^3 of (C) the [1-17^{Lys8}+2H-S(CH$_3$)$_2$]$^{3+}$ product ion from panel A, and (D) the [1-17^{Pro1}+2H-S(CH$_3$)$_2$]$^{3+}$ product ion from panel B. A superscript † indicates sequence ions containing one modified amino acid residue. A superscript * indicates the loss of NH_3. A superscript ○ indicates the loss of H_2O. A superscript ● indicates the addition of H_2O. A dashed line indicates an unmodified sequence ion was observed. A solid line indicates a sequence ion was observed with one modified amino acid.

Figure 2.9 (cont'd)

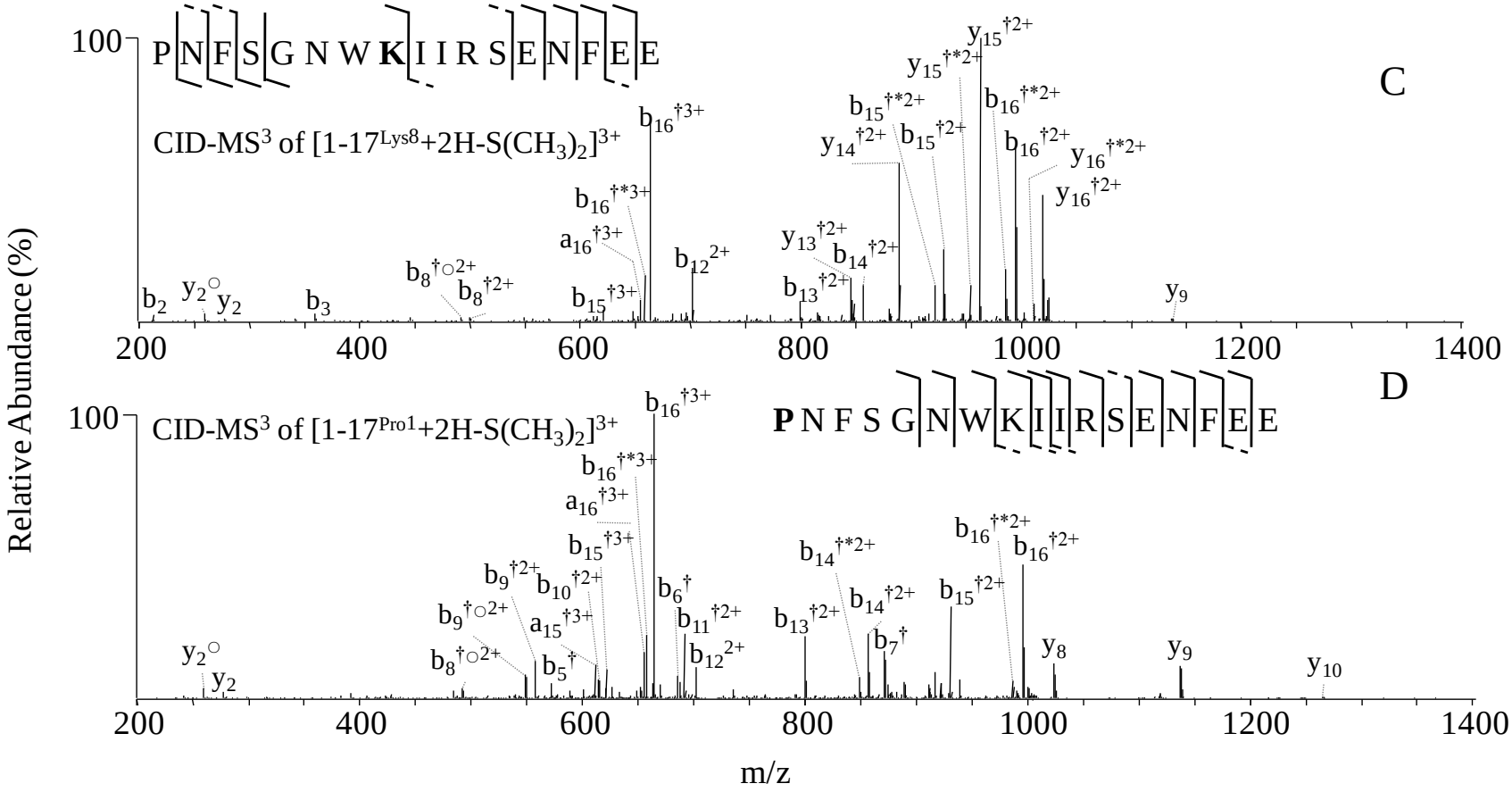

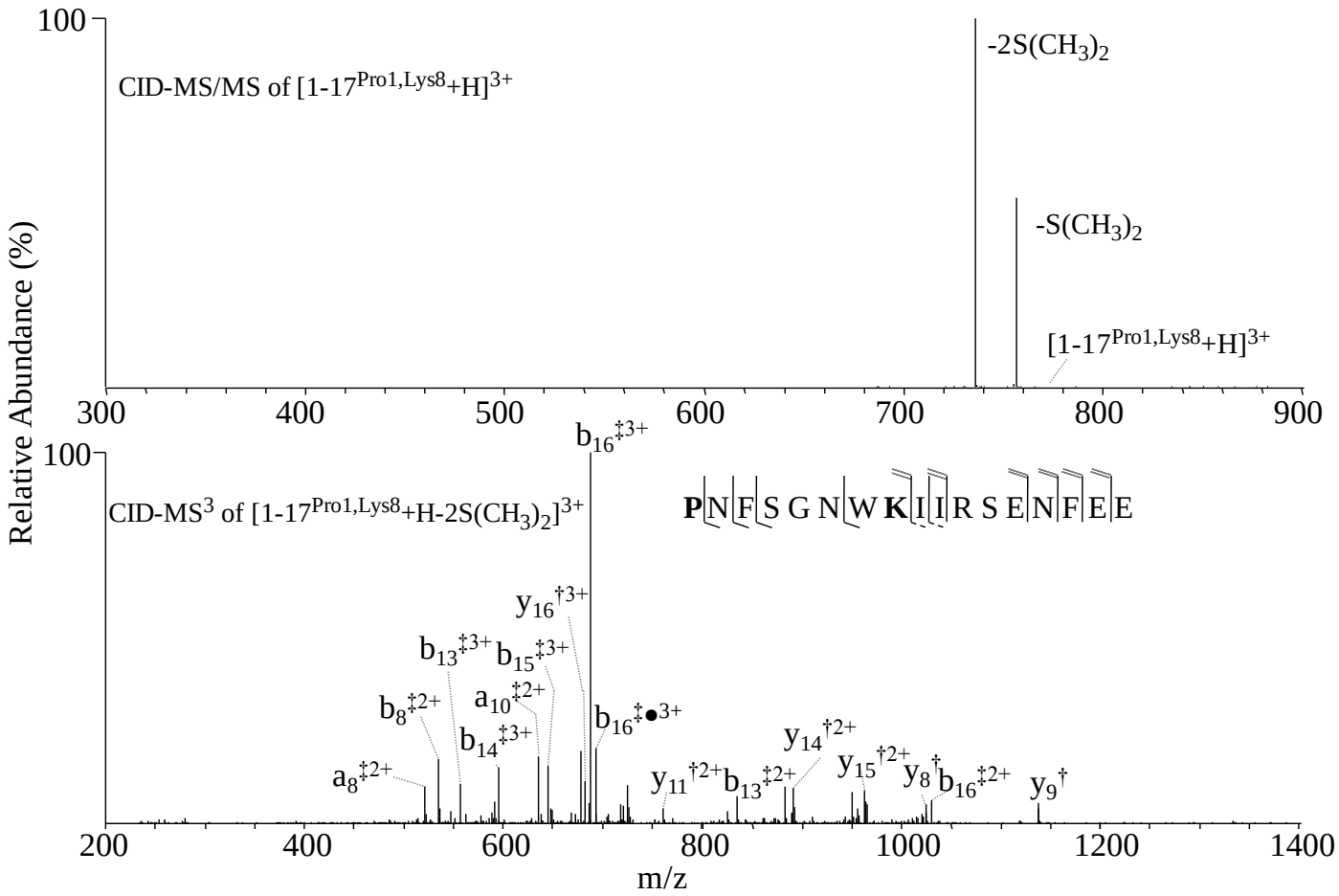

Figure 2.10 Ion trap mass spectrometry characterization of the DMBNHS doubly modified CRABP II peptide, 1-17^{Pro1,Lys8}. CID-MS/MS of (A) triply charged ([1-17^{Pro1,Lys8}+H]$^{3+}$) precursor ions. CID-MS^3 of (B) the [1-17^{Pro1,Lys8}+H-2S(CH$_3$)$_2$]$^{3+}$ product ion from panel A. A superscript † indicates sequence ions containing one modified amino acid residue. A superscript ‡ indicates sequence ions containing two modified amino acid residues. A superscript ○ indicates the loss of H_2O. A superscript ● indicates the addition of H_2O. A dashed line indicates an unmodified sequence ion was observed. A single solid line indicates a sequence ion was observed with one modified amino acid. A double solid line indicates a sequence ion was observed with two modified amino acids.

The results obtained following CID-MS/MS and -MS^3 of the modified forms of peptide 18-42, (LLKVLGVNVMLRKIAVAAASKPAVE) containing three lysine residues (resulting in the potential formation of three singly modified peptides (18-42^{Lys20}, 18-42^{Lys30} and 18-42^{Lys38}), three doubly modified peptides (18-$42^{Lys20, Lys30}$, 18-$42^{Lys20, Lys38}$ and 18-$42^{Lys30, Lys38}$) and one triply modified peptide (18-$42^{Lys20, Lys30, Lys38}$), further demonstrates the utility of the sulfonium ion derivatization approach for the 'targeted' identification and characterization of modified peptide ions. As shown in Figure 2.4, two singly modified forms of the 18-42 peptides were observed. As expected, CID-MS/MS of the triply charged $[18\text{-}42^{Lys38}+2H]^{3+}$ and $[18\text{-}42^{Lys30}+2H]^{3+}$ precursor ions were identical, each giving rise to the exclusive neutral loss of a single $S(CH_3)_2$ group (Figure 2.11 A and 2.11 B). By analyzing the MS^3 spectra obtained by dissociation of the $[18\text{-}42^{Lys38}+2H\text{-}S(CH_3)_2]^{3+}$ and $[18\text{-}42^{Lys30}+2H\text{-}S(CH_3)_2]^{3+}$ product ions, the modification site was located on the Lys_{38} residue for the 18-42^{Lys38} form of the peptide (Figure 2.11 C), and on the Lys_{30} residue for the 18-42^{Lys30} form of the peptide (Figure 2.11 D). No evidence was found for a form of the 18-42 peptide that was singly modified at the Lys_{20} residue, suggesting that this residue was less reactive to the DMBNHS reagent (i.e., less solvent accessible) compared to the adjacent Lys_{30} and Lys_{38} residues (see below for further discussion).

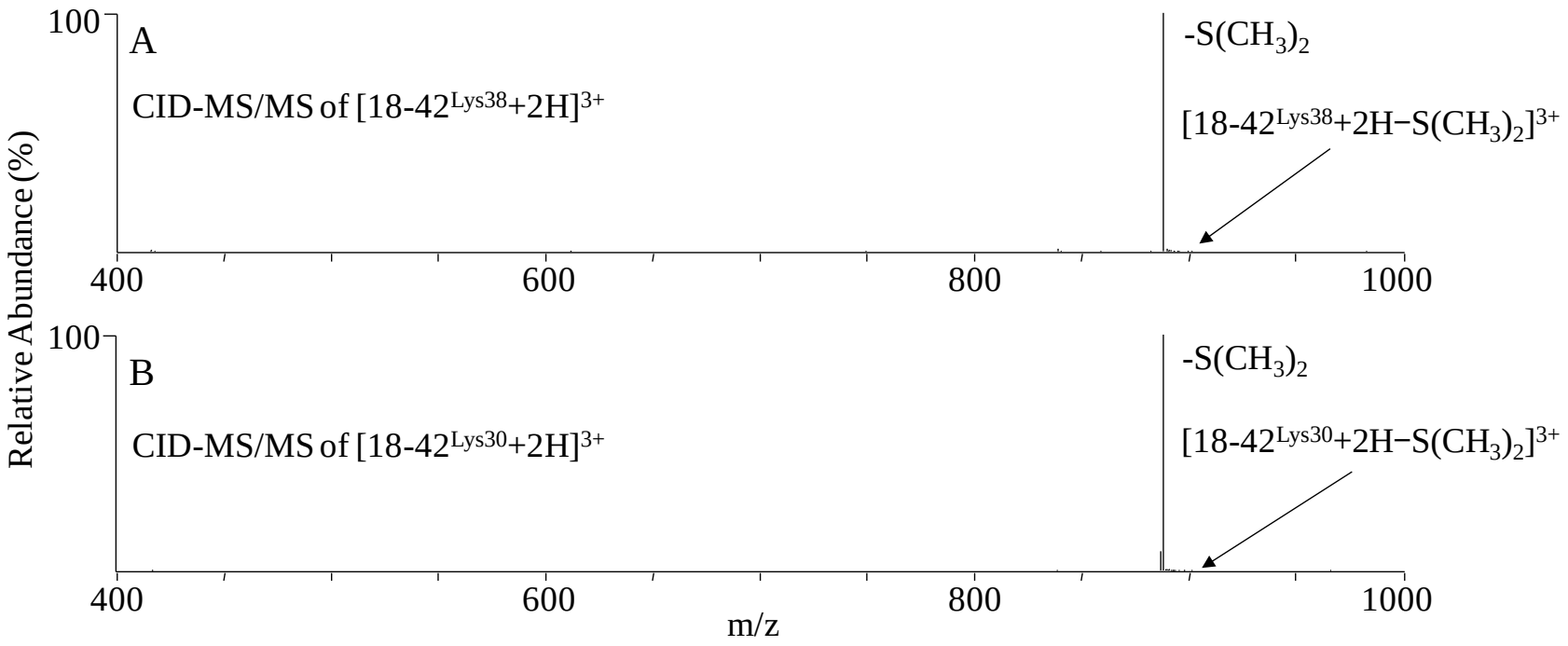

Figure 2.11 Ion trap mass spectrometry characterization of the isomeric DMBNHS singly modified CRABP II peptides, 18-42^{Lys38} and 18-42^{Lys30}. CID-MS/MS of the triply charged (A) [18-42^{Lys38}+2H]$^{3+}$ and (B) [18-42^{Lys30}+2H]$^{3+}$ precursor ions. (C) CID-MS^3 of the [18-42^{Lys38}+2H-S(CH$_3$)$_2$]$^{3+}$ product ion from panel A. (D) CID-MS^3 of the [18-42^{Lys30}+2H-S(CH$_3$)$_2$]$^{3+}$ product ion from panel B. A superscript † indicates sequence ions containing one modified amino acid residue. A dashed line indicates an unmodified sequence ion was observed. A single solid line indicates a sequence ion was observed with one modified amino acid.

Figure 2.11 (cont'd)

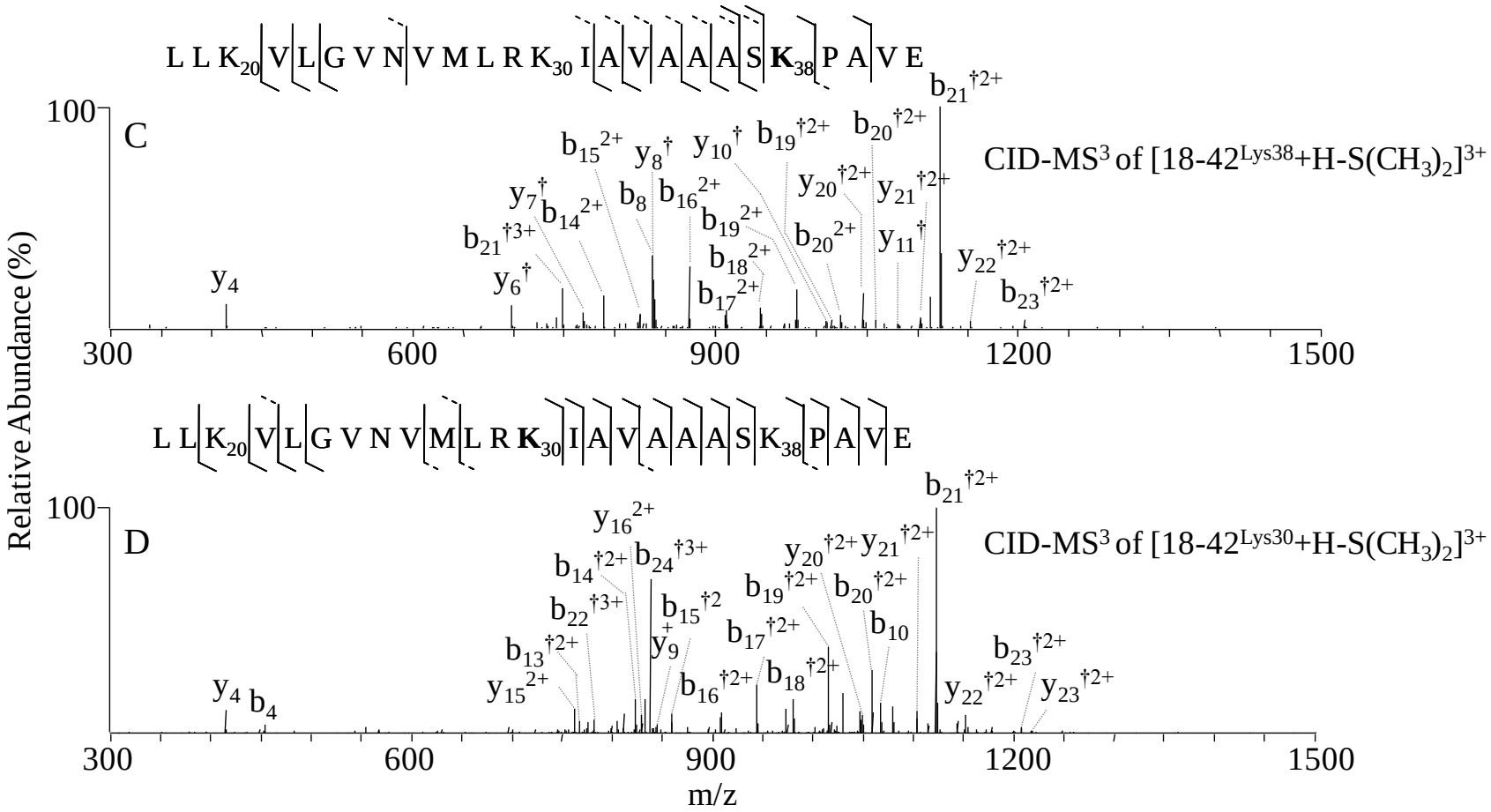

CID-MS/MS of the quadruply charged precursor ions of the three doubly modified 18-42 peptide ions (the 18-42^{Lys20,Lys38} peak was separately resolved while the 18-42^{Lys20,Lys30} and 18-42^{Lys30,Lys38} peaks were closely eluting) each resulted in the exclusive loss of up to two $S(CH_3)_2$ groups, similar to that described above for the 1-13 and 1-17 peptides, indicating the presence of two modifications within the peptides (Figure 2.12). Once again, the loss of two $S(CH_3)_2$ groups was the dominant fragmentation pathway. The MS^3 spectra shown in Figure 2.13 were used to assign the sites of modification to the Lys_{20} and Lys_{38} residues for the 18-42^{Lys20,Lys38} peptide (Figure 2.13 A), the Lys_{20} and Lys_{30} residues for the 18-42^{Lys20,Lys30} peptide (Figure 2.13 B), and the Lys_{30} and Lys_{38} residues for the 18-42^{Lys30,Lys38} peptide (Figure 2.13 C). Because the 18-42^{Lys20,Lys30} and 18-42^{Lys30,Lys38} peptides were not well resolved, several of the ions from the 18-42^{Lys20,Lys30} peptide (e.g., $b_{16}^{\ddagger 2+}$, $b_{17}^{\ddagger 2+}$, and $b_{18}^{\ddagger 2+}$) were also observed in the spectrum from the 18-42^{Lys30,Lys38} peptide.

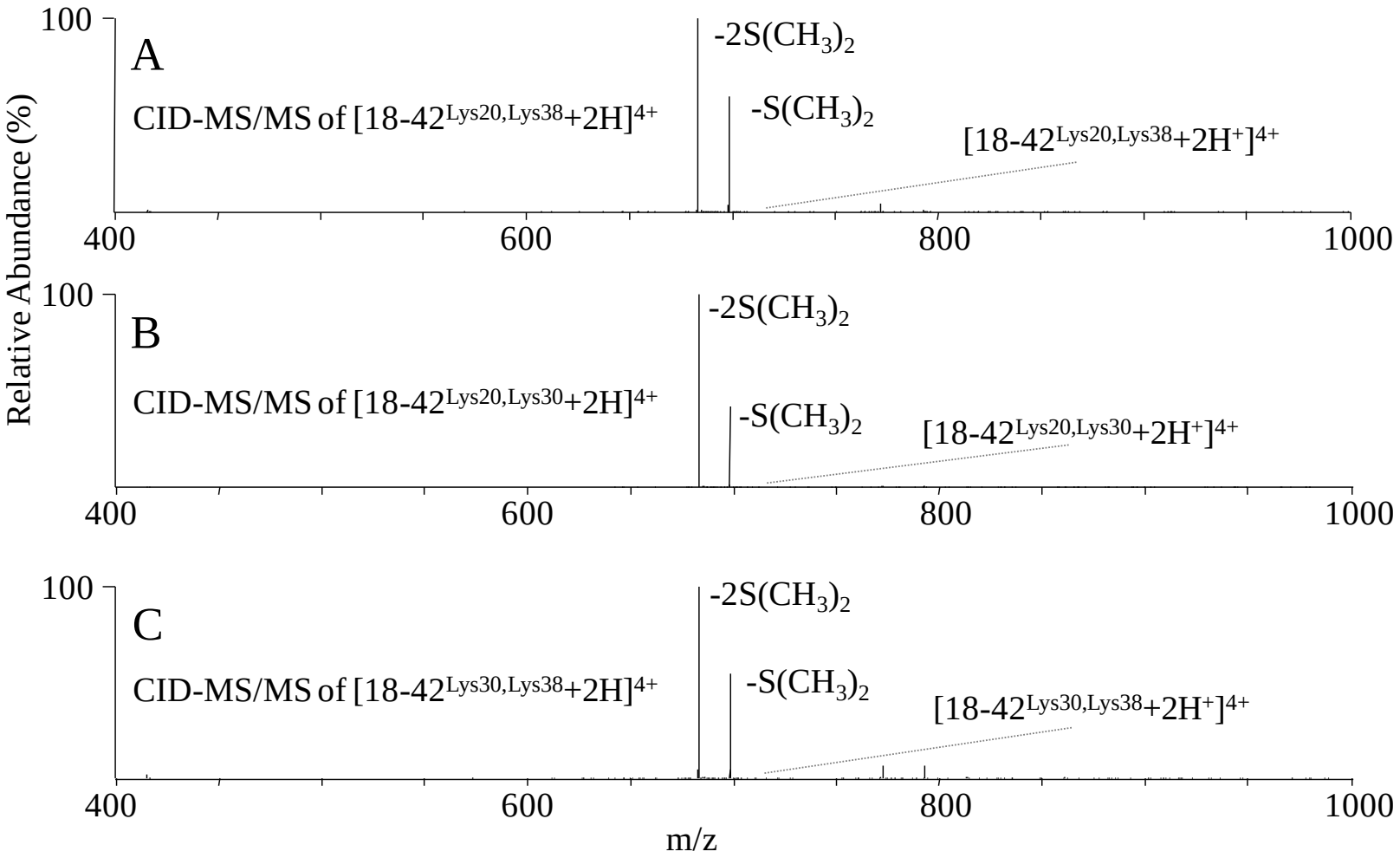

Figure 2.12 CID-MS/MS of the isomeric DMBNHS doubly modified CRABP II peptides, 18-42^{Lys20,Lys38}, 18-42^{Lys20,Lys30}, and 18-42^{Lys30,Lys38}. CID-MS/MS of the quadruply charged (A) [18-42$^{Lys20,\ Lys38}$+2H]$^{4+}$, (B) [18-42^{Lys20,Lys30}+2H]$^{4+}$, and (C) [18-42^{Lys30,Lys38}+2H]$^{4+}$ precursor ions.

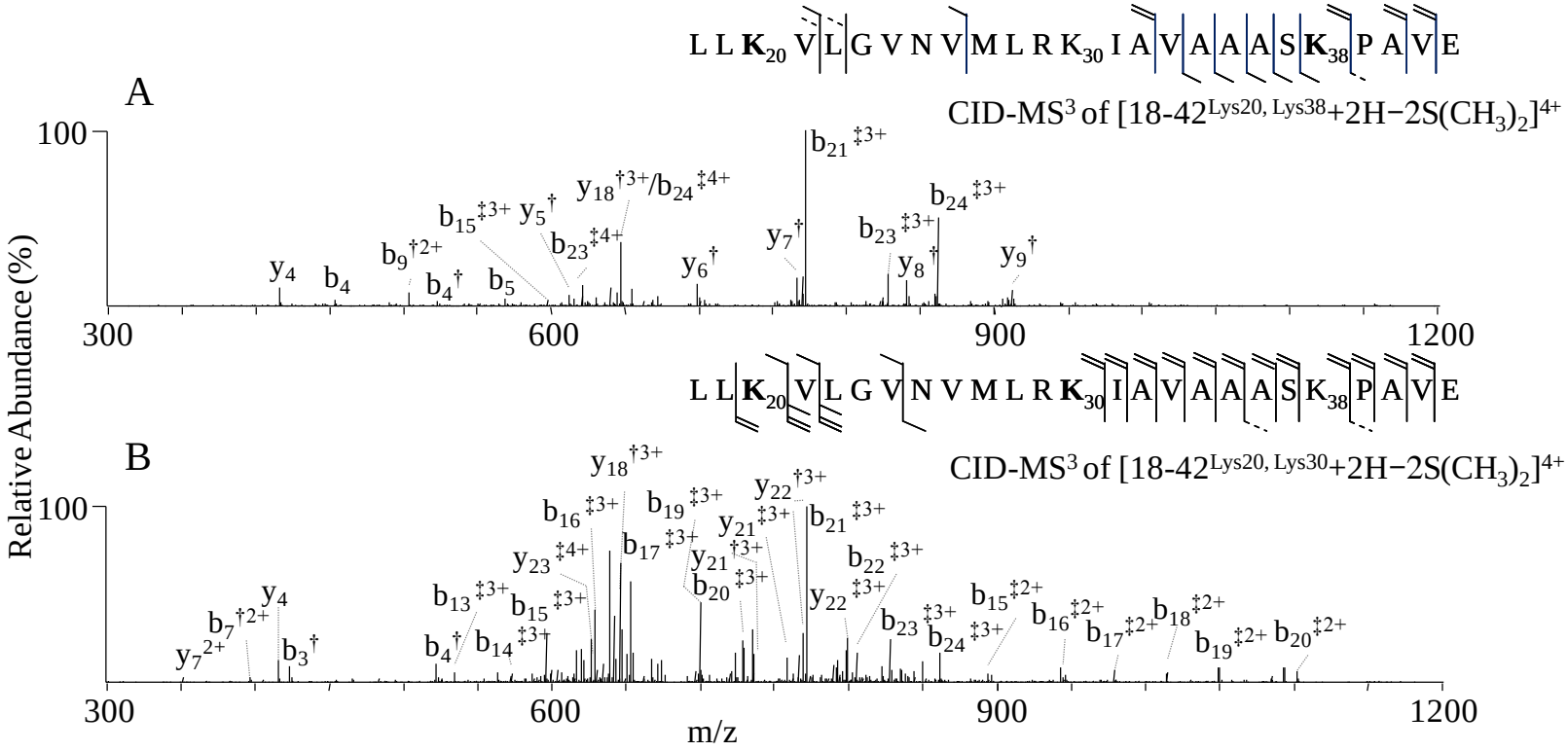

Figure 2.13 CID-MS^3 of the quadruply charged product ions formed by CID-MS/MS of the isomeric DMBNHS doubly modified CRABP II peptides, 18-42^{Lys20,Lys38}, 18-42^{Lys20,Lys30}, and 18-42^{Lys30,Lys38}. (A) CID-MS^3 of the [18-42^{Lys20,Lys38}+2H-2S(CH$_3$)$_2$]$^{4+}$ product ion from Figure 2.9 A. (B) CID-MS^3 of the [18-42^{Lys20,Lys30}+2H-2S(CH$_3$)$_2$]$^{4+}$ product ion from Figure 2.9 B. (C) CID-MS^3 of the [18-42^{Lys30,Lys38}+2H-2S(CH$_3$)$_2$]$^{4+}$ product ion from Figure 2.9 C. A superscript † indicates sequence ions containing one modified amino acid residue. A superscript ‡ indicates sequence ions containing two modified amino acid residues. A dashed line indicates an unmodified sequence ion was observed. A single solid line indicates a sequence ion was observed with one modified amino acid. A double solid line indicates a sequence ion was observed with two modified amino acids.

Figure 2.13 (cont'd)

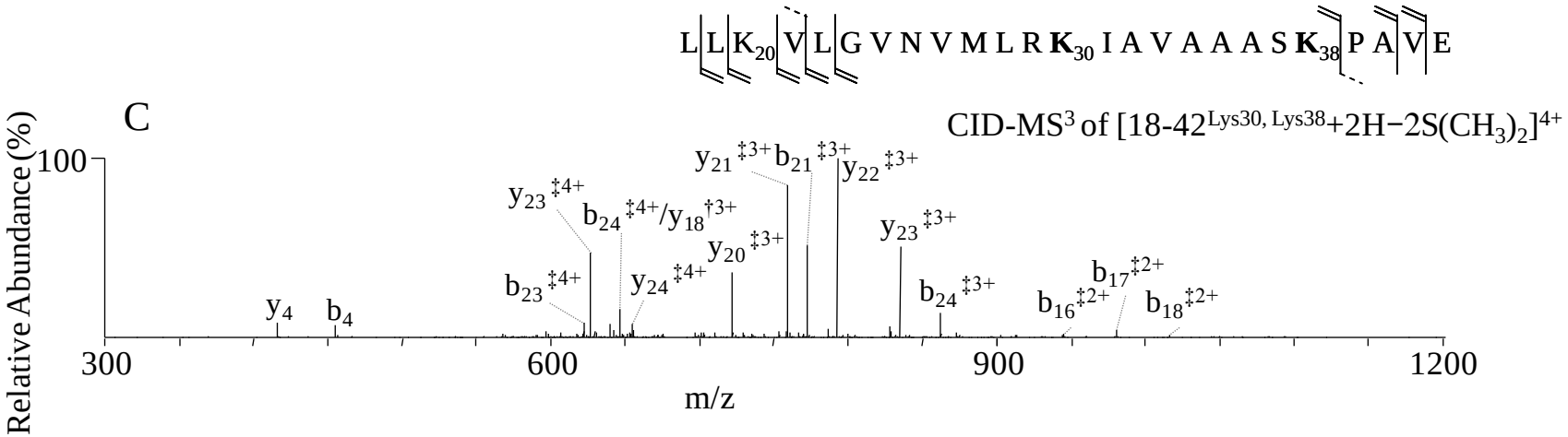

Finally, Figure 2.14 shows the CID-MS/MS and -MS^3 spectra of the quadruply charged precursor ion of the triply modified 18-42^{Lys20,Lys30,Lys38} peptide. MS/MS resulted in the characteristic neutral loss of up to three $S(CH_3)_2$ groups, indicating the presence of three modifications within the peptide, while MS^3 confirmed the identity of the peptide sequence and localization of the modifications on each of the three lysine residues, Lys_{20}, Lys_{30} and Lys_{38}.

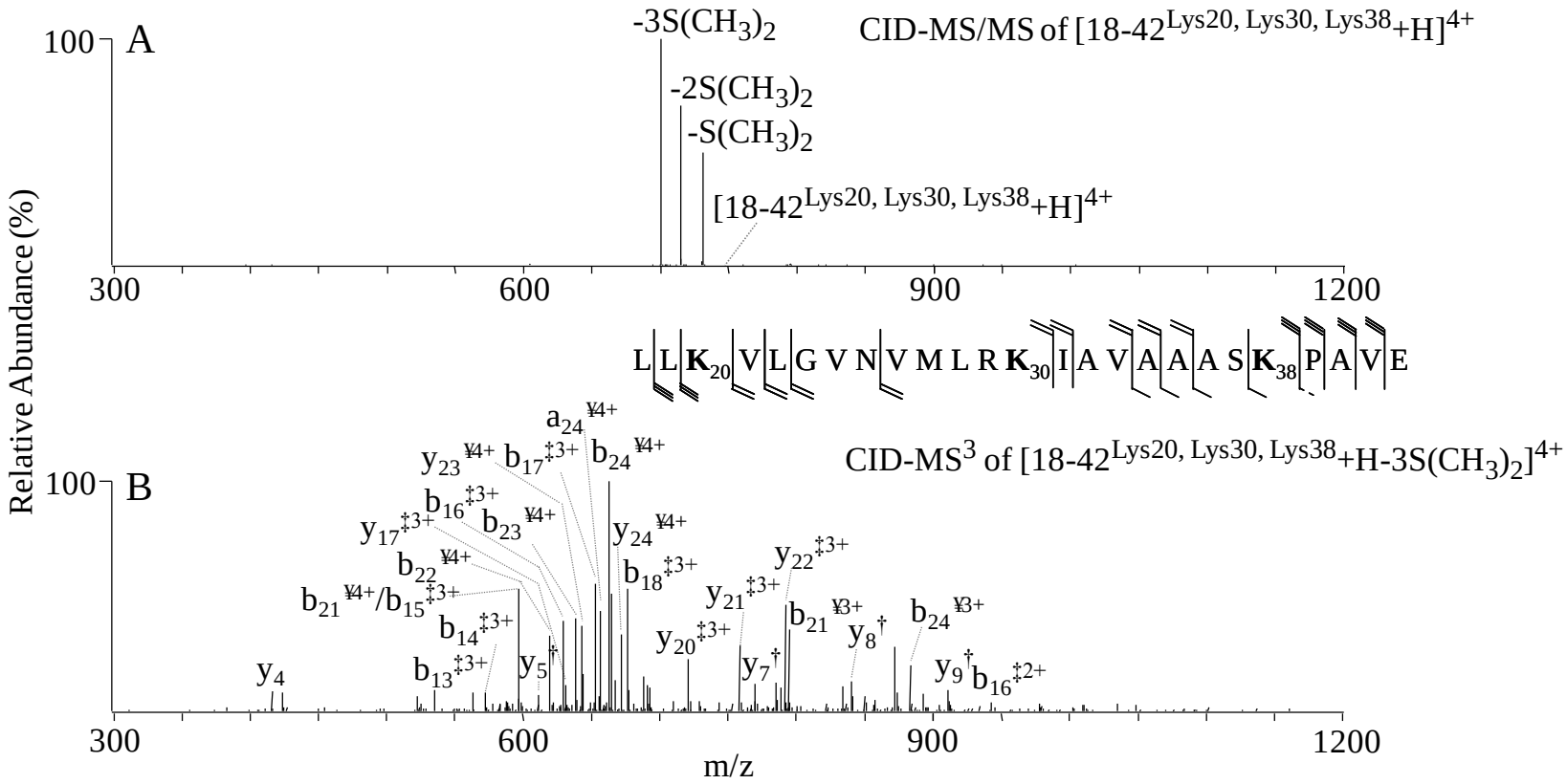

Figure 2.14 Ion trap mass spectrometry characterization of the DMBNHS triply modified CRABP II peptide, 18-42^{Lys20,Lys30,Lys38}. (A) CID-MS/MS of the [18-42^{Lys20,Lys30,Lys38}+H]$^{4+}$ precursor ion. (B) CID-MS^3 of the [18-42^{Lys20,Lys30,Lys38}+H-3S(CH$_3$)$_2$]$^{4+}$ product ion from panel A. A superscript † indicates sequence ions containing one modified amino acid residue. A superscript ‡ indicates sequence ions containing two modified amino acid residues. A superscript ¥ indicates sequence ions containing three modified amino acid residues. A dashed line indicates an unmodified sequence ion was observed. A single solid line indicates a sequence ion was observed with one modified amino acid. A double solid line indicates a sequence ion was observed with two modified amino acids. A triple solid line indicates a sequence ion was observed with three modified amino acids.

For the comparison of the sequence coverage obtained from each of the singly, doubly and triply modified forms of the 18-42 peptide ions at +3 or +4 charge states, Figure 2.15 shows the CID-MS/MS spectra from the triply and quadruply protonated precursor ions of the unmodified 18-42 peptide. Similar to that described above for the 1-13 peptide, comparing the CID-MS^3 spectra from the triply charged singly modified 18-42 peptide ions (i.e. the $[18\text{-}42^{Lys30}+2H]^{3+}$ and $[18\text{-}42^{Lys38}+2H]^{3+}$ in Figure 2.11 C and 2.11 D) with the triply charged unmodified 18-42 peptide ions (i.e. the $[18\text{-}42+3H]^{3+}$ in Figure 2.15), and the CID-MS^3 spectra of the doubly and triply modified 18-41 peptide ions at +4 charge states (i.e. $[18\text{-}42^{Lys20,Lys38}+2H]^{4+}$, $[18\text{-}42^{Lys20,Lys30}+2H]^{4+}$, and $[18\text{-}42^{Lys30,Lys38}+2H]^{4+}$ from Figure 2.11 and $[18\text{-}42^{Lys20,Lys30,Lys38}+H]^{4+}$ from Figure 2.14 B) with the quadruply charged unmodified 18-42 peptide ions, revealed that the sequence coverage obtained from MS^3 spectra of the DMBNHS derivatized peptides was equivalent to, or greater than, that from MS/MS of the unmodified form.

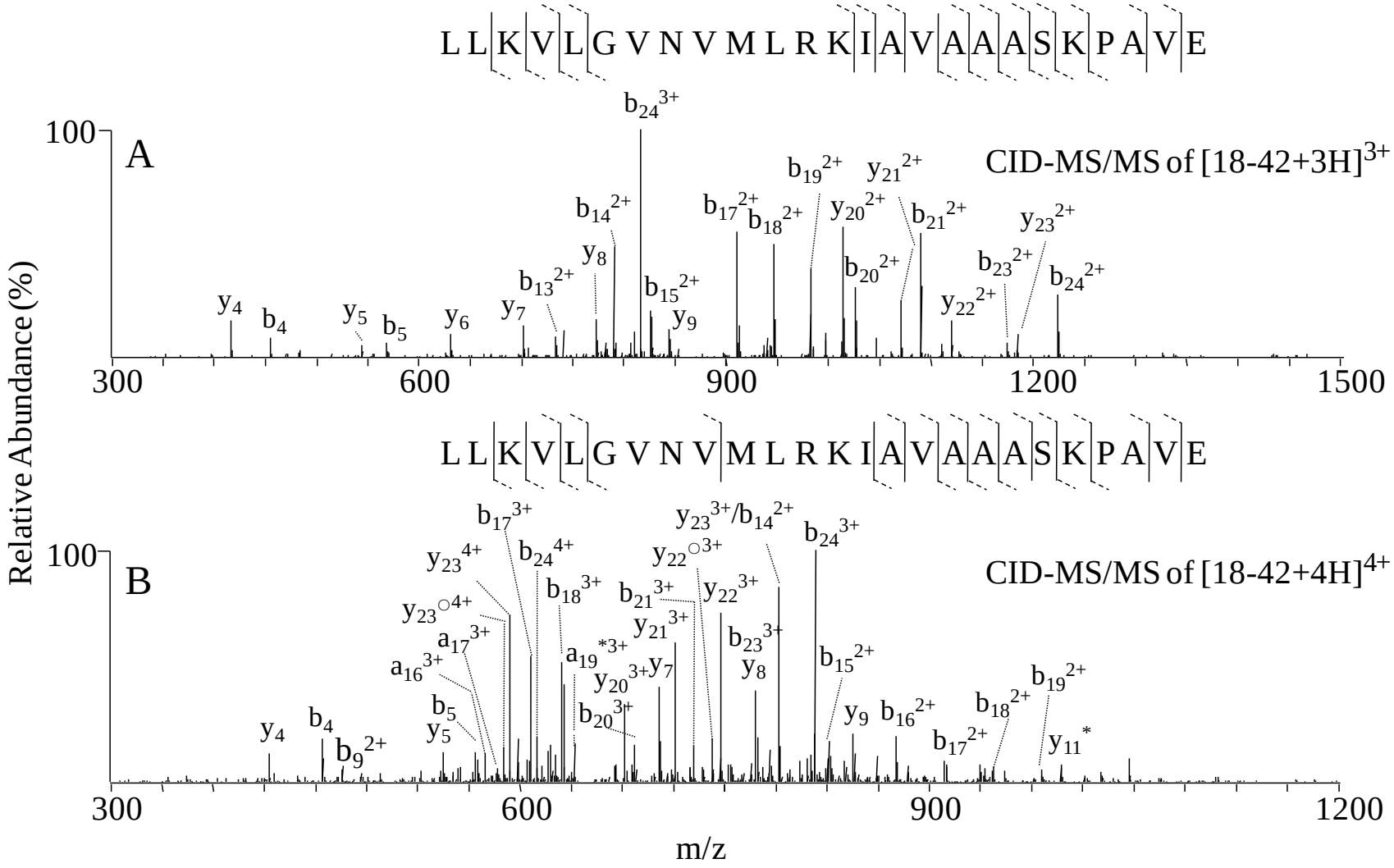

Figure 2.15 CID-MS/MS of the unmodified CRABP II peptide 18-42. CID-MS/MS of the (A) triply charged $[18\text{-}42+3H]^{3+}$ and (B) quadruply charged $[18\text{-}42+4H]^{4+}$ precursor ions.

Peptide 97-112 (QKLLKGEGPKTSWTRE) also has three modifiable sites and it is expected to observe three singly modified forms (i.e., 97-112^{Lys98}, 97-112^{Lys101}, and97-112^{Lys106}), three doubly modified forms (i.e., 97-112^{Lys98,Lys101}, 97-1121^{Lys98,Lys106}, and97-112^{Lys101,Lys106}), and one triply modified form (i.e., 97-112^{Lys98,Lys101,Lys106}) as seen from peptide 18-42. However, the three singly modified forms were eluted closely from the column and could not be separated. As a result, CID-MS^3 of the exclusive neutral loss product ion [97-112$^{Lys98/Lys101/Lys106}$+2H-S$(CH_3)_2$]$^{3+}$ from CID-MS/MS of [97-112$^{Lys98/Lys101/Lys106}$+2H]$^{3+}$ (data no shown) gave rise to a series of sequence ions corresponding to a mixture of the three singly modified forms (i.e., 97-112^{Lys98}, 97-112^{Lys101}, and97-112^{Lys106}), as illustrated in Figure 2.16 A. Similarly, the three doubly modified peptides, 97-112^{Lys98,Lys101}, 97-1121^{Lys98,Lys106}, and 97-112^{Lys101,Lys106}, were also not resolved. Figure 2.16 B shows CID-MS^3 of [97-112$^{Lys98,Lys101/Lys98,Lys106/Lys101,Lys106}$+H-2S$(CH_3)_2$]$^{3+}$ from CID-MS/MS of the isomeric DMBNHS doubly modified CRABP II peptides [97-112$^{Lys98,Lys101/Lys98,Lys106/Lys101,Lys106}$+H]$^{3+}$ and illustrated a mixture of different modification sites. Again, comparison of MS^3 spectra of the DMBNHS modified forms with MS/MS of the unmodified form (Figure 2.16 C) revealed that the derivatized peptides gave similar, or even better, sequence coverage.

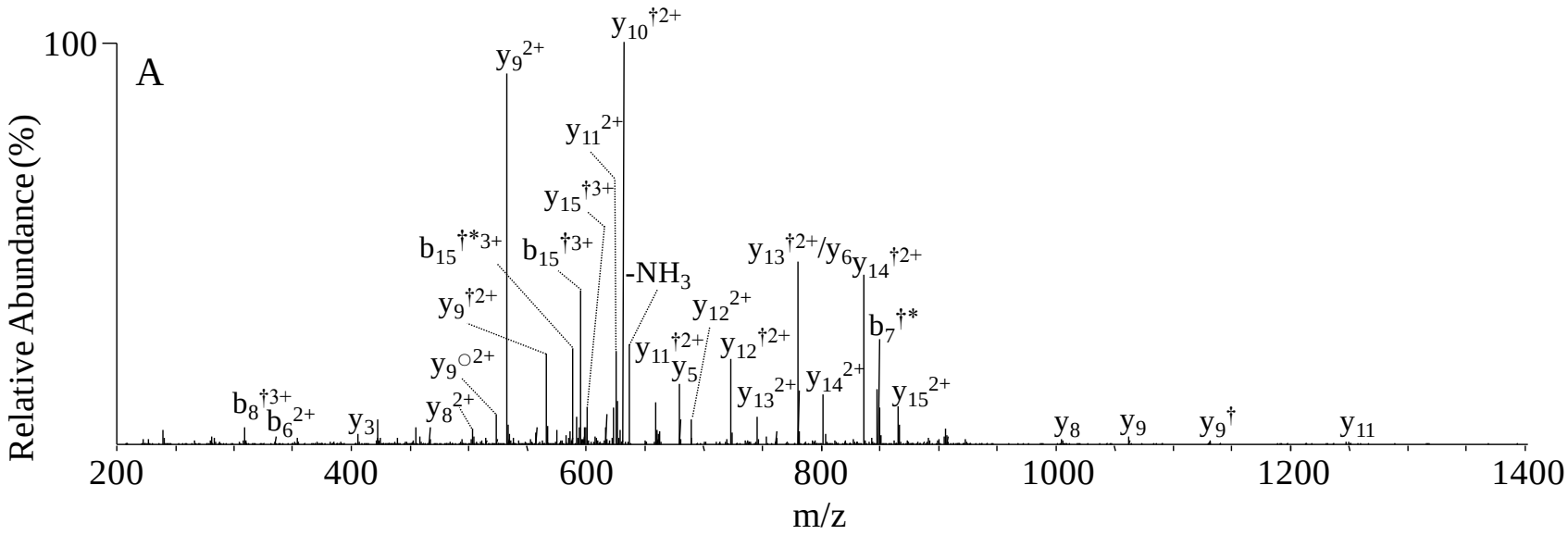

Figure 2.16 Ion trap mass spectrometry characterization of the DMBNHS singly modified peptide, 97-112$^{Lys98/Lys101/Lys106}$, doubly modified peptides, 97-112$^{Lys98,Lys101/Lys98,Lys106/Lys101,Lys106}$, and unmodified peptide, 97-112. (A) CID-MS^3 of the triply charged [97-112$^{Lys98/Lys101/Lys106}$+2H-S(CH$_3$)$_2$]$^{3+}$ product ion formed by CID-MS/MS of the [97-112$^{Lys98/Lys101/Lys106}$+2H]$^{3+}$ precursor ion. (B) CID-MS^3 of the triply charged [97-112$^{Lys98,Lys101/Lys98,Lys106/Lys101,Lys106}$+H-2S(CH$_3$)$_2$]$^{3+}$ product ion formed by CID-MS/MS of the [97-112$^{Lys98,Lys101/Lys98,Lys106/Lys101,Lys106}$+H]$^{3+}$ precursor ion. (C) CID-MS/MS of the triply protonated unmodified peptide ion, [97-112+3H]$^{3+}$. A superscript † indicates sequence ions containing one modified amino acid residue. A superscript ‡ indicates sequence ions containing two modified amino acid residues. A dashed line indicates an unmodified sequence ion was observed. A single solid line indicates a sequence ion was observed with one modified amino acid. A double solid line indicates a sequence ion was observed with two modified amino acids.

Figure 2.16 (cont'd)

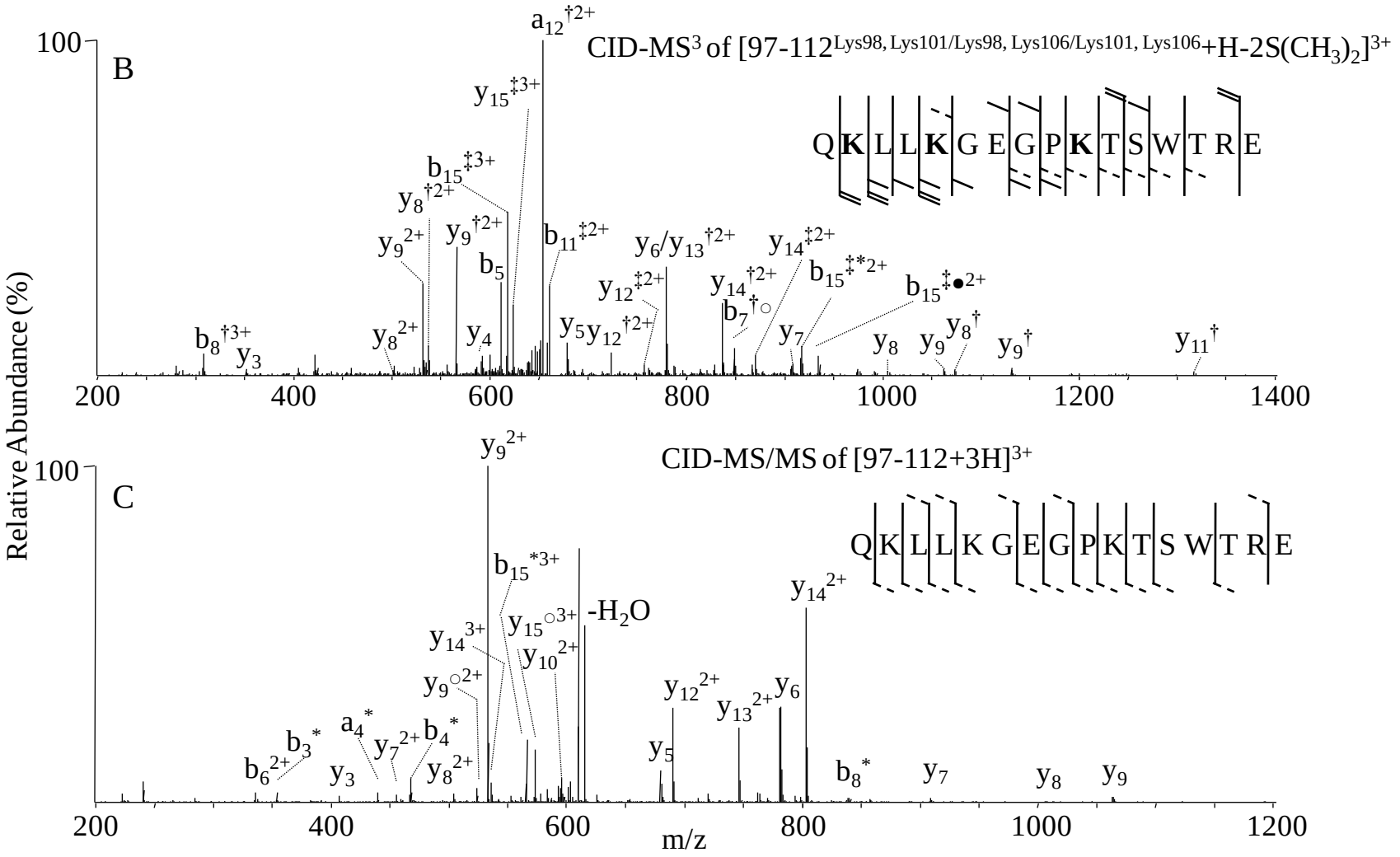

CID-MS/MS of DMBNHS modified forms of peptides containing only one modifiable residues, i.e., 63-70(INFKVGEE), 63-72(INFKVGEEFE), 47-62(GDTFYIKTSTTVRTTE), all resulted in a single product ion formed by the exclusive neutral loss of a $S(CH_3)_2$ (Figure 2.17). $[63\text{-}70^{Lys66}+H\text{-}S(CH_3)_2]^{2+}$ and $[63\text{-}72^{Lys66}+H\text{-}S(CH_3)_2]^{2+}$ has one mobile proton that can move along the peptide backbone while $[47\text{-}62^{Lys53}+H\text{-}S(CH_3)_2]^{2+}$ has a proton sequestered on the arginine residue, however, the observance of dominant neutral loss product ions from all of the three peptides indicates again the characteristic fragmentation pathway of sulfonium ion derivatized peptides are independent of proton mobility.

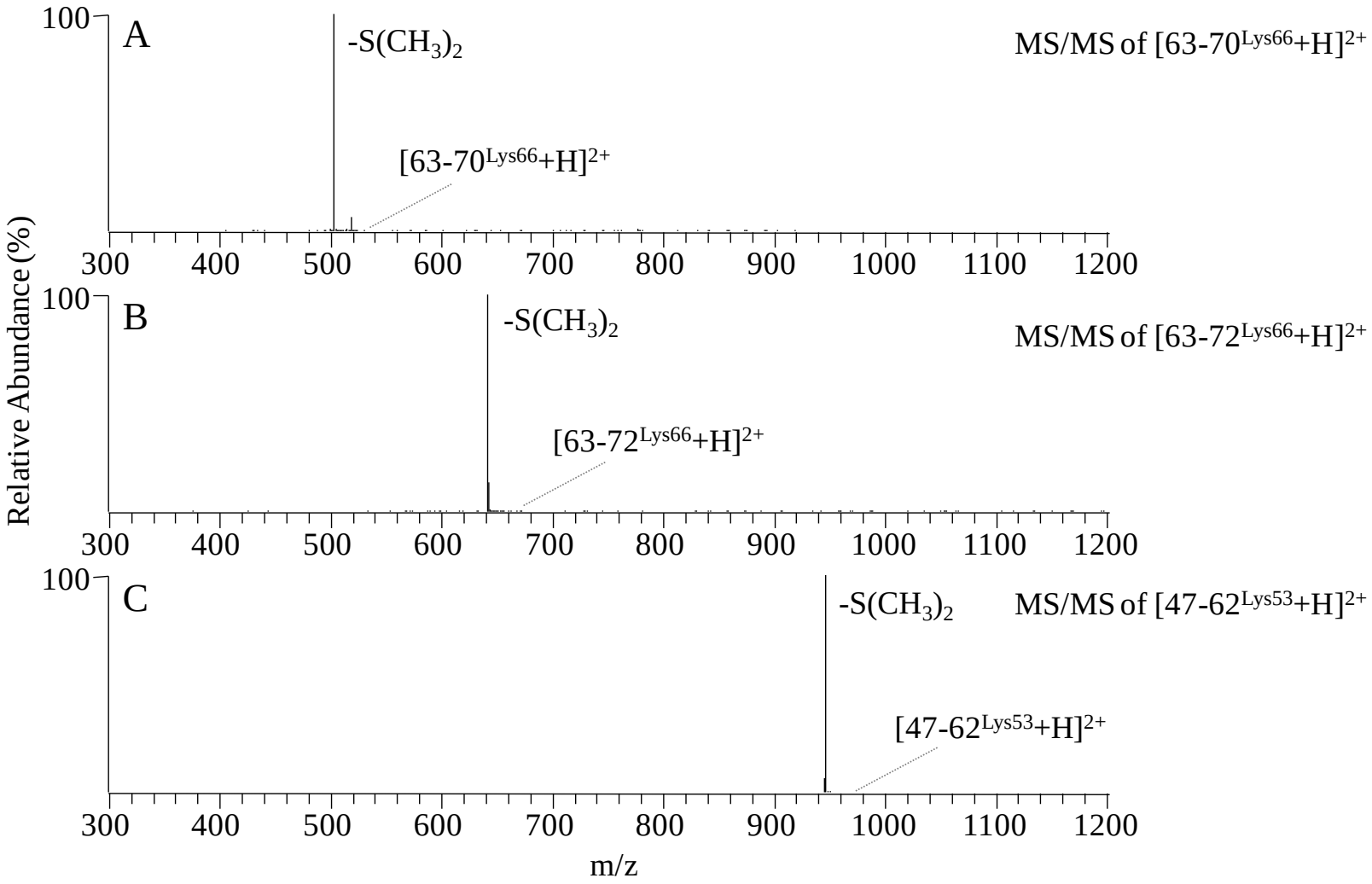

Figure 2.17 CID-MS/MS of the DMBNHS singly modified CRABP II peptides, 63-70^{Lys66}, 63-72^{Lys66}, and 47-62^{Lys53}. CID-MS/MS of the doubly charged (A) [63-70^{Lys66}+H]$^{2+}$, (B) [63-72^{Lys66}+H]$^{2+}$, and (C) [47-62^{Lys66}+H]$^{2+}$ precursor ions.

CID-MS^3 of the doubly charged $[63\text{-}70^{Lys66}+H\text{-}S(CH_3)_2]^{2+}$ product ion (as shown in Figure 2.18 A) formed by CID-MS/MS of the doubly charged DMBNHS singly modified peptide, $[63\text{-}70^{Lys66}+H]^{2+}$, allowed the modification site to be assigned to Lys_{66}. Interpretation of MS/MS of the doubly charged unmodified peptide 63-70, i.e., $[63\text{-}70+2H]^{2+}$ (see Figure 2.18 B), gave almost the same sequence coverage as MS^3 spectrum of $[63\text{-}70^{Lys66}+H\text{-}S(CH_3)_2]^{2+}$, and again demonstrated that the DMBNHS modification does not limit the sequence information obtained by CID fragmentation. Comparison of the m/z of the sequence ions from spectrum of CID-MS^3 of $[63\text{-}70^{Lys66}+H\text{-}S(CH_3)_2]^{2+}$ with CID-MS/MS of $[63\text{-}70^{Lys66}+H]^{2+}$ also provided more confidence with modification site identification.

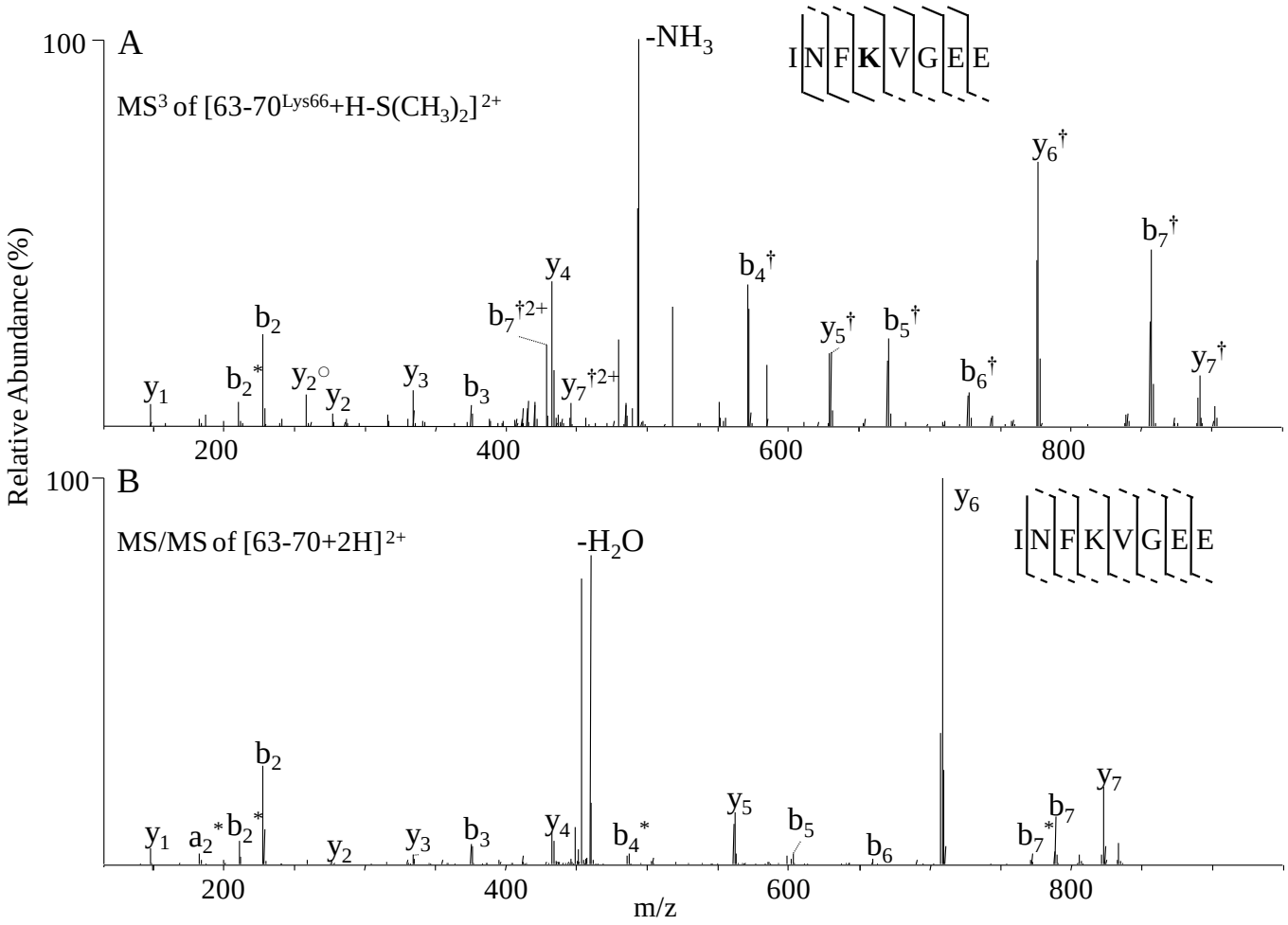

Figure 2.18 Ion trap mass spectrometry characterization of the DMBNHS singly modified peptide, 63-70^{Lys66}, and unmodified peptide, 63-70. CID-MS^3 (A) of the [63-70^{Lys66}+H-S(CH$_3$)$_2$]$^{2+}$ product ion from Figure 2.14 A. CID-MS/MS (B) of [63-70+2H]$^{2+}$. A superscript † indicates sequence ions containing one modified amino acid residue. A dashed line indicates an unmodified sequence ion was observed. A single solid line indicates a sequence ion was observed with one modified amino acid residue.

Peptide 63-72 shares the same modifiable residue, Lys_{66}, with peptide 63-70, and is expected to give the same results (Figure 2.19). Based on the observation of modified and unmodified b and y series sequence ions from Figure 2.19 A as well as the comparison between Figure 2.19 A and 2.19 B, the modification site can be confidently assigned to Lys_{66}. The fragmentation of doubly charged modified and unmodified 63-70 and 63-72 all gave very comprehensive sequence coverage, probably due to the presence of a mobile proton.

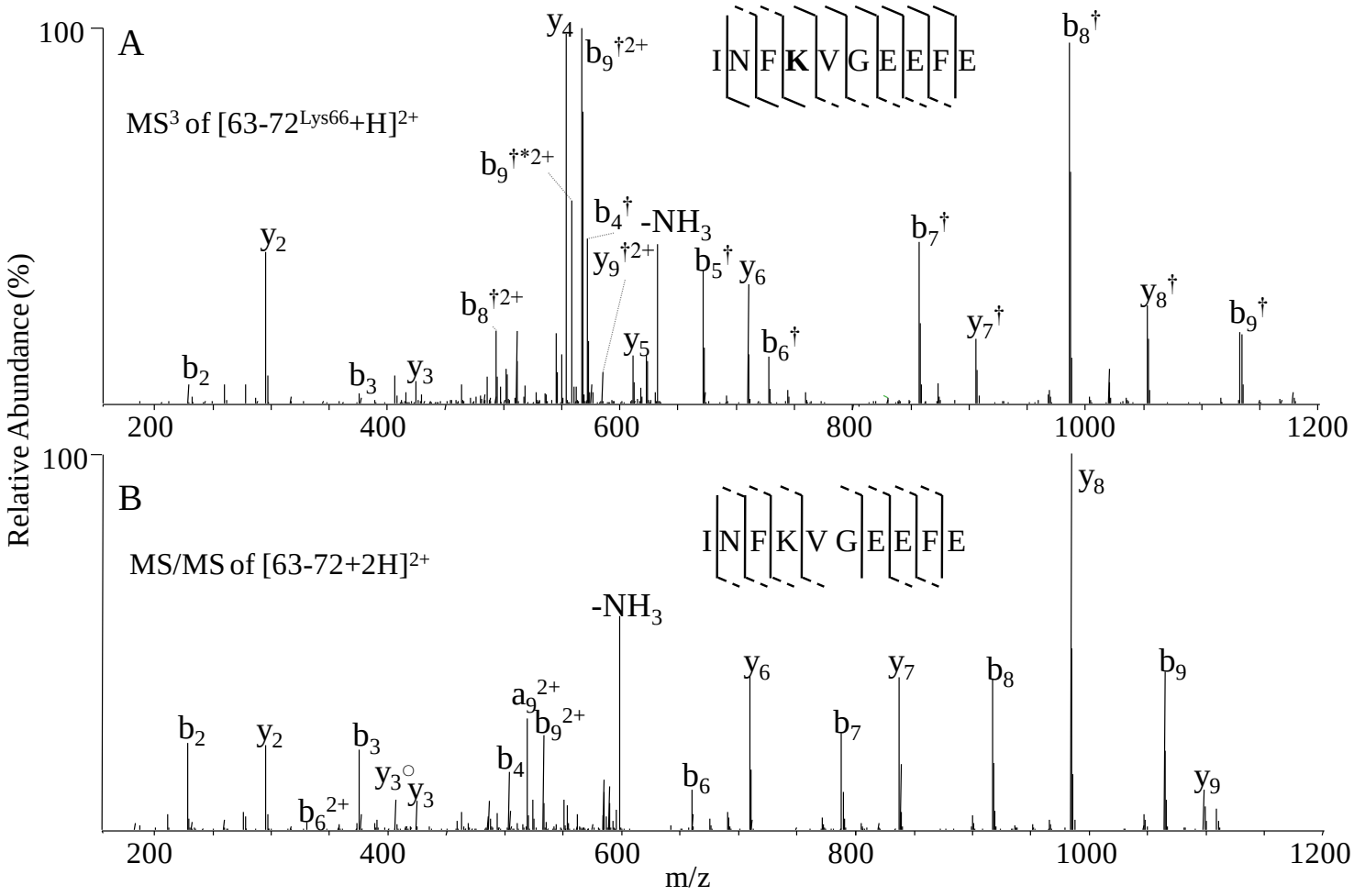

Figure 2.19 Ion trap mass spectrometry characterization of the DMBNHS singly modified peptide, 63-72^{Lys66}, and unmodified peptide, 63-72. CID-MS^3 (A) of the [63-72^{Lys66}+H-S(CH$_3$)$_2$]$^{2+}$ product ion from Figure 2.14 B. CID-MS/MS (B) of [63-72+2H]$^{2+}$. A superscript † indicates sequence ions containing one modified amino acid residue. A dashed line indicates an unmodified sequence ion was observed. A single solid line indicates a sequence ion was observed with one modified amino acid.

Similarly, CID-MS^3 of $[47\text{-}62^{Lys53}+H\text{-}S(CH_3)_2]^{2+}$ (Figure 2.20 A) allowed the DMBNHS modification site to be localized on Lys_{53}. For comparison, CID-MS/MS of unmodified peptide 47-62 was shown in Figure 2.20 B. The same m/z of y_9 and higher mass of $y_{10}^{\dagger}$, $y_{11}^{\dagger}$, and $y_{12}^{\dagger}$ from CID-MS^3 of $[47\text{-}62^{Lys53}+H\text{-}S(CH_3)_2]^{2+}$ (Figure 2.20 A) compared to y_9, y_{10}, y_{11}, and y_{12} from CID-MS/MS of $[47\text{-}62+2H]^{2+}$ (Figure 2.19 B) further confirmed the modification site at Lys_{53}.

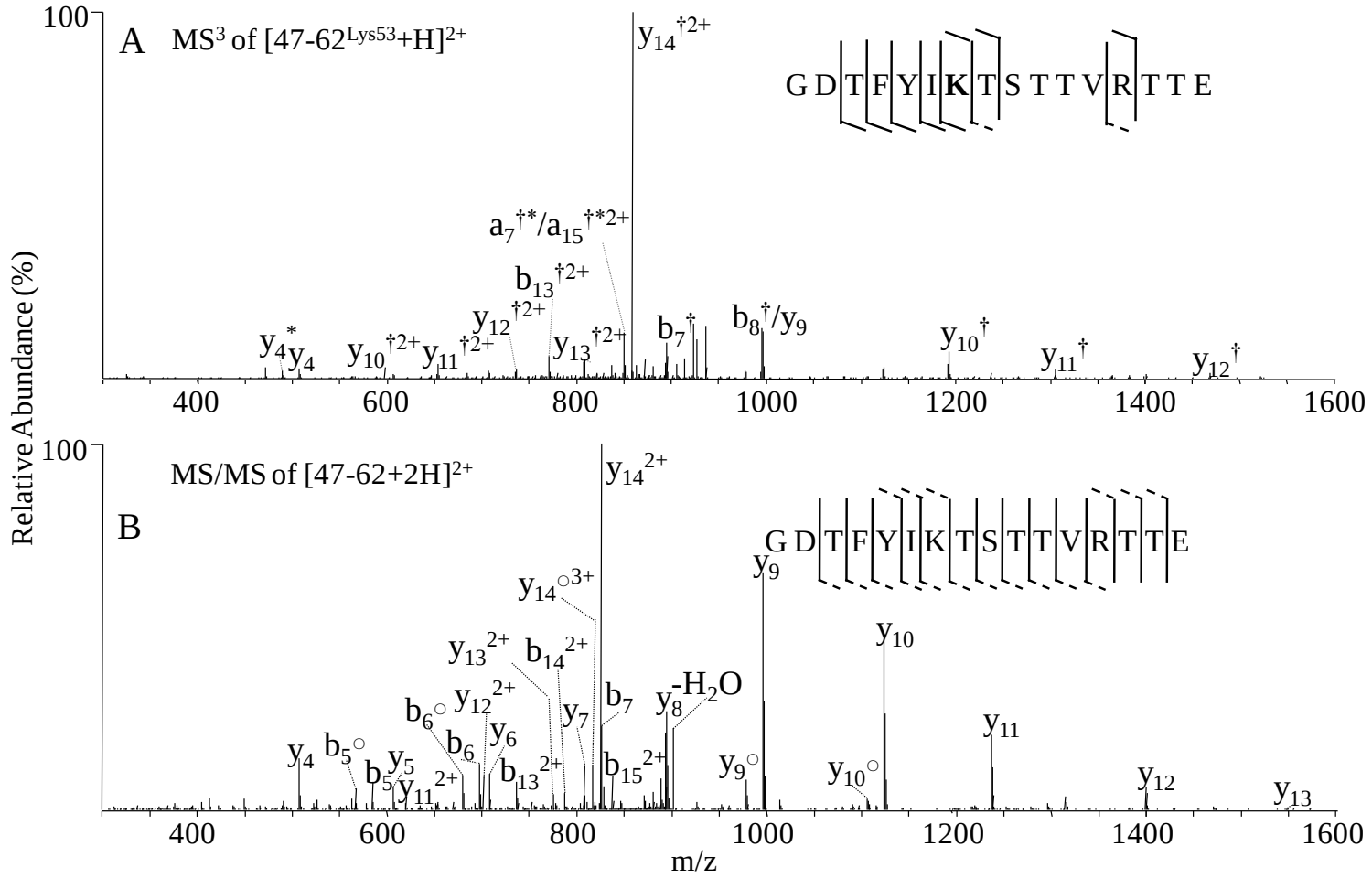

Figure 2.20 Ion trap mass spectrometry characterization of the DMBNHS singly modified peptide, 47-62^{Lys53}, and unmodified peptide, 47-62. CID-MS^3 (A) of the [47-62^{Lys53}+H-S(CH$_3$)$_2$]$^{2+}$ product ion from Figure 2.14 C. CID-MS/MS (B) of [47-62+2H]$^{2+}$. A superscript † indicates sequence ions containing one modified amino acid residue. A dashed line indicates an unmodified sequence ion was observed. A single solid line indicates a sequence ion was observed with one modified amino acid.

2.4.3. Correlation of the Modified Peptide Ion Abundances with the Predicted Solvent Accessibilities of CRABP II

Normalized plots of the relative abundances (summed from all observed charge states) of the unmodified, singly modified, doubly modified, and triply modified peptides versus the stoichiometric ratios of DMBNHS reagent to protein are shown in Figure 2.21. These plots summarize the reactivity of the peptides towards DMBNHS and therefore are indicative of the solvent accessibility of these peptide regions. The experimentally determined solvent accessibilities of the lysine residues in these peptide regions were also compared to the calculated solvent accessibilities, determined using the GetArea program [329] (see Table 1) based on the known NMR solution phase structure of CRABP II [330]. The results are discussed in detail below. Note that the plots shown herein were generated assuming that the ionization efficiency of a given peptide was not affected by the DMBNHS modification, even though enhancement of the ionization efficiencies caused by the incorporation of the sulfonium ion was demonstrated [323]. Also, it was assumed that the magnitude of any enhancement in ionization efficiencies would be similar between peptides, and would therefore not have an impact on determination of the relative solvent accessibilities. Furthermore, the consistency of these results with the predicted solvent accessibilities of the CRABP II lysine residues (see below) suggest that any differences caused by ionization efficiency are not substantial.

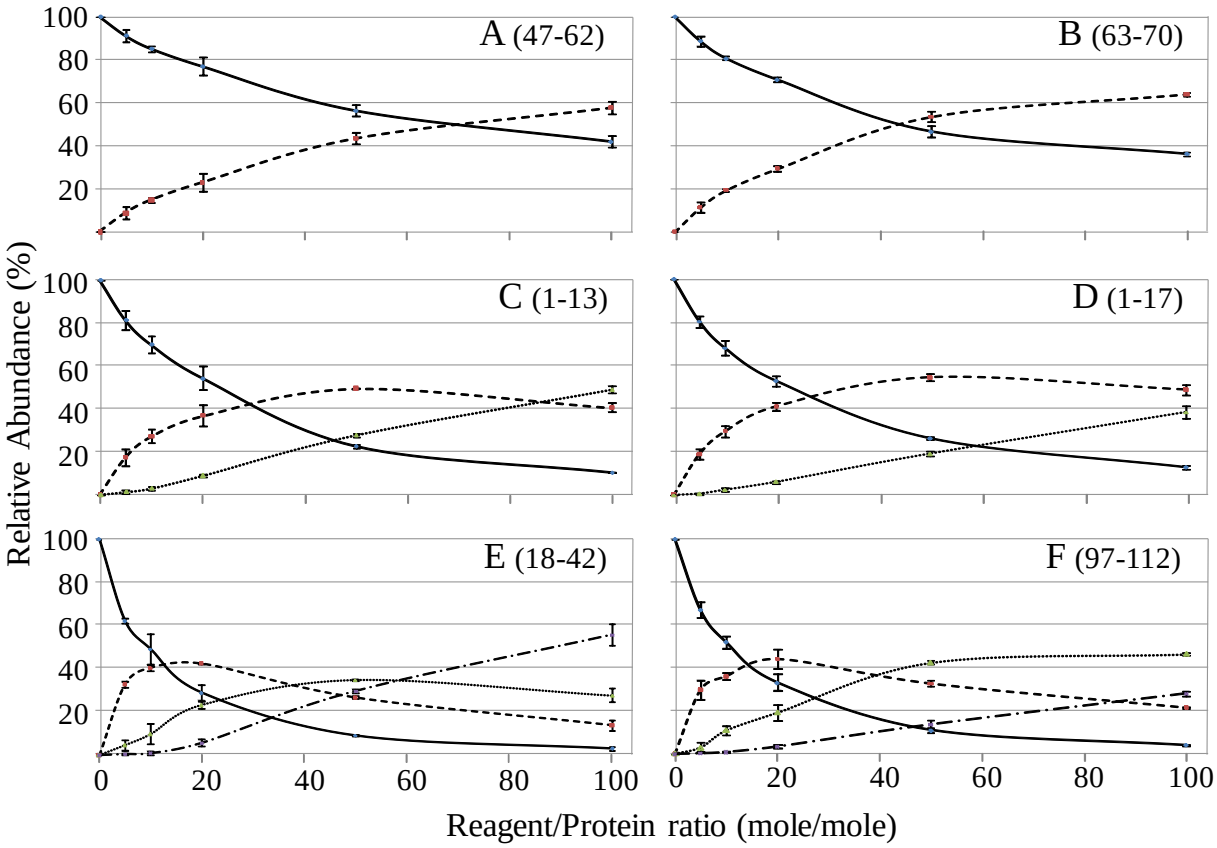

Figure 2.21 Plots of the relative abundances of unmodified peptides (solid line), singly modified peptides (dashed line), doubly modified peptides (dotted line), and triply modified peptides (dashed and dotted line) versus the molar ratios of reagent over protein. (A) peptide 47-62, (B) peptide 63-70, (C) peptide 1-13, (D) peptide 1-17, (E) peptide 18-42 and (F) peptide 97-112. Samples were separately prepared and run in triplicate. Error bars are shown as ±S.D.

Peptides 47-62 (Figure 2.21 A) and 63-70 (Figure 2.21 B) each contain only one lysine residue, Lys_{53} and Lys_{66}, respectively. The peak relative abundance of the singly modified 63-70 peptide (64±1%) was higher than that of the 47-62 peptide (58±3%). These data suggest that Lys_{66} is more accessible to the DMBNHS reagent compared to Lys_{53}. This result is consistent with the GetArea predicted solvent accessibilities of these residues (60.5% for Lys_{66} and 38.3% for Lys_{53}).

Peptides 1-13 and 1-17 contain two identical modifiable residues, Pro_1 (N-terminus) and Lys_8, so their responses to an increasing amount of modification reagent were expected to be the same. However, 1-13 (Figure 2.21 C) showed a higher extent of modification than 1-17 (Figure 2.21 D). This might be due to a difference in the extent of ionization efficiency between the unmodified and modified forms between the two peptides, or a difference in the Glu-C enzyme cleavage activity caused by the modification (i.e. the incorporation of the fixed charge may enhance enzymatic cleavage at the cleavable site closest to the modification). The predicted solvent accessibilities of the Pro_1 and Lys_8 residues are 57.8% and 45.7%, respectively. However, for both the 1-13 and 1-17 peptides, the abundance of the Lys_8 modified peak (e.g., [1-13^{Lys8}] in Figure 2.4 was higher than that of the Pro_1 modified peak (e.g., [1-13^{Pro1} in Figure 2.4]). This is rationalized as being due to differences in the rate of reactivity between the primary ε-amino group of the lysine side chain and the secondary amine functional group of the N-terminal proline residue, respectively, toward the NHS ester of the DMBNHS reagent.

Both peptides 97-112 and 18-42 contain 3 lysine residues. The triply modified 18-42 peptide was observed with a maximum relative abundance of 57±5%, while the triply modified

97-112 peptide was observed with a maximum relative abundance of only 28±1% (compare Figure 2.21 E and 2.21 F, respectively). This overall greater extent of reaction of the 18-42 peptide compared to the 97-112 peptide is consistent with the higher summed predicted solvent accessibilities of the Lys_{20} (49.3%), Lys_{30} (58.1%) and Lys_{38} (93.1%) residues (summed total of 200.5%) versus the Lys_{98} (49.6%), Lys_{101} (72.7%) and Lys_{106} (42.6%) residues (summed total of 164.9%). Also consistent with the predicted solvent accessibilities, which suggest that Lys_{38} is the most exposed residue followed by Lys_{30} and finally Lys_{20}, the intensity of the 18-42^{Lys38} modified peptide was found to be more abundant than the 18-42^{Lys30} modified peptide. Finally, the lack of a singly modified 18-42^{Lys20} peak corresponding to modification at the Lys_{20} residue is consistent with its significantly lower predicted solvent accessibility compared to the Lys_{30} and Lys_{38} residues. Unfortunately, the isomeric singly and doubly modified forms of the 97-112 peptide were not chromatographically resolved. As a result, the predicted solvent accessibilities of each lysine residue could not be correlated with their reactivity. Similarly, the singly, doubly and triply modified forms of the 63-96 peptide containing four modifiable sites (Lys_{66}, Lys_{82}, Lys_{86} and Lys_{92}) were not chromatographically resolved, precluding the ability to correlate their individual reactivity and predicted solvent accessibility. Overall however, the results described above provide strong evidence that the extent of modification of the DMBNHS reagent is correlated with the protein solvent accessibility.

CHAPTER THREE

EXPERIMENTAL METHODS FOR CHAPTER TWO

3.1 Materials

Sodium methanethiolate, γ-butyrolactone, d_6-γ-butyrolactone, 4-bromobutyric acid, thiourea, d_3-iodomethane, tris(hydroxymethyl)aminomethane (Tris), guanidine hydrochloride, and neurotensin were purchased from Sigma-Aldrich (St. Louis, MO, USA). Anhydrous dimethyl sulfoxide (DMSO) (stored over 3Å sieves), N-hydroxyssuccinimide (NHS) and N,N'-dicyclohexylcarbodiimide (DCC) were from Fluka (Switzerland). HCl, NaCl, and KOH were purchased from Columbus Chemical Industries (Columbus, WI, USA). Diethyl ether, KCl, sulfuric acid, dimethylformamide (DMF), and silica gel (200-425 mesh) were from Jade Scientific (Canton, MI, USA). Glacial acetic acid, ethanol, isopropyl alcohol, chloroform, dichloromethane (DCM), and ethyl acetate were from Mallinckrodt Chemicals (Phillipsburg, NJ, USA). Acetonitrile and iodomethane were purchased from EMD Chemicals (San Diego, CA, USA). Sodium hydroxide, sodium phosphate dibasic (crystal), potassium phosphate monobasic (crystal), magnesium sulfate (anhydrous), and formic acid were from Spectrum Chemical Mfg. (Gardena, CA, USA). Trifluoroacetic acid (TFA) was purchased from Pierce (Rockford, IL,

---

Part of the results described in Chapter Three were published in: Lu, Y., Zhou, X., Stemmer, P.M. and Reid, G.E., Sulfonium Ion Derivatization, Isobaric Stable Isotope Labeling and Data Dependent CID- and ETD-MS/MS for Enhanced Phosphopeptide Quantitation, Identification and Phosphorylation Site Characterization. *J. Am. Soc. Mass Spectrom*. **2012**, *23*, 577-593.

USA). Endoprotease Glu-C was purchased from Thermo Fisher Scientific (Waltham, MA, USA). All aqueous solutions were prepared using deionized water obtained from a Barnstead nanopure diamond purification system (Dubuque, IA, USA). CRABP II was supplied by Dr. Babak Borhan (Department of Chemistry, Michigan State University).

^{1}H NMR spectra were performed on a Varian Inova 500 MHz instrument and recorded in parts per million (ppm) referenced to the solvent resonances (δ), with coupling constants (*J*) in hertz (Hz).

3.2 Synthesis of S,S'-Dimethylthiobutanoylhydroxysuccinimide Ester, S,S'-d_3-Dimethylthiobutanoylhydroxysuccinimide Ester, and S,S'-$^{13}C_1$-Dimethylthiobutanoylhydroxysuccinimide Ester

The synthesis of the amine-specific protein modification reagents, S,S'-dimethylthiobutanoylhydroxysuccinimide ester (DMBNHS) **(3),** S,S'-d_3-dimethylthiobutanoylhydroxysuccinimide ester (d_3-DMBNHS) **(3')**, and S,S'-$^{13}C_1$-dimethylthiobutanoylhydroxysuccinimide ester ($^{13}C_1$-DMBNHS) **(3")** ($^{13}C_1$-DMBNHS is being used in a separate study for improved aminophospholipid analysis) was achieved via a three-step process as shown in Scheme 3.1. The details for each step are described below.

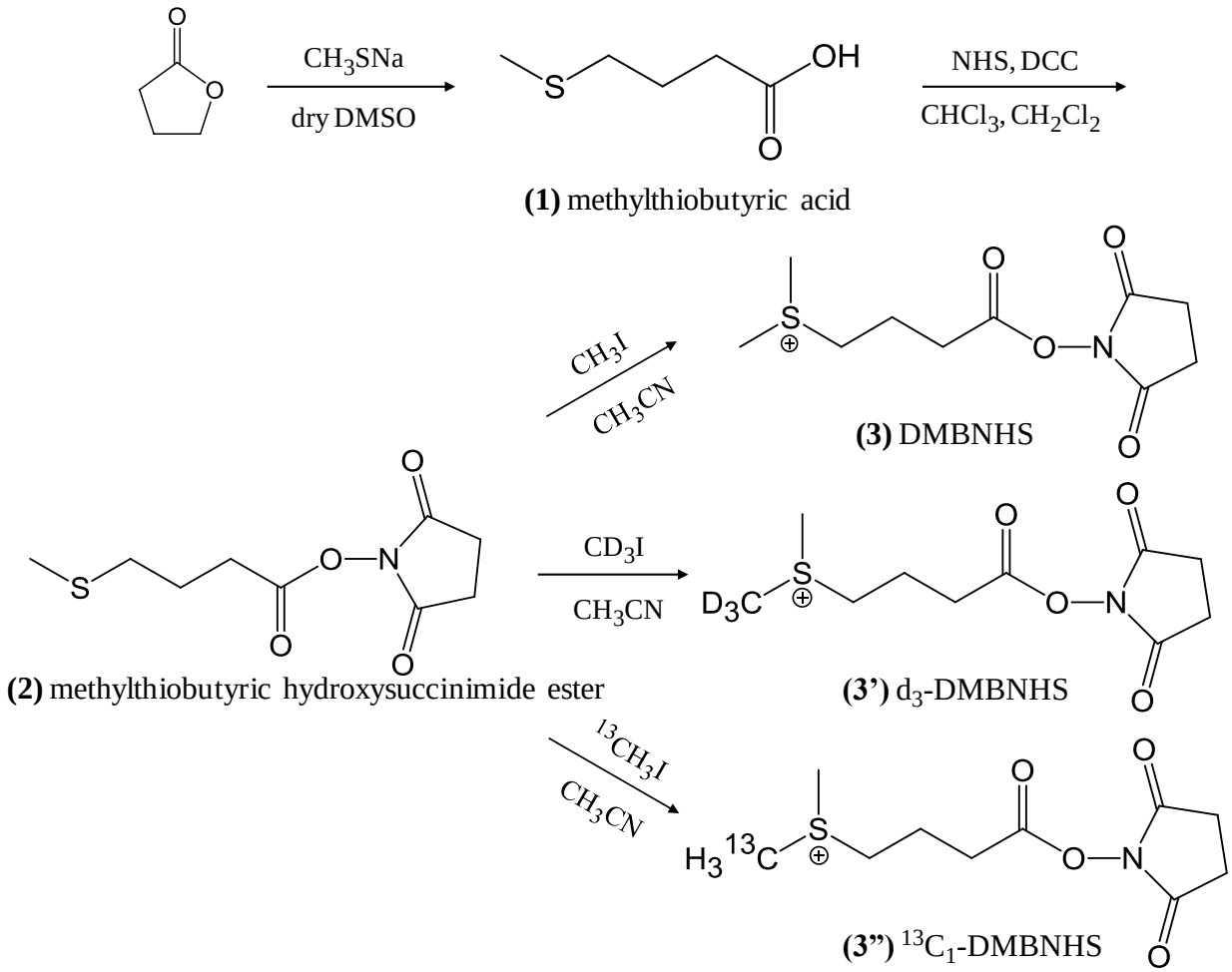

Scheme 3.1 Synthesis of the sulfonium ion containing protein modification reagents, S,S'-dimethylthiobutanoylhydroxysuccinimide ester (DMBNHS) **(3)**, S,S'-d_3-dimethylthiobutanoylhydroxysuccinimide ester (d_3-DMBNHS) **(3')**, and S,S'-^{13}C-dimethylthiobutanoylhydroxysuccinimide ester (^{13}C-DMBNHS) **(3")**.

3.2.1 Synthesis of Methylthiobutyric Acid

Based on the method of Williams *et al*. [331], sodium methanethiolate (6.97 g, 99.5 mmol) and γ-butyrolactone (4.46 mL, 74.63 mmol) were dissolved in 90 mL of anhydrous DMSO, and then the solution was stirred under N_2 atmosphere at room temperature for 6 days. 166 mL of 1M HCl was added to the resulting slurry, and then the aqueous solution was extracted with 6 × 104 mL of diethyl ether. The solvent was evaporated under reduced pressure. The crude product was purified by silica gel column chromatography with 100% ethyl acetate as the solvent to give 5.97 g (yield 60%) of product as a colorless oil. ^{1}H NMR (500 MHz, $CDCl_3$): δ 1.90 (m, 2H, J = 7), 2.07 (s, 3H), 2.47 (t, 2H, J = 7), 2.52 (t, 2H, J = 7.5), 11.15 (s, broad, 1H). The NMR spectrum is shown in Figure 3.1.

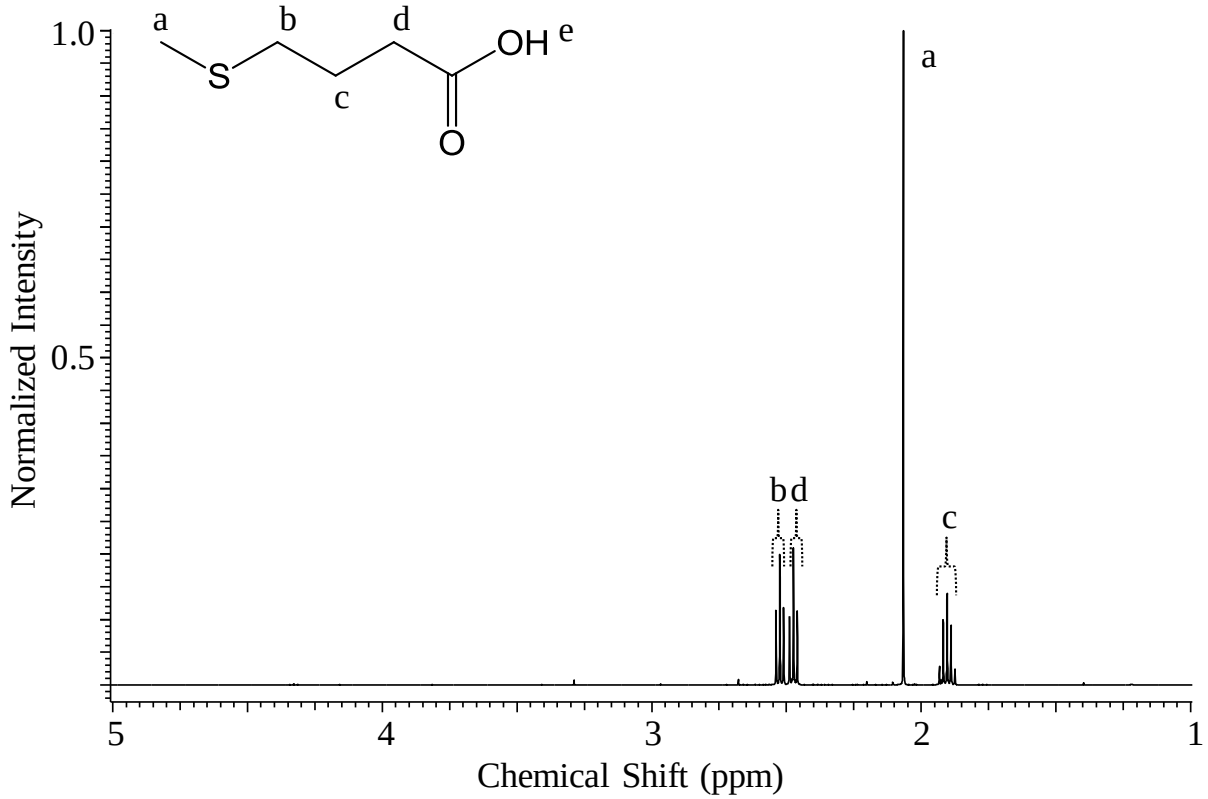

Figure 3.1 ^{1}H NMR characterization of methylthiobutyric acid **(1)**

3.2.2 Synthesis of Methylthiobutyric Hydroxysuccinimide Ester

Under a N_2 atmosphere, NHS (3.80 g, 33 mmol) and **(1)** (4.02 g, 30 mmol) were dissolved in a mixture of $CHCl_3$ (60 mL) and CH_2Cl_2 (30 mL). The mixture was stirred for 5 minutes at room temperature. Then DCC (6.80 g, 33 mmol) was added and a precipitate formed immediately. The resulting suspension was stirred in N_2 atmosphere for 24 hrs. The mixture was then filtered and the filtrate was collected and concentrated under reduced pressure. 5 mL of acetonitrile was then added to the residue and the resulting precipitate was filtered out (this step was repeated twice until no precipitate could be observed in acetonitrile). The resultant solution was dried *in vacuo*, after which 6.08 g (88%) of product was obtained as a white solid. ^{1}H NMR (500MHz, $CDCl_3$): δ 2.02 (m, 2H, J = 7.5), 2.09 (s, 3H), 2.59 (t, 2H, J = 7), 2.75 (t, 2H, J = 7), 2.82 (s, 4H). The NMR spectrum is shown in Figure 3.2.

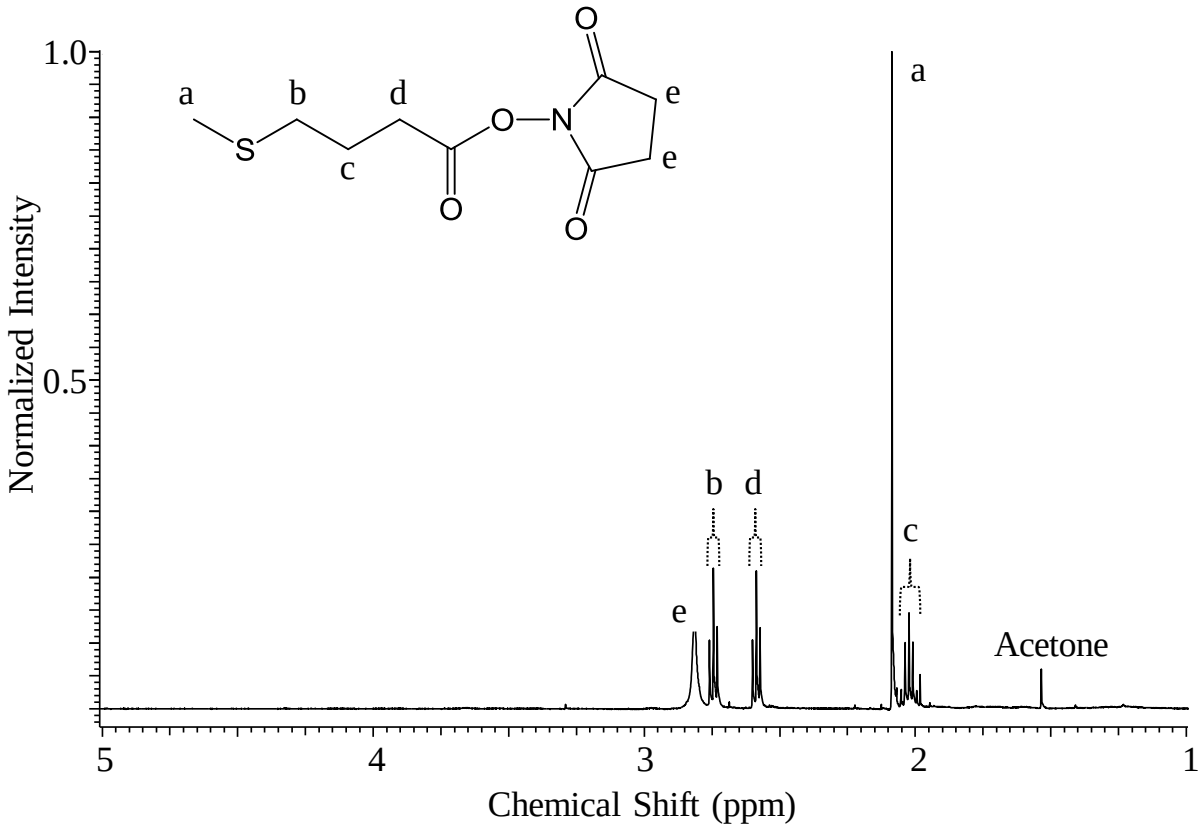

Figure 3.2 ^{1}H NMR characterization of methylthiobutyric hydroxysuccinimide ester **(2)**

3.2.3 Synthesis of DMBNHS, D_3-DMBNHS, and $^{13}C_1$-DMBNHS

Methylthiobutyric hydroxysuccinimide ester **(2)** (0.231 g, 1 mmol) and iodomethane (0.71 g, 5 mmol) were dissolved in 2 mL of CH_3CN followed by stirring in the dark at room temperature for 2 days. The resulting solution was then concentrated under reduced pressure. The resultant yellow solid was washed with 10 mL of DCM then dried *in vacuo* to give 0.28 g (76%) of product **(3)** as yellow crystals. D_3-DMBNHS **(3')** and $^{13}C_1$-DMBNHS **(3")** were synthesized by reacting **(2)** with d_3-iodomethane and $^{13}C_1$-iodomethane, respectively, using the same method described above. The product was stored in the dark. ^{1}H NMR (500 MHz, CD_3CN) of **(3)**: δ 2.16 (m, 2H, *J* = 7.5), 2.77 (s, 4H), 2.81 (s, 6H), 2.85 (t, 2H, *J* = 7.5), 3.29 (t, 2H, *J* = 7.5). ^{1}H NMR (500MHz, CD_3CN) of **(3')**: δ 2.16 (m, 2H, *J* = 7.5), 2.77 (s, 4H), 2.82 (s, 3H), 2.85 (t, 2H, *J* = 7.5), 3.31 (t, 2H, *J* = 7.5). ^{1}H NMR (500MHz, CD_3CN) of **(3")**: δ 2.67, 2.97 (d, 3H, *J* = 146.0), 2.77 (s, 4H), 2.82, 2.83 (d, 3H, J = 4), 2.85 (t, 2H, *J* = 7.0), 3.31 (m, 2H, $^3J_{C\text{-}H}$ = 3.0, $J_{H\text{-}H}$ = 7.5). The NMR spectra of DMBNHS **(3)**, d_3-DMBNHS **(3')**, and $^{13}C_1$-DMBNHS **(3")** are shown in Figure 3.3, Figure 3.4, and Figure 3.5, respectively.

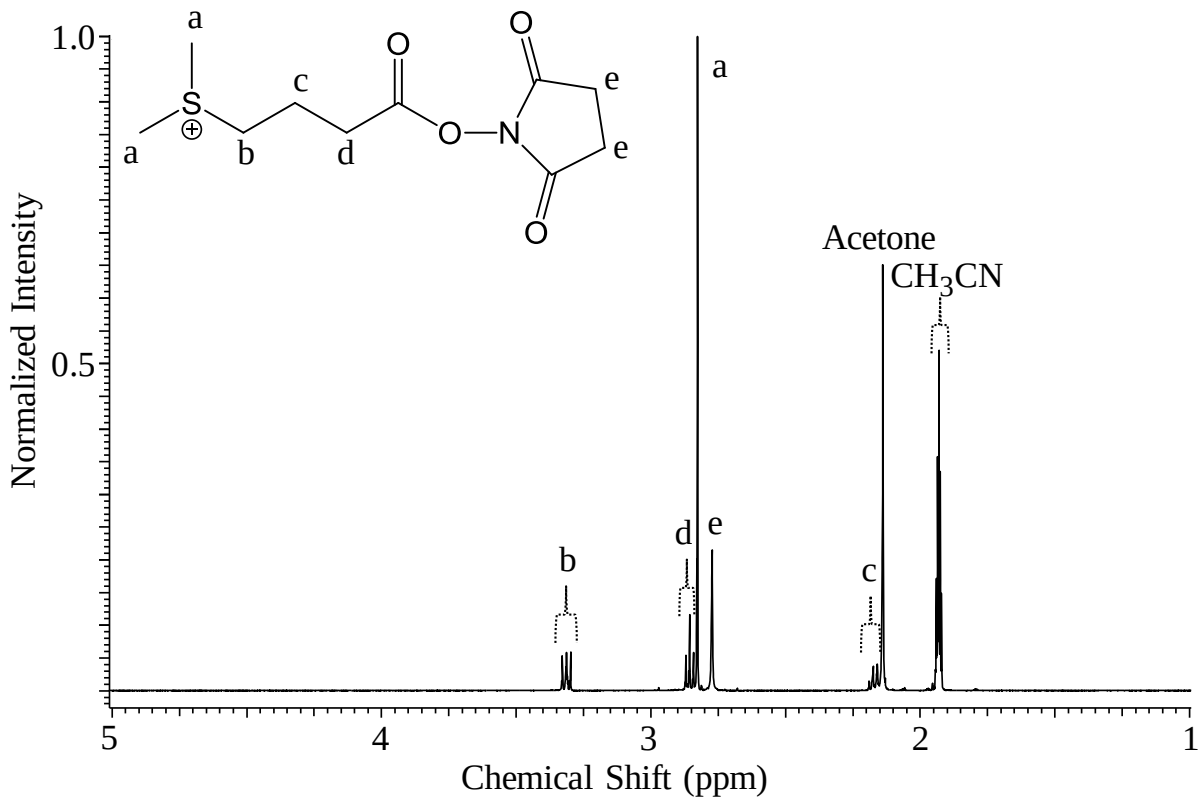

Figure 3.3 ^{1}H NMR characterization of DMBNHS **(3)**

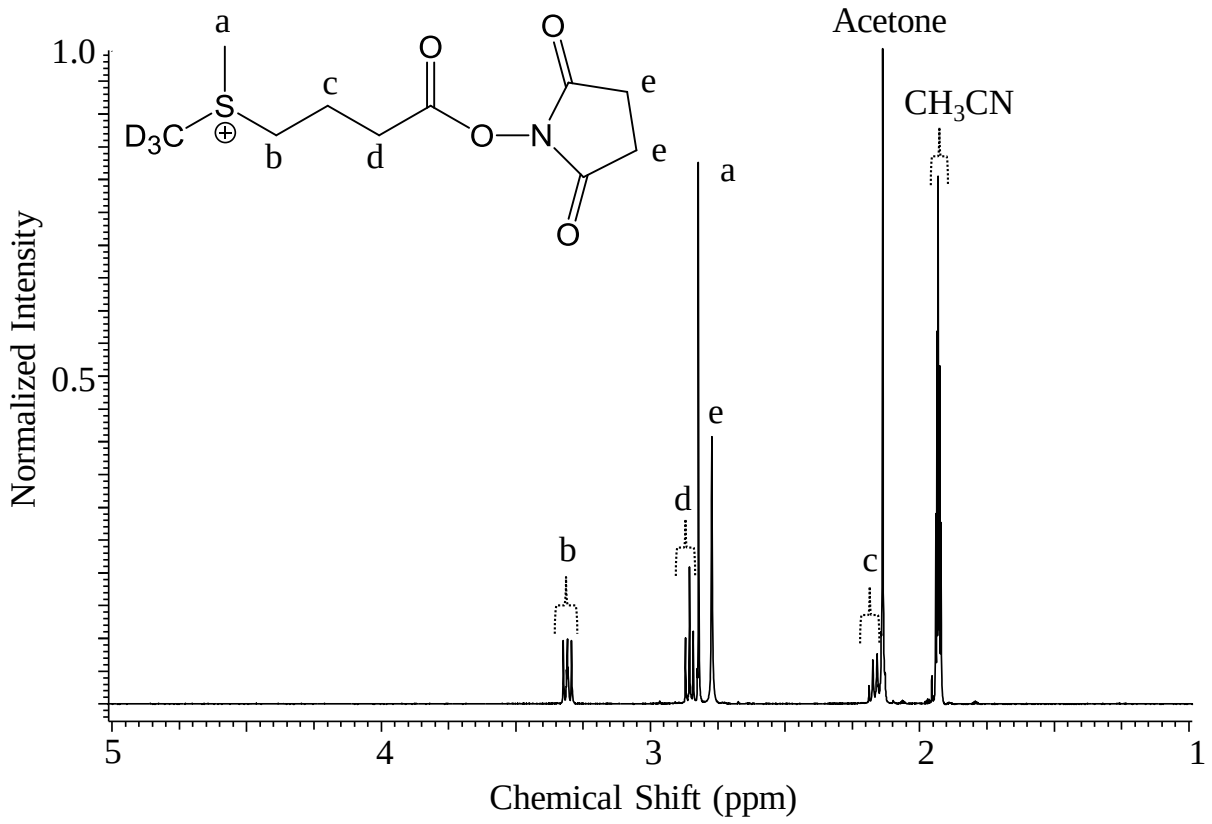

Figure 3.4 ^{1}H NMR characterization of d_3-DMBNHS **(3')**

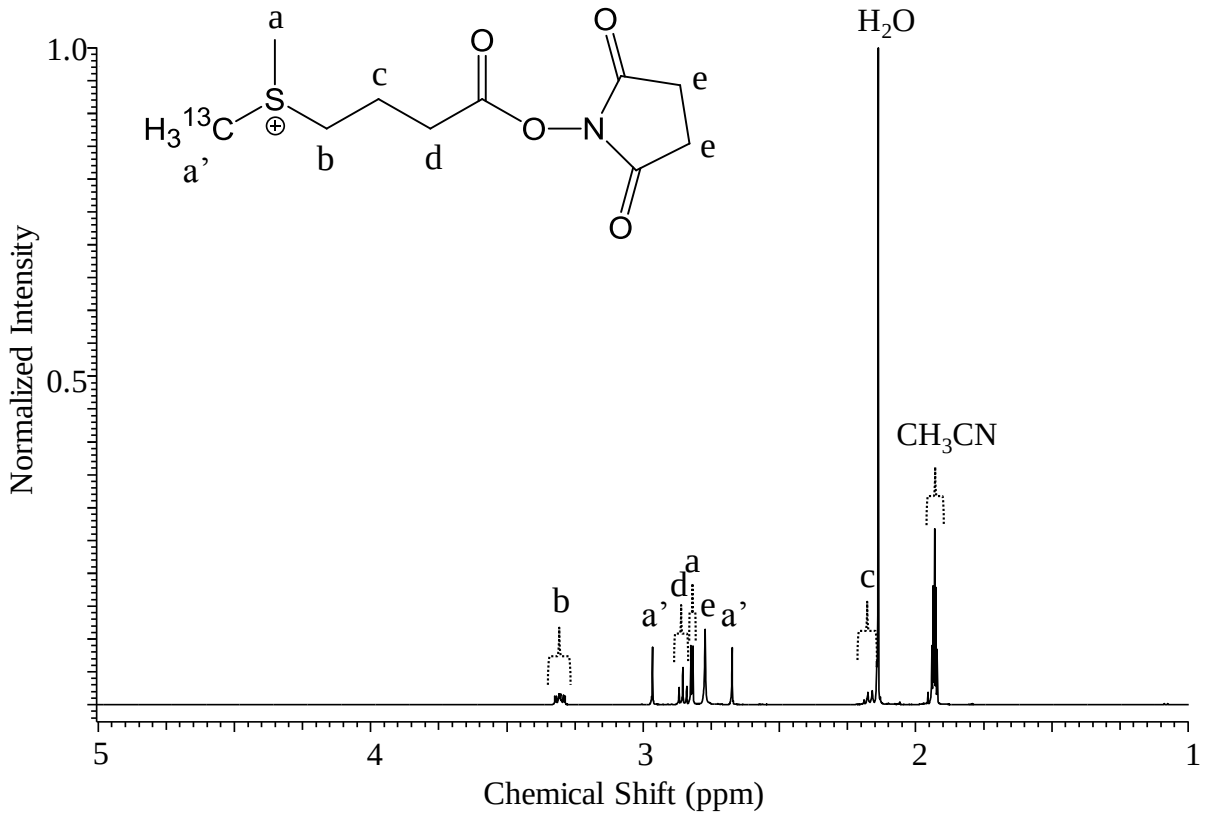

Figure 3.5 ^{1}H NMR characterization of $^{13}C_1$-DMBNHS **(3")**

ESI-MS and CID-MS/MS characterization of **(3), (3')**, and **(3")** are shown in Figure 3.5. Panel A, C, and E show m/z=246.1, m/z=249.1, and m/z=247.1 as the singly charged DMBNHS **(3)**, d_3-DMBNHS **(3')**, and $^{13}C_1$-DMBNHS **(3")**, respectively. CID-MS/MS of $[DMBNHS]^+$, $[d_3\text{-DMBNHS}]^+$, and $^{13}C_1$-DMBNHS (shown in panels B, D, and F) gave a dominant product ion produced by the exclusive neutral loss of dimethylsulfide (62 Da), d_3-dimethylsulfide (65 Da), and $^{13}C_1$-dimethylsulfide (63 Da), respectively.

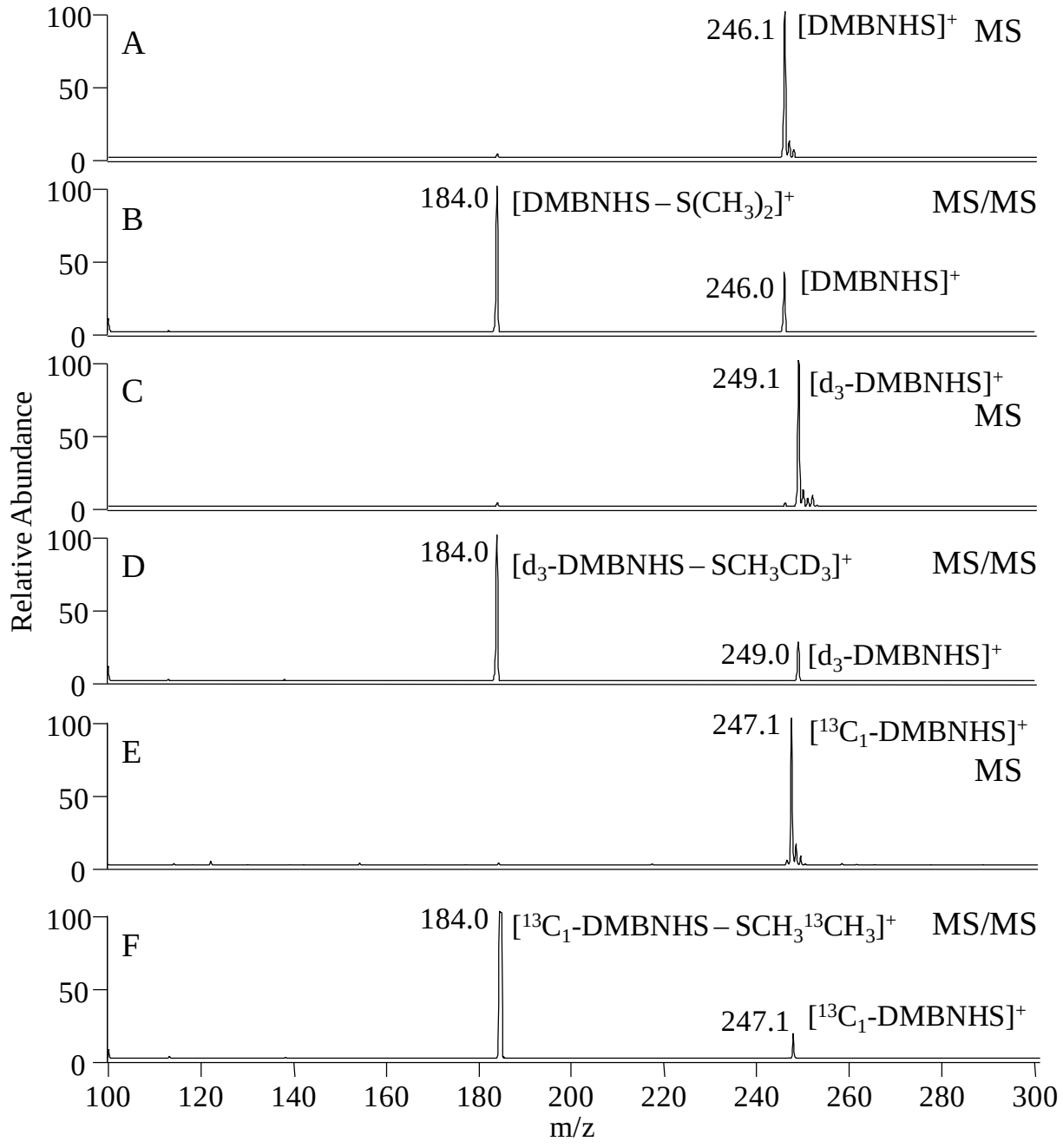

Figure 3.6 Ion trap mass spectrometry characterization of DMBNHS (3), d_3-DMBNHS (3'), and $^{13}C_1$-DMBNHS (3''). ESI-MS of (A) DMBNHS, (C) d_3-DMBNHS, and (E) $^{13}C_1$-DMBNHS (3''). CID-MS/MS of (B) singly charged (3) from panel A, (D) singly charged (3') from panel C, and (F) singly charged (3') from panel E

3.3 Synthesis of S,S'-Dimethylthio-D_6-Butanoylhydroxysuccinimide Ester (d_6-light DMBNHS) and S,S'-D_6-Dimethylthiobutanoylhydroxysuccinimide Ester (d_6-heavy DMBNHS)

A pair of isobaric differential isotope-encoded DMBNHS reagents, S,S'-dimethylthio-d_6-butanoylhydroxysuccinimide ester (d_6-light DMBNHS) and S,S'-d_6-dimethylthiobutanoylhydroxysuccinimide esters (d_6-heavy DMBNHS), were synthesized. Together with DMBNHS, the d_6-light DMBNHS and d_6-heavy DMBNHS reagents were then used in a separate study carried out by Yali Lu in the Reid lab, focused on improving phosphopeptide ESI-MS ionization efficiencies, increased presence or abundance of higher charge state precursor ions, enhanced characterization of phosphorylation sites and phosphopeptide sequences by CID and ETD, and improved differential quantitative analysis [323].

3.3.1 Synthesis of S,S'-Dimethylthio-D_6-Butanoylhydroxysuccinimide Ester (d_6-light DMBNHS)

D_6-light DMBNHS (**(6)** in Scheme 3.2) was synthesized using an analogous method as described for DMBNHS **(3)** with γ-butyrolactone substituted by d_6-γ-butyrolactone as the starting material. The details are provided below.

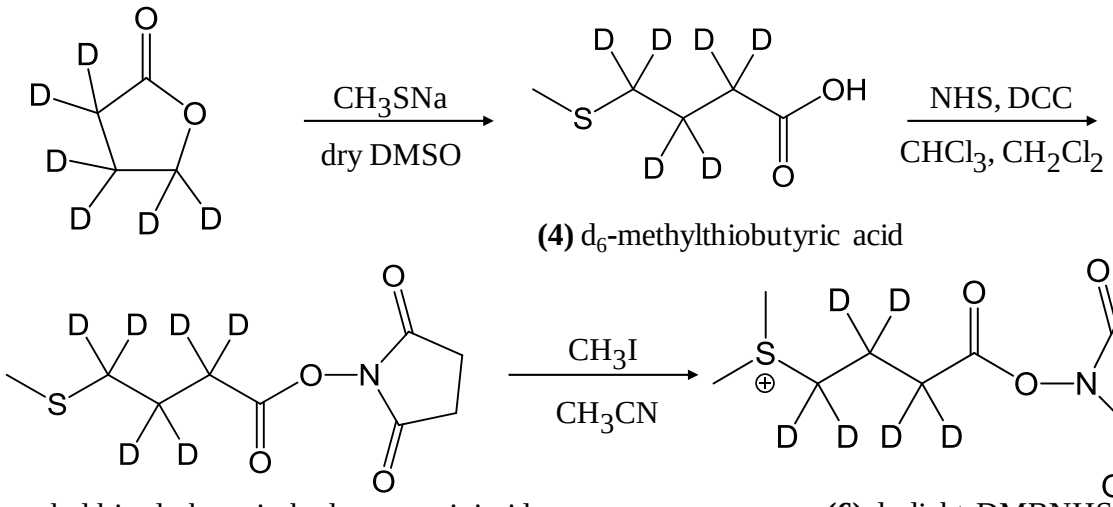

Scheme 3.2 Synthesis of S,S'-dimethylthio-d_6-butanoylhydroxysuccinimide ester, d_6-light DMBNHS.

3.3.1.1 Synthesis of D_6-Methylthiobutyric Acid

Sodium methanethiolate (2.72 g, 34.9 mmol) and d_6-γ-butyrolactone (2.00 mL, 8.73 mmol) were dissolved in 26 mL of anhydrous DMSO, and then the solution was stirred under N_2 atmosphere at room temperature for 119 hrs. 65 mL of 1M HCl was added to the resulting slurry, and then the aqueous solution was extracted with 6 × 40 mL of diethyl ether. The organic extracts were combined, dried over anhydrous $MgSO_4$, and concentrated under reduced pressure. The raw product was redissolved in 100 mL of dichloromethane and washed with 3 × 25 mL of water. After being dried over anhydrous $MgSO_4$ and then *in vacuo*, 3.04 g (90%) of product **(4)** was obtained as a viscous colorless liquid. ^{1}H NMR (500 MHz, $CDCl_3$): δ 2.06 (s, 3H), 11.27 (br, 1H). ^{2}H NMR (500 MHz, $CDCl_3$): δ 1.80 (s, 2H), 2.38 (s, 2H), 2.43 (s, broad, 2H). The ^{1}H NMR and ^{2}H NMR spectra are shown in Figure 3.6 and Figure 3.7, respectively.

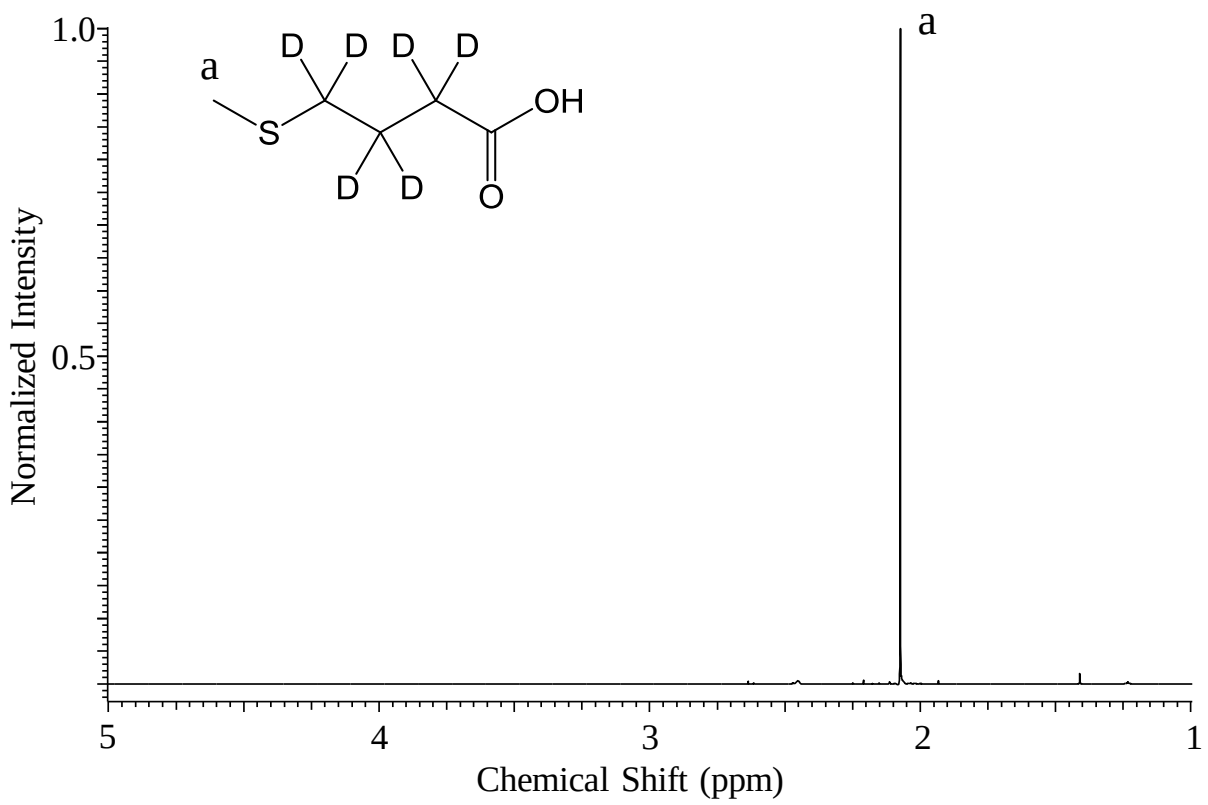

Figure 3.7 ^{1}H NMR characterization of d_6-methylthiobutyric acid **(4)**

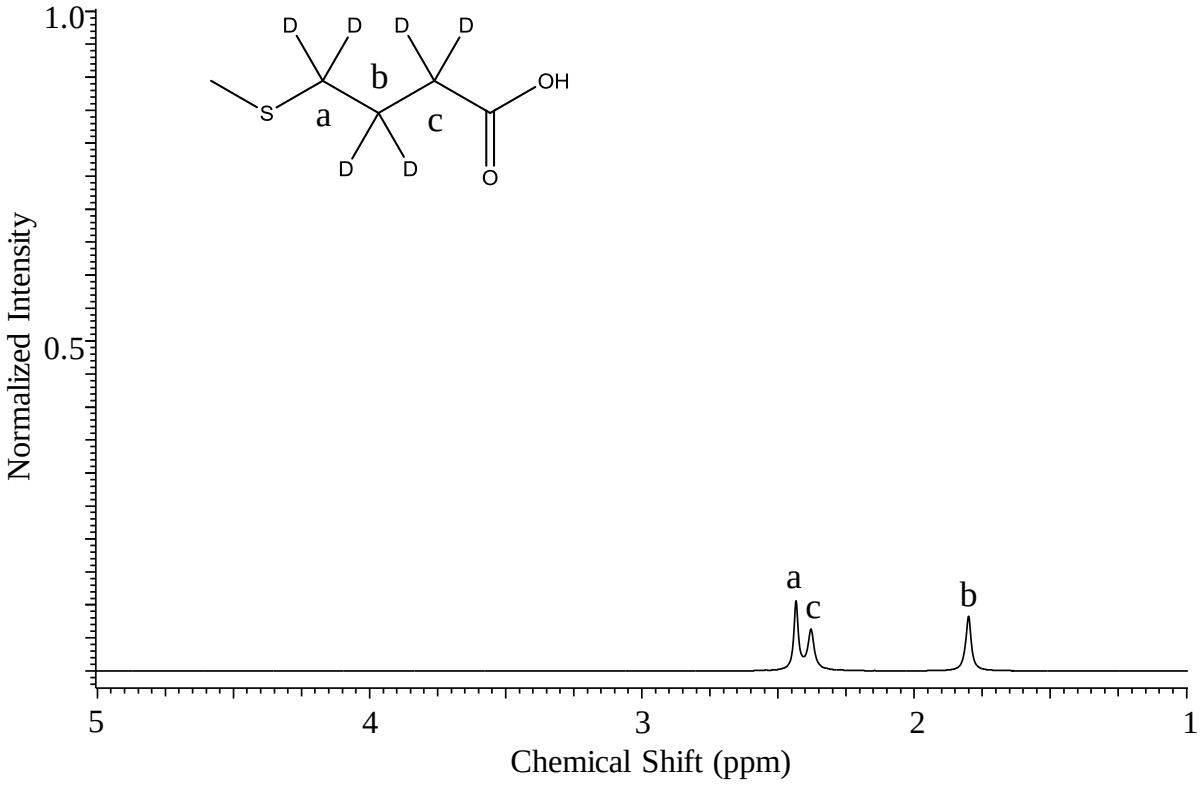

Figure 3.8 ^{2}H NMR characterization of d_6-methylthiobutyric acid **(4)**

3.3.1.2 Synthesis of Methylthio-D_6-Butyric Hydroxysuccinimide Ester

Under a N_2 atmosphere, NHS (1.26 g, 11 mmol) and **(4)** (1.40 g, 10 mmol) were dissolved in a mixture of $CHCl_3$ (20 mL) and CH_2Cl_2 (10 mL). The mixture was stirred for 5 minutes at room temperature. Then DCC (2.27 g, 11 mmol) was added and a precipitate formed immediately. The resulting suspension was stirred in N_2 atmosphere for 18 hrs. The mixture was then filtered and the filtrate was collected and concentrated under reduced pressure. 8 mL of acetonitrile was then added to the residue and the resulting precipitate was filtered out (this step was repeated twice until no precipitate could be observed in acetonitrile). Then acetonitrile (8 mL) was added and the precipitate was filtered out. The solvent was removed *in vacuo* and the ester **(5)** was obtained as a yellow solid with a quantitative yield. ^{1}H NMR (500 MHz, $CDCl_3$): δ 2.07 (s, 3H), 2.82 (s, 4H). The spectrum is shown in Figure 3.8.

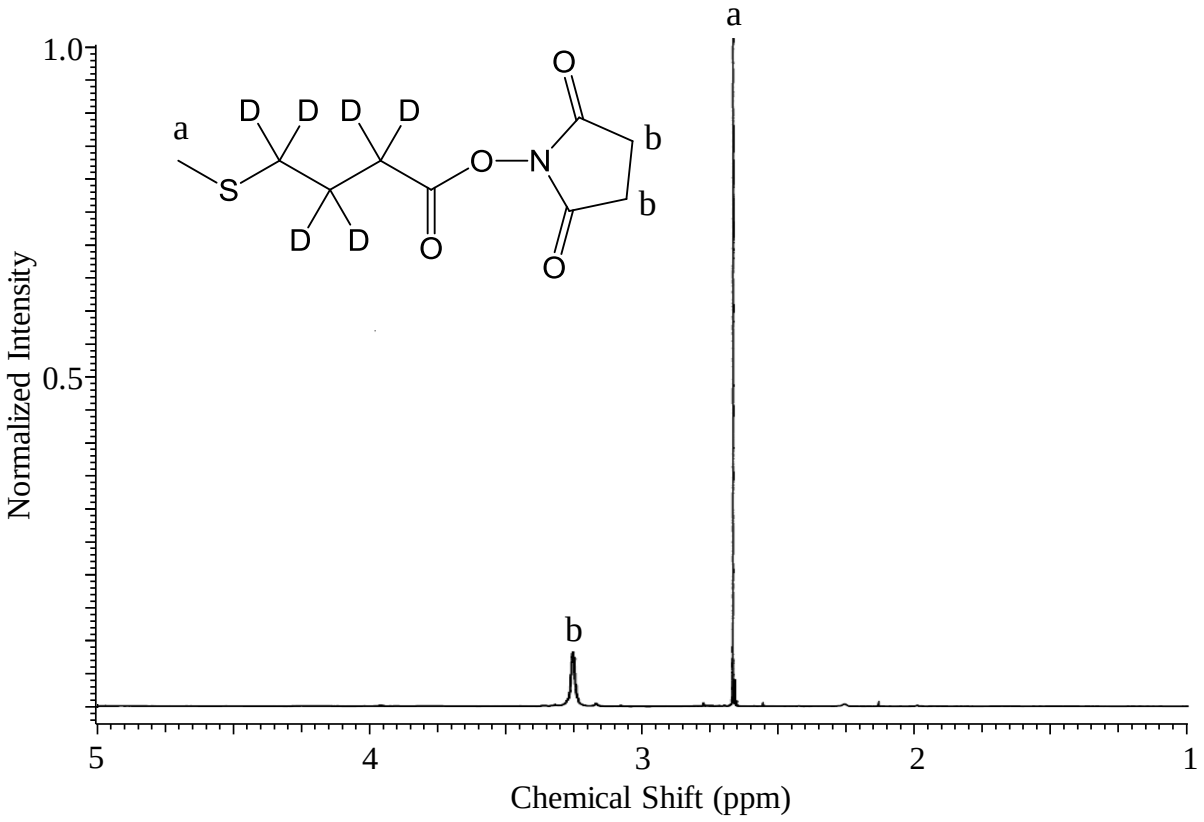

Figure 3.9 ^{1}H NMR characterization of methylthio-d_6-butyric hydroxysuccinimide ester **(5)**

3.3.1.3 Synthesis of D_6-Light DMBNHS

Methylthiobutyric hydroxysuccinimide ester **(5)** (2.23 g, 9.41 mmol) and iodomethane (1.76 mL, 28.23 mmol) were dissolved in 16 mL of CH_3CN followed and stirred in dark at room temperature for 2 days. The resulting solution was then concentrated under reduced pressure. The resultant yellow solid was washed with DCM then dried *in vacuo* to give 3.06 g (86%) of product **(6)** as a pale-yellow solid. The product was stored in the dark. ^1H NMR (500 MHz, CD_3CN): δ 2.77 (s, 4H), 2.83 (s, 6H). The spectrum is shown in Figure 3.9.

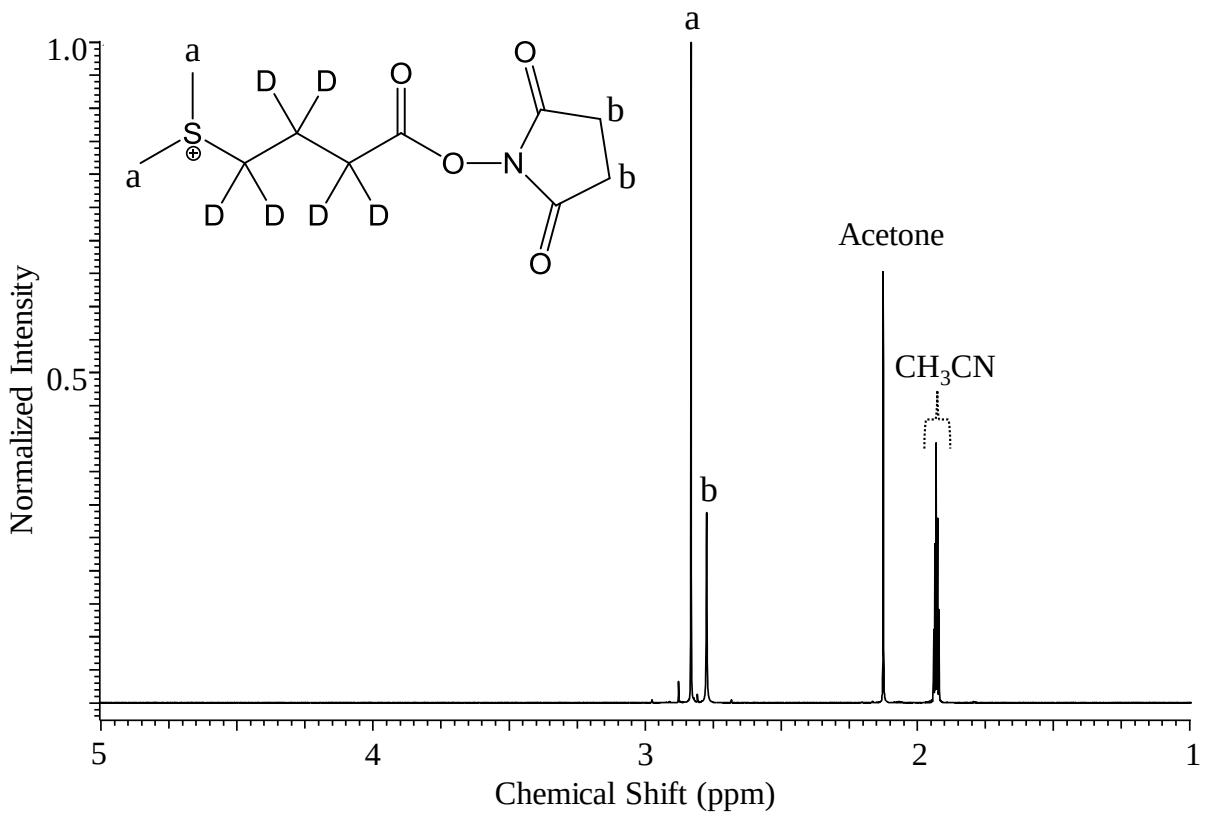

Figure 3.10 ^{1}H NMR characterization of d_6-light DMBNHS **(6)**

ESI-MS and CID-MS/MS characterization of d_6-light DMBNHS **(6)** are shown in Figure 3.10. Panel A shows m/z=252.09 as the singly charged d_6-light DMBNHS **(6)**. A shoulder to the left of m/z=252.09 was observed. This is due to the presence of a d_5-light DMBNHS impurity resulting from the use of a 98% deuterated d_6-γ-butyrolactone as the starting material. CID-MS/MS of the $[d_6\text{-light DMBNHS}]^+$ (shown in panel B) gave an exclusive product ion produced via the neutral loss of d_6-dimethylsulfide (68 Da).

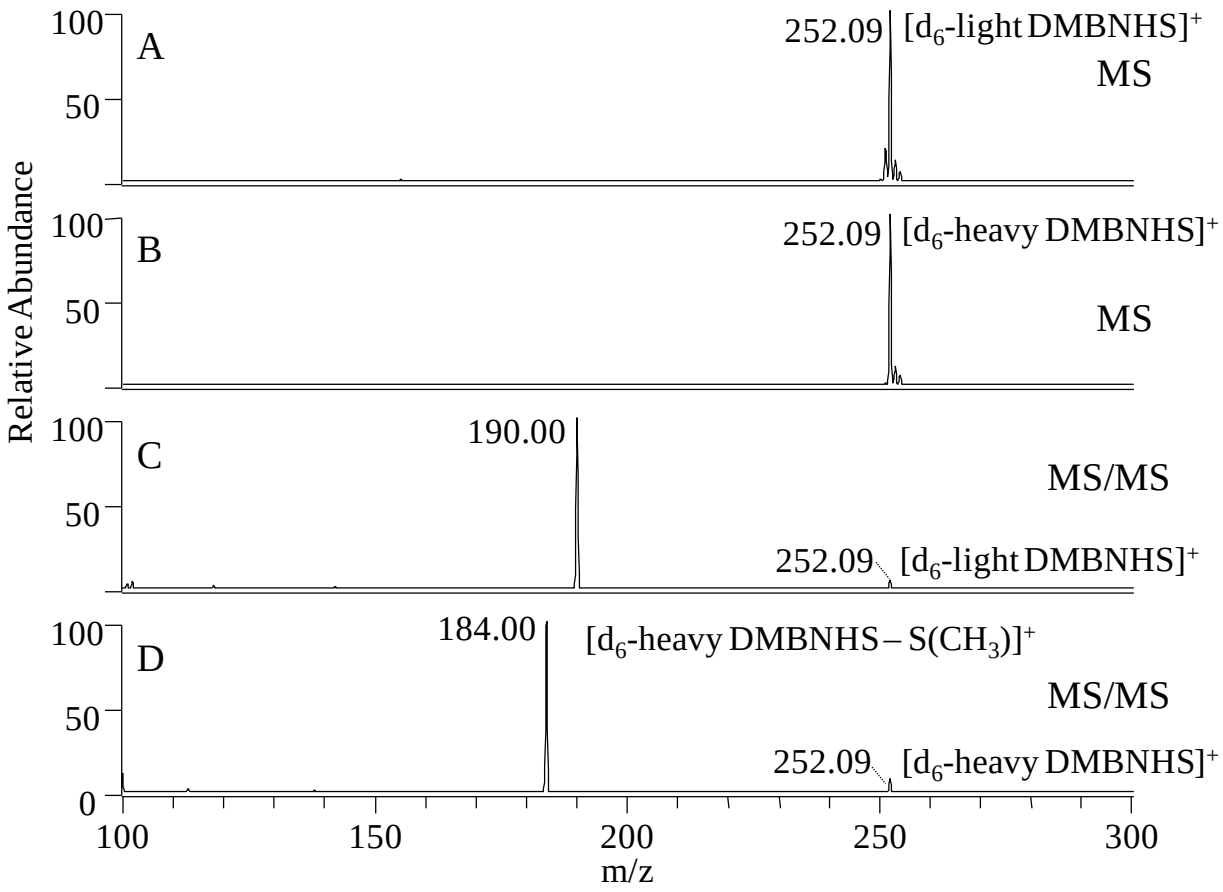

Figure 3.11 Ion trap mass spectrometry characterization of d_6-light DMBNHS **(6)** and d_6-heavy DMBNHS **(10).** ESI-MS of (A) d_6-light DMBNHS and (B) d_6-heavy DMBNHS. CID-MS/MS of (C) singly charged **(6)** from panel A and (D) singly charged **(10)** from panel B.

3.3.2 Synthesis of S,S'-D_6-Dimethylthiobutanoylhydroxysuccinimide Ester (d_6-heavy DMBNHS)

D_6-heavy DMBNHS was synthesized via a four-step process as shown in Scheme 3.3. The details for each step are described below.

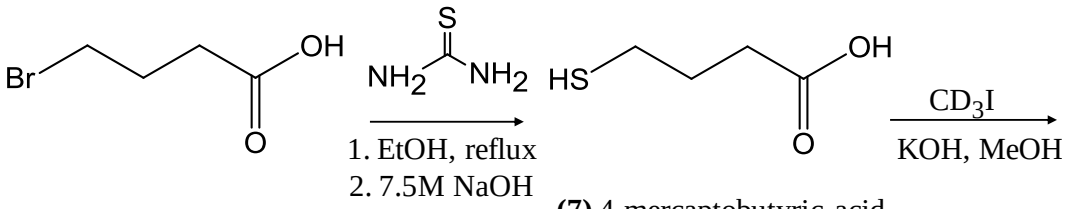

(7) 4-mercaptobutyric acid

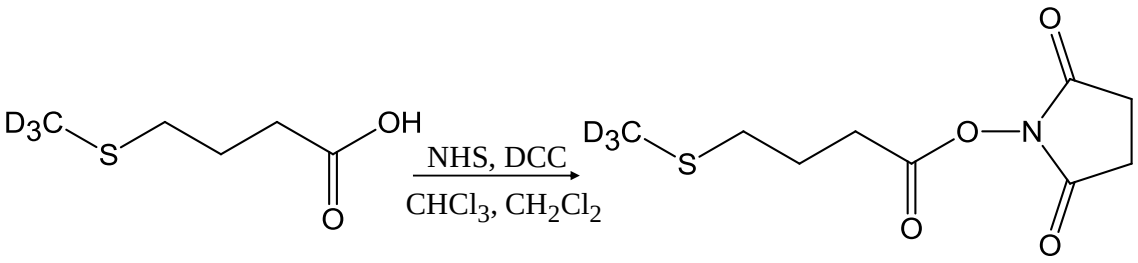

(8) 4-d_3-methylmercaptobutyric acid **(9)** 4-d_3-methylmercaptobutyric hydroxysuccinimide ester

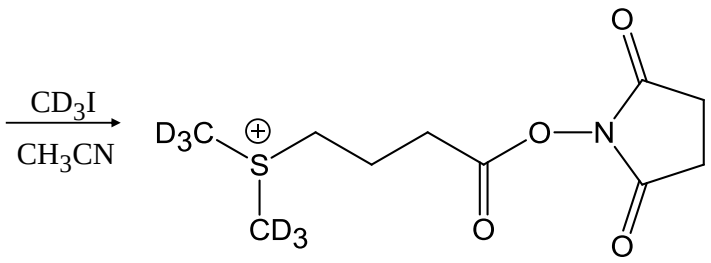

(10) d_6-heavy DMBNHS

Scheme 3.3 Synthesis of d_6-S,S'-dimethylthiobutanoylhydroxysuccinimide ester, d_6-heavy DMBNHS.

3.3.2.1 Synthesis of 4-Mercaptobutyric Acid

Based on the method of Jessing *et. al* [332], 4-bromobutyric acid (8.35 g, 50.0 mmol) and thiourea (5.70 g, 75.0 mmol) were dissolved in 100 mL of ethanol and refluxed overnight. On the second day, the solvent was evaporated under reduced pressure and 65 mL of 7.5 M NaOH (aq) was added. The mixture was reacted at 90 ^{o}C under a N_2 atmosphere. After 16 h reaction, 2M H_2SO_4 was added slowly under stirring until pH=1 in an ice bath. The resulting mixture was extracted with 4 × 60 mL of CH_2Cl_2, dried over anhydrous $MgSO_4$, and concentrated *in vacuo* to give 5.27 g (88%) of the product **(7)** as a colorless oil. ^{1}H NMR (500 MHz, $CDCl_3$): δ 1.33 (t, 1H, *J* = 8.0 Hz), 1.93 (qui, 2H, *J* = 7.0 Hz), 2.50 (t, 2H, *J* = 7.0 Hz), 2.59 (q, 2H, *J* = 7.0 Hz), 11.28 (s, broad, 1H). The NMR spectrum is shown in Figure 3.11.

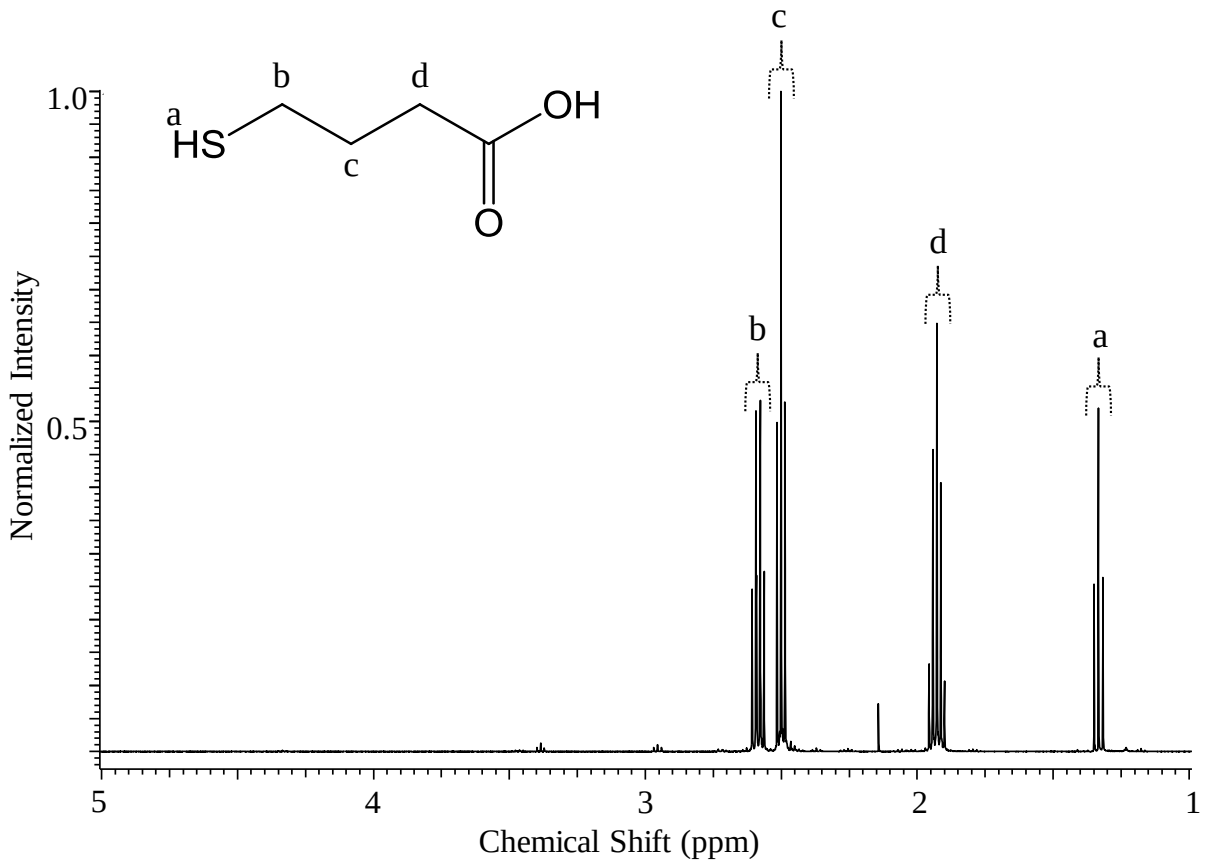

Figure 3.12 ^{1}H NMR characterization of 4-mercaptobutyric acid **(7)**

3.3.2.2 Synthesis of 4-D_3-Methylmercaptobutyric Acid

Adapted from the method of Crouch *et. al* [333], potassium hydroxide (1.31 g, 23.4 mmol) in 2 mL of methanol was added dropwise to **(7)** (1.08 g, 9 mmol) dissolved in 10 mL of methanol in ice bath and stirred for 10 min to be cooled to 0 ^{o}C. D_3-iodomethane (672.4 μL, 10.8 mmol) was added slowly over 10 min and the solution was stirred at room temperature overnight. After evaporating the solvent in reduced pressure, 12 mL of H_2O was added and 2M HCl was added until pH=1. The solution was extracted with 4 × 18 mL of diethyl ether. The organic extracts were combined and dried over anhydrous $MgSO_4$. The solvent was removed *in vacuo* and 858.2 mg (70%) of product **(8)** was obtained as a brown oil. ^{1}H NMR (500 MHz, $CDCl_3$): δ 1.92 (qui, 2H, *J* = 7.0 Hz), 2.48 (t, 2H, *J* = 7.5 Hz), 2.53 (t, 2H, *J* = 7.5 Hz), 11.19 (s, broad, 1H). The spectrum is shown in Figure 3.12.

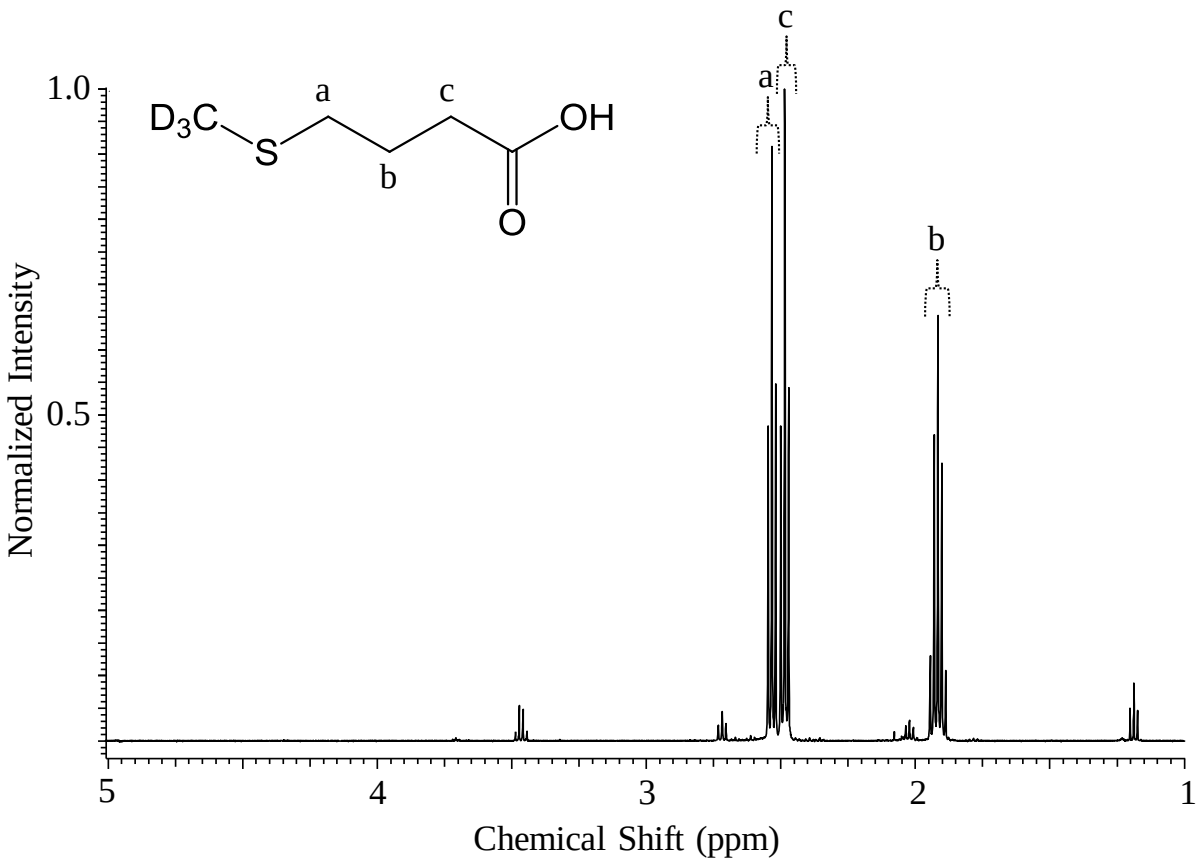

Figure 3.13 ^{1}H NMR characterization of 4-d_3-methylmercaptobutyric acid **(8)**

3.3.2.3 Synthesis of 4-D_3-Methylmercaptobutyric Hydroxysuccinimide Ester

Under a N_2 atmosphere, N-hydroxysuccinimide (792.4 mg, 6.89 mmol) and **(8)** (858.2 mg, 6.26 mmol) were dissolved in a mixture of $CHCl_3$ (15 mL) and CH_2Cl_2 (10 mL). The mixture was stirred for 5 minutes at room temperature. Then N,N'-dicyclohexylcarbodiimide (1419.5 mg, 6.89 mmol) was added and a precipitate formed immediately. The resulting slurry was stirred in N_2 atmosphere. After 18 hrs, the mixture was filtered and the filtrate was collected and concentrated under reduced pressure. Then acetonitrile (3 mL) was added and the precipitate was filtered out. The solvent was removed *in vacuo* and the ester **(9)** was obtained as a yellow solid with a quantitative yield. ^{1}H NMR (500 MHz, $CDCl_3$): δ 2.02 (qui, 2H, J = 7.5 Hz), 2.58 (t, 2H, J = 7.5 Hz), 2.74 (t, 2H, J = 7.0 Hz), 2.82 (s, 4H). The spectrum is shown in Figure 3.13.

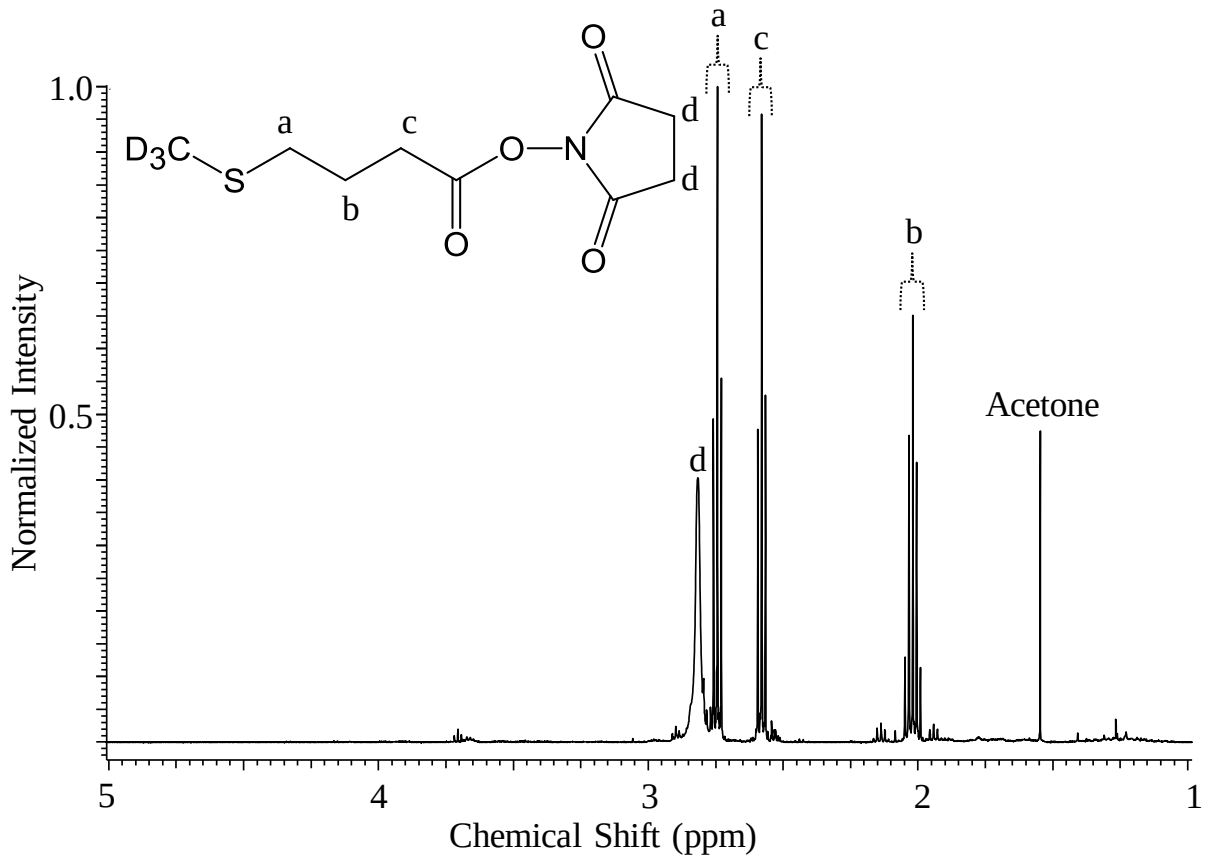

Figure 3.14 ^{1}H NMR characterization of 4-d_3-methylmercaptobutyric hydroxysuccinimide ester **(9)**

3.3.2.4 Synthesis of D_6-Heavy DMBNHS

4-D_3-methylmercaptobutyric hydroxysuccinimide ester **(9)** (933.6 mg, 3.99 mmol) and d_3-iodomethane (1.16 g, 7.98 mmol) were dissolved in CH_3CN (8 mL) and stirred in dark at room temperature for 2 days. The resulting solution was concentrated under reduced pressure. The resultant yellow solid was washed with dichloromethane and then dried *in vacuo* over night to give 1.19 g (79%) of **(10)** as a white powder. The product was stored in the dark. ^{1}H NMR (500MHz, CD_3CN): δ 2.16 (qui, 2H, *J* = 7.5), 2.77 (s, 4H), 2.85 (t, 2H, *J* = 7.5), 3.30 (m, 2H). The spectrum is shown in Figure 3.14.

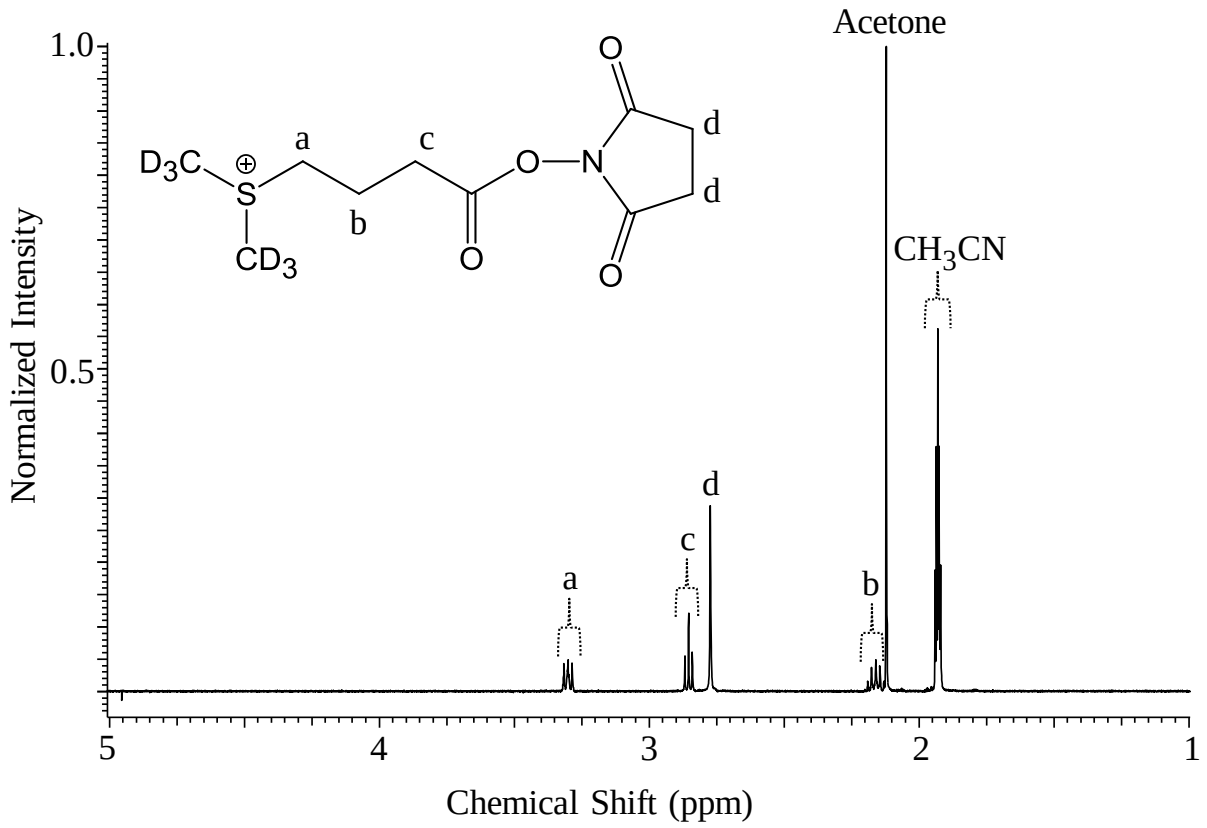

Figure 3.15 ^{1}H NMR characterization of d_6-heavy DMBNHS **(10)**

ESI-MS and CID-MS/MS characterization of d_6-heavy DMBNHS **(10)** are shown in Figure 3.10. Panel C shows m/z=252.09 as the singly charged d_6-heavy DMBNHS **(6)**. CID-MS/MS of the $[d_6\text{-heavy DMBNHS}]^+$ (shown in panel D) gave a dominant product ion produced by the exclusive neutral loss of dimethylsulfide (62 Da). As illustrated in Figure 3.14, d_6-heavy DMBNHS and d_6-light DMBNHS showed the same m/z in ESI-MS but give rise to different product ion with a mass difference of 6 Da under CID-MS/MS.

3.4 Peptide Modification Reaction

20 μg of neurotensin was dissolved in 20 μL of PBS buffer (NaCl: 136.75 mM, $Na_2HPO_4 \cdot 7H_2O$: 8.10 mM, KCl: 2.68 mM, KH_2PO_4: 1.47 mM, pH=7.5) to a concentration of 0.6 mM. Then 0.2 μL of DMBNHS **(3)** dissolved in DMF at a concentration of 60 mM was added to the peptide solution and reacted at room temperature (peptide : reagent = 1 : 1). After 1 hr, the resultant mixture was desalted by Sep-Pak® C18 (Waters, Milford, MA, USA) according to the manufacturer's protocol with elution in 40, 60, and 80% acetonitrile (aq) containing 0.05% formic acid and directly injected to mass spectrometer for analysis without further purification.

3.5 Protein Modification and Digestion

CRABP II (25 μg, 1.60 nmol) was suspended in 100 μL of PBS buffer (NaCl: 136.75 mM, $Na_2HPO_4 \cdot 7H_2O$: 8.10 mM, KCl: 2.68 mM, KH_2PO_4: 1.47 mM). 1 μL of DMBNHS solution dissolved in DMF with concentrations of 8.0 mM (CRABP II : DMBNHS = 1:5), 16 mM (CRABP II : DMBNHS = 1:10), 32 mM (CRABP II : DMBNHS = 1:20), 80 mM (CRABP II : DMBNHS = 1:50), and 160 mM (CRABP II : DMBNHS = 1:100) were added and each of them was incubated at room temperature for 30 min. The reaction was immediately quenched by addition of a 160-fold molar excess of Tris (100 mM, pH 8.26 at 25 ^{o}C) then concentrated to dryness by vacuum centrifugation. 25 μL of PBS buffer containing 6 M guanidine hydrochloride was then added and the protein was denatured at 37 ^{o}C for 1 hr. 225 μL of ddH_2O was added to bring the final volume to 250 μL. The pH was adjusted to 8.0 with 0.2 mM NaOH or HCl prior

to digestion. 5 μL of 0.25 μg/μL Glu-C solution (Glu-C : CRABP II = 1 : 20(w/w)) was added and the reaction mixture was incubated at 31 ^{o}C overnight. The digestion was quenched by adding 3 μL of formic acid and stored at -20 ^{o}C for future analysis.

3.6 Mass Spectrometry of Protein Modification Reagents

3.6.1 Mass Spectrometry of DMBNHS and D_3-DMBNHS

The protein modification reagents, DMBNHS and d_3-DMBNHS were dissolved in acetonitrile to a final concentration at 20 μM and analyzed by a Thermo Scientific model LCQ Deca 3D quadrupole ion trap (Thermo, San Jose, CA, USA) equipped with a nanoelectrospray ionization (nESI) source. The sample was introduced into the mass spectrometer at a flow rate of 2 μL/min. The spray voltage was maintained at 2.5 kV, and the ion transfer tube of the mass spectrometer was set at 150 ℃. The CID-MS/MS analysis used an activation *q* value at 0.25, an activation time of 30 ms, and normalized collision energy at 20. The spectra shown are the average of 30 scans.

3.6.2 Mass Spectrometry of D_6-Light DMBNHS and D_6-Heavy DMBNHS

$^{13}C_1$-DMBNHS, D_6-light DMBNHS, and d_6-heavy DMBNHS were dissolved in acetonitrile to a final concentration at 20 μM and introduced to a Thermo Scientific model LTQ

linear quadrupole ion trap mass spectrometer (Thermo, San Jose, CA, USA) via a chip-based nESI source (Advion NanoMate, Ithaca, NY) operating in infusion mode using an ESI HD_A chip, a spray voltage of 1.4 kV, and a gas pressure of 0.3 psi. The ion transfer tube of the mass spectrometer was set at 150 ℃. The CID-MS/MS analysis used an activation *q* value at 0.25, an activation time of 30 ms, and collision energy at 15. The spectra shown are the average of 30 scans.

3.7 Mass Spectrometry of the Model Peptide

After being desalted by Sep-Pak® C18, the peptide was in ~60% acetonitrile/0.05% formic acid with a concentration at ~15 μM. The modified peptide was then injected to a Thermo Scientific model LTQ linear quadrupole ion trap mass spectrometer (Thermo, San Jose, CA, USA) equipped with a nESI source. The sample was introduced into the mass spectrometer at a flow rate of 2 μL/min. The spray voltage was maintained at 2.5 kV, and the ion transfer tube of the mass spectrometer was set at 150 ℃. The CID-MS/MS and -MS^3 used an activation *q* value at 0.25, an activation time of 30 ms, and normalized collision energy of 12. The spectra shown are the average of 30 scans.

3.8 HPLC-ESI-MS, CID-MS/MS and -MS^3 Analysis of Protein Digests

HPLC-ESI-MS, CID-MS/MS and -MS^3 analyses were performed using a Thermo LTQ linear quadrupole ion trap mass spectrometer (Thermo, San Jose, CA, USA) equipped with an

Advance nESI source and Paradigm MS4 capillary RP-HPLC system (Michrom Bioresources, Auburn, CA, USA). Analyses were performed using automated methods created by the Xcalibur software (Thermo, San Jose, CA, USA). 5 μL of each sample with a concentration at 1.6 pmol/μL in 3% acetic acid/5% acetonitrile was loaded from a Paradigm AS1 autosampler (Michrom Bioresources, Auburn, CA, USA) onto a peptide CapTrap (Michrom Bioresources, Auburn, CA, USA) at a flow rate at 15 μL/min using 0.1% trifluoroacetic acid/ 2% acetonitrile as the loading buffer. After 5 min loading time, the peptides concentrated on the CapTrap were eluted to a 200 μm id × 50 mm fused silica column packed with Magic C18AQ (3 μm, Michrom Bioresources, Auburn, CA, USA) at a flow rate of 2 μL/min using a linear 45 min gradient from 95% solvent A (0.1% formic acid in H_2O) to 50% solvent B (0.1% formic acid in CH_3CN). After gradient separation, the system was cleaned with 80% solvent B for 5 min followed by equilibrium with 95% solvent A for 5 min. The ion transfer tube of the mass spectrometer was set at 180 ℃, and the spray voltage was maintained at 2.0 kV. The activation time was maintained at 30 ms using an activation *q* value of 0.25. The isolation window was maintained at 2.0 m/z while the normalized collision energy was set at 35. All spectra were recorded in centroid mode. The LTQ was operated in a data-dependent constant neutral loss scan (DDCNL) mode by performing CID-MS/MS scans on the 3 most intense peaks from each MS scan, while simultaneously searching for the defined neutral losses (Table 3.1). Here, the neutral losses with m/z variance of ±0.5 were set to account for single, double, and triple $S(CH_3)_2$ neutral losses from $[M^{N+}+(m-N)H]^{m+}$ precursor ions, where M represents the peptide, N represents the number of modifications, and m represents the different observed charge states ranging from +2 to +5. If the targeted neutral loss was detected and appeared above a predefined threshold

abundance of 1.0×10^4 counts, CID-MS^3 was automatically initiated to further fragment the most intense neutral loss product ion. Dynamic exclusion was enabled to analyze ions with the selected data dependent m/z 3 times within 30 s before it was placed on a dynamic exclusion list for a period of 10 s. Characterization of modification sites and peptide sequences were determined manually from interpretation of the MS^3 spectra.

Table 3.1 Summary of the Data Dependent Constant Neutral Loss (DDCNL) MS/MS values employed for the identification of DMBNHS modified Glu-C digest peptides from CRABP II.

Neutral loss (m/z)	Number of $S(CH_3)_2$ neutral losses	Precursor ion
62.00	1	$[M^{N}]^{+a}$
	2	$[M^{N}+(2\text{-}N)H]^{2+a}$
	3	$[M^{N}+(3\text{-}N)H]^{3+a}$
	4	$[M^{N}+(4\text{-}N)H]^{4+a}$
49.60	4	$[M^{N}+(5\text{-}N)H]^{5+a}$
46.50	3	$[M^{N}+(4\text{-}N)H]^{4+a}$
41.33	2	$[M^{N}+(3\text{-}N)H]^{3+a}$
37.20	3	$[M^{N}+(5\text{-}N)H]^{5+a}$
31.00	1	$[M^{N}+(2\text{-}N)H]^{2+a}$
	2	$[M^{N}+(4\text{-}N)H]^{4+a}$
24.80	2	$[M^{N}+(5\text{-}N)H]^{5+a}$
20.67	1	$[M^{N}+(3\text{-}N)H]^{3+a}$
15.50	1	$[M^{N}+(4\text{-}N)H]^{4+a}$
12.40	1	$[M^{N}+(5\text{-}N)H]^{5+a}$

[a] N = number of modifications.

3.9 Data Analysis

3.9.1 Quantitative Analysis of Percent DMBNHS Modification of Model Protein Digests

The percent of unmodified, singly modified, doubly modified, and triply modified peptide were determined as (precursor ion abundance of the corresponding modification state)/(precursor ion abundance summed from all modification states). If multiple charge states for a precursor ion were observed, then abundance was calculated by combing all the charge states.

3.9.2 Computational Analysis

3.9.2.1 Prediction of Solvent Accessibilities

The program GetArea [329] was used, with all parameters set at the default values, to calculate the solvent-accessibilities of lysine amino acid side chains and the N-terminal amino group of CRABP II, based on the reported NMR solution structure, 1BLR [330].

3.9.2.2 Prediction of Proton Affinities

Model structures of the neutral and protonated side chain functional groups of lysine (methylamine), histidine (4-methyl imazadole), and arginine (N-methyl guanidine), as well as the side chain formed via the loss of $S(CH_3)_2$ from the DMBNHS modified peptides (N-methyl iminohydrofuran) were initially optimized at the PM3 semi-empirical level of theory to identify

likely candidates for the global minimum, followed by further optimization at the B3LYP/6-311+G(d,p) level of theory [334]. Single point calculations were then performed at the MP2/6-311+G(2d,p) level of theory. All optimized structures were subjected to vibrational frequency analysis at the B3LYP/6-311+G(d,p) level. Proton affinities (PA) were determined as described previously [335]. Briefly, proton affinities were calculated according to the negative of the enthalpy of the protonation reaction (3.1), as shown in equations (3.2) and (3.3).

$$\mathbf{M} + \mathbf{H}^{+} \rightarrow \mathbf{MH}^{+} \tag{3.1}$$

$$\mathbf{PA} = -\Delta \mathbf{r}\mathbf{H}^{\mathbf{0}}_{\mathbf{298}} \tag{3.2}$$

$$-\Delta \mathbf{r}\mathbf{H}^{\mathbf{0}}_{\mathbf{298}} = \Delta_{\mathbf{r}}\mathbf{E} + \Delta\left(\Delta \mathbf{E}_{\mathbf{t,298}}\right) + \Delta\left(\Delta \mathbf{E}_{\mathbf{t,298}}\right) + \Delta\left(\Delta \mathbf{E}_{\mathbf{v,298}}\right) + \Delta \mathbf{PV} \tag{3.3}$$

In equation (3.3), $\Delta_{\mathbf{r}}\mathbf{E}$, $\Delta\left(\Delta \mathbf{E}_{\mathbf{t,298}}\right)$, $\Delta\left(\Delta \mathbf{E}_{\mathbf{r,298}}\right)$, **and** $\Delta\left(\Delta \mathbf{E}_{\mathbf{v,298}}\right)$ are the difference in electronic, translational, rotational, and vibrational energy correction (from 0 to 298 K) between MH^{+} and M, respectively. $\Delta_{\mathbf{r}}\mathbf{E}$ can be expressed as equation (3.4), where ZPE is the zero-point energy correction of the species.

$$\Delta_{\mathbf{r}}\mathbf{E} = \mathbf{E}_{\mathbf{elec}}(\mathbf{MH}^{+}) - \mathbf{E}_{\mathbf{elec}}(\mathbf{M}) + \mathbf{ZPE}(\mathbf{MH}^{+}) - \mathbf{ZPE}(\mathbf{M}) \tag{3.4}$$

When an ideal condition is assumed, where $\mathbf{\Delta PV = -RT}$, $\mathbf{\Delta\left(\Delta E_{t,298}\right)}$ comes from the contribution of proton and can be expressed as equation (3.5), and $\mathbf{\Delta\left(\Delta E_{r,298}\right) = 0}$.

$$\mathbf{\Delta\left(\Delta E_{t,298}\right) = -\frac{3}{2}R} \tag{3.5}$$

Therefore, equation (3.3) can be rewritten as below,

$$\mathbf{-\Delta rH^{0}_{298} = E_{elec}(MH^{+}) - E_{elec}(M) + ZPE(MH^{+}) - ZPE(M)}$$
$$\mathbf{+\Delta E_{v,298}(MH^{+}) - \Delta E_{v,298}(M) - \frac{5}{2}RT} \tag{3.6}$$

where $\mathbf{E_{elec}(MH^{+}), E_{elec}(M), ZPE(MH^{+}), ZPE(M)}$, $\mathbf{\Delta E_{v,298}(MH^{+}), and\ \Delta E_{v,298}(M)}$ can be obtained from the output of the structural optimization.

CHAPTER FOUR

OXIDATION INDUCED CONFORMATIONAL CHANGE IN CALCINEURIN STUDIED BY FIXED-CHARGE PROTEIN DERIVATIZATION

4.1 Introduction

With the initial success in determining protein surface residue solvent accessibilities of a model protein, CRABP II, the experimental strategy, i.e., combining protein modification by DMBNHS with data dependent multistage tandem mass spectrometry, was further extended to reveal the mechanisms corresponding to oxidation induced inactivation of calcineurin (CN), from a structural perspective.

Calcineurin, also called protein phosphatase 2B (PP2B), is a Ca^{2+}/calmodulin (CaM) activated serine/threonine phosphatase that is widely distributed in mammalian tissues [336]. By dephophorylating selective substrates, CN functions in a signal transduction pathway to regulate gene expression [337] and participates in a wide variety of physiological processes, such as skeletal muscle differentiation and regeneration [338, 339] , cardiac hypertrophy [340], and neuronal signaling [341].

CN is a heterodimeric protein composed of a ~60 kDa catalytic subunit, CNA, and a ~19 kDa regulatory subunit, CNB. As shown in Figure 4.1, CNA consists of 4 domains, a catalytic domain, a CNB binding domain, a CaM interaction region, and an autoinhibitory (AI) motif [336]. The CN active site, which is located in the catalytic domain, contains a binuclear metal center that is critical for dephophorylation activity. The two metals have been identified as Zn,

which is coordinated with Asn_{150A}, His_{199A}, and His_{281A} (the subscript number and letter indicate the residue number and the CN subunit, respectively), and Fe, which is coordinated with Asp_{90A} and His_{92A} [336, 342-345]. The existences of both Fe^{3+}-Zn^{2+} [342, 343, 346, 347] and Fe^{2+}-Zn^{2+} [348, 349] forms have been reported and the oxidation states of Fe in the active enzyme remains inclusive. In the absence of CaM, the catalytic groove which contains the dinuclear metal center is bound with AI and the enzyme is inhibited. CNA is tightly associated with CNB which is a CaM-like protein possessing four Ca^{2+} binding sites [350]. Two of the Ca^{2+} binding sites, which are located close to the C-terminus, have relatively high affinity and are occupied under normal conditions with Ca^{2+} concentration lower than 10^{-7} M, whereas the two Ca^{2+} binding sites close to N-terminus have relatively low affinity [351-353]. Ca^{2+}/CaM regulated CN activation is proposed to occur via a disinhibition mechanism. More specifically, the extracellular stimulation induced elevation of intracellular Ca^{2+} concentration causes changes to both CNB and CaM. The occupancy of the two low-affinity sites located on the N-terminus of CNB under increased Ca^{2+} concentration causes a small conformational change in its tightly associated CNA and facilitates the binding with CaM [351]. At the same time, CaM activation caused by Ca^{2+} binding enables its interaction with the target sequence, i.e., the CaM binding domain, in CNA and induces a conformational change which removes the AI domain from the catalytic site and activates CN.

CN subunit A (CNA): ~60 kDa

*MSEPKAIDPKLST*TDRVVKAVPFPPSHRLTAKEVFDNDGKPRVDILKAHLM$_{51}$KEGRLEESVALRIITEGA
SILRQEKNLLDIDAPVTVCGDIHGQFFDLM$_{99}$KLFEVGGSPANTRYLFLGDYVDRGYFSIECVLYLWALKILY
PKTLFLLRGNHECRHLTEYFTFKQECKIKYSERVYDACM$_{179}$DAFDCLPLAALM$_{191}$NQQFLCVHGGLS
PEINTLDDIRKLDRFKEPPAYGPM$_{227}$CDILWSDPLEDFGNEKTQEHFTHNTVRGCSYFYSYPAVCEFLQH
NNLLSILRAHEAQDAGYRM$_{290}$YRKSQTTGFPSLITIFSAPNYLDVYNNKAAVLKYENNVM$_{329}$NIRQF
NCSPHPYWLPNFM$_{347}$DVFTWSLPFVGEKVTEM$_{364}$LVNVLNICS*DDELGSEEDGFDGATAAARKEVIR*
NKIRAIGKM$_{406}$ARVFSVLREESESVLTLKGLTPTGM$_{431}$LPSGVLSGGKQTLQSATVEAIEADEAIKGFS
PQHKITSFEEAKGLDRINERM$_{483}$PPRRDAM$_{490}$PSDANLNSINKALTSETNGTDSNGSNSSNIQ

CN subunit B (CNB): ~19 kDa

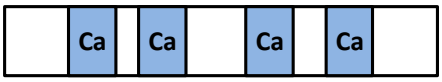

MGNEASYPLEM$_{11}$CSHFDADEIKRLGKRFKKLDLDNSGSLSVEEFM$_{44}$SLPELQQNPLVQRVIDIFDTDG
NGEVDFKEFIEGVSQFSVKGDKEQKLRFAFRIYDM$_{101}$DKDGYISNGELFQVLKM$_{118}$M$_{119}$VGNNL
KDTQLQQIVDKTIINADKDGDGRISFEEFCAVVGGLDIHKKM$_{166}$VVDV

Figure 4.1 Protein domains and sequences of CNA and CNB. The CNA subunit, whose sequence was obtained from UnitProt entry Q08209, includes a catalytic domain (14_A-342_A, where the number and subscript letter indicate the residue number and the corresponding CN subunit, respectively), a CNB binding motif (343_A-373_A), a CaM interaction domain (390_A-414_A), and an autoinhibitory region (469_A-486_A). The CNB subunit, whose sequence was from UnitProt entry P63098, contains four EF-hand Ca^{2+}-binding domains (EF-hand I ranges from 18_B to 50_B with 31_B-42_B as the first Ca^{2+} binding region; EF-hand II ranges from 51_B to 85_B with 63_B-74_B as the second Ca^{2+} binding region; EF-hand III ranges from 87_B to 122_B with 100_B-111_B as the third Ca^{2+} binding region; EF-hand IV ranges from 128_B to 163_B with 141_B-152_B as the fourth Ca^{2+} binding region). The sequences not visible in the electron map from PDB entry 1AUI [344] are in italic text.

Besides being regulated by CaM, CN is also reported to be inactivated by H_2O_2- or superoxide-induced oxidation both *in vivo* and *in vitro* [354-358]. Several mechanisms have been proposed. One mechanism postulated that the redox regulation of CN is induced by the formation of a disulfide bridge between two vicinal cysteine residues in the catalytic region of CNA [347]. However, how the bridging affects CN enzymatic activity remains unclear as the only pair of conserved cysteine residues (Cys_{228A} and Cys_{256A}) which could form the disulfide bond are not close to the active dinuclear metal center [344, 345]. The author proposed a bridging-induced conformational change in the catalytic domain of CNA as the cause of inactivation; however, this hypothesis has not been demonstrated experimentally. Another mechanism suggests that the binuclear active site exists as Fe^{2+}-Zn^{2+} and the CN inactivation is caused by the oxidation of Fe^{2+} to Fe^{3+} [349]. However, this finding is in conflict with many previous studies demonstrating Fe^{3+}-Zn^{2+} as the active form with maximum activity, based on kinetic and spectroscopic characterization [343, 346, 347] and comparison with the metal cluster center in purple acid phosphatase [346]. Recently, Carruthers *et. al.* proposed another mechanism suggesting that oxidative inactivation of CN is caused by the inhibition of CN-CaM interaction due to the oxidation of Met_{406A} located in the CaM binding motif of CNA [359]. They determined Met_{406A} to be highly susceptible to oxidation. Oxidation of Met_{406A} was found to result in a decreased CaM/CN binding affinity, which was suspected to contribute to CN inactivation. However, it was found that a CN mutant with Met_{406A} changed to Leu ($M_{406A}L$) also showed reduced activity upon oxidation, indicating oxidation induced CN inactivation is not, at least not only, mediated by Met_{406A} oxidation.

Here, as an extension of the initial study by Carruthers *et. al.*[359], it is proposed that oxidation causes a conformational change to CN, which may impair CN/CaM binding and inhibit CN activation. In order to demonstrate this hypothesis, the relative rates of H_2O_2 induced oxidative modification of methionine residues within CN were first determined using a multi-enzyme digestion strategy coupled with HPLC-ESI-MS and CID-MS/MS analysis. Then, the analytical strategy developed in Chapter 2 involving protein surface labeling using DMBNHS and data-dependent multistage tandem mass spectrometry, was applied to characterize changes in CN conformation before and after oxidation.

4.2 Quantification of the Susceptibility of Methionine Residues towards Oxidation

To determine the sensitivity of Met residues within CN to oxidation by H_2O_2, CN was incubated with 12 mM H_2O_2 for 0, 15, 30, 45, 60, 120, and 240 min, then digested with Lys-C, trypsin, or Glu-C, and analyzed in triplicate by capillary HPLC-ESI-MS and CID-MS/MS. The MS spectra were acquired in an Orbitrap mass analyzer with 60,000 resolution, while CID/ETD-MS/MS scans were acquired in an ion trap. The peptides were identified by their monoisotopic m/z obtained from the MS spectra acquired with high mass accuracy in the Orbitrap mass analyzer and further confirmed by sequence ions from the MS/MS spectra acquired in the ion trap. The observed Met residues and the corresponding peptides from the three different digests, and from Carruthers's results [359], are listed and compared in Table 4.1. 15 of the total 19 Met residues were observed. It was noted that the sequence coverage obtained here from Lys-C digest

were different from the study by Carruthers *et. al.* [359]. This is likely attributed to differences in chromatographic separation used in each individual study.

Table 4.1 Summary of Methionine residues observed from different proteolytic digests of CN and the predicted solvent accessibilities.

Met residue	Peptides observed from the corresponding digests				Predicted solvent accessibilities [c]
	trypsin digest	Glu-C digest	Lys-C digest	Lys-C digest from Carruthers [b]	
Met_{51A} [a]		34_A-53_A			38.60%
Met_{99A}	77_A-100_A			77_A-100_A	6.60%
Met_{227A}	218_A-243_A and 220_A-243_A		220_A-243_A	220_A-243_A	2.80%
Met_{329A}	324_A-332_A				4.10%
Met_{364A}	361_A-392_A	364_A-394_A	361_A-393_A		0.40%
Met_{406A}		395_A-416_A	406_A-424_A	406_A-424_A	N/A
Met_{431A}	425_A-441_A	419_A-450_A	425_A-441_A	425_A-441_A	N/A
$Met_{483A,490A}$		482_A-506_A	475_A-501_A	475_A-501_A	17.5%(Met_{483A}); N/A(Met_{490A})
Met_{490A}	488_A-501_A				N/A
Met_{11B}		11_B-19_B		2_B-21_B	12.30%
Met_{44B}	30_B-57_B	43_B-48_B		29_B-73_B	43.80%
Met_{101B}	98_B-117_B	90_B-111_B	92_B-103_B	92_B-103_B	26.70%
$Met_{118B,119B}$			118_B-125_B		30.8%(Met_{118B}); 3.9%(Met_{119B})
Met_{166B}	166_B-170_B	153_B-170_B	166_B-170_B		0.30%

[a] The subscript number and letter indicate the residue number and the corresponding CN subunit, respectively.

[b] These data were obtained from Reference [359].

[c] Solvent accessibilities were predicted based on the CN crystal structure from PDB entry 1AUI [344], by using the GetArea program [329].

Table 4.1 shows that some peptides contain two Met residues. For example, 482_A-506_A (peptide 482-506 from CNA) from the Glu-C digest and 475_A-501_A from the Lys-C digest contain Met_{483A} and Met_{490A}, while 118_B-125_B from the Lys-C digest contains Met_{118B} and Met_{119B}. It is expected that two isomeric forms exist for the singly oxidized forms of these peptides. To determine the oxidation rate constant for each Met residue, the relative abundance of peptides containing the corresponding Met residue in the reduced form needs to be obtained. All of the three pairs of singly oxidized isomers, i.e., 482_A-506_A, 475_A-501_A, and 118_B-125_B, were chromatographically resolved and their oxidation sites were identified by CID- and ETD-MS/MS. For example, Figure 4. 2 A shows the CID-MS/MS spectrum of singly oxidized 482_A-506_A with the oxidation site at Met_{490A}. Based on the observation of oxidized sequence ions, i.e., $[b_{11}+O]^{2+}$, $[b_{12}+O]^{2+}$, $[b_{16}+O]^{2+}$, $[b_{17}{}^{*}+O\text{-}SOCH_4]^{2+}$, $[b_{18}+O]^{2+}$, $[b_{19}+O]^{2+}$, $[b_{20}+O]^{2+}$, $[b_{21}+O]^{3+}$, $[b_{22}+O]^{3+}$, $[b_{23}+O]^{3+}$, $[b_{24}+O]^{3+}$ (* indicates the loss of NH_3), and $[y_{23}+O]^{2+}$, and unoxidized sequence ions, i.e., $b_6{}^{2+}$, $b_7{}^{2+}$, $b_8{}^{2+}$, y_6, y_7, y_{16}, and y_{18}, $b_8{}^{2+}$, the oxidation site can be assigned to Met_{490A}. In contrast to Figure 4.2 A, Figure 4.2 B shows $[b_6+O]^{2+}$, $[b_7+O]^{2+}$, and $[b_8+O]^{2+}$ and unoxidized $y_{23}{}^{2+}$ illustrating Met_{483A} as the oxidation site. ETD-MS/MS was performed to further confirm the oxidation site. Figure 4.2 C is the ETD-MS/MS spectrum of 482_A-506_A with the oxidation site at Met_{490A}. More complete sequence coverage was obtained. The presence of reduced sequence ions, i.e., c_5, c_6-1, c_7-1, c_8-1, z_6+1, z_7+1, z_8+1, z_9+1, z_{10}+1, z_{11}+1, z_{12}+1, z_{13}+1, and z_{14}+1, and oxidized sequence ions, i.e., c_{10}+O, c_{11}+O,

c_{12}+O, c_{13}+O, c_{14}+O, c_{15}+O, c_{16}+O, $[c_{20}+O]^{2+}$, $[c_{21}+O]^{2+}$, $[c_{22}+O]^{2+}$, $[c_{23}+O]^{2+}$, z_{15}+O, z_{17}+O+1, z_{18}+O+1, and z_{19}+O+1, allowed the localization of the oxidation site at Met_{490A}. Similarly, the ETD-MS/MS spectrum shown in Figure 4.2 D allows the oxidation site to be located on Met_{483A}. Comparing to the CID-MS/MS spectra, ETD-MS/MS spectra provided much more reliable and abundant sequence information resulting from more evenly distributed cleavages along the peptide backbone. For example, CID-MS/MS of 482_A-$506_A^{Met490A}$ (482_A-506_A with Met_{490A} oxidized) at the +3 charge state gave rise to a sequence coverage of 40% (19 out of a total of 48 possible sequence ions) while ETD-MS/MS of the same peptide ion showed 60% sequence coverage. Similarly, sequence coverage of 31% was obtained from CID-MS/MS of 482_A-$506_A^{Met483A}$ at the +3 charge state whereas 65% sequence coverage was observed from the ETD-MS/MS spectrum. The poorer sequence coverage obtained from CID-MS/MS spectra is attributed to the facile loss of sulfenic acid which occurs when the number of protons on a peptide ion is less than or equal to the number of basic residues in the peptide [13]. Because of the radical-driven cleavage mechanism of ETD, the neutral loss of sulfenic acid is not observed in ETD-MS/MS and sequence information can be more readily obtained [360]. The oxidation sites for the isomers of singly oxidized 475_A-501_A and 118_B-125_B were also identified by CID and ETD-MS/MS (data not shown). Therefore, the oxidation rates of each observed Met residues can be unambiguously quantified.

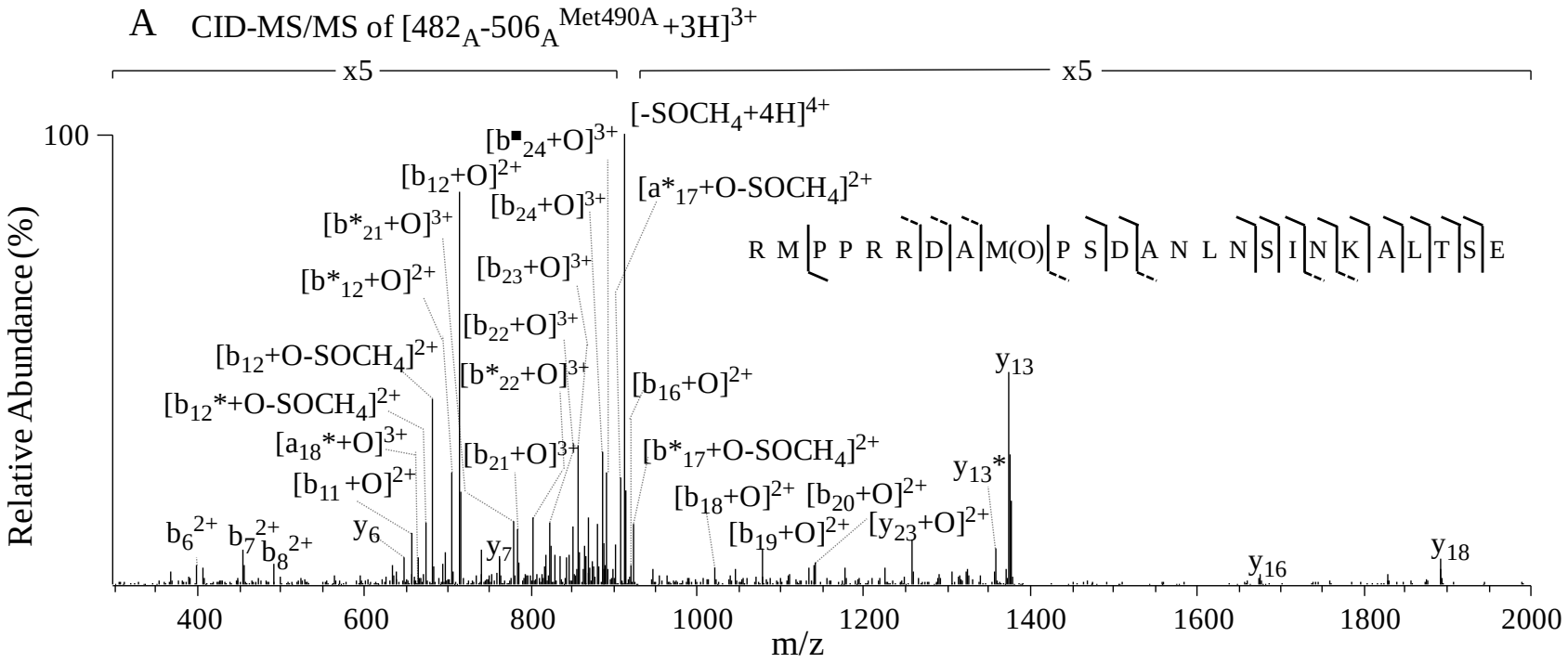

Figure 4.2 Ion trap mass spectrometry characterization of the isomers of singly oxidized 482_A-506_A containing either oxidized Met_{483A} or oxidized Met_{490A}. (A) CID-MS/MS of $[482_A\text{-}506_A{}^{Met490A}+3H]^{3+}$. (B) CID-MS/MS of $[482_A\text{-}506_A{}^{Met483A}+3H]^{3+}$. (C) ETD-MS/MS of $[482_A\text{-}506_A{}^{Met490A}+3H]^{3+}$. (D) ETD-MS/MS of $[482_A\text{-}506_A{}^{Met483A}+3H]^{3+}$. A superscript † indicates sequence ions containing one modified amino acid residue. "+O" indicates the sequence ion contains oxidation site. A superscript ○ indicates the loss of H_2O. A superscript * indicates the loss of NH_3. A superscript ● indicates the addition of H_2O. A dashed line indicates an unoxidized sequence ion was observed. A solid line indicates an oxidized sequence ion was observed.

Figure 4.2 (cont'd)

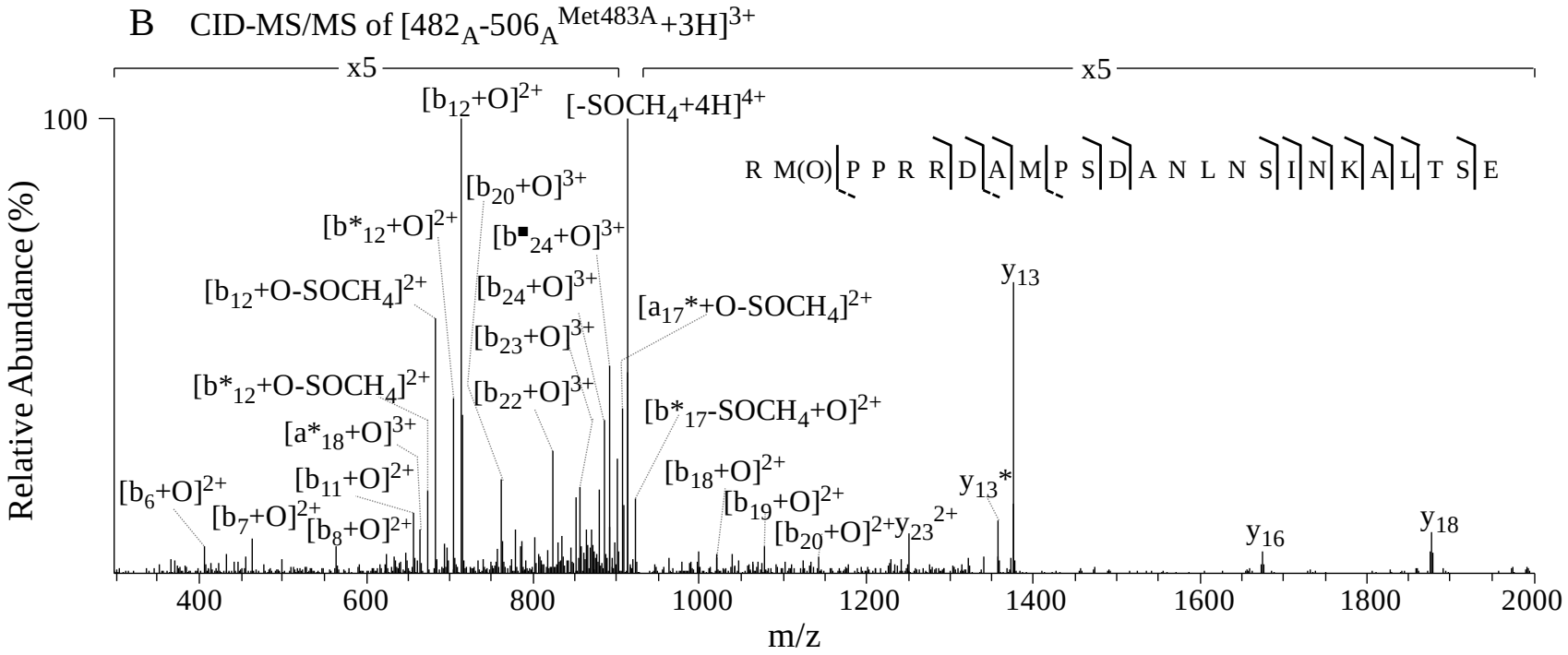

Figure 4.2 (cont'd)

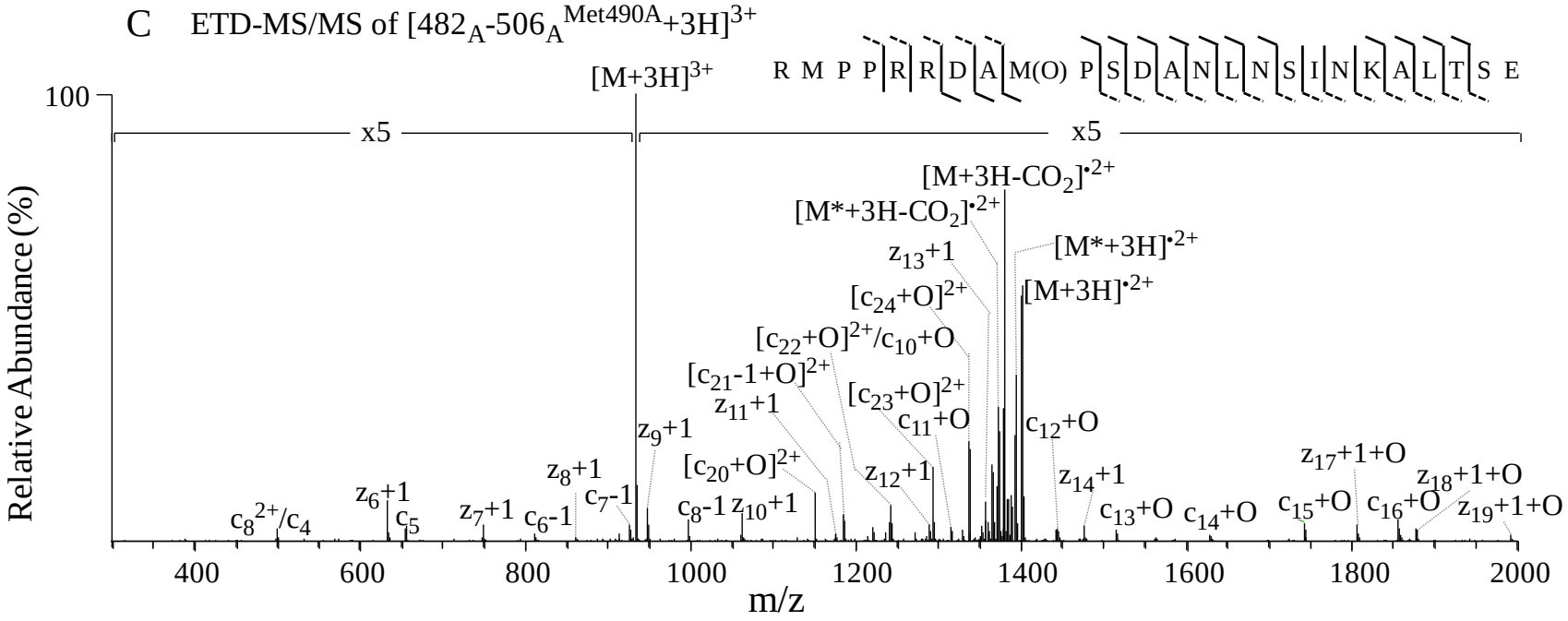

Figure 4.2 (cont'd)

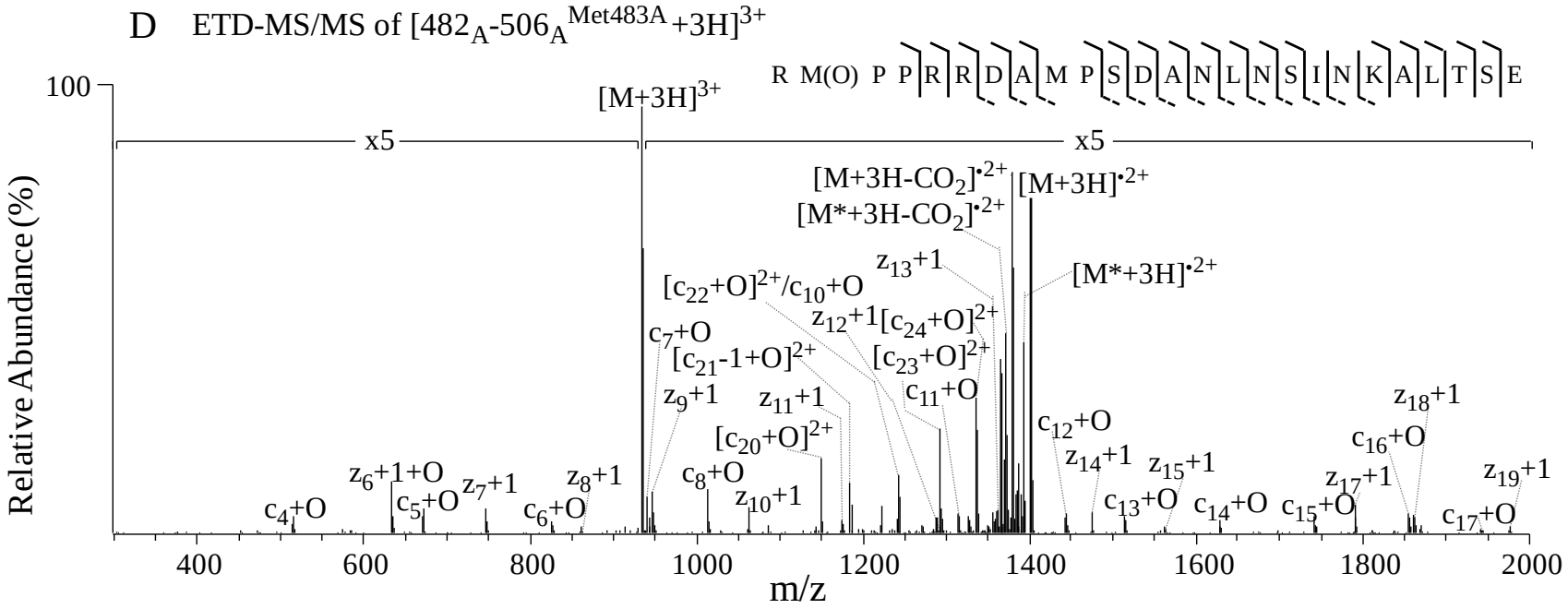

Plots of the percentage of native peptides versus H_2O_2 oxidation time are shown in Figure 4.3 and were used to calculate the pseudo-first order reaction rate constants (k_{ox}) as shown in Figure 4.4. As can be seen from Figure 4.3 C, E, F, G, H, I, and L that CN peptides containing the same Met residue but from different digests show almost the same extent of decrease in the percentage of native form with increased H_2O_2 incubation time. CN Lys-C digests show a slightly higher extent of oxidation, which might be due to a small variance in H_2O_2 concentration during the sample preparation process. Nonetheless, the oxidation rate constants are consistent among different digests as shown in Figure 4.4.

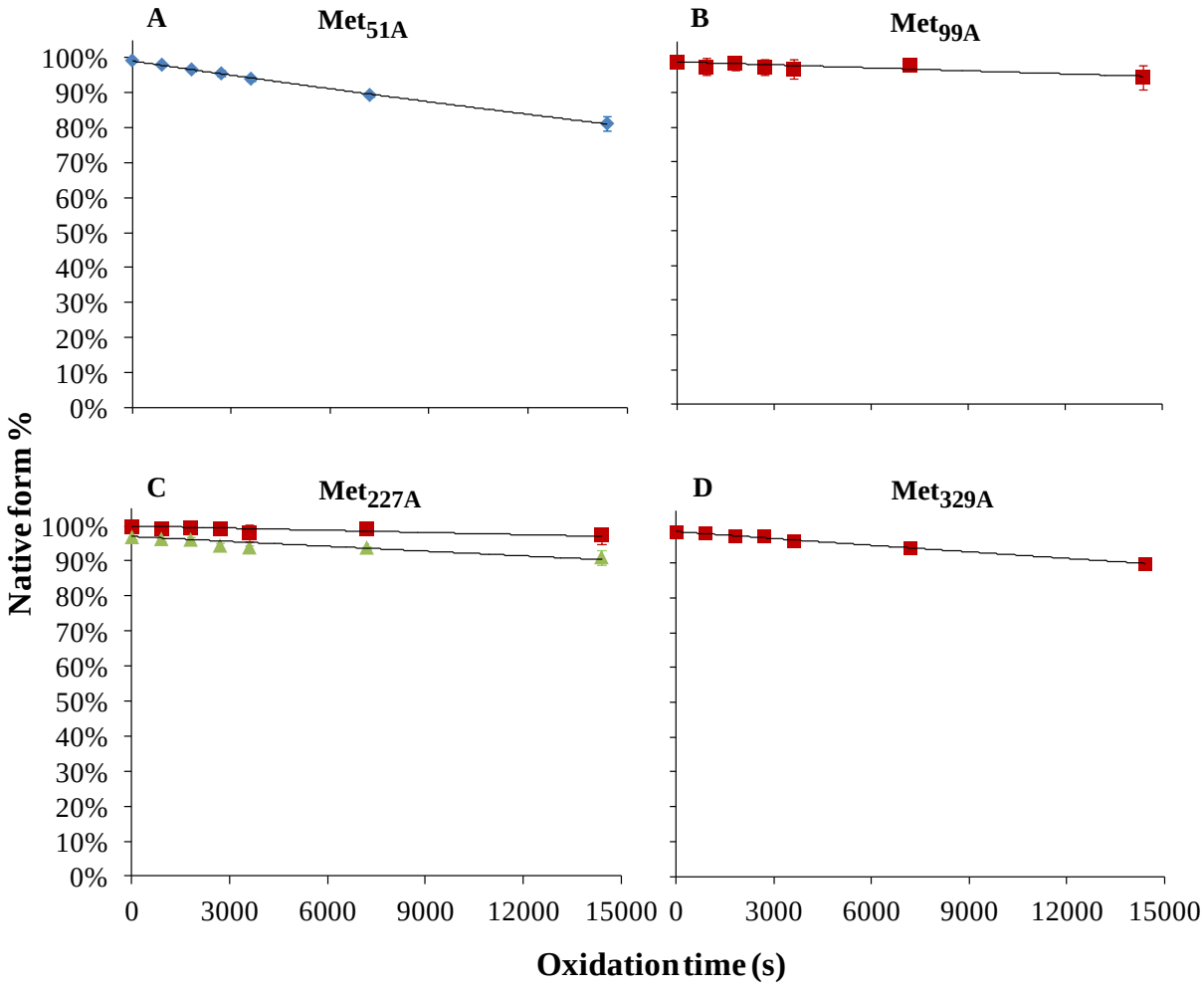

Figure 4.3 Percentage of Met containing CN peptides from Glu-C digest (♦) or trypsin digest (■) or Lys-C digest (▲) remaining in the reduced form following treatment with 12 mM H_2O_2 for 0, 15, 30, 45, 60, 120, and 240 min. (A) peptides containing Met_{51A}, (B) peptides containing Met_{99A}, (C) peptides containing Met_{227A}, (D) peptides containing Met_{329A}, (E) peptides containing Met_{364A}, (F) peptides containing Met_{406A}, (G) peptides containing Met_{431A}, (H) peptides containing Met_{483A}, (I) peptides containing Met_{490A}, (J) peptides containing Met_{11B}, (K) peptides containing Met_{44B}, (L) peptides containing Met_{101B}, (M) peptides containing Met_{118B}, (N) peptides containing Met_{119B}, (O) peptides containing Met_{166B}. All analysis were run by HPLC-ESI-MS and CID-MS/MS in triplicate. Error bars are shown as ± standard deviation.

Figure 4.3. (cont'd)

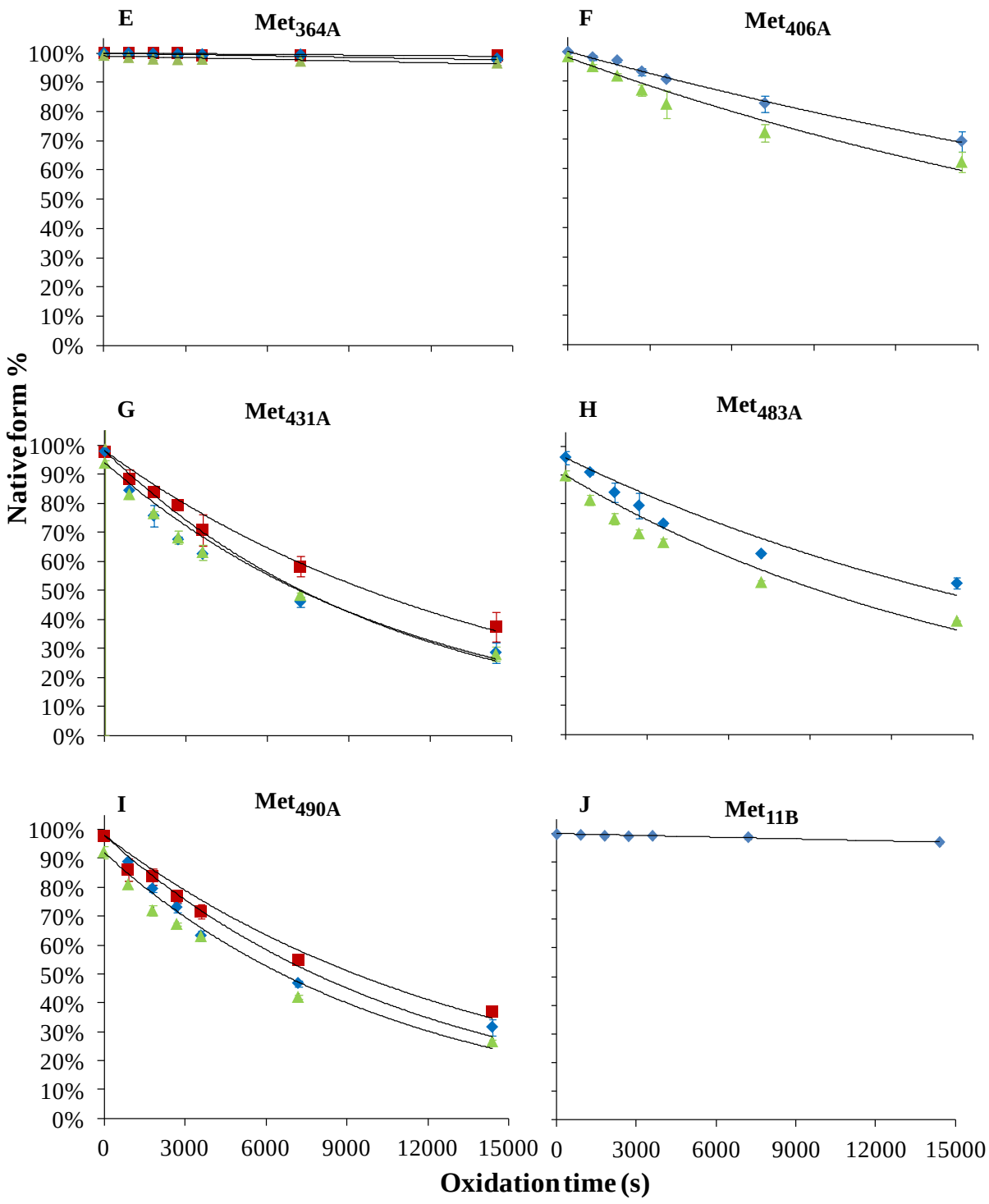

Figure 4.3. (cont'd)

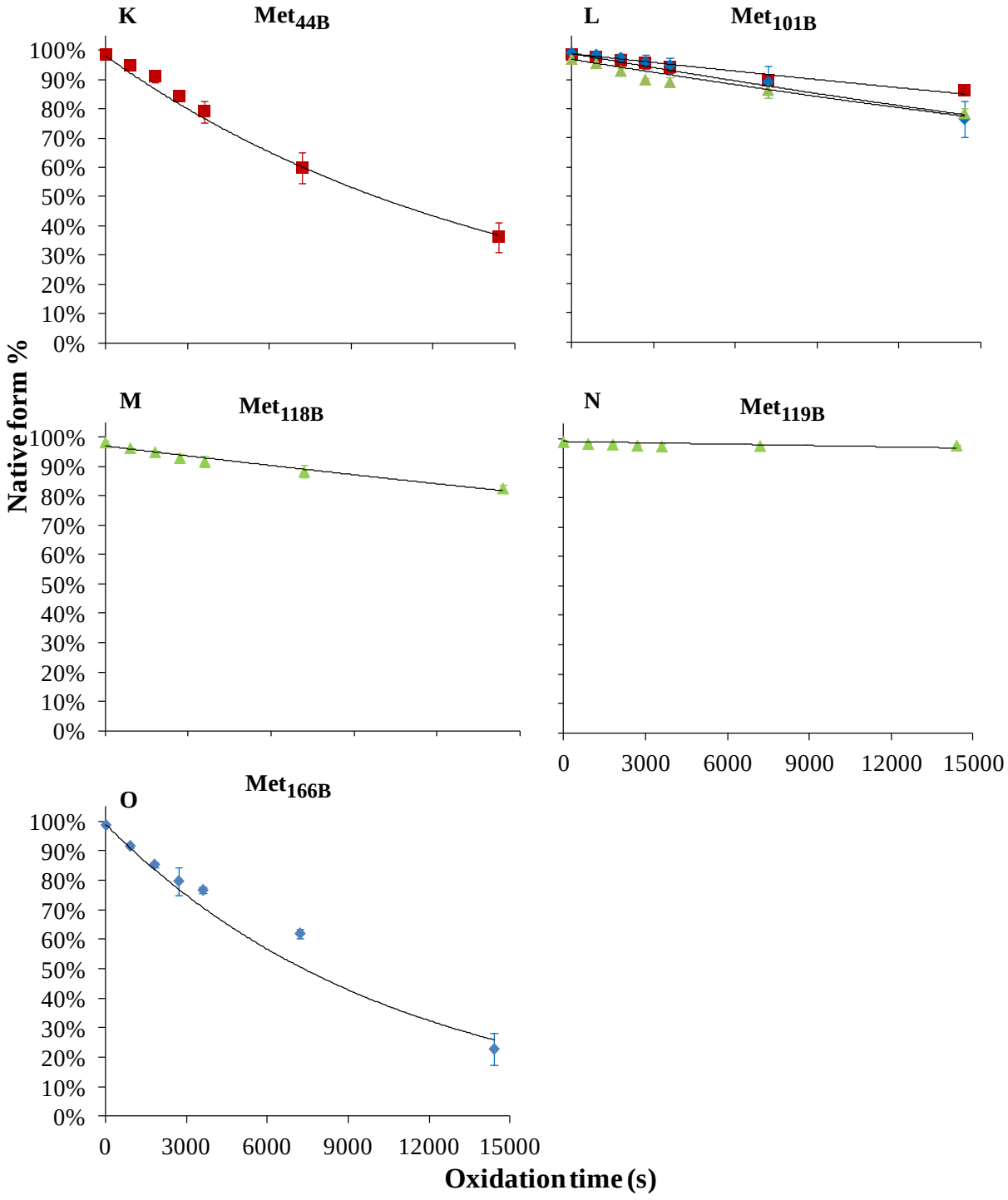

The pseudo-first-order oxidation rate constants of the observed Met residues are summarized and compared (shown as solid labels in Figure 4.4). The rate constants determined by Carruthers *et.al.* [359] are also included and represented by open labels. The Met residues with k_{ox} higher than 2.0×10^{-5} s^{-1} are considered susceptible towards oxidation. In general, the results obtained by the multi enzyme digestion strategy applied here and from Carruthers *et. al.* were consistent, except for residue Met_{11B} and Met_{44B}. These discrepancies might be due to the small variations in conformation between these two batches of proteins. Furthermore, Met_{11B} is considered to be buried based on the predicted solvent accessibility (SA) at 12.3%. Also, the N-terminal of the human CNB used here was myristoylated, while the SA was predicted based on the crystal structure of a human CNB with free N-terminal. However, the crystal structure of a bovine CN with CNB N-terminal myristoylated shows that the extended myristoyl group is laid over 1_B-12_B and thus further blocking the SA of this region [345]. Therefore, the actual SA of Met_{11B} is expected to be lower than 12.3%, which supports the low oxidation rate constant determined here. Generally, the relative susceptibilities of observed Met residues determined here show good correlation with the calculated solvent accessibility based on the known crystal structure [344]. However, it should be noted that Met_{483A} and Met_{166B} have relatively low solvent exposure but show high sensitivity towards oxidation. These differences might be a reflection of the different conformations proteins adopt in the dynamic state and in the static state, as both Met_{483A} (located on the linker region between the CaM binding and autoinhibitory domain) and Met_{166B} (located on CNB C-terminal) reside on the flexible region based on the crystal structure. The oxidation rate constants determined here are expected to be based on the

native structure of CN; however, secondary oxidation of the oxidized CN, whose conformation may be perturbed (discussed in Section 4.3), may also occur. To have an idea of to what extent the protein may undergo secondary oxidation, the probability of a protein being singly oxidized (P(1 ox)) and double oxidized (P(2 ox)) upon being oxidized for 15 min were calculated using equation (4.1) and (4.2), respectively.

$$P(1\ ox) = \sum_{i=1}^{19} p_i \left(\prod_{j=1, j\neq i}^{19} (1 - p_j)\right) \quad (4.1)$$

$$P(2\ ox) = \left\{\sum_{i=1}^{19} p_{i1} \cdot p_{i2} \left(\prod_{j=1, j\neq i1, j\neq i2}^{19} (1 - p_j)\right)\right\}/2! \quad (4.2)$$

In these equations, $p_{i,j}$ is the probability of a specific Met residue being oxidized and were determined from the percentage of unmodified Met residue from CN oxidized for 15 min (as shown in Figure 4.3). 4 Met residues located in the catalytical domain were not observed, which may be due to the lack of enzyme cleavage sites in the corresponding regions. The probability for these 4 missing Met residues to be oxidized was estimated to be 2.1% by averaging the oxidation probability of observed Met residues within the same functional domain. It was determined that P(1 ox) = 39%, and P(2 ox) = 19%, indicating that 39 % of the protein may experience secondary oxidation when being incubated in H_2O_2 for longer than 15 min and at least 19 % of the protein already underwent secondary oxidation at 15 min oxidation time point. Therefore, the oxidation rate constants determined here were attributed to the oxidation susceptibility of Met residues from both the native CN and oxidized CN. Nonetheless, the apparent k_{ox} was still indicative of the susceptibility of CN Met residues towards oxidation.

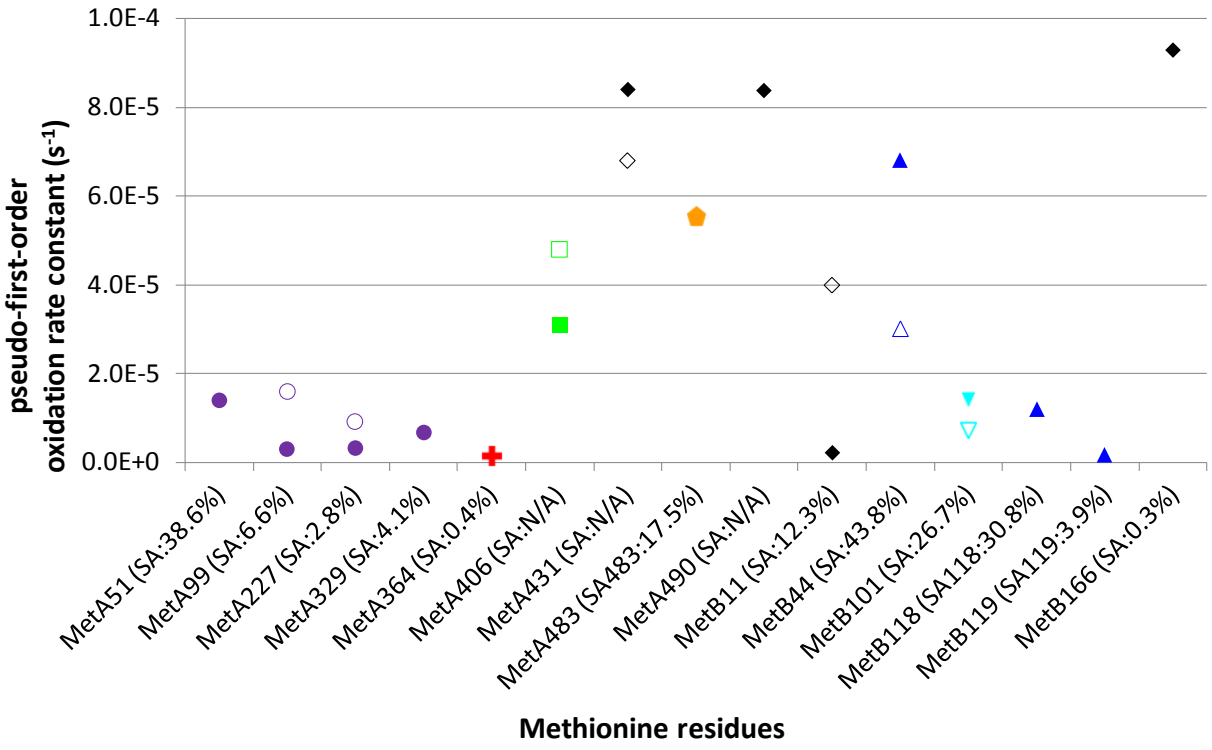

Figure 4.4 Pseudo-first-order oxidation rate constant determined for each observed CN Met residue located in catalytic domain (●), CNB binding domain (✚), CaM binding domain (■), and autoinhibitory region (⬟), CNA binding region (▲), Ca^{2+} binding domain (▼), and non-functional regions (♦). Open labels indicate the data obtained by Carruthers *et. al.* [359] with Met residues residing in catalytic domain (○), CaM binding domain (□),CNA binding domain (Δ), Ca^{2+} binding domain (∇), and non-functional regions (◊).The x-axis labels show the Met residue and the corresponding solvent accessibilities (SA).

The observed CN Met residues show a wide range in the sensitivity towards oxidation with the lowest k_{ox} at 1.5×10^{-6} s^{-1} (Met_{364A}) the highest k_{ox} at 9.3×10^{-5} s^{-1} (Met_{166B}), as illustrated in Figure 4.3. Interestingly, CNA Met residues which are highly susceptible to oxidation (with k_{ox} higher than 2.0×10^{-5} s^{-1}) are all located in the CN regulatory region which includes the CaM binding domain (Met_{406A}), the linker region between the CaM binding and autoinhibitory domains (Met_{431A}), the autoinhibitory domain (Met_{483A}), and the C-terminal (Met_{490A}). The two oxidation sensitive Met residues on the CNB subunit are located on the N-terminal CNA binding domain (Met_{44B}) and the C-terminus (Met_{166B}). Importantly, Met_{44B} is close to the first Ca^{2+} binding region (31_B-42_B) which is one of the two low-affinity sites that play a role in CN activation under elevated Ca^{2+} concentrations [351-353]. Correlation of the Met residues determined to be susceptible towards oxidation with the Lys residues showed large conformational change upon oxidation will be discussed later.

4.3 Quantitative Characterization of Calcineurin Surface Residue Accessibility by DMBNHS Modification

To determine if oxidation could cause a conformational change in CN, native CN and CN oxidized for 15, 30, 45, and 60 min were modified by DMBNHS with a DMBNHS/CN reaction molar ratio at 0, 5, 10, 20, 50 and 100. The concentration of DMF was kept at 1% during the protein modification reaction to maintain CN native structure. The labeled CN was then digested by Glu-C overnight. Potential modification of Lys residues by DMBNHS would cause missed cleavages at Lys residue C-termini if trypsin or Lys-C was used as the digestion enzyme. This could cause the loss of DMBNHS modification information and the generation of large peptides that may not be compatible with a C18 column. Therefore, Glu-C was used here instead of trypsin or Lys-C. 23 of a total of 45 Lys residues were observed, as summarized in Table 4.2. The fraction of peptides containing the unmodified Lys residue from native CN and CN oxidized for various time periods were plotted against the DMBNHS/CN molar ratio and illustrated in Figure 4.5. It can be clearly seen that DMBNHS modification of oxidized CN occurred to a greater extent compared to native CN, indicating that protein started unfolding upon oxidation. This protein unfolding process happened as early as 15 min after being oxidized. Longer oxidation times did not cause a further unfolding of CN and the corresponding extents of DMBNHS modification could be fit into a single rate constant.

Table 4.2 Summary of DMBNHS modification rate constants determined for Lysine residues observed from Glu-C digests of native CN and CN oxidized for different time periods.

Lys residue	Peptide	Predicted SA [a]	Oxidation Time (min)	k_{DMBNHS} (M^{-1} s^{-1})
Lys_{40A}	34_A-44_A	69.00%	0	1.0×10^{-7}
			15	1.5×10^{-6}
			30	1.6×10^{-6}
			40	1.7×10^{-6}
			60	1.6×10^{-6}
Lys_{40A}	34_A-53_A	69.00%	0	5.0×10^{-7}
			15	8.3×10^{-6}
			30	8.3×10^{-6}
			40	7.8×10^{-6}
			60	9.4×10^{-6}
Lys_{47A}		45.30%	0	1.2×10^{-6}
			15	1.8×10^{-6}
			30	1.8×10^{-6}
			40	1.7×10^{-6}
			60	1.8×10^{-6}
Lys_{52A}		64.20%	0	1.2×10^{-6}
			15	1.8×10^{-6}
			30	1.8×10^{-6}
			40	2.0×10^{-6}
			60	2.1×10^{-6}

Table 4.2 (cont'd)

Lys residue	Peptide	Predicted SA [a]	Oxidation Time (min)	k_{DMBNHS} (M^{-1} s^{-1})
Lys_{393A}	364_A-394_A	N/A	0	1.3×10^{-6}
			15	2.3×10^{-6}
			30	2.4×10^{-6}
			40	2.2×10^{-6}
			60	2.1×10^{-6}
	373_A-394_A	N/A	0	1.2×10^{-6}
			15	2.0×10^{-6}
			30	1.9×10^{-6}
			40	1.7×10^{-6}
			60	1.9×10^{-6}
Lys_{399A}	395_A-416_A	N/A	0	4.0×10^{-7}
			15	1.1×10^{-6}
			30	1.5×10^{-6}
			40	1.7×10^{-6}
			60	2.3×10^{-6}
Lys_{405A}		N/A	0	6.3×10^{-7}
			15	1.3×10^{-6}
			30	1.4×10^{-6}
			40	1.6×10^{-6}
			60	1.9×10^{-6}

Table 4.2 (cont'd)

Lys residue	Peptide	Predicted SA [a]	Oxidation Time (min)	k_{DMBNHS} (M^{-1} s^{-1})
$Lys_{424A,441A}$	419_A-450_A	N/A	0	1.6×10^{-6}
			15	2.6×10^{-6}
			30	2.5×10^{-6}
			40	2.2×10^{-6}
			60	2.8×10^{-6}
Lys_{424A} [b]	419_A-450_A	3.80%	0	3.2×10^{-7}
			15	1.2×10^{-6}
Lys_{441A} [b]		49.80%	0	1.0×10^{-7}
			15	1.6×10^{-7}
Lys_{459A}	451_A-472_A	N/A	0	8.9×10^{-7}
			15	1.3×10^{-6}
			30	1.5×10^{-6}
			40	1.3×10^{-6}
			60	1.2×10^{-6}
	457_A-472_A	N/A	0	1.4×10^{-6}
			15	2.2×10^{-6}
			30	2.2×10^{-6}
			40	2.1×10^{-6}
			60	2.3×10^{-6}

Table 4.2 (cont'd)

Lys residue	Peptide	Predicted SA [a]	Oxidation Time (min)	k_{DMBNHS} (M^{-1} s^{-1})
Lys_{466A}	451_A-472_A	N/A	0	1.4×10^{-6}
			15	2.3×10^{-6}
			30	2.3×10^{-6}
			40	2.3×10^{-6}
			60	2.6×10^{-6}
	457_A-472_A	N/A	0	1.7×10^{-6}
			15	2.6×10^{-6}
			30	2.5×10^{-6}
			40	2.3×10^{-6}
			60	2.6×10^{-6}
Lys_{474A}	473_A-481_A	51.90%	0	7.2×10^{-7}
			15	1.9×10^{-6}
			30	2.0×10^{-6}
			40	1.7×10^{-6}
			60	1.9×10^{-6}
Lys_{501A}	482_A-506_A	N/A	0	1.9×10^{-6}
			15	3.3×10^{-6}
			30	3.3×10^{-6}
			40	3.1×10^{-6}
			60	3.0×10^{-6}

Table 4.2 (cont'd)

Lys residue	Peptide	Predicted SA [a]	Oxidation Time (min)	k_{DMBNHS} (M^{-1} s^{-1})
$Lys_{21B, 25B, 28B, 29B}$	20_B-42_B	83.4% (Lys_{21B}); 70.1% (Lys_{25B}); 85.2% (Lys_{28B}); 58.5% (Lys_{29B})	0	2.9×10^{-6}
			15	5.0×10^{-6}
			30	5.5×10^{-6}
			40	5.1×10^{-6}
			60	6.2×10^{-6}
Lys_{21B} [b]	20_B-42_B	83.40%	0	1.7×10^{-6}
			15	2.7×10^{-6}
Lys_{73B}	70_B-77_B	37.20%	0	4.9×10^{-7}
			15	1.1×10^{-6}
			30	1.2×10^{-6}
			40	1.1×10^{-6}
			60	1.4×10^{-6}
Lys_{85B}	75_B-89_B	68.50%	0	1.8×10^{-6}
			15	2.7×10^{-6}
			30	2.7×10^{-6}
			40	2.4×10^{-6}
			60	2.9×10^{-6}
Lys_{88B}		54.50%	0	2.2×10^{-6}
			15	3.5×10^{-6}
			30	3.2×10^{-6}
			40	2.8×10^{-6}
			60	2.9×10^{-6}

Table 4.2 (cont'd)

Lys residue	Peptide	Predicted SA [a]	Oxidation Time (min)	k_{DMBNHS} (M^{-1} s^{-1})
$Lys_{91B, 103B}$	90_B-111_B	3.8% (Lys_{91B}); 49.8%(Lys_{103B})	0	3.8×10^{-7}
			15	1.4×10^{-6}
			30	1.7×10^{-6}
			40	1.5×10^{-6}
			60	1.8×10^{-6}
Lys_{91B} [b]	90_B-111_B	3.80%	0	3.2×10^{-7}
			15	1.2×10^{-6}
Lys_{103B} [b]		49.80%	0	1.0×10^{-7}
			15	1.6×10^{-7}
Lys_{164B}	153_B-170_B	75%	0	1.2×10^{-6}
			15	2.3×10^{-6}
			30	2.2×10^{-6}
			40	2.3×10^{-6}
			60	2.1×10^{-6}
Lys_{165B}		61%	0	1.3×10^{-6}
			15	2.3×10^{-6}
			30	2.0×10^{-6}
			40	2.9×10^{-6}
			60	2.7×10^{-6}

[a] Solvent accessibilities were predicted based on the CN crystal structure from PDB entry 1AUI [344], by using the GetArea program [329].

[b] Calculation of k_{DMBNHS} of these residues were based on the relative intensities of ETD fragment ions.

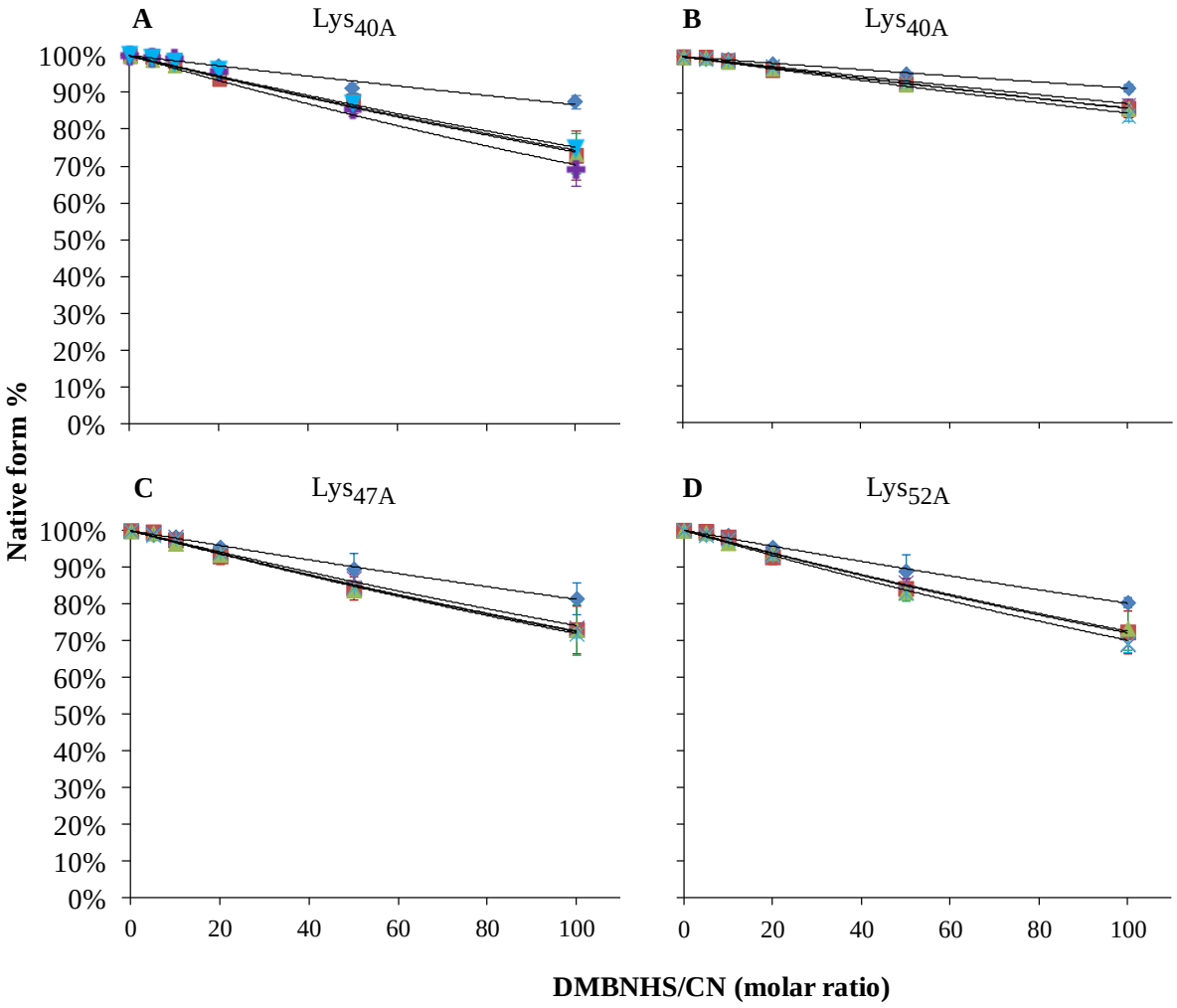

Figure 4.5 Plots of the relative abundances of unmodified Lysine residues versus the molar ratios of DMBNHS over CN. Percentage of (A) unmodified Lys_{40A} from 34_A-44_A, (B) unmodified Lys_{40A} from 34_A-53_A, (C) unmodified Lys_{47A} from 34_A-53_A, (D) Lys_{52A} from 34_A-53_A, (E) Lys_{393A} from 364_A-394_A and (F) 373_A-394_A, (G) Lys_{399A} from 395_A-416_A, (H) Lys_{405A} from 395_A-416_A, (I) Lys_{424A} and Lys_{441A} from 419_A-450_A, (J) Lys_{424A} from 419_A-450_A, (K) Lys_{441A} from 419_A-450_A, (L) Lys_{459A} from 451_A-472_A and (M) 457_A-472_A, (N) Lys_{466A} from 451_A-472_A and (O) 457_A-472_A, (P) Lys_{474A} from 473_A-481_A, (Q) Lys_{501A} from 482_A-506_A, (R) Lys_{21B}, Lys_{25B}, Lys_{28B}, and Lys_{29B} from 19_B-42_B, (S) Lys_{21B} from 19_B-42_B, (T) Lys_{73B} from 70_B-77_B, (U) Lys_{85B} from 75_B-89_B, (V) Lys_{88B} from 75_B-89_B, (W) Lys_{91B} and Lys_{103B} from 90_B-111_B, (X) Lys_{91B} from 90_B-111_B, (Y) Lys_{103B} from 90_B-111_B, (Z) Lys_{164B} from 153_B-170_B, and (AA) Lys_{165B} from 153_B-170_B digested from native CN (♦), CN oxidized for 15 min (■), 30 min (▲), 45 min (▼), and 60 min (✚). All data were run in triplicate. Error bars are shown as ± standard deviation.

Figure 4.5. (cont'd)

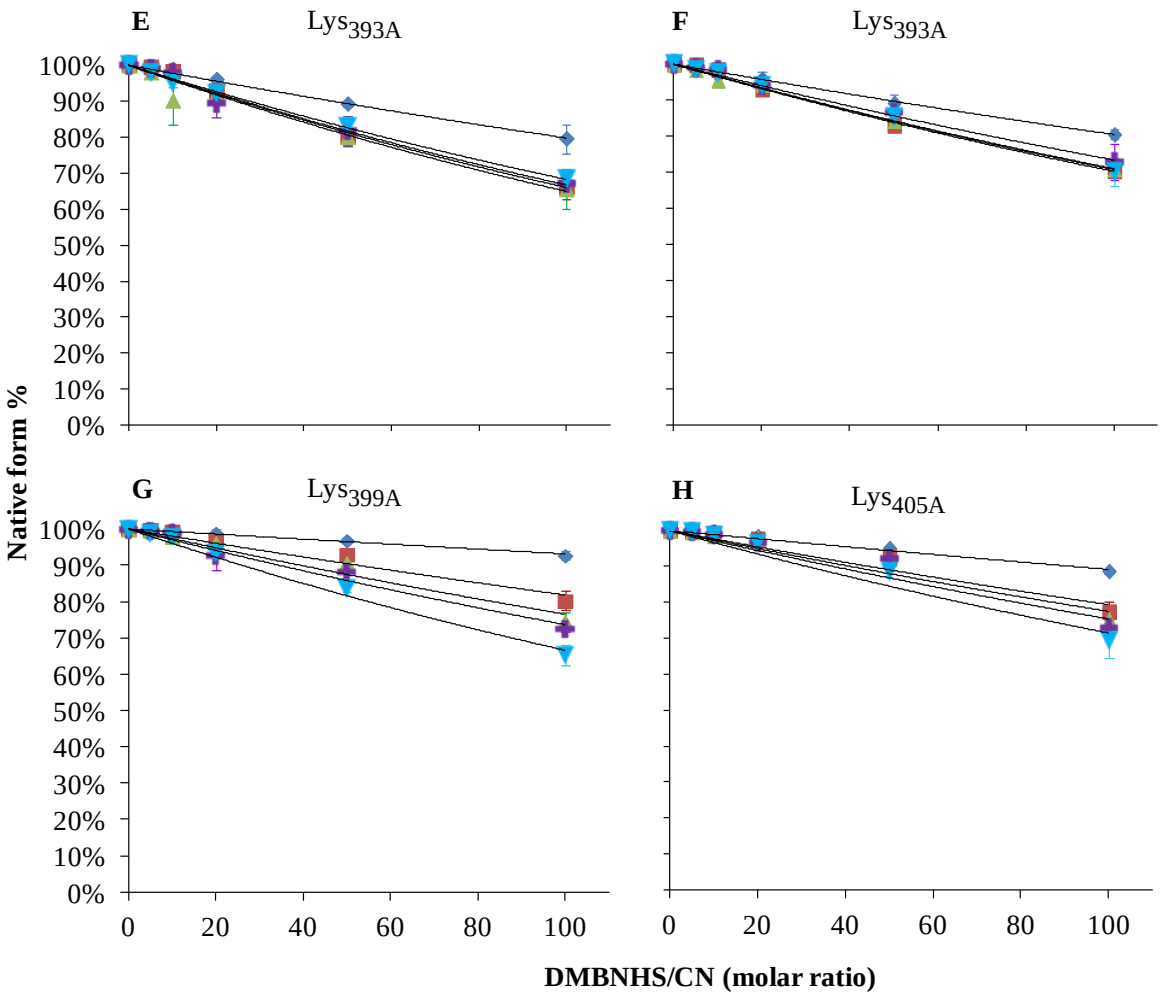

Figure 4.5. (cont'd)

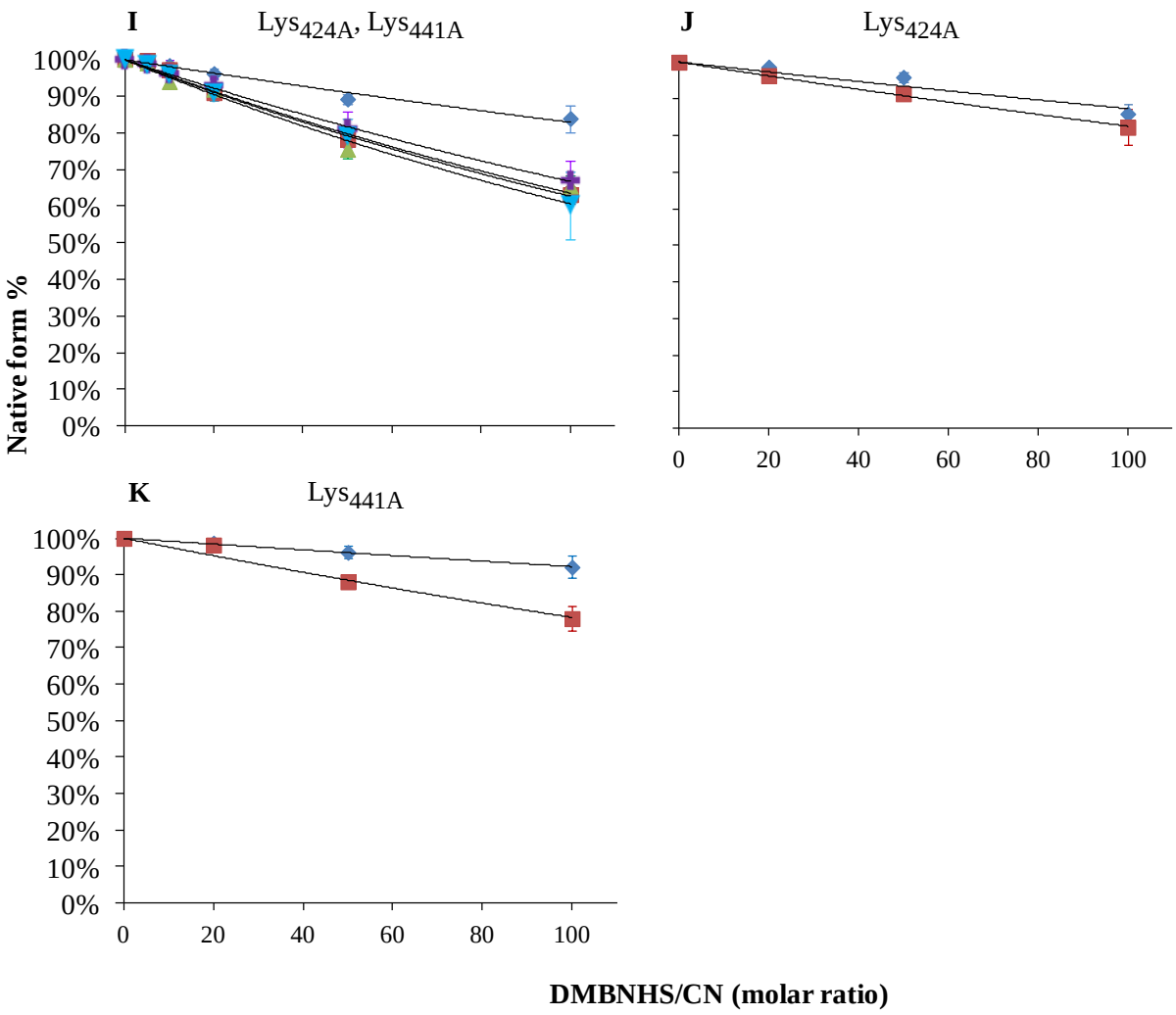

Figure 4.5. (cont'd)

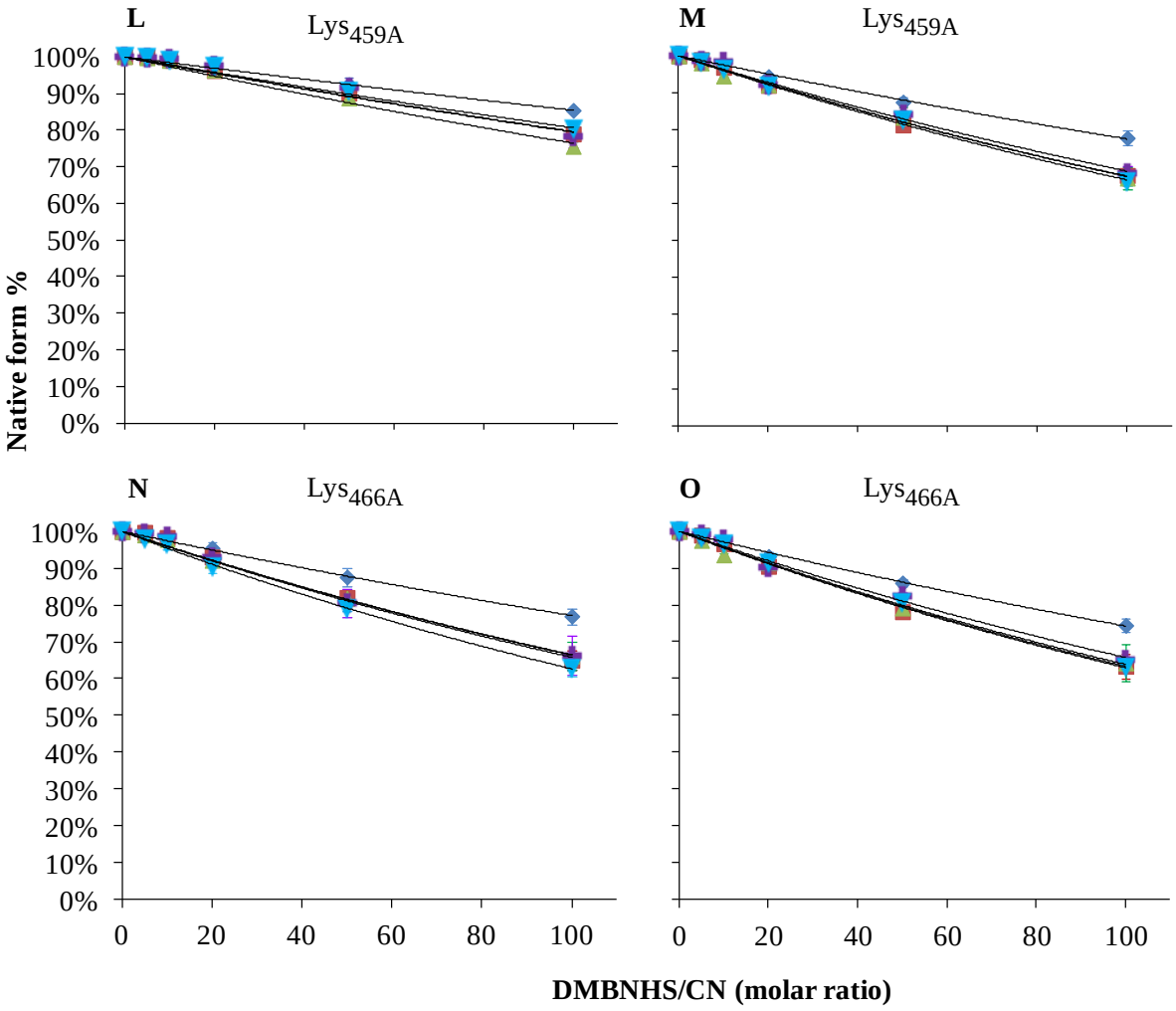

Figure 4.5. (cont'd)

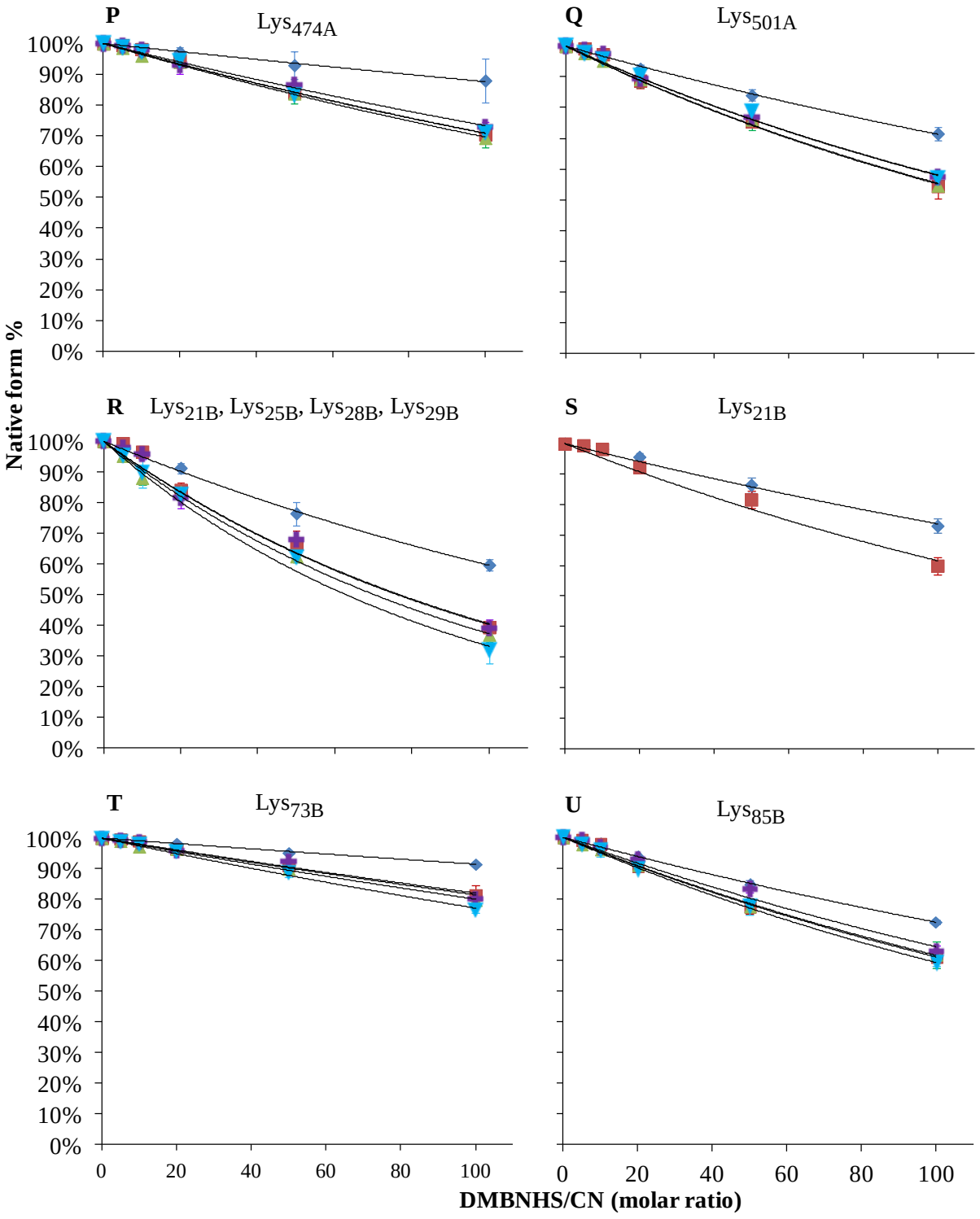

Figure 4.5. (cont'd)

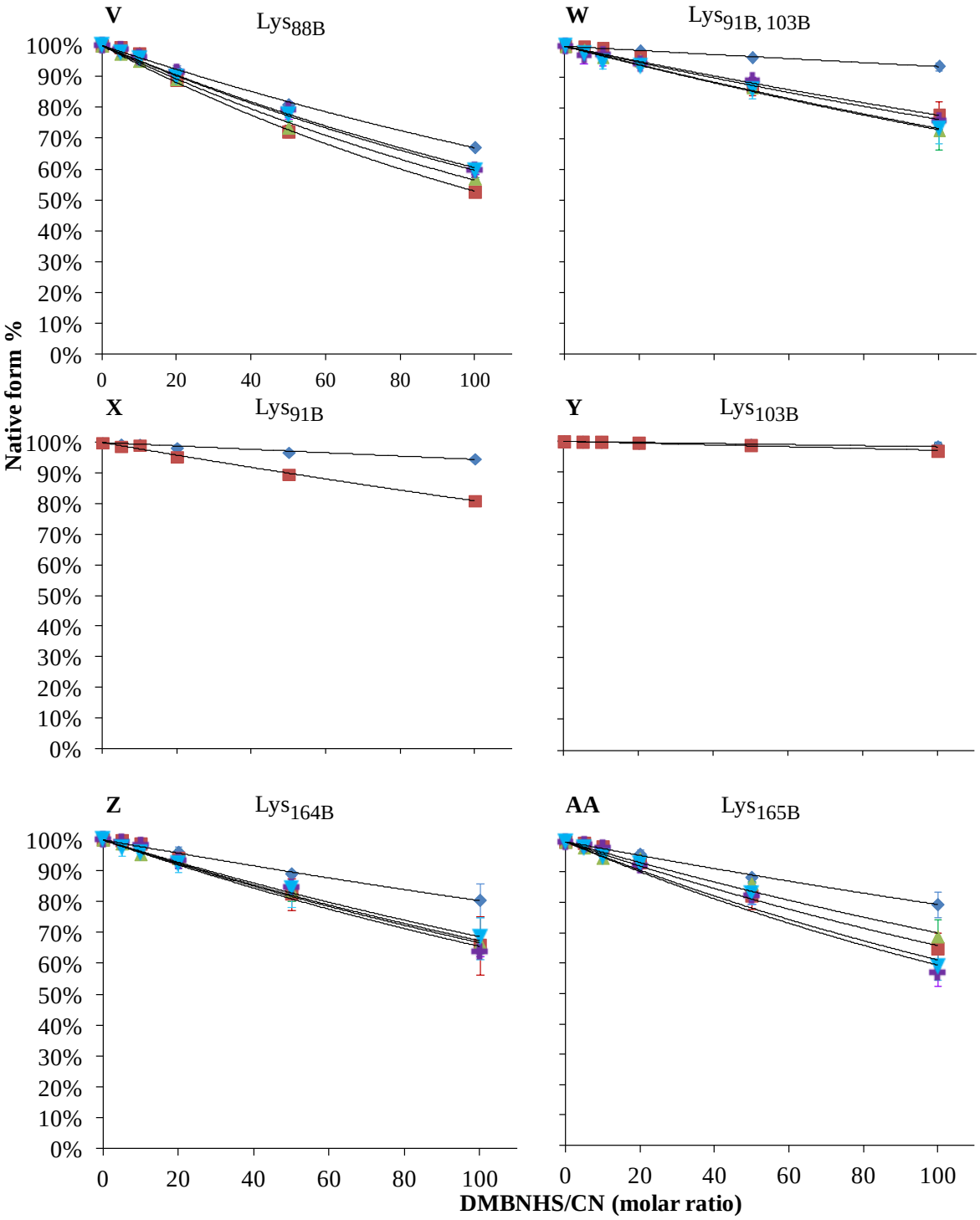

It is important to note that some peptides contain multiple Lys residues and thus isomeric DMBNHS modified peptides were generated. Among those peptides, the isomeric forms of modified 34_A-53_A, 394_A-416_A, 419_A-450_A, 451_A-472_A, 457_A-472_A, 75_B-89_B, and 153_B-170_B were resolved during HPLC separation. The modification sites were identified by CID-MS^3 and ETD-MS/MS and thus DMBNHS modification rate constants can be determined for each individual Lys residue. However, the isomers of some modified peptides closely eluted and the relative abundance could not be measured for each isomer based on the MS intensity. In order to quantify the amount of individual unmodified Lys residue from these peptides, the relative abundances of the MS/MS fragment ions characteristic for the corresponding modification site were used to calculate the DMBNHS modification rate constant. Targeted ETD-MS/MS was performed for the modified peptide isomers digested from native CN and CN oxidized for 15 min. ETD-MS/MS was favored over CID-MS^3 for the quantification purpose mainly because of the higher sequence coverage of ETD technique and, most importantly, the reduced sources of error for quantification due to the lower fragmentation stage required by ETD. The ETD-MS/MS spectrum (Figure 4.6 A) of singly modified 90_B-111_B at the +5 charge state shows the coexistence of the sequence ions corresponding to the DMBNHS modification at Lys_{91B} and Lys_{103B}, confirming the co-elution of 90_B-111_B^{Lys90B} (peptide 90_B-111_B with DMBNHS modification located at Lys_{90B}) and 90_B-$111_B^{Lys103B}$. The intensities of the c_2 (indicating the modification at Lys_{103B}) and $c_2^{\dagger}$ (indicating the modification at Lys_{91B}) were used to obtain the relative abundances of unmodified Lys_{91B} and Lys_{103B}, respectively, and the determined second-order DMBNHS modification rate constants are shown in Figure 4.5 X and Y. Similarly,

the DMBNHS modification rate constants were quantified for Lys_{424A} and Lys_{441A} individually from 419_A-450_A based on the relative abundances of the c_6 and $c_6^{\dagger}$ ions (as shown in Figure 4.6 B) characteristic of the modification site on Lys_{441A} and Lys_{424A}, respectively. However, due to the low abundance of singly modified 419_A-450_A, the c_6 and $c_6^{\dagger}$ ions could hardly be observed when CN was modified by a low molar excess of DMBNHS, such that the percentage of unmodified Lys_{441A} or Lys_{424A} were only calculated for CN modified by DMBNHS at 20, 50, and 100 fold molar excess (as shown in Figure 4.5 K and J). For peptides containing more than two modifiable sites, such as 19_B-42_B, DMBNHS modification rate constants could only be quantified for the first and last Lys residue within the peptide. Because the modified Lys residues sitting between the first and last residues can only be observed together with the N- or C-terminal Lys residue, the intensities of these fragment ions can not be assigned to any specific Lys residue in this case. Therefore, k_{DBMNHS} could only be determined individually for Lys_{21B} and Lys_{29B}. However, Lys_{29B} is adjacent to Lys_{28B} in sequence and the mass addition upon DMBNHS modification (130 Da) is close to the mass of a Lys residue (128 Da). As a result, the singly modified sequence ions containing only Lys_{29B} (i.e., the $c_{14}^{\dagger}$ in Figure 4.6 C) could be hardly differentiated from unmodified sequence ions containing both Lys_{28B} and Lys_{29B} (i.e., the c_{15}+1 in Figure 4.6 C), and the DMBNHS modification rate constant was not individually determined for Lys_{29B}. k_{DBMNHS} was quantified for Lys_{21B} from 19_B-42_B based on the relative abundances of the c_2 and $c_2^{\dagger}$ ions (as shown in Figure 4.5 S). It is noteworthy to point

out that the rate constants determined from the abundances of fragment ions are not correlated with actual extent of DMBNHS modification as the abundances of fragment ions are affected by a variety of factors including ETD cleavage bias at different sites and different ionization efficiency of product ions. However, the variance in fragment intensity brought by these factors should be consistent from run to run when the same peptides are analyzed. Therefore, the fold increase in DMBNHS modification rate constants upon oxidation (as shown in Figure 4.7 and described later) is indicative of the extent of conformational change at the specific region of CN.

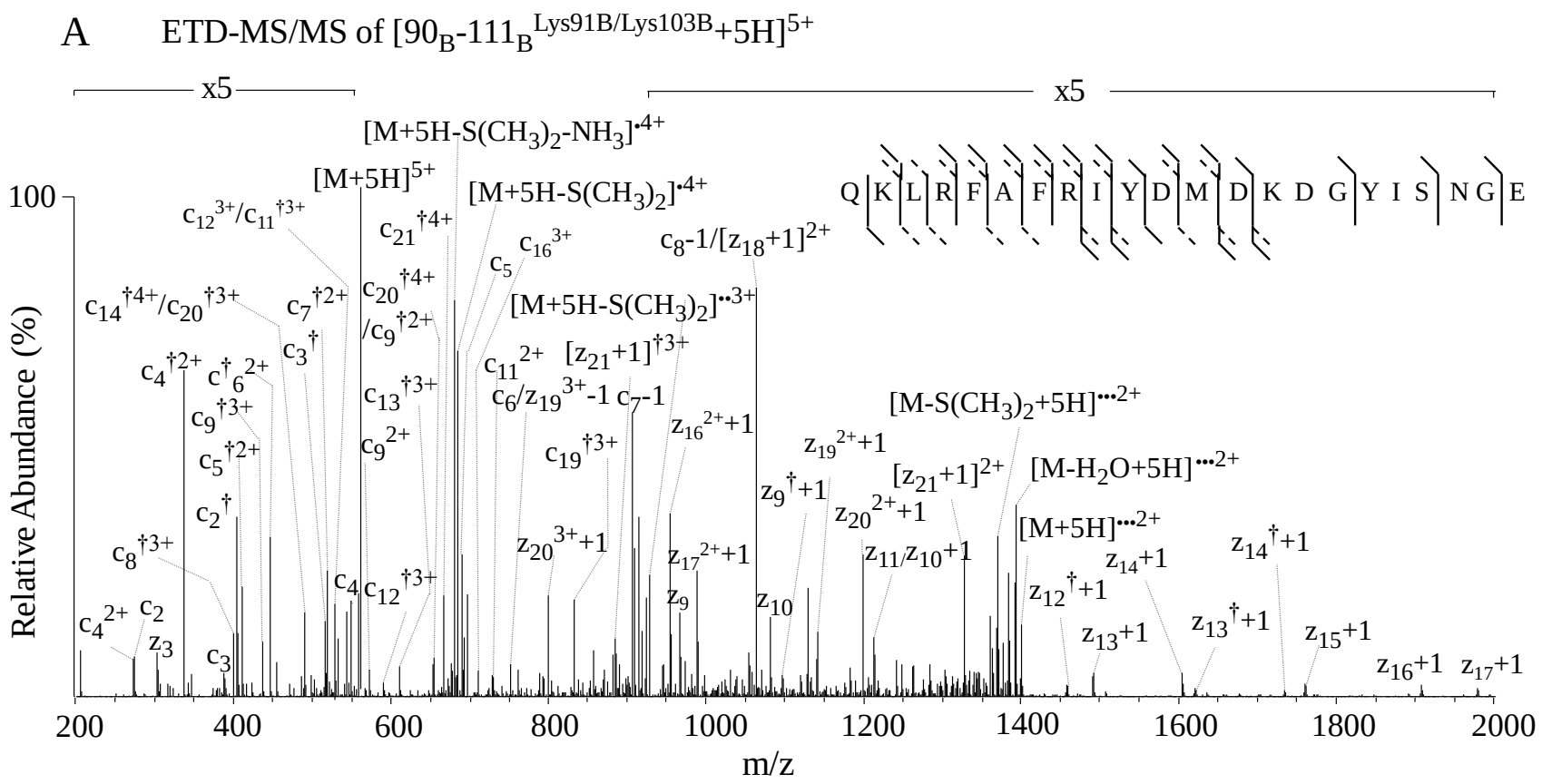

Figure 4.6 Ion trap mass spectrometry characterization of the co-eluting isomers of singly modified 90_B-111_B containing Lys_{91B} and Lys_{103B}, 419_A-450_A containing Lys_{424A} and Lys_{424A}, and 19_B-42_B containing Lys_{21B}, Lys_{25B}, Lys_{28B}, and Lys_{29B}. (A) ETD-MS/MS of $[90_B\text{-}111_B{}^{Lys91B/Lys103B}+5H]^{5+}$. (B) ETD-MS/MS of $[419_A\text{-}450_A{}^{Lys424A/Lys441A}+4H]^{4+}$. (C) ETD-MS/MS of $[19_B\text{-}42_B{}^{Lys21A/Lys25A/Lys28A/Lys29A}+4H]^{4+}$. A superscript † indicates sequence ions containing one modified amino acid residue. A superscript ○ indicates the loss of H_2O. A superscript * indicates the loss of NH_3. A dashed line indicates an unmodified sequence ion was observed. A solid line indicates a singly modified sequence ion was observed.

Figure 4.6 (cont'd)

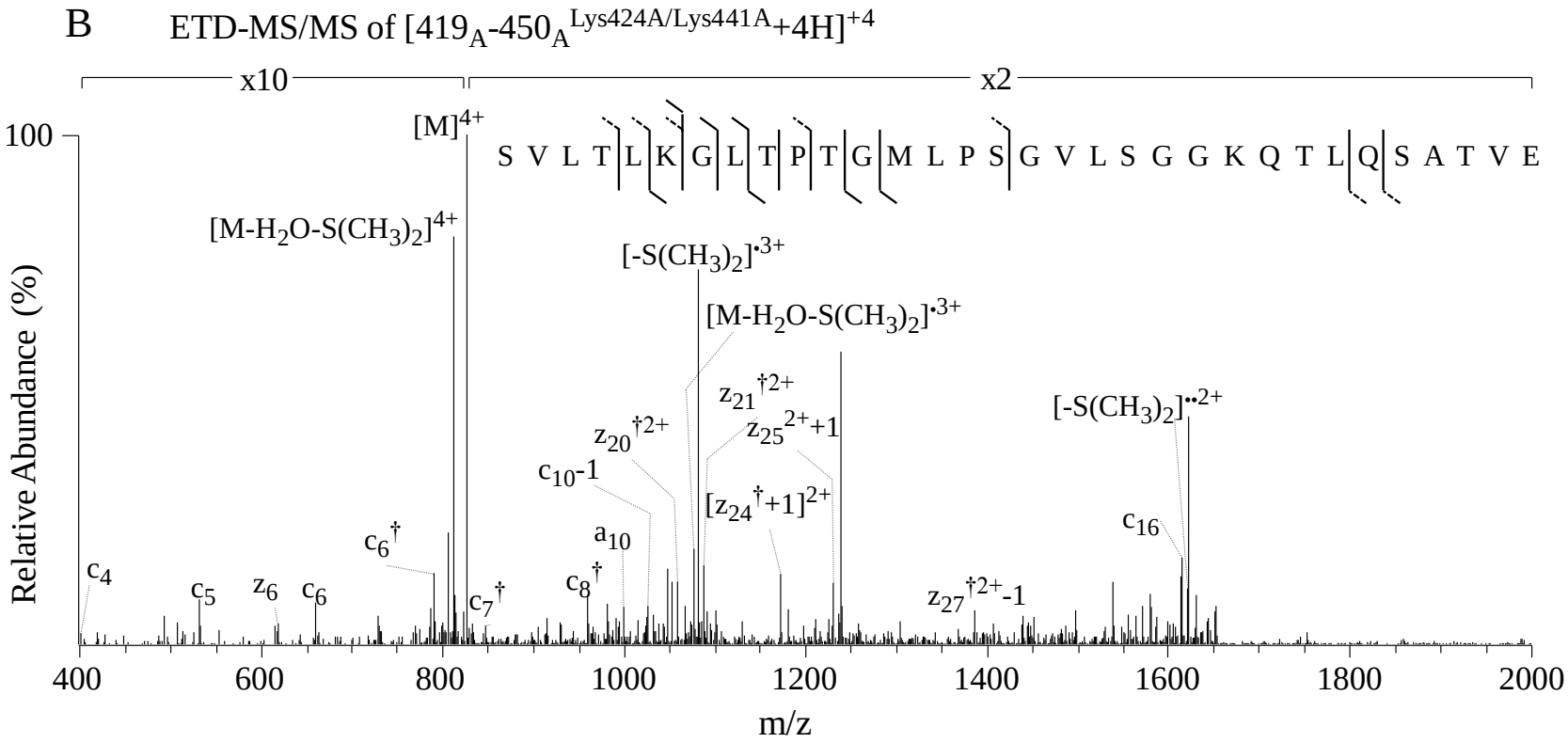

Figure 4.6 (cont'd)

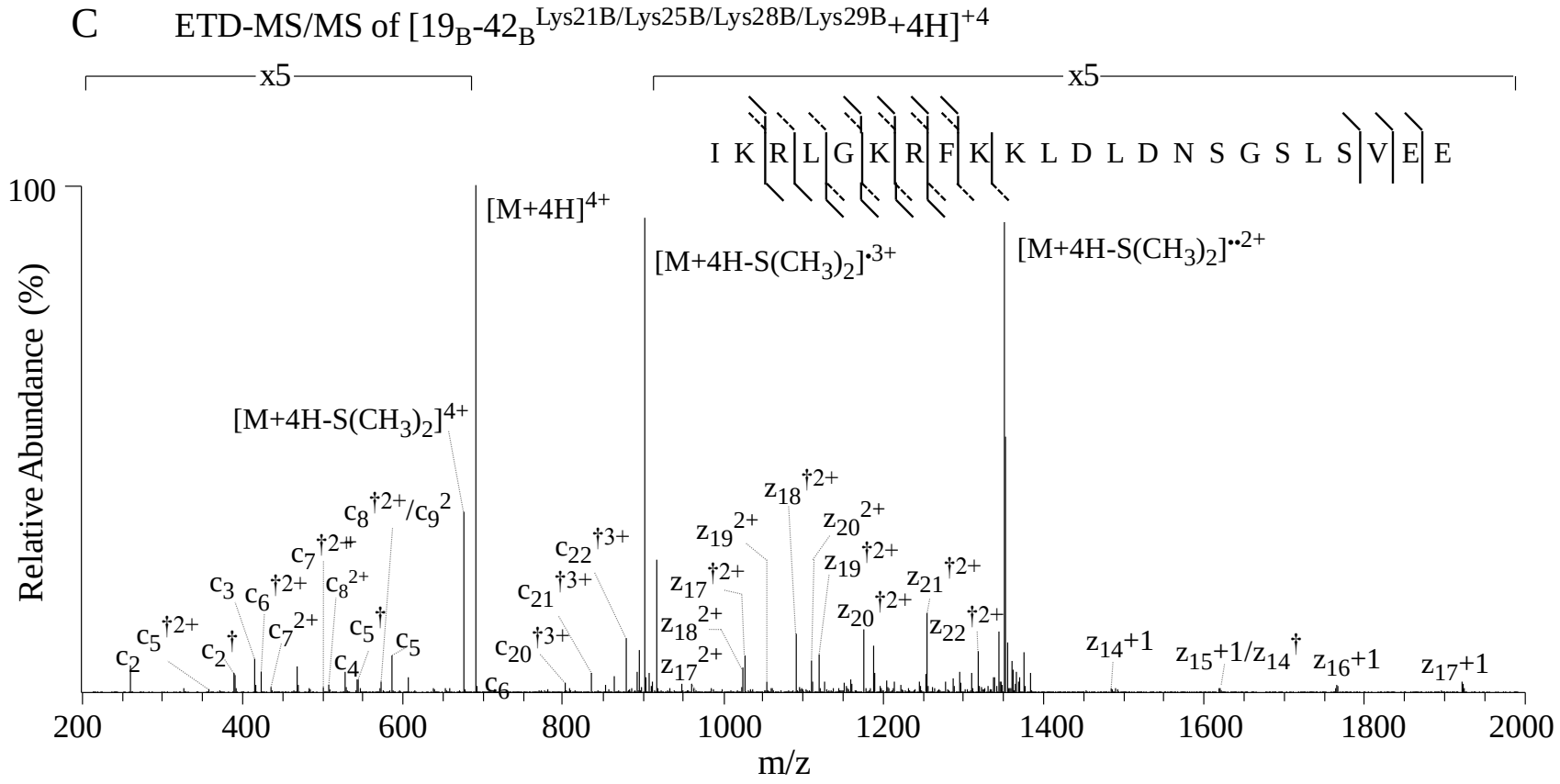

The second-order DMBNHS modification rate constants determined from the plots in Figure 4.5 are summarized in Table 4.2. It is interesting to notice that the DMBNHS modification rate constants of Lys_{459A} and Lys_{466A} determined from 451_A-472_A from native CN (k_{DMBNHS} of Lys_{459A} = 8.9 × 10^{-7} $M^{-1}s^{-1}$, k_{DMBNHS} of Lys_{466A} = 1.4 × 10^{-6} $M^{-1}s^{-1}$) were lower than those determined from 457_A-472_A from native CN (k_{DMBNHS} of Lys_{459A} = 1.4 × 10^{-6} $M^{-1}s^{-1}$, k_{DMBNHS} of Lys_{466A} = 1.7 × 10^{-6} $M^{-1}s^{-1}$). The similar differences in Lys reactivity were observed between 451_A-472_A and 457_A-472_A from CN oxidized for different time periods (as shown in Table 4.2). One possible explanation is that the incorporation of the fixed charge could enhance enzymatic cleavage when the cleavable site is close to the modification site. Also, the enhancement of ionization efficiency caused by the incorporation of a fixed charge is expected to affect shorter peptides more than longer peptides [323]. This is consistent with previous data showing a higher extent of DMBNHS modification for CRABP II peptide 1-13 compared to 1-18 (see Figure 2.21 C and D). However, no apparent difference in DMBNHS modification rate constants was observed between 364_A-394_A and 373_A-394_A both containing Lys_{393A}. This is expected as the DMBNHS modification of Lys_{393A} could only affect the efficiency of the cleavage at the C-terminal of Glu_{394A} of both peptides. 364_A-394_A and 373_A-394_A only differ at the N-terminus which are too far away from Lys_{393A} and the cleavage is not affected by DMBNHS modification. Furthermore, incorporation of only one fixed charge to the peptide would not enhance the ionization efficiency of the peptide as much as incorporation of two fixed charges. Despite the variation in DMBNHS modification rate caused

by digestion and ionization efficiency, the fold change of DMBNHS modification rate constants (described below) used to quantify CN conformational change upon oxidation remained consistent among different peptides containing the same Lys residues. For example, after being oxidized for 15 min, the fold increases in DMBNHS modification rate constant of Lys_{459A} from 451_A-472_A and 457_A-472_A were determined to be 1.44 and 1.54-fold, respectively, with a standard deviation of 0.08.

To study the CN structure under the least perturbation conditions, the extent of CN conformational change upon oxidation was characterized by dividing the DMBNHS modification rate constant of a Lys residue from CN oxidized for 15 min by the DMBNHS modification rate constant of the same Lys residue from native CN giving the fold increase of DMBNHS modification rate constants induced by oxidation (as illustrated in Figure 4.8). Lys residues showed > 2 fold increase in modification rate constants are considered to experience large extent of conformational changes. It can be seen from Figure 4.8 that these Lys residues are located in the CaM binding domain (Lys_{393A} and Lys_{405A}), the linker region between CaM binding and AI domains (Lys_{441A}), and the AI domain (Lys_{474A}) of CNA, and the Ca^{2+} binding regions (Lys_{73B}) and the CNA binding domain (Lys_{91B}) of CNB. Similar to the locations of oxidation sensitive Met residues, the Lys residues that showed a significant increase in k_{DMBNHS} upon oxidation are also located in the CN domains involved in Ca^{2+}/CaM binding and activation.

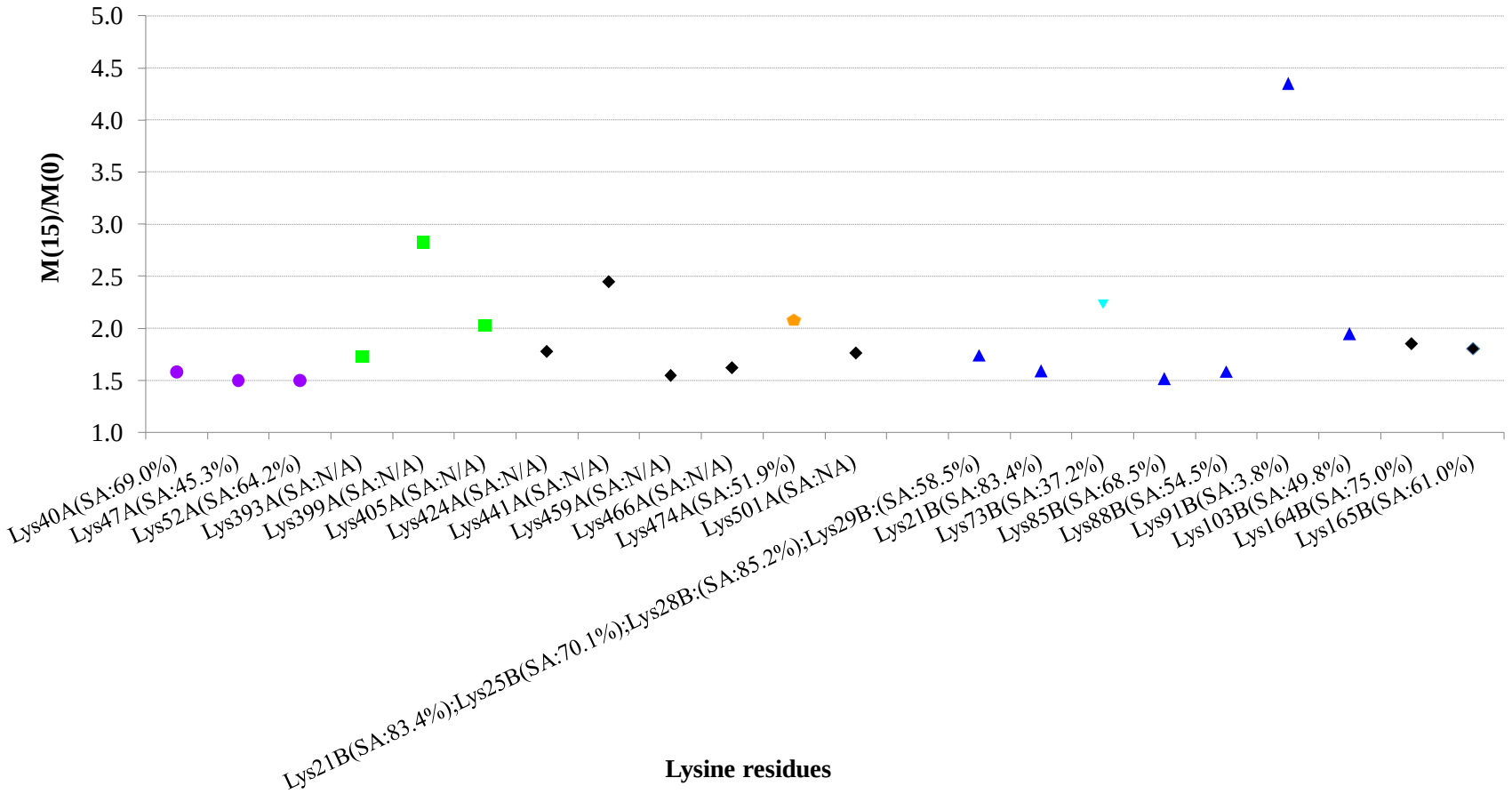

Figure 4.7 The ratio of second-order DMBNHS modification rate constants determined for observed Lys residues from oxidized CN (15 min) over the DMBNHS modification rate constants determined for the corresponding Lys residues from native CN. CN Lys residues located in catalytic domain (●), CaM binding domain (■), and autoinhibitory region (⬟), CNA binding region (▲), Ca^{2+} binding domain (▼), and non-functional regions (♦).The x-axis labels indicate the Lys residue and the corresponding solvent accessibilities (SA).

Lys_{91B} showed the largest fold-increase of modification upon CN oxidation. Interestingly, the ε-amino group of Lys_{91B} is hydrogen-bonded to the amide carbonyl group of Met_{166B}, the Met residue that exhibited the highest susceptibility towards oxidation (as shown in Figure 4.4). Therefore, it is expected that oxidation of Met_{166B} caused a subtle perturbation to its local chemical environment and broke the hydrogen bonding between Met_{166B} and Lys_{91B} thus exposing the ε-amino group of Lys_{91B} to DMBNHS modification.

Lys_{73B} also showed a relatively large change in SA (2.2 fold increase). However, no Met residues are sequentially close or hydrogen-bonded to Lys_{73B}. It is expected that the conformational change around Lys_{73B} may be caused by oxidation of one or several remote Met residue(s). One possible remote oxidation site is Met_{44B}, which was also determined to be highly susceptible to oxidation (shown in Figure 4.4). Oxidation of Met_{44B}, which is located in the first Ca^{2+} binding region (31_B-42_B), may induce a conformational change to the second Ca^{2+} binding domain (63_B-74_B) which involves Lys_{73B}, as these two Ca^{2+} sites are less than 11.1 Å away from each other. Upon being saturated with Ca^{2+}, these two N-terminal low-affinity Ca^{2+} binding sites have been demonstrated to activate CN by direct CNB/CNA interaction [353, 361] and by facilitating CaM/CNA binding [353, 361]. Therefore, conformational change in these two Ca^{2+} binding sites might inhibit the CNB or/and CaM regulated CN activation.

Lys_{399A} and Lys_{405A} which are located within the CaM binding domain also showed > 2 fold increase in modification rate constant. Conformational changes in this region may directly impair CN/CaM binding and inhibit CN activation. Met_{406A} is directly adjacent to Lys_{405A}, so it is reasonable that Met_{406A} oxidation would affect the chemical environment around Lys_{405A}. No Met residue was found close to Lys_{399A} in sequence. Both Lys_{399A} and Lys_{405A} are not visible in the electron map, so Met residues that are spatially close to them in the folded tertiary structure cannot be determined.

Lys_{441A} residing on the linker region between the CaM and AI domains showed a 2.8 fold increase in its SA after oxidation. However, the Met residues whose oxidation may cause the conformational change to the region around Lys_{441A} can not be identified, as Lys_{441A} is not visible in the electron map and the Met residues located close to it can not be determined. However, oxidation of Met_{431A} which is located within AI domain and has been determined to be highly susceptible towards oxidation (see Figure 4.4) may induce a conformational change in the region around Lys_{441A}. Also, it has been demonstrated that CaM binding induces an extensive folding not only to the CaM binding domain but also to the region between it and the AI domain [361, 362]. Therefore, it is plausible to propose that structural change in the CaM binding domain might induce a conformational change in the linker region between the CaM binding and the AI domains, and *vice versa*.

The Lys residue in the AI domain, Lys_{474A}, also illustrated a DMBNHS modification rate constant increase greater than 2 fold indicating a conformational change in AI domain. This conformational change may cause AI to bind with the active metal center more tightly and hamper the displacement of AI from the catalytic site upon Ca^{2+}/CaM binding. Also, CaM binding induced displacement of AI domain from catalytic center involves an extensive conformational change in the regulatory region ranging from the CaM binding domain to the AI domain. Therefore, the oxidation induced conformational changes occurred on CaM binding domain and the linker region between the CaM binding and AI domains may also have a negative effect on the removal of AI domain from the catalytic center upon CaM binding and cause CN inactivation. Met_{483A}, located close to the C-terminal of AI domain, and Met_{490A} exhibited high susceptibility towards oxidation are close to Lys_{474A} in sequence. However, it is not clear whether the oxidation of Met_{483A} and Met_{490A} could cause the conformational change in the region around Lys_{474A}, as no Met residues observable from the electron map was found to be in direct contact with Lys_{474A}.

4.4 Conclusions and Future Directions

The results presented here showed the initial support for the hypothesis that the oxidation induces a conformational change in CN which may cause CN inactivation by impairing the CN binding with Ca^{2+} and CaM and inhibiting displacement of AI domain

from the catalytic center. The Met residues showing a high susceptibility towards oxidation and Lys residues showing a large increase in solvent accessibility upon oxidation are all located in CN domains involved in Ca^{2+}/CaM binding and activation, i.e., CaM binding domain, the linker region between CaM binding and AI domains, the AI domain, the Ca^{2+} binding site, and the CNA binding domain.

It is beneficial to extend this study to give further insight into the oxidation induced CN inactivation via inhibited CaM/CN interaction from a structural perspective. First of all, most of the SA information from the CN catalytic domain are missing here and the percent of unmodified Lys resides can not be determined individually. These problems can be addressed by using multiple enzymes (such as Glu-C and chymotrypsin) to digest DMBNHS modified CN or by utilizing other protein labeling techniques, such as HDX, to provide complementary information as opposed to Lys-specific chemical labeling. Also, it would be interesting to engineer a series of CN mutants with a Met residue of interests exchanged for another amino acid insensitive to oxidation, such as Leu, to locate the Met residue(s) responsible for the oxidation induced CN conformational change. Furthermore, it would be beneficial to study the SA change of CaM/CN complex before and after oxidation to quantitatively characterize the inhibited CaM/CN interaction associated with oxidation.

CHAPTER FIVE

EXPERIMENTAL METHODS FOR CHAPTER FOUR

5.1 Materials

All chemicals were of analytical reagent (AR) grade if not otherwise stated. Ethylene glycol-bis(2-aminoethylether)-N,N,N′,N′-tetraacetic acid (EGTA), dithiothreitol (DTT), iodoacetamide, bovine catalase, tris(hydroxymethyl)aminomethane (Tris base), tris(hydroxymethyl)aminomethane hydrochloride (Tris-HCl), and HEPES were purchased from Sigma-Aldrich (St. Louis, MO, USA). KCl, $MgCl_2$, $CaCl_2$, and H_2O_2 (30% solution) were purchased from Columbus Chemical Industries (Columbus, WI, USA). Dimethylformamide (DMF) was from Jade Scientific (Canton, MI, USA). Glacial acetic acid and water (HPLC grade) were from Mallinckrodt Chemicals (Phillipsburg, NJ, USA). Acetonitrile (HPLC grade) and iodomethane were purchased from EMD Chemicals (San Diego, CA, USA). Sodium hydroxide (NaOH) and formic acid were from Spectrum Chemical Mfg. (Gardena, CA, USA). Trifluoroacetic acid (TFA) was purchased from Pierce (Rockford, IL, USA). S,S'-dimethylthiobutanoylhydroxysuccinimide ester (DMBNHS) was prepared using the method described in Section 3.2. Mass spectrometry grade Glu-C was purchased from Thermo Fisher Scientific (Waltham, MA, USA). Sequencing grade modified trypsin was from Promega (Madison, WI, USA). Sequencing grade Lys-C was obtained from Roche

Diagnostics (Indianapolis, IN, USA). Calcineurin (CN) was supplied by Dr. Paul Stemmer (Institute of Environmental Health Sciences, Wayne State University).

5.2 Quantification of Calcineurin Methionine Residues Oxidation Rates

5.2.1 Oxidation of Calcineurin

Six aliquots of 200 μL of 0.40 μg/μL CN (4.06 μM) solution in 10 mM HEPES buffer (pH 7.6) (10 mM HEPES, 100 mM KCl, 1 mM $MgCl_2$) and 0.1 mM $CaCl_2$ were oxidized by adding 10 μL of 250 mM H_2O_2 (final H_2O_2 concentration: 12 mM). Then, the 6 samples were incubated at room temperature in the dark for 15, 30, 45, 60, 120, and 240 min, separately. Immediately after oxidation, 40 μL of 31.25 μg/mL catalase in 10 mM HEPES buffer (pH 7.6) was added to each sample and allowed to react at room temperature for 5 min to stop the oxidation. A native CN sample was prepared by adding 50 μL of 10 mM HEPES buffer (pH 7.6) to 200 μL of 0.40 μg/μL CN solution in 10 mM HEPES buffer (pH 7.6). After oxidation, each sample was equally divided into 9 aliquots with 3 aliquots digested immediately and 6 aliquots used for DMBNHS modification (to be described later).

5.2.2 Calcineurin Digestion Using Multiple Enzymes

The 3 aliquots of each CN sample with 0, 15, 30, 45, 60, 120, and 240 min oxidation in H_2O_2 (from Section 5.2.1) were diluted with 10 mM HEPES buffer (pH 7.6)

to a final volume of 44 μL followed by addition of 8 μL of 10 mM EGTA. Reduction of CN was performed by addition of 2 μL of 0.1 M DTT (final concentration: 4 mM) followed by incubation at 60 ^{o}C for 30 min. 2 μL of 0.25 M iodoacetamide (final concentration: 10 mM) was then added and the reaction was incubated at room temperature for 1 hr in the dark. 2 μL of 0.1 M DTT was added to inactivate excess iodoacetamide at room temperature for 30 min. The resultant samples were diluted with 10 mM HEPES buffer (pH 7.6) to a final volume of 70 μL. For digestion using Glu-C, the pH of one aliquot of each of the CN sample was adjusted to 8.0 with 0.2 M NaOH followed by addition of 4 μL of 0.1 μg/μL Glu-C in H_2O (Glu-C:CN=1:20 (w/w)). The digestion was performed at 30 ^{o}C overnight (16 hr). For trypsin digestion, the pH of the second aliquot of each of the CN sample was adjusted to 7.8 with 0.2 M NaOH. 4 μL of 0.2 μg/μL trypsin in H_2O (trypsin:CN=1:10 (w/w)) was added and the reaction mixture was incubated at 37 ^{o}C overnight (16 hr). For CN digestion by Lys-C, the pH of the third aliquot of each of the CN sample was brought up to 8.0 with 0.2 M NaOH followed by addition of 4 μL of 0.2 μg/μL Lys-C in H_2O (Lys-C:CN=1:10 (w/w)). The Lys-C digestion was kept at 37 ^{o}C overnight (16 hr). Finally, 0.5 μL of formic acid was added to quench the digestion and the CN samples were stored at -20 ^{o}C until further analysis.

5.2.3 HPLC-ESI-MS and CID/ETD-MS/MS Analysis of Calcineurin Digests

HPLC-ESI-MS and CID/ETD-MS/MS analyses were performed using a Thermo Scientific Orbitrap Velos ETD mass spectrometer (Thermo, San Jose, CA, USA) coupled to an Advance nESI source and Paradigm MS4 capillary RP-HPLC system (Michrom Bioresources, Auburn, CA, USA). Analyses were performed using automated methods created by the Xcalibur software (Thermo, San Jose, CA, USA). 5 μL of each sample with a concentration at 0.2 pmol/μL in 3% acetic acid/5% acetonitrile was loaded from a Paradigm AS1 autosampler (Michrom Bioresources, Auburn, CA, USA) onto a peptide CapTrap (Michrom Bioresources, Auburn, CA, USA) at a flow rate at 15 μL/min using 0.1% trifluoroacetic acid/ 2% acetonitrile as the loading buffer. After 5 min loading time, the peptides concentrated on the peptide CapTrap (Michrom Bioresources, Auburn, CA, USA) were eluted onto a 200 μm id × 50 mm fused silica column packed with Magic C18AQ (3 μm, Michrom Bioresources, Auburn, CA, USA) at a flow rate of 2 μL/min using a linear 45 min gradient from 95% solvent A (0.1% formic acid in H_2O) to 50% solvent B (0.1% formic acid in CH_3CN). After gradient separation, the system was cleaned with 80% solvent B for 5 min followed by equilibrium with 95% solvent A for 5 min.

The spray voltage was maintained at 1.4 kV. The ion transfer tube of the mass spectrometer was set at 250 ℃, and the S-lens is set at 57%. The full MS scans were acquired from m/z 300 – 2000 in the Orbitrap mass analyzer with 60,000 resolution. Full scans were taken at AGC target value 2.0×10^5 and with 10 ms maximum injection time in the ion trap. All spectra were recorded in centroid mode.

The mass spectrometer was programmed to operate in a data-dependent mode. In both CID- and ETD-MS/MS analysis, the 5 most intense ions (signal threshold was set at 1.0×10^4 counts) from the survey MS scan were isolated with an isolation window of 2.0 m/z. During CID-MS/MS, using an AGC target value of 1.0×10^4 and a 100 ms maximum injection time in the ion trap, the isolated ions were fragmented with a normalized collision energy of 35 using an activation time of 10 ms and activation *q* value of 0.25. In ETD-MS/MS, the AGC target value and maximum injection time for analyte ions remained the same as in CID-MS/MS experiments while the AGC target value and maximum injection time of the reagent ion, i.e., fluoranthene anion, were set as 2.0×10^4 and 100 ms, respectively. ETD was carried out with supplemental activation enabled with normalized energy of 15. The reaction time was optimized as 100 ms for the 2+ charge state and proportionally scaled down for higher charge states, i.e., a 66 ms activation time for the 3+ charge state, a 50 ms activation time for the 4+ charge state, etc. Dynamic exclusion was enabled to perform CID/ETD-MS/MS experiments on the ions with same m/z 3 times within 30 s before it was placed on a dynamic exclusion list for a period of 10 s. All MS/MS spectra were acquired in the ion trap with normal scan rate in centroid mode.

5.2.4 Data Analysis

5.2.4.1 Prediction of Solvent Accessibilities

The program GetArea [329] was used, with all parameters set at the default values, to calculate the solvent-accessibilities of methionine residue side chains of CN, based on the reported crystal structure, 1AUI [344].

5.2.4.2 Determination of the Oxidation Rates of Calcineurin Methionine Residues

Characterization of oxidation sites and peptide sequences were determined manually from interpretation of the CID- and ETD-MS/MS spectra. The percent of Met containing peptides in their native state was calculated as (relative abundance of the native peptides)/(relative abundance of the native peptides + relative abundance of the oxidized peptides). The relative abundances were determined from the full MS intensity averaged over the corresponding extracted ion chromatographic peaks at 30% peak height. If multiple charge states for a precursor ion were observed, then abundance was calculated by combing all the charge states. The percent of native peptides from triplicate HPLC-ESI-MS analysis were averaged and used for the determination of pseudo-first-order oxidation rate constants.

5.3 Quantitative Analysis of Calcineurin Conformational Changes Associated with Oxidation

5.3.1 DMBNHS Modification of Native and Oxidized Calcineurin Followed by Protein Digestion by Glu-C

The 6 aliquots of each of the CN samples oxidized for 0, 15, 30, 45, and 60 min obtained from Section 5.2.1 were used for following DMBNHS modifications. To each CN sample from each oxidation time point, 1 μL of DMBNHS solution dissolved in 25%DMF/75%H_2O (prepared immediately before usage) with concentrations of 0.0 mM (CN : DMBNHS = 1:0), 0.5 mM (CN : DMBNHS = 1:5), 1.0 mM (CN : DMBNHS = 1:10), 2 mM (CN : DMBNHS = 1:20), 5 mM (CN : DMBNHS = 1:50), and 10 mM (CN : DMBNHS = 1:100) were added and each of them was incubated at room temperature for 30 min. The reaction was immediately quenched for 5 min at room temperature by addition of 8 μL of Tris (pH 8.3 at 25 ^{o}C) at a 160-fold molar excess over DMBNHS. Similar to the methods used in Section 5.2.2, each of the CN samples were diluted to a final volume of 44 μL with 10 mM HEPES buffer (pH 7.6) followed by addition of 8 μL of 10 mM EGTA. The resultant CN samples were incubated with 4 mM DTT at 60 ^{o}C for 30 min, followed by a reaction with 10 mM iodoacetamide at room temperature for 1 hr in the dark, and inactivation of excess iodoacetamide by 4 mM DTT at room temperature for 30 min. The resultant samples were diluted with 10 mM HEPES buffer (pH 7.6) to a final volume of 70 μL. The pH was adjusted to 8.0 with 0.2 mM NaOH prior to digestion. 4 μL of 0.1 μg/μL Glu-C solution was added (Glu-C:CN=1:20 (w/w) and the reaction mixture was incubated at 30 ^{o}C overnight (16 hr). The digestion was stopped by addition of 0.5 μL of formic acid and the quenched samples were stored at -20 ^{o}C for future analysis.

5.3.2 HPLC-ESI-MS, CID-MS/MS, -MS^3, and ETD-MS/MS Analysis of DMBNHS Modified Calcineurin Digests

HPLC-ESI-MS, CID-MS/MS, -MS^3, and ETD-MS/MS analyses were performed using a Thermo Orbitrap Velos ETD mass spectrometer (Thermo, San Jose, CA, USA) equipped with an Advance nESI source and Paradigm MS4 capillary RP-HPLC system (Michrom Bioresources, Auburn, CA, USA). Analyses were performed using automated methods created by the Xcalibur software (Thermo, San Jose, CA, USA). 5 μL of each sample with a concentration at 0.35 pmol/μL in 3% acetic acid/5% acetonitrile was loaded from a Paradigm AS1 autosampler (Michrom Bioresources, Auburn, CA, USA) onto a peptide CapTrap (Michrom Bioresources, Auburn, CA, USA) at a flow rate at 15 μL/min using 0.1% trifluoroacetic acid/ 2% acetonitrile as the loading buffer. After 5 min loading time, the peptides concentrated on the CapTrap were eluted to a 200 μm id × 50 mm fused silica column packed with Magic C18AQ (3 μm, Michrom Bioresources, Auburn, CA, USA) at a flow rate of 2 μL/min using a linear 70 min gradient from 95% solvent A (0.1% formic acid in H_2O) to 50% solvent B (0.1% formic acid in CH_3CN). After gradient separation, the system was cleaned with 80% solvent B for 5 min followed by equilibrium with 95% solvent A for 5 min.

The spray voltage was maintained at 1.4 kV. The ion transfer tube was set at 250 ℃ and S-lens value was at 57%. The full MS scans were acquired from m/z 300 to 2000 in the Orbitrap mass analyzer with a resolution of 60,000. Full scans were taken at AGC

target value 2.0×10^5 and with 10 ms maximum injection time in the ion trap. All MS, MS/MS, and MS^3 spectra were acquired in centroid mode.

In CID-MS/MS and -MS^3 analysis, the precursor ions were isolated with an isolation window of 2.0 m/z using AGC target value 1.0×10^4 and 100 ms as the maximum injection time. CID was performed with normalized collision energy of 35 using an activation time of 10 ms and activation *q* value of 0.25. Dynamic exclusion was enabled to perform CID/ETD-MS/MS experiments on the ions with same m/z 3 times within 30 s before it was placed on a dynamic exclusion list for a period of 10 s. Similar to the method described in Section 3.8, the mass spectrometer was operated in a data-dependent constant neutral loss scan (DDCNL) mode by performing CID-MS/MS scans on the 5 most intense peaks from each MS survey scan, while simultaneously searching for the defined neutral losses (Table 3.1). Here, the neutral losses with m/z variance of ±0.5 were set to account for single, double, and triple $S(CH_3)_2$ neutral losses from $[M^{N+}+(m-N)H]^{m+}$ precursor ions, where M represents the peptide, N represents the number of modifications, and m represents the different observed charge states ranging from +2 to +5. If the targeted neutral loss was detected and appeared above a predefined threshold abundance of 1.0×10^4 counts, CID-MS^3 was automatically initiated to further fragment the most intense neutral loss product ion. All the MS/MS and MS^3 spectra were acquired in ion trap with normal scan rate.

Targeted ETD-MS/MS experiments were performed in a data-independent mode where only the precursor ions of interests were selected for targeted analysis by ETD-

MS/MS. Targeted ETD-MS/MS of each peptide of interests were started at least 0.5 min earlier than the starting time point and 0.5 min later than the end time point of the retention time predicted from previous HPLC-ESI-MS, CID-MS/MS and -MS^3 runs as described above. ETD-MS/MS of all observed charge states were performed following each full MS scan. With a maximum injection time of 100 ms, the analyte ions and reagent ions (fluoranthene anions) were accumulated in the ion trap with an AGC target value of 1.0×10^4 and 2.0×10^5, respectively. Supplemental activation was enabled with a normalized energy at 15. The activation time from 60 ms to 100 ms was optimized for the 2+ charge state and proportionally scaled down for higher charge states (e.g., if a 60 ms reaction time was used for 2+ charge state, then a 40 ms reaction time would be used for 3+ charge state, a 30 ms reaction time would be used for 4+ charge state, etc.).

5.3.3 Data Analysis

5.3.3.1 Prediction of Solvent Accessibilities

With all parameters set at the default values, GetArea [329] was used to estimate the solvent-accessibilities of CN lysine residue side chains, based on the reported crystal structure, 1AUI [344].

5.3.3.2 Quantitative Analysis of the Extent of DMBNHS Modification of Calcineurin Lysine Residues

DMBNHS modification sites and peptide sequences were confirmed by manual inspection of the CID-MS/MS, -MS^3 and ETD-MS/MS spectra. The relative abundances were determined from MS or ETD-MS/MS spectra averaged over the corresponding chromatographic peaks at 30% peak height. If multiple charge states for a precursor ion were present, the relative abundance from each charge state was summed. For peptides with only one modifiable site, the percent of unmodified Lys residues was calculated as equation (5.1), where MS(UN) indicate the relative MS abundances of unmodified peptides and MS (M) indicates the relative MS abundances of the modified peptides with different numbers of modification. In this particular case, singly modified state was present and thus $\sum MS(M) = MS(1M)$, where MS(1M) indicates the relative MS abundances of singly modified peptides. For peptides with multiple modifiable sites and whose isomeric modified forms were resolved chromatographically, the total abundance of a specific unmodified Lys residue is summed from both the unmodified peptides and partially modified peptides with the specific Lys residue unmodified. Therefore, the fraction of a specific unmodified Lys residue was determined as equation (5.2), where MS(pM with the Lys residue under investigation unmodified) indicates the relative MS abundances of the specific partially modified peptides isomers with the Lys under investigation remaining unmodified. For peptides with multiple modifiable sites and whose isomeric modified forms co-eluted during HPLC separation, the relative abundance of the partially modified peptides isomers with different sites of modification could not be determined from MS intensity. In this case, the relative abundance of ETD-MS/MS fragment ions characteristic for the corresponding modification site(s) was used together with relative MS abundances to determine the relative abundances of each

isomer, as illustrated in equation (5.3), where MS/MS(the specific fragment ions characteristic of the Lys residue under investigation unmodified) indicates the relative ETD-MS/MS abundances of the fragment ions characteristic of the partially modified peptides with the Lys residue under investigation remaining unmodified and MS/MS(the specific fragment ion characteristic of a certain Lys residue unmodified) indicates the relative ETD-MS/MS abundances of the specific fragment ions, which is the same type of ions as that used in MS/MS(the specific fragment ions characteristic of the Lys residue under investigation unmodified), characteristic of the unmodification of any Lys residues. The percent of native peptides from triplicate HPLC-ESI-MS, CID-MS/MS, -MS^3 and ETD-MS/MS analysis were averaged and used for the determination of second-order DMBNHS modification rate constants.

$$\frac{\mathbf{MS(UN)}}{\mathbf{MS(UN)}+\sum \mathbf{MS(M)}} \tag{5.1}$$

$$\frac{\mathbf{MS(UN)}+\sum \mathbf{MS(pM\ with\ the\ Lys\ residue\ under\ investigation\ unmodified)}}{\mathbf{MS(UN)}+\sum \mathbf{MS(M)}} \tag{5.2}$$

$$\frac{\mathbf{MS(UN)}+\sum \mathbf{MS(pM)}\times\frac{\mathbf{MS/MS(the\ specific\ fragment\ ions\ characterisitic\ of\ the\ Lys\ residue\ under\ investigation\ unmodified)}}{\sum \mathbf{MS/MS(the\ specific\ fragment\ ion\ characteristic\ of\ a\ certain\ Lys\ residue\ unmodified)}}}{\mathbf{MS(UN)}+\sum \mathbf{MS(M)}} \tag{5.3}$$

REFERENCES

References

1. Chait, B.T. Mass Spectrometry in the Postgenomic Era. *Annual Review of Biochemistry*, **2011**, *80*, 239-246.

2. Yates, J.R.; Ruse, C.I.; Nakorchevsky, A. Proteomics by Mass Spectrometry: Approaches, Advances, and Applications. *Annual Review of Biomedical Engineering*, **2009**, *11*, 49-79.

3. Helsens, K.; Martens, L.; Vandekerckhove, J.; Gevaert, K. Mass Spectrometry-Driven Proteomics: an Introduction. *Methods in Molecular Biology*, **2011**, *753*, 1-27.

4. Fenn, J.B.; Mann, M.; Meng, C.K.; Wong, S.F.; Whitehouse, C.M. Electrospray Ionization for Mass Spectrometry of Large Biomolecules. *Science*, **1989**, *246*, 64-71.

5. Tanaka, K.; Waki, H.; Ido, Y.; Akita, S.; Yoshida, Y.; Yoshida, T.; Matsuo, T. Protein and Polymer Analyses up to m/z 100 000 by Laser Ionization Time-of-Flight Mass Spectrometry. *Rapid Communications in Mass Spectrometry*, **1988**, *2*, 151-153.

6. Karas, M.; Hillenkamp, F. Laser Desorption Ionization of Proteins with Molecular Masses Exceeding 10,000 Daltons. *Analytical Chemistry*, **1988**, *60*, 2299-2301.

7. Jennings, K.R. The Changing Impact of the Collision-Induced Decomposition of Ions on Mass Spectrometry. *International Journal of Mass Spectrometry*, **2000**, *200*, 479-493.

8. Steen, H.; Mann, M. The ABC's (and XYZ's) of Peptide Sequencing. *Nature Reviews Molecular Cell Biology*, **2004**, *5*, 699-711.

9. Schlosser, A.; Lehmann, W.D. Five-Membered Ring Formation in Unimolecular Reactions of Peptides: a Key Structural Element Controlling Low-Energy Collision-Induced Dissociation of Peptides. *Journal of Mass Spectrometry*, **2000**, *35*, 1382-1390.

10. Wysocki, V.H.; Tsaprailis, G.; Smith, L.L.; Breci, L.A. Mobile and Localized Protons: a Framework for Understanding Peptide Dissociation. *Journal of Mass Spectrometry*, **2000**, *35*, 1399-1406.

11. Kapp, E.A.; Schütz, F.; Reid, G.E.; Eddes, J.S.; Moritz, R.L.; O'Hair, R.A.J.; Speed, T.P.; Simpson, R.J. Mining a Tandem Mass Spectrometry Database To Determine the Trends and Global Factors Influencing Peptide Fragmentation. *Analytical Chemistry*, **2003**, *75*, 6251-6264.

12. Palumbo, A.M.; Reid, G.E. Evaluation of Gas-Phase Rearrangement and Competing Fragmentation Reactions on Protein Phosphorylation Site Assignment Using Collision Induced Dissociation-MS/MS and MS^3. *Analytical Chemistry*, **2008**, *80*, 9735-9747.

13. Reid, G.E.; Roberts, K.D.; Kapp, E.A.; Simpson, R.J. Statistical and Mechanistic Approaches to Understanding the Gas-Phase Fragmentation Behavior of Methionine Sulfoxide Containing Peptides. *Journal of Proteome Research*, **2004**, *3*, 751-759.

14. Hoffmann, E.d.; Stroobant, V. Mass Spectrometry: Principles and Applications. 3 Ed. *Chichester : John Wiley & Sons, New Jersey*, **2007**.

15. Morris, H.R.; Paxton, T.; Dell, A.; Langhorne, J.; Berg, M.; Bordoli, R.S.; Hoyes, J.; Bateman, R.H. High Sensitivity Collisionally-activated Decomposition Tandem Mass Spectrometry on a Novel Quadrupole/Orthogonal-acceleration Time-of-flight Mass Spectrometer. *Rapid Communications in Mass Spectrometry*, **1996**, *10*, 889-896.

16. Zubarev, R.A.; Kelleher, N.L.; McLafferty, F.W. Electron Capture Dissociation of Multiply Charged Protein Cations. A Nonergodic Process. *Journal of the American Chemical Society*, **1998**, *120*, 3265-3266.

17. Syka, J.E.P.; Coon, J.J.; Schroeder, M.J.; Shabanowitz, J.; Hunt, D.F. Peptide and Protein Sequence Analysis by Electron Transfer Dissociation Mass Spectrometry. *Proceedings of the National Academy of Sciences of the United States of America*, **2004**, *101*, 9528-9533.

18. Coon, J.J.; Ueberheide, B.; Syka, J.E.P.; Dryhurst, D.D.; Ausio, J.; Shabanowitz, J.; Hunt, D.F. Protein Identification Using Sequential Ion/Ion Reactions and Tandem Mass Spectrometry. *Proceedings of the National Academy of Sciences of the United States of America*, **2005**, *102*, 9463-9468.

19. Coon, J.J.; Syka, J.E.P.; Schwartz, J.C.; Shabanowitz, J.; Hunt, D.F. Anion Dependence in the Partitioning Between Proton and Electron Transfer in Ion/Ion Reactions. *International Journal of Mass Spectrometry*, **2004**, *236*, 33-42.

20. McLafferty, F.W.; Horn, D.M.; Breuker, K.; Ge, Y.; Lewis, M.A.; Cerda, B.; Zubarev, R.A.; Carpenter, B.K. Electron Capture Dissociation of Gaseous Multiply Charged Ions by Fourier-Transform Ion Cyclotron Resonance. *Journal of The American Society for Mass Spectrometry*, **2001**, *12*, 245-249.

21. Zubarev, R.A. Reactions of Polypeptide Ions with Electrons in the Gas Phase. *Mass Spectrometry Reviews*, **2003**, *22*, 57-77.

22. Armirotti, A.; Damonte, G. Achievements and Perspectives of Top-Down Proteomics. *Proteomics*, **2010**, *10*, 3566-3576.

23. Coon, J.J. Collisions or Electrons? Protein Sequence Analysis in the 21st Century. *Analytical Chemistry*, **2009**, *81*, 3208-3215.

24. Zubarev, R.A.; Horn, D.M.; Fridriksson, E.K.; Kelleher, N.L.; Kruger, N.A.; Lewis, M.A.; Carpenter, B.K.; McLafferty, F.W. Electron Capture Dissociation for Structural

Characterization of Multiply Charged Protein Cations. *Analytical Chemistry*, **2000**, *72*, 563-573.

25. Good, D.M.; Wirtala, M.; McAlister, G.C.; Coon, J.J. Performance Characteristics of Electron Transfer Dissociation Mass Spectrometry. *Molecular & Cellular Proteomics*, **2007**, *6*, 1942-1951.

26. Swaney, D.L.; McAlister, G.C.; Wirtala, M.; Schwartz, J.C.; Syka, J.E.P.; Coon, J.J. Supplemental Activation Method for High-Efficiency Electron-Transfer Dissociation of Doubly Protonated Peptide Precursors. *Analytical Chemistry*, **2006**, *79*, 477-485.

27. Bushey, J.M.; Baba, T.; Glish, G.L. Simultaneous Collision Induced Dissociation of the Charge Reduced Parent Ion during Electron Capture Dissociation. *Analytical Chemistry*, **2009**, *81*, 6156-6164.

28. Zubarev, R.A. Electron-Capture Dissociation Tandem Mass Spectrometry. *Current Opinion in Biotechnology*, **2004**, *15*, 12-16.

29. Silivra, O.; Kjeldsen, F.; Ivonin, I.; Zubarev, R. Electron Capture Dissociation of Polypeptides in a Three-Dimensional Quadrupole Ion Trap: Implementation and First Results. *Journal of The American Society for Mass Spectrometry*, **2005**, *16*, 22-27.

30. Ding, L.; Brancia, F.L. Electron Capture Dissociation in a Digital Ion Trap Mass Spectrometer. *Analytical Chemistry*, **2006**, *78*, 1995-2000.

31. Baba, T.; Hashimoto, Y.; Hasegawa, H.; Hirabayashi, A.; Waki, I. Electron Capture Dissociation in a Radio Frequency Ion Trap. *Analytical Chemistry*, **2004**, *76*, 4263-4266.

32. Reid, G.E.; McLuckey, S.A. 'Top Down' Protein Characterization via Tandem Mass Spectrometry. *Journal of Mass Spectrometry*, **2002**, *37*, 663-675.

33. Henzel, W.; Watanabe, C.; Stults, J. Protein Identification: the Origins of Peptide Mass Fingerprinting. *Journal of The American Society for Mass Spectrometry*, **2003**, *14*, 931-942.

34. Hunt, D.F.; Yates, J.R.; Shabanowitz, J.; Winston, S.; Hauer, C.R. Protein Sequencing by Tandem Mass Spectrometry. *Proceedings of the National Academy of Sciences*, **1986**, *83*, 6233-6237.

35. Eng, J.K.; Mccormack, A.L.; Yates, J.R. An Approach to Correlate Tandem Mass-Spectral Data of Peptides with Amino-Acid-Sequences in a Protein Database. *Journal of The American Society for Mass Spectrometry*, **1994**, *5*, 976-989.

36. MacCoss, M.J.; Wu, C.C.; Yates, J.R. Probability-Based Validation of Protein Identifications Using a Modified SEQUEST Algorithm. *Analytical Chemistry*, **2002**, *74*, 5593-5599.

37. Anderson, D.C.; Li, W.Q.; Payan, D.G.; Noble, W.S. A New Algorithm for the Evaluation of Shotgun Peptide Sequencing in Proteomics: Support Vector Machine Classification of Peptide MS/MS Spectra and SEQUEST Scores. *Journal of Proteome Research*, **2003**, *2*, 137-146.

38. Perkins, D.N.; Pappin, D.J.C.; Creasy, D.M.; Cottrell, J.S. Probability-Based Protein Identification by Searching Sequence Databases Using Mass Spectrometry Data. *Electrophoresis*, **1999**, *20*, 3551-3567.

39. Fenyo, D.; Beavis, R.C. A Method for Assessing the Statistical Significance of Mass Spectrometry-Based Protein Identifications Using General Scoring Schemes. *Analytical Chemistry*, **2003**, *75*, 768-774.

40. Biemann, K.; Papayannopoulos, I.A. Amino Acid Sequencing of Proteins. *Accounts of Chemical Research*, **1994**, *27*, 370-378.

41. Aebersold, R.; Mann, M. Mass Spectrometry-Based Proteomics. *Nature*, **2003**, *422*, 198-207.

42. Monteoliva, L.; Albar, J.P. Differential Proteomics: an Overview of Gel and Non-Gel Based Approaches. *Briefings in Functional Genomics*, **2004**, *3*, 220-239.

43. Perrot, M.; Sagliocco, F.; Mini, T.; Monribot, C.; Schneider, U.; Shevchenko, A.; Mann, M.; Jeno, P.; Boucherie, H. Two-Dimensional Gel Protein Database of Saccharomyces Cerevisiae (update 1999). *Electrophoresis*, **1999**, *20*, 2280-2298.

44. Link, A.J.; Eng, J.; Schieltz, D.M.; Carmack, E.; Mize, G.J.; Morris, D.R.; Garvik, B.M.; Yates, J.R., 3rd Direct Analysis of Protein Complexes Using Mass Spectrometry. *Nature Biotechnology*, **1999**, *17*, 676-682.

45. Washburn, M.P.; Wolters, D.; Yates, J.R., 3rd Large-Scale Analysis of the Yeast Proteome by Multidimensional Protein Identification Eechnology. *Nature Biotechnology*, **2001**, *19*, 242-247.

46. McLafferty, F.W.; Kelleher, N.L.; Lin, H.Y.; Valaskovic, G.A.; Aaserud, D.J.; Fridriksson, E.K. Top Down Versus Bottom up Protein Characterization by Tandem High-Resolution Mass Spectrometry. *Journal of the American Chemical Society*, **1999**, *121*, 806-812.

47. Siuti, N.; Kelleher, N.L. Decoding Protein Modifications Using Top-Down Mass Spectrometry. *Nature Methods*, **2007**, *4*, 817-821.

48. Huber, C.; Huber, L. Special Focus on Top-Down Proteomics. *Proteomics*, **2010**, *10*, 3564-3565.

49. Cui, W.; Rohrs, H.W.; Gross, M.L. Top-Down Mass Spectrometry: Recent Developments, Applications and Perspectives. *Analyst*, **2011**.

50. Marshall, A.G.; Hendrickson, C.L.; Jackson, G.S. Fourier Transform Ion Cyclotron Resonance Mass Spectrometry: a Primer. *Mass Spectrometry Reviews*, **1998**, *17*, 1-35.

51. Hu, Q.Z.; Noll, R.J.; Li, H.Y.; Makarov, A.; Hardman, M.; Cooks, R.G. The Orbitrap: a New Mass Spectrometer. *Journal of Mass Spectrometry*, **2005**, *40*, 430-443.

52. Zhai, H.; Han, X.; Breuker, K.; McLafferty, F.W. Consecutive Ion Activation for Top Down Mass Spectrometry: Improved Protein Sequencing by Nozzle-Skimmer Dissociation. *Analytical Chemistry*, **2005**, *77*, 5777-5784.

53. Han, X.; Jin, M.; Breuker, K.; McLafferty, F.W. Extending Top-Down Mass Spectrometry to Proteins with Masses Greater than 200 Kilodaltons. *Science*, **2006**, *314*, 109-112.

54. Fersht, A.R. From the First Protein Structures to Our Current Knowledge of Protein Folding: Delights and Scepticisms. *Nature Reviews Molecular Cell Biology*, **2008**, *9*, 650-654.

55. Dobson, C.M. Protein Folding and Misfolding. *Nature*, **2003**, *426*, 884-890.

56. Frauenfelder, H.; Chen, G.; Berendzen, J.; Fenimore, P.W.; Jansson, H.; McMahon, B.H.; Stroe, I.R.; Swenson, J.; Young, R.D. A Unified Model of Protein Dynamics. *Proceedings of the National Academy of Sciences*, **2009**, *106*, 5129-5134.

57. Vinson, V.J. Proteins in Motion. *Science*, **2009**, *324*, 197.

58. Tollinger, M.; Skrynnikov, N.R.; Mulder, F.A.A.; Forman-Kay, J.D.; Kay, L.E. Slow Dynamics in Folded and Unfolded States of an SH3 Domain. *Journal of the American Chemical Society*, **2001**, *123*, 11341-11352.

59. Konermann, L.; Pan, J.X. Calcium-Induced Structural Transitions of the Calmodulin-Melittin System Studied by Electrospray Mass Spectrometry: Conformational Subpopulations and Metal-Unsaturated Intermediates. *Biochemistry*, **2010**, *49*, 3477-3486.

60. Korzhnev, D.M.; Religa, T.L.; Banachewicz, W.; Fersht, A.R.; Kay, L.E. A Transient and Low-Populated Protein-Folding Intermediate at Atomic Resolution. *Science*, **2010**, *329*, 1312-1316.

61. Dyson, H.J.; Wright, P.E. Intrinsically Unstructured Proteins and Their Functions. *Nature Reviews Molecular Cell Biology*, **2005**, *6*, 197-208.

62. Sugase, K.; Dyson, H.J.; Wright, P.E. Mechanism of Coupled Folding and Binding of an Intrinsically Disordered Protein. *Nature*, **2007**, *447*, 1021-U1011.

63. Huang, Y.J.; Montelione, G.T. Structural Biology: Proteins Flex to Function. *Nature*, **2005**, *438*, 36-37.

64. Qian, B.; Raman, S.; Das, R.; Bradley, P.; McCoy, A.J.; Read, R.J.; Baker, D. High-Resolution Structure Prediction and the Crystallographic Phase Problem. *Nature*, **2007**, *450*, 259-264.

65. Iribarne, J.V.; Thomson, B.A. On the Evaporation of Small Ions from Charged Droplets. *Journal of Chemical Physics*, **1976**, *64*, 2287-2294.

66. Dole, M.; Mack, L.L.; Hines, R.L.; Mobley, R.C.; Ferguson, L.D.; Alice, M.B. Molecular Beams of Macroions *Journal of Chemical Physics*, **1968**, *49*, 2240-2249.

67. Kebarle, P.; Verkerk, U.H. Electrospray: From Ions in Solution to Ions in the Gas Phase, What We Know Now. *Mass Spectrometry Reviews*, **2009**, *28*, 898-917.

68. Konermann, L.; Ferguson, P.L.; Kuprowski, M.C.; Boys, B.L.; Wilson, D.J.; Pan, J.X. Protein Folding and Protein-Ligand Interactions Monitored by Electrospray Mass Spectrometry. *Current Analytical Chemistry*, **2009**, *5*, 186-204.

69. Hamdy, O.; Julian, R. Reflections on Charge State Distributions, Protein Structure, and the Mystical Mechanism of Electrospray Ionization. *Journal of The American Society for Mass Spectrometry*, **2012**, *23*, 1-6.

70. Chowdhury, S.K.; Katta, V.; Chait, B.T. Probing Conformational Changes in Proteins by Mass Spectrometry. *Journal of the American Chemical Society*, **1990**, *112*, 9012-9013.

71. Nesatyy, V.J.; Suter, M.J.F. On the Conformation-Dependent Neutralization Theory and Charging of Individual Proteins and Their Non-Covalent Complexes in the Gas Phase. *Journal of Mass Spectrometry*, **2004**, *39*, 93-97.

72. Samalikova, M.; Grandori, R. Role of opposite charges in protein electrospray ionization mass spectrometry. *Journal of Mass Spectrometry*, **2003**, *38*, 941-947.

73. Grandori, R. Origin of the conformation dependence of protein charge-state distributions in electrospray ionization mass spectrometry. *Journal of Mass Spectrometry*, **2003**, *38*, 11-15.

74. Smith, R.D.; Loo, J.A.; Loo, R.R.O.; Busman, M.; Udseth, H.R. Principles and Practice of Electrospray Ionization-Mass Spectrometry for Large Polypeptides and Proteins. *Mass Spectrometry Reviews*, **1991**, *10*, 359-452.

75. Konermann, L. A Minimalist Model for Exploring Conformational Effects on the Electrospray Charge State Distribution of Proteins. *The Journal of Physical Chemistry B*, **2007**, *111*, 6534-6543.

76. Grandori, R. Electrospray-Ionization Mass Spectrometry for Protein Conformational Studies. *Current Organic Chemistry*, **2003**, *7*, 1589-1603.

77. Ben-Nissan, G.; Sharon, M. Capturing protein structural kinetics by mass spectrometry. *Chemical Society Reviews*, **2011**, *40*, 3627-3637.

78. Frimpong, A.K.; Abzalimov, R.R.; Uversky, V.N.; Kaltashov, I.A. Characterization of Intrinsically Disordered Proteins with Electrospray Ionization Mass Spectrometry: Conformational Heterogeneity of alpha-Synuclein. *Proteins-Structure Function and Bioinformatics*, **2010**, *78*, 714-722.

79. Grandori, R.; Testa, L.; Brocca, S.; Samalikova, M.; Santambrogio, C.; Alberghina, L. Electrospray ionization-mass spectrometry conformational analysis of isolated domains of an intrinsically disordered protein. *Biotechnology Journal*, **2011**, *6*, 96-100.

80. Zamani, L.; Lindholm, J.; Ilag, L.L.; Jacobsson, S.P. Discrimination among IgG1-kappa Monoclonal Antibodies Produced by Two Cell Lines Using Charge State Distributions in NanoESI-TOF Mass Spectra. *Journal of The American Society for Mass Spectrometry*, **2009**, *20*, 1030-1036.

81. Konermann, L.; Collings, B.A.; Douglas, D.J. Cytochrome c Folding Kinetics Studied by Time-Resolved Electrospray Ionization Mass Spectrometry. *Biochemistry*, **1997**, *36*, 5554-5559.

82. Theorell, H.; Åkesson, Å. Studies on Cytochrome c. II. the Optical Properties of Pure Cytochrome c and Some of Its Derivatives. *Journal of the American Chemical Society*, **1941**, *63*, 1812-1818.

83. Beechem, J.M.; Ameloot, M.; Brand, L. Global and Target Analysis of Complex Decay Phenomena. *Analytical Instrumentation*, **1985**, *14*, 379-402.

84. Pan, J.; Konermann, L. Calcium-Induced Structural Transitions of the Calmodulin−Melittin System Studied by Electrospray Mass Spectrometry: Conformational Subpopulations and Metal-Unsaturated Intermediates. *Biochemistry*, **2010**, *49*, 3477-3486.

85. Boys, B.L.; Konermann, L. Folding and Assembly of Hemoglobin Monitored by Electrospray Mass Spectrometry Using an On-line Dialysis System. *Journal of The American Society for Mass Spectrometry*, **2007**, *18*, 8-16.

86. Santambrogio, C.; Ricagno, S.; Sobott, F.; Colombo, M.; Bolognesi, M.; Grandori, R. Characterization of β2-Microglobulin Conformational Intermediates Associated to Different Fibrillation Conditions. *Journal of Mass Spectrometry*, **2011**, *46*, 734-741.

87. Bai, Y.; Milne, J.S.; Mayne, L.; Englander, S.W. Primary Structure Effects on Peptide Group Hydrogen Exchange. *Proteins: Structure, Function, and Bioinformatics*, **1993**, *17*, 75-86.

88. Rand, K.D.; Lund, F.W.; Amon, S.; Jørgensen, T.J.D. Investigation of Amide Hydrogen Back-Exchange in Asp and His Repeats Measured by Hydrogen ($^{1}H/^{2}H$) Exchange Mass Spectrometry. *International Journal of Mass Spectrometry*, **2011**, *302*, 110-115.

89. Smith, D.L.; Deng, Y.; Zhang, Z. Probing the Non-covalent Structure of Proteins by Amide Hydrogen Exchange and Mass Spectrometry. *Journal of Mass Spectrometry*, **1997**, *32*, 135-146.

90. Konermann, L.; Pan, J.X.; Liu, Y.H. Hydrogen Exchange Mass Spectrometry for Studying Protein Structure and Dynamics. *Chemical Society Reviews*, **2011**, *40*, 1224-1234.

91. Deng, Y.; Zhang, Z.; Smith, D. Comparison of Continuous and Pulsed Labeling Amide Hydrogen Exchange/Mass Spectrometry for Studies of Protein Dynamics. *Journal of The American Society for Mass Spectrometry*, **1999**, *10*, 675-684.

92. Engen, J.R. Analysis of Protein Conformation and Dynamics by Hydrogen/Deuterium Exchange MS. *Analytical Chemistry*, **2009**, *81*, 7870-7875.

93. Marcsisin, S.; Engen, J. Hydrogen Exchange Mass Spectrometry: What Is It and What Can It Tell Us? *Analytical and Bioanalytical Chemistry*, **2010**, *397*, 967-972.

94. Konermann, L.; Simmons, D.A. Protein-Folding Kinetics and Mechanisms Studied by Pulse-Labeling and Mass Spectrometry. *Mass Spectrometry Reviews*, **2003**, *22*, 1-26.

95. Zhang, Z.; Smith, D.L. Determination of Amide Hydrogen Exchange by Mass Spectrometry: A New Tool for Protein Structure Elucidation. *Protein Science*, **1993**, *2*, 522-531.

96. Wang, L.; Pan, H.; Smith, D.L. Hydrogen Exchange-Mass Spectrometry. *Molecular & Cellular Proteomics*, **2002**, *1*, 132-138.

97. Wu, Y.; Kaveti, S.; Engen, J.R. Extensive Deuterium Back-Exchange in Certain Immobilized Pepsin Columns Used for H/D Exchange Mass Spectrometry. *Analytical Chemistry*, **2006**, *78*, 1719-1723.

98. Busby, S.A.; Chalmers, M.J.; Griffin, P.R. Improving Digestion Efficiency under H/D Exchange Conditions with Activated Pepsinogen Coupled Columns. *International Journal of Mass Spectrometry*, **2007**, *259*, 130-139.

99. Jones, L.M.; Zhang, H.; Vidavsky, I.; Gross, M.L. Online, High-Pressure Digestion System for Protein Characterization by Hydrogen/Deuterium Exchange and Mass Spectrometry. *Analytical Chemistry*, **2010**, *82*, 1171-1174.

100. López-Ferrer, D.; Petritis, K.; Robinson, E.W.; Hixson, K.K.; Tian, Z.; Lee, J.H.; Lee, S.-W.; Tolić, N.; Weitz, K.K.; Belov, M.E.; Smith, R.D.; Paša-Tolić, L. Pressurized Pepsin Digestion in Proteomics. *Molecular & Cellular Proteomics*, **2011**, *10*.

101. Astorga-Wells, J.; Landreh, M.; Johansson, J.; Bergman, T.; Jornvall, H. A Membrane Cell for On-Line Hydrogen/Deuterium Exchange to Dtudy Protein Folding and Protein-Protein Interactions by Mass Spectrometry. *Molecular & Cellular Proteomics*, **2011**.

102. Liuni, P.; Rob, T.; Wilson, D.J. A Microfluidic Reactor for Rapid, Low-Pressure Proteolysis with On-Chip Electrospray Ionization. *Rapid Communications in Mass Spectrometry*, **2010**, *24*, 315-320.

103. Landreh, M.; Astorga-Wells, J.; Johansson, J.; Bergman, T.; Jörnvall, H. New Developments in Protein Structure-Function Analysis by MS and Use of Hydrogen-Deuterium Exchange Microfluidics. *Febs Journal*, **2011**, *278*, 3815-3821.

104. Lam, T.T.; Lanman, J.K.; Emmett, M.R.; Hendrickson, C.L.; Marshall, A.G.; Prevelige, P.E. Mapping of Protein:Protein Contact Surfaces by Hydrogen/Deuterium Exchange, Followed by On-Line High-Performance Liquid Chromatography-Electrospray Ionization Fourier-Transform Ion-Cyclotron-Resonance Mass Analysis. *Journal of Chromatography A*, **2002**, *982*, 85-95.

105. Emmett, M.R.; Kazazic, S.; Marshall, A.G.; Chen, W.; Shi, S.D.H.; Bolaños, B.; Greig, M.J. Supercritical Fluid Chromatography Reduction of Hydrogen/Deuterium Back Exchange in Solution-Phase Hydrogen/Deuterium Exchange with Mass Spectrometric Analysis. *Analytical Chemistry*, **2006**, *78*, 7058-7060.

106. Zhang, H.-M.; Bou-Assaf, G.; Emmett, M.; Marshall, A. Fast Reversed-Phase Liquid Chromatography to Reduce Back Exchange and Increase Throughput in H/D Exchange Monitored by FT-ICR Mass Spectrometry. *Journal of The American Society for Mass Spectrometry*, **2009**, *20*, 520-524.

107. Wu, Y.; Engen, J.; Hobbins, W. Ultra Performance Liquid Chromatography (UPLC) Further Improves Hydrogen/Deuterium Exchange Mass Spectrometry. *Journal of The American Society for Mass Spectrometry*, **2006**, *17*, 163-167.

108. Chalmers, M.J.; Busby, S.A.; Pascal, B.D.; Southern, M.R.; Griffin, P.R. A Two-Stage Differential Hydrogen Deuterium Exchange Method for the Rapid Characterization of Protein/Ligand Interactions. *Journal of Biomolecular Techniques*, **2007**, *18*, 194-204.

109. Wales, T.E.; Fadgen, K.E.; Gerhardt, G.C.; Engen, J.R. High-Speed and High-Resolution UPLC Separation at Zero Degrees Celsius. *Analytical Chemistry*, **2008**, *80*, 6815-6820.

110. Houde, D.; Arndt, J.; Domeier, W.; Berkowitz, S.; Engen, J.R. Characterization of IgG1 Conformation and Conformational Dynamics by Hydrogen/Deuterium Exchange Mass Spectrometry. *Analytical Chemistry*, **2009**, *81*, 5966-5966.

111. Jørgensen, T.J.D.; Gårdsvoll, H.; Ploug, M.; Roepstorff, P. Intramolecular Migration of Amide Hydrogens in Protonated Peptides upon Collisional Activation. *Journal of the American Chemical Society*, **2005**, *127*, 2785-2793.

112. Abzalimov, R.R.; Kaltashov, I.A. Controlling Hydrogen Scrambling in Multiply Charged Protein Ions during Collisional Activation: Implications for Top-Down Hydrogen/Deuterium Exchange MS Utilizing Collisional Activation in the Gas Phase. *Analytical Chemistry*, **2010**, *82*, 942-950.

113. Rand, K.D.; Adams, C.M.; Zubarev, R.A.; Jørgensen, T.J.D. Electron Capture Dissociation Proceeds with a Low Degree of Intramolecular Migration of Peptide Amide Hydrogens. *Journal of the American Chemical Society*, **2008**, *130*, 1341-1349.

114. Abzalimov, R.R.; Kaplan, D.A.; Easterling, M.L.; Kaltashov, I.A. Protein Conformations Can Be Probed in Top-Down HDX MS Experiments Utilizing Electron Transfer Dissociation of Protein Ions Without Hydrogen Scrambling. *Journal of The American Society for Mass Spectrometry*, **2009**, *20*, 1514-1517.

115. Zehl, M.; Rand, K.D.; Jensen, O.N.; Jørgensen, T.J.D. Electron Transfer Dissociation Facilitates the Measurement of Deuterium Incorporation into Selectively Labeled Peptides with Single Residue Resolution. *Journal of the American Chemical Society*, **2008**, *130*, 17453-17459.

116. Rand, K.D.; Zehl, M.; Jensen, O.N.; Jørgensen, T.J.D. Protein Hydrogen Exchange Measured at Single-Residue Resolution by Electron Transfer Dissociation Mass Spectrometry. *Analytical Chemistry*, **2009**, *81*, 5577-5584.

117. Pan, J.; Han, J.; Borchers, C.H.; Konermann, L. Hydrogen/Deuterium Exchange Mass Spectrometry with Top-Down Electron Capture Dissociation for Characterizing Structural Transitions of a 17 kDa Protein. *Journal of the American Chemical Society*, **2009**, *131*, 12801-12808.

118. Pan, J.X.; Han, J.; Borchers, C.H.; Konermann, L. Characterizing Short-Lived Protein Folding Intermediates by Top-Down Hydrogen Exchange Mass Spectrometry. *Analytical Chemistry*, **2010**, *82*, 8591-8597.

119. Pan, J.; Han, J.; Borchers, C.H.; Konermann, L. Conformer-Specific Hydrogen Exchange Analysis of Aβ(1–42) Oligomers by Top-Down Electron Capture Dissociation Mass Spectrometry. *Analytical Chemistry*, **2011**, *83*, 5386-5393.

120. Ghaemmaghami, S.; Fitzgerald, M.C.; Oas, T.G. A Quantitative, High-Throughput Screen for Protein Stability. *Proceedings of the National Academy of Sciences*, **2000**, *97*, 8296-8301.

121. Fitzgerald, M.C.; Powell, K.D. Accuracy and Precision of a New H/D Exchange- and Mass Spectrometry-Based Technique for Measuring the Thermodynamic Properties of Protein-Peptide Complexes. *Biochemistry*, **2003**, *42*, 4962-4970.

122. Powell, K.D.; Ghaemmaghami, S.; Wang, M.Z.; Ma, L.; Oas, T.G.; Fitzgerald, M.C. A General Mass Spectrometry-Based Assay for the Quantitation of Protein−Ligand Binding Interactions in Solution. *Journal of the American Chemical Society*, **2002**, *124*, 10256-10257.

123. Tang, L.; Roulhac, P.L.; Fitzgerald, M.C. H/D Exchange and Mass Spectrometry-Based Method for Biophysical Analysis of Multidomain Proteins at the Domain Level. *Analytical Chemistry*, **2007**, *79*, 8728-8739.

124. Dearmond, P.D.; West, G.M.; Anbalagan, V.; Campa, M.J.; Patz, E.F.; Fitzgerald, M.C. Discovery of Novel Cyclophilin A Ligands Using an H/D Exchange- and Mass Spectrometry-Based Strategy. *Journal of Biomolecular Screening*, **2010**, *15*, 1051-1062.

125. Zhu, M.M.; Rempel, D.L.; Du, Z.; Gross, M.L. Quantification of Protein−Ligand Interactions by Mass Spectrometry, Titration, and H/D Exchange: PLIMSTEX. *Journal of the American Chemical Society*, **2003**, *125*, 5252-5253.

126. Zhu, M.; Rempel, D.; Gross, M. Modeling Sata from Titration, Amide H/D Exchange, and Mass Spectrometry to Obtain Protein-Ligand Binding Constants. *Journal of The American Society for Mass Spectrometry*, **2004**, *15*, 388-397.

127. Sperry, J.B.; Shi, X.; Rempel, D.L.; Nishimura, Y.; Akashi, S.; Gross, M.L. A Mass Spectrometric Approach to the Study of DNA-binding Proteins: Interaction of Human TRF2 with Telomeric DNA. *Biochemistry*, **2008**, *47*, 1797-1807.

128. Sperry, J.B.; Huang, R.Y.C.; Zhu, M.M.; Rempel, D.L.; Gross, M.L. Hydrophobic Peptides Affect Binding of Calmodulin and Ca^{2+} as Explored by H/D Amide Exchange and Mass Spectrometry. *International Journal of Mass Spectrometry*, **2011**, *302*, 85-92.

129. Huang, R.Y.C.; Rempel, D.L.; Gross, M.L. HD Exchange and PLIMSTEX Determine the Affinities and Order of Binding of Ca2+ with Troponin C. *Biochemistry*, **2011**, *50*, 5426-5435.

130. Ma, L.; Fitzgerald, M.C. A New H/D Exchange- and Mass Spectrometry-Based Method for Thermodynamic Analysis of Protein-DNA Interactions. *Chemistry & Biology*, **2003**, *10*, 1205-1213.

131. Xu, G.; Chance, M.R. Hydroxyl Radical-Mediated Modification of Proteins as Probes for Structural Proteomics. *Chemical Reviews*, **2007**, *107*, 3514-3543.

132. Sharp, J.S.; Becker, J.M.; Hettich, R.L. Protein Surface Mapping by Chemical Oxidation: Structural Analysis by Mass Spectrometry. *Analytical Biochemistry*, **2003**, *313*, 216-225.

133. Watson, C.; Janik, I.; Zhuang, T.; Charvátová, O.; Woods, R.J.; Sharp, J.S. Pulsed Electron Beam Water Radiolysis for Submicrosecond Hydroxyl Radical Protein Footprinting. *Analytical Chemistry*, **2009**, *81*, 2496-2505.

134. Xu, G.; Chance, M.R. Radiolytic Modification of Acidic Amino Acid Residues in Peptides: Probes for Examining Protein−Protein Interactions. *Analytical Chemistry*, **2004**, *76*, 1213-1221.

135. Kiselar, J.G.; Maleknia, S.D.; Sullivan, M.; Downard, K.M.; Chance, M.R. Hydroxyl Radical Probe of Protein Surfaces Using Synchrotron X-ray Radiolysis and Mass Spectrometry. *International Journal of Radiation Biology*, **2002**, *78*, 101-114.

136. Guan, J.-Q.; Vorobiev, S.; Almo, S.C.; Chance, M.R. Mapping the G-Actin Binding Surface of Cofilin Using Synchrotron Protein Footprinting. *Biochemistry*, **2002**, *41*, 5765-5775.

137. Tong, X.; Wren, J.C.; Konermann, L. Effects of Protein Concentration on the Extent of γ-Ray-Mediated Oxidative Labeling Studied by Electrospray Mass Spectrometry. *Analytical Chemistry*, **2007**, *79*, 6376-6382.

138. Ottinger, L.M.; Tullius, T.D. High-Resolution in Vivo Footprinting of a Protein−DNA Complex Using γ-Radiation. *Journal of the American Chemical Society*, **2000**, *122*, 5901-5902.

139. Xu, G.; Chance, M.R. Radiolytic Modification and Reactivity of Amino Acid Residues Serving as Structural Probes for Protein Footprinting. *Analytical Chemistry*, **2005**, *77*, 4549-4555.

140. Smedley, J.G.; Sharp, J.S.; Kuhn, J.F.; Tomer, K.B. Probing the pH-Dependent Prepore to Pore Transition of Bacillus anthracis Protective Antigen with Differential Oxidative Protein Footprinting. *Biochemistry*, **2008**, *47*, 10694-10704.

141. Takamoto, K.; Chance, M.R. Radiolytic Protein Footprinting with Mass Spectrometry to Probe the Structure of Macromolecular Complexes. *Annual Review of Biophysics and Biomolecular Structure*, **2006**, *35*, 251-276.

142. Sharp, J.S.; Becker, J.M.; Hettich, R.L. Analysis of Protein Solvent Accessible Surfaces by Photochemical Oxidation and Mass Spectrometry. *Analytical Chemistry*, **2004**, *76*, 672-683.

143. Aye, T.T.; Low, T.Y.; Sze, S.K. Nanosecond Laser-Induced Photochemical Oxidation Method for Protein Surface Mapping with Mass Spectrometry. *Analytical Chemistry*, **2005**, *77*, 5814-5822.

144. Hambly, D.; Gross, M. Laser Flash Photolysis of Hydrogen Peroxide to Oxidize Protein Solvent-Accessible Residues on the Microsecond Timescale. *Journal of The American Society for Mass Spectrometry*, **2005**, *16*, 2057-2063.

145. Gau, B.C.; Sharp, J.S.; Rempel, D.L.; Gross, M.L. Fast Photochemical Oxidation of Protein Footprints Faster than Protein Unfolding. *Analytical Chemistry*, **2009**, *81*, 6563-6571.

146. Gau, B.C.; Chen, H.; Zhang, Y.; Gross, M.L. Sulfate Radical Anion as a New Reagent for Fast Photochemical Oxidation of Proteins. *Analytical Chemistry*, **2010**, *82*, 7821-7827.

147. Nabuchi, Y.; Asoh, Y.; Takayama, M. Folding Analysis of Hormonal Polypeptide Calcitonins and the Oxidized Calcitonins Using Electrospray Ionization Mass Spectrometry Combined with H/D Exchange. *Journal of The American Society for Mass Spectrometry*, **2004**, *15*, 1556-1564.

148. Xu, G.; Kiselar, J.; He, Q.; Chance, M.R. Secondary Reactions and Strategies To Improve Quantitative Protein Footprinting. *Analytical Chemistry*, **2005**, *77*, 3029-3037.

149. Guan, J.-Q.; Chance, M.R. Structural Proteomics of Macromolecular Assemblies Using Oxidative Footprinting and Mass Spectrometry. *Trends in biochemical sciences*, **2005**, *30*, 583-592.

150. Buxton, G.V.; Greenstock, C.L.; Phillips Helman, W.; Ross, A.B. Critical Review of rate constants for reacitons of hydrated electrons. *Journal of Physical and Chemical Reference Data*, **1988**, *17*, 513-886.

151. Hawkins, C.L.; Davies, M.J. Generation and Propagation of Radical Reactions on Proteins. *Biochimica et Biophysica Acta - Bioenergetics*, **2001**, *1504*, 196-219.

152. Venkatesh, S.; Tomer, K.B.; Sharp, J.S. Rapid Identification of Oxidation-Induced Conformational Changes by Kinetic Analysis. *Rapid Communications in Mass Spectrometry*, **2007**, *21*, 3927-3936.

153. Wang, L.; Chance, M.R. Structural Mass Spectrometry of Proteins Using Hydroxyl Radical Based Protein Footprinting. *Analytical Chemistry*, **2011**, *83*, 7234-7241.

154. Kiselar, J.G.; Datt, M.; Chance, M.R.; Weiss, M.A. Structural Analysis of Proinsulin Hexamer Assembly by Hydroxyl Radical Footprinting and Computational Modeling. *Journal of Biological Chemistry*, **2011**, *286*, 43710-43716.

155. Yang, Y.; Hua, Q.-x.; Liu, J.; Shimizu, E.H.; Choquette, M.H.; Mackin, R.B.; Weiss, M.A. Solution Structure of Proinsulin. *Journal of Biological Chemistry*, **2010**, *285*, 7847-7851.

156. Hambly, D.; Gross, M. Laser Flash Photochemical Oxidation to Locate Heme Binding and Conformational Changes in Myoglobin. *International Journal of Mass Spectrometry*, **2007**, *259*, 124-129.

157. Zhang, H.; Gau, B.C.; Jones, L.M.; Vidavsky, I.; Gross, M.L. Fast Photochemical Oxidation of Proteins for Comparing Structures of Protein-Ligand Complexes: the Calmodulin-Peptide Model System. *Analytical Chemistry*, **2011**, *83*, 311-318.

158. Oztug Durer, Z.A.; Kamal, J.K.A.; Benchaar, S.; Chance, M.R.; Reisler, E. Myosin Binding Surface on Actin Probed by Hydroxyl Radical Footprinting and Site-Directed Labels. *Journal of Molecular Biology*, **2011**, *414*, 204-216.

159. Jones, L.M.; B. Sperry, J.; A. Carroll, J.; Gross, M.L. Fast Photochemical Oxidation of Proteins for Epitope Mapping. *Analytical Chemistry*, **2011**, *83*, 7657-7661.

160. Gau, B.; Garai, K.; Frieden, C.; Gross, M.L. Mass Spectrometry-Based Protein Footprinting Characterizes the Structures of Oligomeric Apolipoprotein E2, E3, and E4. *Biochemistry*, **2011**, *50*, 8117-8126.

161. Schorzman, A.N.; Perera, L.; Cutalo-Patterson, J.M.; Pedersen, L.C.; Pedersen, L.G.; Kunkel, T.A.; Tomer, K.B. Modeling of the DNA-binding site of yeast Pms1 by mass spectrometry. *DNA Repair*, **2011**, *10*, 454-465.

162. Stocks, B.B.; Konermann, L. Structural Characterization of Short-Lived Protein Unfolding Intermediates by Laser-Induced Oxidative Labeling and Mass Spectrometry. *Analytical Chemistry*, **2009**, *81*, 20-27.

163. Stocks, B.B.; Konermann, L. Time-Dependent Changes in Side-Chain Solvent Accessibility during Cytochrome c Folding Probed by Pulsed Oxidative Labeling and Mass Spectrometry. *Journal of Molecular Biology*, **2010**, *398*, 362-373.

164. Stocks, B.B.; Rezvanpour, A.; Shaw, G.S.; Konermann, L. Temporal Development of Protein Structure during S100A11 Folding and Dimerization Probed by Oxidative Labeling and Mass Spectrometry. *Journal of Molecular Biology*, **2011**, *409*, 669-679.

165. Chen, J.; Rempel, D.L.; Gross, M.L. Temperature Jump and Fast Photochemical Oxidation Probe Submillisecond Protein Folding. *Journal of the American Chemical Society*, **2010**, *132*, 15502-15504.

166. Pan, Y.; Konermann, L. Membrane Protein Structural Insights from Chemical Labeling and Mass Spectrometry. *Analyst*, **2010**, *135*.

167. Barrera, N.P.; Robinson, C.V. Advances in the Mass Spectrometry of Membrane Proteins: From Individual Proteins to Intact Complexes. *Annual Review of Biochemistry*, **2011**, *80*, 247-271.

168. Maleknia, S.D.; Brenowitz, M.; Chance, M.R. Millisecond Radiolytic Modification of Peptides by Synchrotron X-rays Identified by Mass Spectrometry. *Analytical Chemistry*, **1999**, *71*, 3965-3973.

169. Pan, Y.; Stocks, B.B.; Brown, L.; Konermann, L. Structural Characterization of an Integral Membrane Protein in Its Natural Lipid Environment by Oxidative Methionine Labeling and Mass Spectrometry. *Analytical Chemistry*, **2009**, *81*, 28-35.

170. Pan, Y.; Brown, L.; Konermann, L. Mapping the Structure of an Integral Membrane Protein under Semi-Denaturing Conditions by Laser-Induced Oxidative Labeling and Mass Spectrometry. *Journal of Molecular Biology*, **2009**, *394*, 968-981.

171. Pan, Y.; Brown, L.; Konermann, L. Site-Directed Mutagenesis Combined with Oxidative Methionine Labeling for Probing Structural Transitions of a Membrane Protein by Mass Spectrometry. *Journal of The American Society for Mass Spectrometry*, **2010**, *21*, 1947-1956.

172. Pan, Y.; Brown, L.; Konermann, L. Kinetic Folding Mechanism of an Integral Membrane Protein Examined by Pulsed Oxidative Labeling and Mass Spectrometry. *Journal of Molecular Biology*, **2011**, *410*, 146-158.

173. Gupta, S.; Bavro, V.N.; D'Mello, R.; Tucker, S.J.; Vénien-Bryan, C.; Chance, M.R. Conformational Changes During the Gating of a Potassium Channel Revealed by Structural Mass Spectrometry. *Structure*, **2010**, *18*, 839-846.

174. Sharp, J.S.; Sullivan, D.M.; Cavanagh, J.; Tomer, K.B. Measurement of Multisite Oxidation Kinetics Reveals an Active Site Conformational Change in Spo0F as a Result of Protein Oxidation†. *Biochemistry*, **2006**, *45*, 6260-6266.

175. Liu, J.; Konermann, L. Irreversible Thermal Denaturation of Cytochrome c Studied by Electrospray Mass Spectrometry. *Journal of The American Society for Mass Spectrometry*, **2009**, *20*, 819-828.

176. Saladino, J.; Liu, M.; Live, D.; Sharp, J.S. Aliphatic Peptidyl Hydroperoxides as a Source of Secondary Oxidation in Hydroxyl Radical Protein Footprinting. *Journal of The American Society for Mass Spectrometry*, **2009**, *20*, 1123-1126.

177. Jones, S.; van Heyningen, P.; Berman, H.M.; Thornton, J.M. Protein-DNA Interactions: A Structural Analysis. *Journal of Molecular Biology*, **1999**, *287*, 877-896.

178. Tsai, C.-J.; Lin, S.L.; Wolfson, H.J.; Nussinov, R. Studies of protein-protein interfaces: A statistical analysis of the hydrophobic effect. *Protein Science*, **1997**, *6*, 53-64.

179. Suckau, D.; Mak, M.; Przybylski, M. Protein Surface Topology-Probing by Selective Chemical Modification and Mass Spectrometric Peptide Mapping. *Proceedings of the National Academy of Sciences of the United States of America*, **1992**, *89*, 5630-5634.

180. Glocker, M.O.; Borchers, C.; Fiedler, W.; Suckau, D.; Przybylski, M. Molecular Characterization of Surface Topology in Protein Tertiary Structures by Amino-Acylation and Mass Spectrometric Peptide Mapping. *Bioconjugate Chemistry*, **1994**, *5*, 583-590.

181. Ehrhard, B.; Misselwitz, R.; Welfle, K.; Hausdorf, G.; Glaser, R.W.; Schneider-Mergener, J.; Welfle, H. Chemical Modification of Recombinant HIV-1 Capsid Protein p24 Leads to the Release of a Hidden Epitope Prior to Changes of the Overall Folding of the Protein. *Biochemistry*, **1996**, *35*, 9097-9105.

182. Przybylski, M.; Glocker, M.O.; Nestel, U.; Schnaible, V.; Bluggel, M.; Diederichs, K.; Weckesser, J.; Schad, M.; Schmid, A.; Welte, W.; Benz, R. X-ray Crystallographic and Mass Spectrometric Structure Determination and Functional Characterization of Succinylated Porin from Rhodobacter Capsulatus: Implications for Ion Selectivity and Single-Channel Conductance. *Protein Science*, **1996**, *5*, 1477-1489.

183. Glocker, M.O.; Bauer, S.H.; Kast, J.; Volz, J.; Przybylski, M. Characterization of Specific Noncovalent Protein Complexes by UV Matrix-Assisted Laser Desorption Ionization Mass Spectrometry. *Journal of Mass Spectrometry*, **1996**, *31*, 1221-1227.

184. Williams, J.; Tomer, K.; Hioe, C.; Zolla-Pazner, S.; Norris, P. The Antigenic Determinants on HIV p24 for CD4+ T Cell Inhibiting Antibodies as Determined by Limited Proteolysis, Chemical Modification, and Mass Spectrometry. *Journal of The American Society for Mass Spectrometry*, **2006**, *17*, 1560-1569.

185. Giovanni, R.; Anna Maria, S.; Simona, A.; Chiara, D.; Ambrosio; Andrea, S. Mass Spectrometry-Based Approaches for Structural Studies on Protein Complexes at Low-Resolution. *Current Proteomics*, **2007**, *4*, 1-16.

186. Zappacosta, F.; Ingallinella, P.; Scaloni, A.; Pessi, A.; Bianchi, E.; Sollazzo, M.; Tramontano, A.; Marino, G.; Pucci, P. Surface Topology of Minibody by Selective Chemical Modifications and Mass Spectrometry. *Protein Science*, **1997**, *6*, 1901-1909.

187. Vachet, R.W.; Mendoza, V.L. Probing Protein Structure by Amino Acid-Specific Covalent Labeling and Mass Spectrometry. *Mass Spectrometry Reviews*, **2009**, *28*, 785-815.

188. Hager-Braun, C.; Hochleitner, E.; Gorny, M.; Zolla-Pazner, S.; Bienstock, R.; Tomer, K. Characterization of a Discontinuous Epitope of the HIV Envelope Protein gp120 Recognized by a Human Monoclonal Antibody Using Chemical Modification and Mass Spectrometric Analysis. *Journal of The American Society for Mass Spectrometry*, **2010**, *21*, 1687-1698.

189. Hochleitner, E.O.; Borchers, C.; Parker, C.; Bienstock, R.J.; Tomer, K.B. Characterization of a Discontinuous Epitope of the Human Immunodeficiency Virus (HIV) Core Protein p24 by Epitope Excision and Differential Chemical Modification Followed by Mass Spectrometric Peptide Mapping Analysis. *Protein Science*, **2000**, *9*, 487-496.

190. Scholten, A.; Visser, N.; van den Heuvel, R.; Heck, A. Analysis of Protein-Protein Interaction Surfaces Using a Combination of Efficient Lysine Acetylation and NanoLC-MALDI-MS/MS Applied to the E9:Im9 Bacteriotoxin-Immunity Protein Complex. *Journal of The American Society for Mass Spectrometry*, **2006**, *17*, 983-994.

191. McKee, C.J.; Kessl, J.J.; Norris, J.O.; Shkriabai, N.; Kvaratskhelia, M. Mass Spectrometry-Based Footprinting of Protein–Protein Interactions. *Methods*, **2009**, *47*, 304-307.

192. Knock, S.L.; Miller, B.T.; Blankenship, J.E.; Nagle, G.T.; Smith, J.S.; Kurosky, A. N-Acylation of Aplysia Egg-Laying Hormone with Biotin. Characterization of Bioactive and Inactive Derivatives. *Journal of Biological Chemistry*, **1991**, *266*, 24413-24419.

193. Shell, S.M.; Hess, S.; Kvaratskhelia, M.; Zou, Y. Mass Spectrometric Identification of Lysines Involved in the Interaction of Human Replication Protein A with Single-Stranded DNA. *Biochemistry*, **2004**, *44*, 971-978.

194. Kvaratskhelia, M.; Miller, J.T.; Budihas, S.R.; Pannell, L.K.; Grice, S.F.J.L. Identification of Specific HIV-1 Reverse Transcriptase Contacts to the Viral RNA:tRNA Complex by Mass Spectrometry and a Primary Amine Selective Reagent. *Proceedings of the National Academy of Sciences of the United States of America*, **2002**, *99*, 15988-15993.

195. Carven, G.J.; Stern, L.J. Probing the Ligand-Induced Conformational Change in HLA-DR1 by Selective Chemical Modification and Mass Spectrometric Mapping†. *Biochemistry*, **2005**, *44*, 13625-13637.

196. Lehman, J.A.; Hoelz, D.J.; Turchi, J.J. DNA-Dependent Conformational Changes in the Ku Heterodimer. *Biochemistry*, **2008**, *47*, 4359-4368.

197. Sharp, J.S.; Nelson, S.; Brown, D.; Tomer, K.B. Structural Characterization of the E2 Glycoprotein from Sindbis by Lysine Biotinylation and LC-MS/MS. *Virology*, **2006**, *348*, 216-223.

198. Azim-Zadeh, O.; Hillebrecht, A.; Linne, U.; Marahiel, M.A.; Klebe, G.; Lingelbach, K.; Nyalwidhe, J. Use of Biotin Derivatives to Probe Conformational Changes in Proteins. *Journal of Biological Chemistry*, **2007**, *282*, 21609-21617.

199. Blodgett, D.M.; De Zutter, J.K.; Levine, K.B.; Karim, P.; Carruthers, A. Structural Basis of GLUT1 Inhibition by Cytoplasmic ATP. *The Journal of General Physiology*, **2007**, *130*, 157-168.

200. Gabant, G.; Augier, J.; Armengaud, J. Assessment of Solvent Residues Accessibility Using Three Sulfo-NHS-Biotin Reagents in Parallel: Application to Footprint Changes of a Methyltransferase upon Binding its Substrate. *Journal of Mass Spectrometry*, **2008**, *43*, 360-370.

201. Wang, X.; Kim, S.-H.; Ablonczy, Z.; Crouch, R.K.; Knapp, D.R. Probing Rhodopsin−Transducin Interactions by Surface Modification and Mass Spectrometry. *Biochemistry*, **2004**, *43*, 11153-11162.

202. Novak, P.; Kruppa, G.H.; Young, M.M.; Schoeniger, J. A Top-Down Method for the Determination of Residue-Specific Solvent Accessibility in Proteins. *Journal of Mass Spectrometry*, **2004**, *39*, 322-328.

203. Nuss, J.E.; Sweeney, D.J.; Alter, G.M. Reactivity-Based Analysis of Domain Structures in Native Replication Protein A. *Biochemistry*, **2006**, *45*, 9804-9818.

204. Mendoza, V.L.; Antwi, K.; Baron-Rodriguez, M.A.; Blanco, C.; Vachet, R.W. Structure of the Preamyloid Dimer of β-2-Microglobulin from Covalent Labeling and Mass Spectrometry. *Biochemistry*, **2010**, *49*, 1522-1532.

205. Mendoza, V.L.; Barón-Rodríguez, M.A.; Blanco, C.; Vachet, R.W. Structural Insights into the Pre-Amyloid Tetramer of β-2-Microglobulin from Covalent Labeling and Mass Spectrometry. *Biochemistry*, **2011**, *50*, 6711-6722.

206. Thumm, M.; Hoenes, J.; Pfleiderer, G. S-methylthioacetimidate is a New Reagent for the Amidination of Proteins at Low pH. *Biochimica et Biophysica Acta - General Subjects*, **1987**, *923*, 263-267.

207. Beardsley, R.L.; Reilly, J.P. Quantitation Using Enhanced Signal Tags: A Technique for Comparative Proteomics. *Journal of Proteome Research*, **2002**, *2*, 15-21.

208. Janecki, D.J.; Beardsley, R.L.; Reilly, J.P. Probing Protein Tertiary Structure with Amidination. *Analytical Chemistry*, **2005**, *77*, 7274-7281.

209. Liu, X.; Broshears, W.C.; Reilly, J.P. Probing the Structure and Activity of Trypsin with Amidination. *Analytical Biochemistry*, **2007**, *367*, 13-19.

210. Beardsley, R.L.; Running, W.E.; Reilly, J.P. Probing the Structure of the Caulobacter crescentus Ribosome with Chemical Labeling and Mass Spectrometry. *Journal of Proteome Research*, **2006**, *5*, 2935-2946.

211. Fitzgerald, M.C.; Xu, Y.; Falk, I.N.; Hallen, M.A. Mass Spectrometry- and Lysine Amidination-Based Protocol for Thermodynamic Analysis of Protein Folding and Ligand Binding Interactions. *Analytical Chemistry*, **2011**, *83*, 3555-3562.

212. Bogan, A.A.; Thorn, K.S. Anatomy of hot spots in protein interfaces. *Journal of Molecular Biology*, **1998**, *280*, 1-9.

213. Riordan, J.F. Arginyl residues and anion binding sites in proteins. *Molecular and Cellular Biochemistry*, **1979**, *26*, 71-92.

214. Akinsiku, O.T.; Yu, E.T.; Fabris, D. Mass spectrometric investigation of protein alkylation by the RNA footprinting probe kethoxal. *Journal of Mass Spectrometry*, **2005**, *40*, 1372-1381.

215. Leitner, A.; Amon, S.; Rizzi, A.; Lindner, W. Use of the arginine-specific butanedione/phenylboronic acid tag for analysis of peptides and protein digests using matrix-assisted laser desorption/ionization mass spectrometry. *Rapid Communications in Mass Spectrometry*, **2007**, *21*, 1321-1330.

216. Riordan, J.F. Functional arginyl residues in carboxypeptidase A. Modification with butanedione. *Biochemistry*, **1973**, *12*, 3915-3923.

217. Leitner, A.; Lindner, W. Functional Probing of Arginine Residues in Proteins Using Mass Spectrometry and an Arginine-Specific Covalent Tagging Concept. *Analytical Chemistry*, **2005**, *77*, 4481-4488.

218. Liu, Y.; Kvaratskhelia, M.; Hess, S.; Qu, Y.; Zou, Y. Modulation of Replication Protein A Function by Its Hyperphosphorylation-induced Conformational Change Involving DNA Binding Domain B. *Journal of Biological Chemistry*, **2005**, *280*, 32775-32783.

219. Gao, Y.; Wang, Y. Site-Selective Modifications of Arginine Residues in Human Hemoglobin Induced by Methylglyoxal. *Biochemistry*, **2006**, *45*, 15654-15660.

220. Zhang, L.; Lilyestrom, W.; Li, C.; Scherer, T.; van Reis, R.; Zhang, B. Revealing a Positive Charge Patch on a Recombinant Monoclonal Antibody by Chemical Labeling and Mass Spectrometry. *Analytical Chemistry*, **2011**, *83*, 8501-8508.

221. Krell, T.; Pitt, A.R.; Coggins, J.R. The use of electrospray mass spectrometry to identify an essential arginine residue in type II dehydroquinases. *Febs Letters*, **1995**, *360*, 93-96.

222. Wood, T.D.; Guan, Z.; Borders, C.L.; Chen, L.H.; Kenyon, G.L.; McLafferty, F.W. Creatine kinase: Essential arginine residues at the nucleotide binding site identified by

chemical modification and high-resolution tandem mass spectrometry. *Proceedings of the National Academy of Sciences*, **1998**, *95*, 3362-3365.

223. Schepens, I.; Ruelland, E.; Miginiac-Maslow, M.; Le Maréchal, P.; Decottignies, P. The Role of Active Site Arginines of Sorghum NADP-Malate Dehydrogenase in Thioredoxin-dependent Activation and Activity. *Journal of Biological Chemistry*, **2000**, *275*, 35792-35798.

224. Wu, X.; Chen, S.G.; Petrash, J.M.; Monnier, V.M. Alteration of Substrate Selectivity through Mutation of Two Arginine Residues in the Binding Site of Amadoriase II from Aspergillus sp. *Biochemistry*, **2002**, *41*, 4453-4458.

225. Calvete, J.J.; Campanero-Rhodes, M.A.; Raida, M.; Sanz, L. Characterisation of the conformational and quaternary structure-dependent heparin-binding region of bovine seminal plasma protein PDC-109. *Febs Letters*, **1999**, *444*, 260-264.

226. Carven, G.J.; Stern, L.J. Probing the Ligand-Induced Conformational Change in HLA-DR1 by Selective Chemical Modification and Mass Spectrometric Mapping. *Biochemistry*, **2005**, *44*, 13625-13637.

227. Fiedler, W.; Borchers, C.; Macht, M.; Deininger, S.-O.; Przybylski, M. Molecular Characterization of a Conformational Epitope of Hen Egg White Lysozyme by Differential Chemical Modification of Immune Complexes and Mass Spectrometric Peptide Mapping. *Bioconjugate Chemistry*, **1998**, *9*, 236-241.

228. Hager-Braun, C.; Tomer, K.B. Characterization of the Tertiary Structure of Soluble CD4 Bound to Glycosylated Full-Length HIVgp120 by Chemical Modification of Arginine Residues and Mass Spectrometric Analysis. *Biochemistry*, **2002**, *41*, 1759-1766.

229. Iacob, R.E.; Keck, Z.; Olson, O.; Foung, S.K.H.; Tomer, K.B. Structural elucidation of critical residues involved in binding of human monoclonal antibodies to hepatitis C virus E2 envelope glycoprotein. *Biochimica et Biophysica Acta - Proteins & Proteomics*, **2008**, *1784*, 530-542.

230. Edith Wilson, M.; Hirs, C.H.W.; Serge, N.T. Modification of Histidyl Residues in Proteins by Diethylpyrocarbonate. *Methods in Enzymology*, **1977**, *Volume 47*, 431-442.

231. Melchior, W.B.; Fahrney, D. Ethoxyformylation of Proteins. Reaction of Ethoxyformic Anhydride with α-chymotrypsin, Pepsin, and Pancreatic Ribonuclease at pH 4. *Biochemistry*, **1970**, *9*, 251-258.

232. Kalkum, M.; Przybylski, M.; Glocker, M.O. Structure Characterization of Functional Histidine Residues and Carbethoxylated Derivatives in Peptides and Proteins by Mass Spectrometry. *Bioconjugate Chemistry*, **1998**, *9*, 226-235.

233. Mendoza, V.L.; Vachet, R.W. Protein Surface Mapping Using Diethylpyrocarbonate with Mass Spectrometric Detection. *Analytical Chemistry*, **2008**, *80*, 2895-2904.

234. Glocker, M.O.; Kalkum, M.; Yamamoto, R.; Schreurs, J. Selective Biochemical Modification of Functional Residues in Recombinant Human Macrophage Colony-Stimulating Factor β (rhM-CSF β): Identification by Mass Spectrometry. *Biochemistry*, **1996**, *35*, 14625-14633.

235. Hnízda, A.; Šantrůček, J.; Šanda, M.; Strohalm, M.; Kodíček, M. Reactivity of Histidine and Lysine Side-Chains with Diethylpyrocarbonate - A Method to Identify Surface Exposed Residues in Proteins. *Journal of Biochemical and Biophysical Methods*, **2008**, *70*, 1091-1097.

236. Dage, J.L.; Sun, H.; Halsall, H.B. Determination of Diethylpyrocarbonate-Modified Amino Acid Residues in α1-Acid Glycoprotein by High-Performance Liquid Chromatography Electrospray Ionization–Mass Spectrometry and Matrix-Assisted Laser Desorption/Ionization Time-of-Flight–Mass Spectrometry. *Analytical Biochemistry*, **1998**, *257*, 176-185.

237. Hobbs, C.A.; Deterding, L.J.; Perera, L.; Bobay, B.G.; Thompson, R.J.; Darden, T.A.; Cavanagh, J.; Tomer, K.B. Structural Characterization of the Conformational Change in Calbindin-D28k upon Calcium Binding Using Differential Surface Modification Analyzed by Mass Spectrometry. *Biochemistry*, **2009**, *48*, 8603-8614.

238. Srikanth, R.; Mendoza, V.L.; Bridgewater, J.D.; Zhang, G.; Vachet, R.W. Copper Binding to β-2-Microglobulin and Its Pre-Amyloid Oligomers. *Biochemistry*, **2009**, *48*, 9871-9881.

239. Qin, K.; Yang, Y.; Mastrangelo, P.; Westaway, D. Mapping Cu(II) Binding Sites in Prion Proteins by Diethyl Pyrocarbonate Modification and Matrix-assisted Laser Desorption Ionization-Time of Flight (MALDI-TOF) Mass Spectrometric Footprinting. *Journal of Biological Chemistry*, **2002**, *277*, 1981-1990.

240. Carraway, K.L.; Koshland Jr, D.E.; Hirs, C.H.W.; Timasheff, S.N. Carbodiimide Modification of Proteins. *Methods in Enzymology*, **1972**, *Volume 25*, 616-623.

241. Akashi, S.; Shirouzu, M.; Terada, T.; Ito, Y.; Yokoyama, S.; Takio, K. Characterization of the Structural Difference between Active and Inactive Forms of the Ras Protein by Chemical Modification Followed by Mass Spectrometric Peptide Mapping. *Analytical Biochemistry*, **1997**, *248*, 15-25.

242. Izumi, S.; Kaneko, H.; Yamazaki, T.; Hirata, T.; Kominami, S. Membrane Topology of Guinea Pig Cytochrome P450 17α Revealed by a Combination of Chemical Modifications and Mass Spectrometry. *Biochemistry*, **2003**, *42*, 14663-14669.

243. Sanderson, R.J.; Mosbaugh, D.W. Identification of Specific Carboxyl Groups on Uracil-DNA Glycosylase Inhibitor Protein That Are Required for Activity. *Journal of Biological Chemistry*, **1996**, *271*, 29170-29181.

244. Zhang, H.; Shen, W.; Rempel, D.; Monsey, J.; Vidavsky, I.; Gross, M.L.; Bose, R. Carboxyl-Group Footprinting Maps the Dimerization Interface and Phosphorylation-induced Conformational Changes of a Membrane-associated Tyrosine Kinase. *Molecular & Cellular Proteomics*, **2011**, *10*.

245. Britto, P.J.; Knipling, L.; Wolff, J. The Local Electrostatic Environment Determines Cysteine Reactivity of Tubulin. *Journal of Biological Chemistry*, **2002**, *277*, 29018-29027.

246. Yem, A.W.; Epps, D.E.; Mathews, W.R.; Guido, D.M.; Richard, K.A.; Staite, N.D.; Deibel, M.R. Site-Specific Chemical Modification of Interleukin-1 β by Acrylodan at Cysteine 8 and Lysine 103. *Journal of Biological Chemistry*, **1992**, *267*, 3122-3128.

247. Lapko, V.N.; Jiang, X.-Y.; Smith, D.L.; Song, P.-S. Surface Topography of Phytochrome A Deduced from Specific Chemical Modification with Iodoacetamide. *Biochemistry*, **1998**, *37*, 12526-12535.

248. Apuy, J.L.; Park, Z.-Y.; Swartz, P.D.; Dangott, L.J.; Russell, D.H.; Baldwin, T.O. Pulsed-Alkylation Mass Spectrometry for the Study of Protein Folding and Dynamics: Development and Application to the Study of a Folding/Unfolding Intermediate of Bacterial Luciferase. *Biochemistry*, **2001**, *40*, 15153-15163.

249. Kehoe, J.J.; Brodkorb, A.; Mollé, D.; Yokoyama, E.; Famelart, M.-H.; Bouhallab, S.; Morris, E.R.; Croguennec, T. Determination of Exposed Sulfhydryl Groups in Heated β-Lactoglobulin A Using IAEDANS and Mass Spectrometry. *Journal of Agricultural and Food Chemistry*, **2007**, *55*, 7107-7113.

250. Su, D.; Delaplane, S.; Luo, M.; Rempel, D.L.; Vu, B.; Kelley, M.R.; Gross, M.L.; Georgiadis, M.M. Interactions of Apurinic/Apyrimidinic Endonuclease with a Redox Inhibitor: Evidence for an Alternate Conformation of the Enzyme. *Biochemistry*, **2011**, *50*, 82-92.

251. Macpherson, L.J.; Dubin, A.E.; Evans, M.J.; Marr, F.; Schultz, P.G.; Cravatt, B.F.; Patapoutian, A. Noxious Compounds Activate TRPA1 Ion Channels Through Covalent Modification of Cysteines. *Nature*, **2007**, *445*, 541-545.

252. Bauer, P.J.; Krause, E. Accessibility of Cysteines in the Native Bovine Rod cGMP-Gated Channel. *Biochemistry*, **2005**, *44*, 1624-1634.

253. Apuy, J.L.; Chen, X.; Russell, D.H.; Baldwin, T.O.; Giedroc, D.P. Ratiometric Pulsed Alkylation/Mass Spectrometry of the Cysteine Pairs in Individual Zinc Fingers of MRE-

Binding Transcription Factor-1 (MTF-1) as a Probe of Zinc Chelate Stability. *Biochemistry*, **2001**, *40*, 15164-15175.

254. Krieger, C.C.; An, X.; Tang, H.-Y.; Mohandas, N.; Speicher, D.W.; Discher, D.E. Cysteine Shotgun-Mass Spectrometry (CS-MS) Reveals Dynamic Sequence of Protein Structure Changes within Mutant and Stressed Cells. *Proceedings of the National Academy of Sciences*, **2011**, *108*, 8269-8274.

255. Whitehurst, C.B.; Soderblom, E.J.; West, M.L.; Hernandez, R.; Goshe, M.B.; Brown, D.T. Location and Role of Free Cysteinyl Residues in the Sindbis Virus E1 and E2 Glycoproteins. *Journal of Virology*, **2007**, *81*, 6231-6240.

256. Yu, M.; Romer, K.A.; Nieland, T.J.F.; Xu, S.; Saenz-Vash, V.; Penman, M.; Yesilaltay, A.; Carr, S.A.; Krieger, M. Exoplasmic Cysteine Cys384 of the HDL Receptor SR-BI is Critical for Its Sensitivity to a Small-Molecule Inhibitor and Normal Lipid Transport Activity. *Proceedings of the National Academy of Sciences*, **2011**, *108*, 12243-12248.

257. Happersberger, H.P.; Przybylski, M.; Glocker, M.O. Selective Bridging of Bis-Cysteinyl Residues by Arsonous Acid Derivatives as an Approach to the Characterization of Protein Tertiary Structures and Folding Pathways by Mass Spectrometry. *Analytical Biochemistry*, **1998**, *264*, 237-250.

258. West, G.M.; Tang, L.; Fitzgerald, M.C. Thermodynamic Analysis of Protein Stability and Ligand Binding Using a Chemical Modification- and Mass Spectrometry-Based Strategy. *Analytical Chemistry*, **2008**, *80*, 4175-4185.

259. West, G.M.; Thompson, J.W.; Soderblom, E.J.; Dubois, L.G.; DeArmond, P.D.; Moseley, M.A.; Fitzgerald, M.C. Mass Spectrometry-Based Thermal Shift Assay for Protein−Ligand Binding Analysis. *Analytical Chemistry*, **2010**, *82*, 5573-5581.

260. West, G.M.; Tucker, C.L.; Xu, T.; Park, S.K.; Han, X.; Yates, J.R.; Fitzgerald, M.C. Quantitative Proteomics Approach for Identifying Protein–Drug Interactions in Complex Mixtures Using Protein Stability Measurements. *Proceedings of the National Academy of Sciences*, **2010**.

261. Froelich, J.M.; Kaplinghat, S.; Reid, G.E. Automated Neutral Loss and Data Dependent Energy Resolved "Pseudo MS^3" for the Targeted Identification, Characterization and Quantitative Analysis of Methionine-Containing Peptides. *European Journal of Mass Spectrometry*, **2008**, *14*, 219-229.

262. Reid, G.E.; Roberts, K.D.; Simpson, R.J.; O'Hair, R.A. Selective Identification and Quantitative Analysis of Methionine Containing Peptides by Charge Derivatization and Tandem Mass Spectrometry. *Journal of The American Society for Mass Spectrometry*, **2005**, *16*, 1131-1150.

263. Amunugama, M.; Roberts, K.D.; Reid, G.E. Mechanisms for the Selective Gas-Phase Fragmentation Reactions of Methionine Side Chain Fixed Charge Sulfonium Ion Containing Peptides. *Journal of The American Society for Mass Spectrometry*, **2006**, *17*, 1631-1642.

264. Sokolovsky, M.; Harell, D.; Riordan, J.F. Reaction of Tetranitromethane with Sulfhydryl Groups in Proteins. *Biochemistry*, **1969**, *8*, 4740-4745.

265. Houston, L.L.; Walsh, K.A. Transient Inactivation of Trypsin by Mild Acetylation with N-cetylimidazole. *Biochemistry*, **1970**, *9*, 156-166.

266. Koshland, M.E.; Englberger, F.M.; Erwin, M.J.; Gaddone, S.M. Modification of Amino Acid Residues in Anti-p-azobenzenearsonic Acid Antibody during Extensive Iodination. *Journal of Biological Chemistry*, **1963**, *238*, 1343-1348.

267. Lennon, C.W.; Cox, H.D.; Hennelly, S.P.; Chelmo, S.J.; McGuirl, M.A. Probing Structural Differences in Prion Protein Isoforms by Tyrosine Nitration. *Biochemistry*, **2007**, *46*, 4850-4860.

268. Šantrůček, J.; Strohalm, M.; Kadlčík, V.; Hynek, R.; Kodíček, M. Tyrosine Residues Modification Studied by MALDI-TOF Mass Spectrometry. *Biochemical and Biophysical Research Communications*, **2004**, *323*, 1151-1156.

269. Leite, J.F.; Cascio, M. Probing the Topology of the Glycine Receptor by Chemical Modification Coupled to Mass Spectrometry. *Biochemistry*, **2002**, *41*, 6140-6148.

270. Hobba, G.D.; Forbes, B.E.; Parkinson, E.J.; Francis, G.L.; Wallace, J.C. The Insulin-like Growth Factor (IGF) Binding Site of Bovine Insulin-like Growth Factor Binding Protein-2 (bIGFBP-2) Probed by Iodination. *Journal of Biological Chemistry*, **1996**, *271*, 30529-30536.

271. Horton, H.R.; Koshland, D.E. A Highly Reactive Colored Reagent with Selectivity for the Tryptophan Residue in Proteins. 2-Hydroxy-5-nitrobenzyl Bromide1. *Journal of the American Chemical Society*, **1965**, *87*, 1126-1132.

272. Spande, T.F.; Witkop, B.; Hirs, C.H.W. Determination of the Tryptophan Content of Proteins with N-bromosuccinimide. *Methods in Enzymology*, **1967**, *Volume 11*, 498-506.

273. Strohalm, M.; Šantrůček, J.; Hynek, R.; Kodíček, M. Analysis of Tryptophan Surface Accessibility in Proteins by MALDI-TOF Mass Spectrometry. *Biochemical and Biophysical Research Communications*, **2004**, *323*, 1134-1138.

274. Fears, K.P.; Sivaraman, B.; Powell, G.L.; Wu, Y.; Latour, R.A. Probing the Conformation and Orientation of Adsorbed Enzymes Using Side-Chain Modification. *Langmuir*, **2009**, *25*, 9319-9327.

275. Marie, G.; Serani, L.; Laprévote, O.; Cahuzac, B.; Guittet, E.; Felenbok, B. Differential Chemical Labeling of the AlcR DNA-Binding Domain from Aspergillas Nidulans Versus Its Complex with a 16-mer DNA Target: Identification of an Essential Tryptophan Involved in the Recognition and the Interaction with the Nucleic Acid. *Protein Science*, **2001**, *10*, 99-107.

276. Ladner, C.L.; Turner, R.J.; Edwards, R.A. Development of Indole Chemistry to Label Tryptophan Residues in Protein for Determination of Tryptophan Surface Accessibility. *Protein Science*, **2007**, *16*, 1204-1213.

277. Richards, F.M.; Lamed, R.; Wynn, R.; Patel, D.; Olack, G. Methylene as a Possible Universal Footprinting Reagent that will Include Hydrophobic Surface Areas: Overview and Feasibility: Properties of Diazirine as a Precursor. *Protein Science*, **2000**, *9*, 2506-2517.

278. Craig, P.O.; Ureta, D.B.; Delfino, J.M. Probing Protein Conformation with a Minimal Photochemical Reagent. *Protein Science*, **2002**, *11*, 1353-1366.

279. Craig, P.O.; Gómez, G.E.; Ureta, D.B.; Caramelo, J.J.; Delfino, J.M. Experimentally Approaching the Solvent-Accessible Surface Area of a Protein: Insights into the Acid Molten Globule of Bovine α-Lactalbumin. *Journal of Molecular Biology*, **2009**, *394*, 982-993.

280. Ureta, D.B.; Craig, P.O.; Gómez, G.E.; Delfino, J.M. Assessing Native and Non-native Conformational States of a Protein by Methylene Carbene Labeling: The Case of Bacillus licheniformis β-Lactamase. *Biochemistry*, **2007**, *46*, 14567-14577.

281. Turro, N.J.; Cha, Y.; Gould, I.R. Reactivity and Intersystem Crossing of Singlet Methylene in Solution. *Journal of the American Chemical Society*, **1987**, *109*, 2101-2107.

282. Gómez, G.; Mundo, M.; Craig, P.; Delfino, J. Probing Protein Surface with a Solvent Mimetic Carbene Coupled to Detection by Mass Spectrometry. *Journal of The American Society for Mass Spectrometry*, **2012**, *23*, 30-42.

283. Jumper, C.C.; Schriemer, D.C. Mass Spectrometry of Laser-Initiated Carbene Reactions for Protein Topographic Analysis. *Analytical Chemistry*, **2011**, *83*, 2913-2920.

284. Sinz, A. Chemical Cross-Linking and Mass Spectrometry to Map Three-Dimensional Protein Structures and Protein-Protein Interactions. *Mass Spectrometry Reviews*, **2006**, *25*, 663-682.

285. Schilling, B.; Row, R.H.; Gibson, B.W.; Guo, X.; Young, M.M. MS2Assign, Automated Assignment and Nomenclature of Tandem Mass Spectra of Chemically Crosslinked Peptides. *Journal of The American Society for Mass Spectrometry*, **2003**, *14*, 834-850.

286. Singh, P.; Panchaud, A.; Goodlett, D.R. Chemical Cross-Linking and Mass Spectrometry as a Low-Resolution Protein Structure Determination Technique. *Analytical Chemistry*, **2010**, *82*, 2636-2642.

287. Alley, S.C.; Ishmael, F.T.; Jones, A.D.; Benkovic, S.J. Mapping Protein−Protein Interactions in the Bacteriophage T4 DNA Polymerase Holoenzyme Using a Novel Trifunctional Photo-cross-linking and Affinity Reagent. *Journal of the American Chemical Society*, **2000**, *122*, 6126-6127.

288. Fujii, N.; Jacobsen, R.B.; Wood, N.L.; Schoeniger, J.S.; Guy, R.K. A Novel Protein Crosslinking Reagent for the Determination of Moderate Resolution Protein Structures by Mass Spectrometry (MS3-D). *Bioorganic & Medicinal Chemistry Letters*, **2004**, *14*, 427-429.

289. Chowdhury, S.M.; Du, X.; Tolić, N.; Wu, S.; Moore, R.J.; Mayer, M.U.; Smith, R.D.; Adkins, J.N. Identification of Cross-Linked Peptides after Click-Based Enrichment Using Sequential Collision-Induced Dissociation and Electron Transfer Dissociation Tandem Mass Spectrometry. *Analytical Chemistry*, **2009**, *81*, 5524-5532.

290. Muller, D.R.; Schindler, P.; Towbin, H.; Wirth, U.; Voshol, H.; Hoving, S.; Steinmetz, M.O. Isotope-Tagged Cross-Linking Reagents. A new Tool in Mass Spectrometric Protein Interaction Analysis. *Analytical Chemistry*, **2001**, *73*, 1927-1934.

291. Chen, X.; Chen, Y.H.; Anderson, V.E. Protein Cross-Links: Universal Isolation and Characterization by Isotopic Derivatization and Electrospray Ionization Mass Spectrometry. *Analytical Biochemistry*, **1999**, *273*, 192-203.

292. Petrotchenko, E.V.; Serpa, J.J.; Borchers, C.H. Use of a Combination of Isotopically Coded Cross-Linkers and Isotopically Coded N-Terminal Modification Reagents for Selective Identification of Inter-peptide Crosslinks. *Analytical Chemistry*, **2010**, *82*, 817-823.

293. Petritis, B.O.; Qian, W.J.; Camp, D.G., 2nd; Smith, R.D. A Simple Procedure for Effective Quenching of Trypsin Activity and Prevention of ^{18}O-Labeling Back-Exchange. *Journal of Proteome Research*, **2009**, *8*, 2157-2163.

294. Back, J.W.; Notenboom, V.; de Koning, L.J.; Muijsers, A.O.; Sixma, T.K.; de Koster, C.G.; de Jong, L. Identification of Cross-Linked Peptides for Protein Interaction Studies Using Mass Spectrometry and ^{18}O Labeling. *Analytical Chemistry*, **2002**, *74*, 4417-4422.

295. Bennett, K.L.; Kussmann, M.; Bjork, P.; Godzwon, M.; Mikkelsen, M.; Sorensen, P.; Roepstorff, P. Chemical Cross-Linking with Thiol-Cleavable Reagents Combined with Differential Mass Spectrometric Peptide Mapping - a Novel Approach to Assess Intermolecular Protein Contacts. *Protein Science*, **2000**, *9*, 1503-1518.

296. Petrotchenko, E.V.; Olkhovik, V.K.; Borchers, C.H. Isotopically Coded Cleavable Cross-Linker for Studying Protein-Protein Interaction and Protein Complexes. *Molecular & Cellular Proteomics*, **2005**, *4*, 1167-1179.

297. Petrotchenko, E.V.; Xiao, K.; Cable, J.; Chen, Y.; Dokholyan, N.V.; Borchers, C.H. BiPS, a Photocleavable, Isotopically Coded, Fluorescent Cross-linker for Structural Proteomics. *Molecular & Cellular Proteomics*, **2009**, *8*, 273-286.

298. Back, J.W.; Hartog, A.F.; Dekker, H.L.; Muijsers, A.O.; de Koning, L.J.; de Jong, L. A New Crosslinker for Mass Spectrometric Analysis of the Quaternary Structure of Protein Complexes. *Journal of The American Society for Mass Spectrometry*, **2001**, *12*, 222-227.

299. Tang, X.; Munske, G.R.; Siems, W.F.; Bruce, J.E. Mass Spectrometry Identifiable Cross-Linking Strategy for Studying Protein−Protein Interactions. *Analytical Chemistry*, **2005**, *77*, 311-318.

300. Soderblom, E.J.; Goshe, M.B. Collision-Induced Dissociative Chemical Cross-Linking Reagents and Methodology: Applications to Protein Structural Characterization Using Tandem Mass Spectrometry Analysis. *Analytical Chemistry*, **2006**, *78*, 8059-8068.

301. Dreiocker, F.; Müller, M.Q.; Sinz, A.; Schäfer, M. Collision-Induced Dissociative Chemical Cross-Linking Reagent for Protein Structure Characterization: Applied Edman Chemistry in the Gas Phase. *Journal of Mass Spectrometry*, **2010**, *45*, 178-189.

302. Muller, M.Q.; Dreiocker, F.; Ihling, C.H.; Schafer, M.; Sinz, A. Fragmentation Behavior of a Thiourea-Based Reagent for Protein Structure Analysis by Collision-Induced Dissociative Chemical Cross-Linking. *Journal of Mass Spectrometry*, **2010**, *45*, 880-891.

303. Muller, M.Q.; Dreiocker, F.; Ihling, C.H.; Schafer, M.; Sinz, A. Cleavable Cross-Linker for Protein Structure Analysis: Reliable Identification of Cross-Linking Products by Tandem MS. *Analytical Chemistry*, **2010**, *82*, 6958-6968.

304. Clifford-Nunn, B.; Showalter, H.D.; Andrews, P.C. Quaternary Diamines as Mass Spectrometry Cleavable Crosslinkers for Protein Interactions. *Journal of The American Society for Mass Spectrometry*, **2012**, *23*, 201-212.

305. Paizs, B.; Suhai, S. Fragmentation Pathways of Protonated Peptides. *Mass Spectrometry Reviews*, **2005**, *24*, 508-548.

306. Lu, Y.; Tanasova, M.; Borhan, B.; Reid, G.E. Ionic Reagent for Controlling the Gas-Phase Fragmentation Reactions of Cross-Linked Peptides. *Analytical Chemistry*, **2008**, *80*, 9279-9287.

307. Schulze, W.X.; Usadel, B. Quantitation in Mass-Spectrometry-Based Proteomics. *Annual Review of Plant Biology*, **2010**, *61*, 491-516.

308. Bondarenko, P.V.; Chelius, D.; Shaler, T.A. Identification and Relative Quantitation of Protein Mixtures by Enzymatic Digestion Followed by Capillary Reversed-Phase Liquid Chromatography-Tandem Mass Spectrometry. *Analytical Chemistry*, **2002**, *74*, 4741-4749.

309. Wang, W.; Zhou, H.; Lin, H.; Roy, S.; Shaler, T.A.; Hill, L.R.; Norton, S.; Kumar, P.; Anderle, M.; Becker, C.H. Quantification of proteins and metabolites by mass spectrometry without isotopic labeling or spiked standards. *Analytical Chemistry*, **2003**, *75*, 4818-4826.

310. Gao, J.; Opiteck, G.J.; Friedrichs, M.S.; Dongre, A.R.; Hefta, S.A. Changes in the Protein Expression of Yeast as a Function of Carbon Source. *Journal of Proteome Research*, **2003**, *2*, 643-649.

311. Asara, J.M.; Christofk, H.R.; Freimark, L.M.; Cantley, L.C. A Label-Free Quantification Method by MS/MS TIC Compared to SILAC and Spectral Counting in a Proteomics Screen. *Proteomics*, **2008**, *8*, 994-999.

312. Ong, S.E.; Mann, M. Mass Spectrometry-Based Proteomics Turns Quantitative. *Nature Chemical Biology*, **2005**, *1*, 252-262.

313. Gygi, S.P.; Rist, B.; Gerber, S.A.; Turecek, F.; Gelb, M.H.; Aebersold, R. Quantitative Analysis of Complex Protein Mixtures Using Isotope-Coded Affinity Tags. *Nature Biotechnology*, **1999**, *17*, 994-999.

314. Hansen, K.C.; Schmitt-Ulms, G.; Chalkley, R.J.; Hirsch, J.; Baldwin, M.A.; Burlingame, A.L. Mass Spectrometric Analysis of Protein Mixtures at Low Levels Using Cleavable ^{13}C-Isotope-Coded Affinity Tag and Multidimensional Chromatography. *Molecular & Cellular Proteomics*, **2003**, *2*, 299-314.

315. Boersema, P.J.; Raijmakers, R.; Lemeer, S.; Mohammed, S.; Heck, A.J.R. Multiplex Peptide Stable Isotope Dimethyl Labeling for Quantitative Proteomics. *Nature Protocols*, **2009**, *4*, 484-494.

316. Hsu, J.-L.; Huang, S.-Y.; Chow, N.-H.; Chen, S.-H. Stable-Isotope Dimethyl Labeling for Quantitative Proteomics. *Analytical Chemistry*, **2003**, *75*, 6843-6852.

317. Boersema, P.J.; Aye, T.T.; van Veen, T.A.B.; Heck, A.J.R.; Mohammed, S. Triplex Protein Quantification Based on Stable Isotope Labeling by Peptide Dimethylation Applied to Cell and Tissue Lysates. *Proteomics*, **2008**, *8*, 4624-4632.

318. Ross, P.L.; Huang, Y.N.; Marchese, J.N.; Williamson, B.; Parker, K.; Hattan, S.; Khainovski, N.; Pillai, S.; Dey, S.; Daniels, S.; Purkayastha, S.; Juhasz, P.; Martin, S.; Bartlet-Jones, M.; He, F.; Jacobson, A.; Pappin, D.J. Multiplexed Protein Quantitation in Saccharomyces Cerevisiae Using Amine-Reactive Isobaric Tagging Reagents. *Molecular & Cellular Proteomics*, **2004**, *3*, 1154-1169.

319. Choe, L.; D'Ascenzo, M.; Relkin, N.R.; Pappin, D.; Ross, P.; Williamson, B.; Guertin, S.; Pribil, P.; Lee, K.H. 8-Plex Quantitation of Changes in Cerebrospinal Fluid Protein Expression in Subjects Undergoing Intravenous Immunoglobulin Treatment for Alzheimer's Disease. *Proteomics*, **2007**, *7*, 3651-3660.

320. Thompson, A.; Schäfer, J.; Kuhn, K.; Kienle, S.; Schwarz, J.; Schmidt, G.; Neumann, T.; Hamon, C. Tandem Mass Tags: A Novel Quantification Strategy for Comparative Analysis of Complex Protein Mixtures by MS/MS. *Analytical Chemistry*, **2003**, *75*, 1895-1904.

321. Dayon, L.; Hainard, A.; Licker, V.; Turck, N.; Kuhn, K.; Hochstrasser, D.F.; Burkhard, P.R.; Sanchez, J.-C. Relative Quantification of Proteins in Human Cerebrospinal Fluids by MS/MS Using 6-Plex Isobaric Tags. *Analytical Chemistry*, **2008**, *80*, 2921-2931.

322. Li, S.; Zeng, D. CILAT - A New Reagent for Quantitative Proteomics. *Chemical Communications*, **2007**.

323. Lu, Y.; Zhou, X.; Stemmer, P.; Reid, G. Sulfonium Ion Derivatization, Isobaric Stable Isotope Labeling and Data Dependent CID- and ETD-MS/MS for Enhanced Phosphopeptide Quantitation, Identification and Phosphorylation Site Characterization. *Journal of The American Society for Mass Spectrometry*, **2012**, *23*, 577-593.

324. Sierakowski, J.; Amunugama, M.; Roberts, K.D.; Reid, G.E. Substituent Effects on the Gas-Phase Fragmentation Reactions of Sulfonium Ion Containing Peptides. *Rapid Communications in Mass Spectrometry*, **2007**, *21*, 1230-1238.

325. Roberts, K.D.; Reid, G.E. Leaving Group Effects on the Selectivity of the Gas-Phase Fragmentation Reactions of Side Chain Fixed-Charge-Containing Peptide Ions. *Journal of Mass Spectrometry*, **2007**, *42*, 187-198.

326. Kalkhof, S.; Sinz, A. Chances and Pitfalls of Chemical Cross-Linking with Amine-Reactive N-Hydroxysuccinimide Esters. *Analytical and Bioanalytical Chemistry*, **2008**, *392*, 305-312.

327. Lu, Y., *Ionic Cross-Linking Reagents and Tandem Mass Spectrometry for Mapping Structures of Proteins and Protein Complexes*, in *Master's thesis submitted to Michigan State University*. 2008.

328. Leavell, M.D.; Novak, P.; Behrens, C.R.; Schoeniger, J.S.; Kruppa, G.H. Strategy for Selective Chemical Cross-Linking of Tyrosine and Lysine Residues. *Journal of The American Society for Mass Spectrometry*, **2004**, *15*, 1604-1611.

329. Fraczkiewicz, R.; Braun, W. Exact and Efficient Analytical Calculation of the Accessible Surface Areas and Their Gradients for Macromolecules. *Journal of Computational Chemistry*, **1998**, *19*, 319-333.

330. Wang, L.C.; Li, Y.; Abildgaard, F.; Markley, J.L.; Yan, H.G. NMR Solution Structure of Type II Human Cellular Retinoic Acid Binding Protein: Implications for Ligand Binding. *Biochemistry*, **1998**, *37*, 12727-12736.

331. Williams, K.A.; Doi, J.T.; Musker, W.K. Neighboring-Group Participation in Organic Redox Reactions .10. The Kinetic and Mechanistic Effects of Imidazole and Benzimidazole Nitrogen on Thioether Oxidations. *Journal of Organic Chemistry*, **1985**, *50*, 4-10.

332. Jessing, M.; Brandt, M.; Jensen, K.J.; Christensen, J.B.; Boas, U. Thiophene Backbone Amide Linkers, a New Class of Easily Prepared and Highly Acid-Labile Linkers for Solid-Phase Synthesis†. *The Journal of Organic Chemistry*, **2006**, *71*, 6734-6741.

333. Crouch, N.P.; Adlington, R.M.; Baldwin, J.E.; Lee, M.H.; MacKinnon, C.H. A Mechanistic Rationalisation for the Substrate Specificity of Recombinant Mammalian 4-Hydroxyphenylpyruvate Dioxygenase (4-HPPD). *Tetrahedron*, **1997**, *53*, 6993-7010.

334. Frisch, M.J.T., G. W.; Schlegel, H. B.; Scuseria, G. E.; Robb, M. A.; Cheeseman, J. R.; Montgomery, Jr., J. A.; Vreven, T.; Kudin, K. N.; Burant, J. C.; Millam, J. M.; Iyengar, S. S.; Tomasi, J.; Barone, V.; Mennucci, B.; Cossi, M.; Scalmani, G.; Rega, N.; Petersson, G. A.; Nakatsuji, H.; Hada, M.; Ehara, M.; Toyota, K.; Fukuda, R.; Hasegawa, J.; Ishida, M.; Nakajima, T.; Honda, Y.; Kitao, O.; Nakai, H.; Klene, M.; Li, X.; Knox, J. E.; Hratchian, H. P.; Cross, J. B.; Bakken, V.; Adamo, C.; Jaramillo, J.; Gomperts, R.; Stratmann, R. E.; Yazyev, O.; Austin, A. J.; Cammi, R.; Pomelli, C.; Ochterski, J. W.; Ayala, P. Y.; Morokuma, K.; Voth, G. A.; Salvador, P.; Dannenberg, J. J.; Zakrzewski, V. G.; Dapprich, S.; Daniels, A. D.; Strain, M. C.; Farkas, O.; Malick, D. K.; Rabuck, A. D.; Raghavachari, K.; Foresman, J. B.; Ortiz, J. V.; Cui, Q.; Baboul, A. G.; Clifford, S.; Cioslowski, J.; Stefanov, B. B.; Liu, G.; Liashenko, A.; Piskorz, P.; Komaromi, I.; Martin, R. L.; Fox, D. J.; Keith, T.; Al-Laham, M. A.; Peng, C. Y.; Nanayakkara, A.; Challacombe, M.; Gill, P. M. W.; Johnson, B.; Chen, W.; Wong, M. W.; Gonzalez, C.; Pople, J. A. Gaussian 03 (Revision B.04), Gaussian, Inc., Pittsburgh, PA. **2003**.

335. Lioe, H.; O'Hair, R.A.J.; Gronert, S.; Austin, A.; Reid, G.E. Experimental and Theoretical Proton Affinities of Methionine, Methionine Sulfoxide and Their N- and C-terminal Derivatives. *International Journal of Mass Spectrometry*, **2007**, *267*, 220-232.

336. Rusnak, F.; Mertz, P. Calcineurin: Form and Function. *Physiological Reviews*, **2000**, *80*, 1483-1521.

337. Schulz, R.A.; Yutzey, K.E. Calcineurin Signaling and NFAT Activation in Cardiovascular and Skeletal Muscle Development. *Developmental Biology*, **2004**, *266*, 1-16.

338. Sakuma, K.; Yamaguchi, A. The Functional Role of Calcineurin in Hypertrophy, Regeneration, and Disorders of Skeletal Muscle. *Journal of Biomedicine and Biotechnology*, **2010**, *2010,* 721219.

339. Mallinson, J.; Meissner, J.; Chang, K.C. Chapter 2. Calcineurin Signaling and the Slow Oxidative Skeletal Muscle Fiber Type. *International Review of Cell and Molecular Biology*, **2009**, *277*, 67-101.

340. Agrawal, R.; Agrawal, N.; Koyani, C.N.; Singh, R. Molecular Targets and Regulators of Cardiac Hypertrophy. *Pharmacological Research*, **2010**, *61,* 269-280.

341. Fujiwara, A.; Kakizawa, S.; Eno, M. Induction of Cerebellar Long-Term Depression Requires Activation of Calcineurin in Purkinje Cells. *Neuropharmacology*, **2007**, *52*, 1663-1670.

342. King, M.M.; Huang, C.Y. The Calmodulin-Dependent Activation and Deactivation of the Phosphoprotein Phosphatase, Calcineurin, and the Effect of Nucleotides, Pyrophosphate, and Divalent Metal-Ions - Identification of Calcineurin as a Zn and Fe Metalloenzyme. *Journal of Biological Chemistry*, **1984**, *259,* 8847-8856.

343. Yu, L.; Haddy, A.; Rusnak, F. Evidence That Calcineurin Accommodates an Active-Site Binuclear Metal Center. *Journal of the American Chemical Society*, **1995**, *117,* 10147-10148.

344. Kissinger, C.R.; Parge, H.E.; Knighton, D.R.; Lewis, C.T.; Pelletier, L.A.; Tempczyk, A.; Kalish, V.J.; Tucker, K.D.; Showalter, R.E.; Moomaw, E.W.; Gastinel, L.N.; Habuka, N.; Chen, X.H.; Maldonado, F.; Barker, J.E.; Bacquet, R.; Villafranca, J.E. Crystal-Structures of Human Calcineurin and the Human Fkbp12-Fk506-Calcineurin Complex. *Nature*, **1995**, *378*, 641-644.

345. Griffith, J.P.; Kim, J.L.; Kim, E.E.; Sintchak, M.D.; Thomson, J.A.; Fitzgibbon, M.J.; Fleming, M.A.; Caron, P.R.; Hsiao, K.; Navia, M.A. X-Ray Structure of Calcineurin Inhibited by the Immunophilin Immunosuppressant Fkbp12-Fk506 Complex. *Cell*, **1995**, *82*, 507-522.

346. Yu, L.; Golbeck, J.; Yao, J.; Rusnak, F. Spectroscopic and Enzymatic Characterization of the Active Site Dinuclear Metal Center of Calcineurin: Implications for a Mechanistic Role. *Biochemistry*, **1997**, *36,* 10727-10734.

347. Bogumil, R.; Namgaladze, D.; Schaarschmidt, D.; Schmachtel, T.; Hellstern, S.; Mutzel, R.; Ullrich, V. Inactivation of Calcineurin by Hydrogen Peroxide and Phenylarsine Oxide - Evidence for a Dithiol-Disulfide Equilibrium and Implications for Redox Regulation. *European Journal of Biochemistry*, **2000**, *267,* 1407-1415.

348. Oin, K.F.; Khangulov, S.; Liu, C.; Huang, C.Y. Role of Fe Ion in Calcineurin Studied by Erp and Activity Measurements. *Faseb Journal*, **1995**, *9,* A1347-A1347.

349. Namgaladze, D.; Hofer, H.W.; Ullrich, V. Redox Control of Calcineurin by Targeting the Binuclear Fe^{2+}-Zn^{2+} Center at the Enzyme Active Site. *Journal of Biological Chemistry*, **2002**, *277*, 5962-5969.

350. Aitken, A.; Klee, C.B.; Cohen, P. The Structure of the B-Subunit of Calcineurin. *European Journal of Biochemistry*, **1984**, *139*, 663-671.

351. Gallagher, S.C.; Gao, Z.-H.; Li, S.; Dyer, R.B.; Trewhella, J.; Klee, C.B. There Is Communication between All Four Ca^{2+}-Bindings Sites of Calcineurin B. *Biochemistry*, **2001**, *40*, 12094-12102.

352. Yang, S.-A.; Klee, C.B. Low Affinity Ca^{2+}-Binding Sites of Calcineurin B Mediate Conformational Changes in Calcineurin A. *Biochemistry*, **2000**, *39*, 16147-16154.

353. Stemmer, P.M.; Klee, C.B. Dual Calcium Ion Regulation of Calcineurin by Calmodulin and Calcineurin B. *Biochemistry*, **1994**, *33*, 6859-6866.

354. Filosto, S.; Fry, W.; Knowlton, A.A.; Goldkorn, T. Neutral Sphingomyelinase 2 (nSMase2) is a Phosphoprotein Regulated by Calcineurin (PP2B). *Journal of Biological Chemistry*, **2010**, *285*, 10213-10222.

355. Wang, X.T.; Culotta, V.C.; Klee, C.B. Superoxide Dismutase Protects Calcineurin from Inactivation. *Nature*, **1996**, *383*, 434-437.

356. Sommer, D.; Fakata, D.L.; Swanson, S.A.; Stemmer, P.M. Modulation of the Phosphatase Activity of Calcineurin by Oxidants and Antioxidants *in vitro*. *European Journal of Biochemistry*, **2000**, *267*, 2312-2322.

357. Reiter, T.A.; Abraham, R.T.; Choi, M.; Rusnak, F. Redox Regulation of Calcineurin in T-Lymphocytes. *Journal of Biological Inorganic Chemistry*, **1999**, *4*, 632-644.

358. Namgaladze, D.; Shcherbyna, L.; Kienhofer, J.; Hofer, H.W.; Ullrich, V. Superoxide Targets Calcineurin Signaling in Vascular Endothelium. *Biochemical and Biophysical Research Communications*, **2005**, *334*, 1061-1067.

359. Carruthers, N.J.; Stemmer, P.M. Methionine Oxidation in the Calmodulin-Binding Domain of Calcineurin Disrupts Calmodulin Binding and Calcineurin Activation. *Biochemistry*, **2008**, *47*, 3085-3095.

360. Srikanth, R.; Wilson, J.; Bridgewater, J.; Numbers, J.; Lim, J.; Olbris, M.; Kettani, A.; Vachet, R. Improved Sequencing of Oxidized Cysteine and Methionine Containing Peptides Using Electron Transfer Dissociation. *Journal of The American Society for Mass Spectrometry*, **2007**, *18*, 1499-1506.

361. Shen, X.; Li, H.; Ou, Y.; Tao, W.; Dong, A.; Kong, J.; Ji, C.; Yu, S. The Secondary Structure of Calcineurin Regulatory Region and Conformational Change Induced by Calcium/Calmodulin Binding. *Journal of Biological Chemistry*, **2008**, *283*, 11407-11413.

362. Rumi-Masante, J.; Rusinga, F.I.; Lester, T.E.; Dunlap, T.B.; Williams, T.D.; Dunker, A.K.; Weis, D.D.; Creamer, T.P. Structural Basis for Activation of Calcineurin by Calmodulin. *Journal of Molecular Biology*, **2012**, *415*, 307-317.